Coolside Waste Management Research

Final Report
April 23, 1991- June 30, 1996

Work Performed Under Contract No.: DE-AC21-91MC28162

For
U.S. Department of Energy
Office of Fossil Energy
Federal Energy Technology Center
Morgantown Site
P.O. Box 880
Morgantown, West Virginia 26507-0880

By
Center for Applied Energy Research
University of Kentucky
3572 Iron Works Pike
Lexington, Kentucky 40511-8433

Disclaimer

Table of Contents

COOLSIDE WASTE MANAGEMENT RESEARCH
Final Report
Executive Summary

Introduction

This final report summarizes the important aspects of the project, but it does not present all of the data that was produced. Further details maybe found in the monthly and quarterly reports that were filed with the Morgantown Energy Technology Center. This report is organized into six chapters which present the important conclusions of the principal areas of investigation. A summary of the more significant observations follows.

Project Summary

Background and Methodology

This study was initiated during a successful test of the Coolside flue gas desulfurization technology at Ohio Edison's Edgewater generating station in 1991. Coolside is a lime duct injection technology which is installed on the downstream side of the last heat exchanger (Chapter 1). As tested by Ohio Edison, it also employs an alkali reagent, in this case $NaOH$, to enhance sulfur capture.

The overall goal of the this study was to develop sufficient chemical and physical data to insure the environmentally safe disposal of the material. A related project conducted in conjunction with CONSOL Research and Development investigated the utilization potential of the material. Two areas were chosen for

particular emphasis. These are the elemental release or leaching characteristics of the material and the geotechnical characteristics of the material.

The methodology and approach for the geotechnical work (Chapter 3) included the laboratory classification of the waste as an engineering material and laboratory investigations of the its strength and swell properties as a function of compaction. Field studies included the controlled emplacement of the material under varying degrees of compaction. During the fill the geotechnical properties of the materials were measured. The lysimeters were excavated at the end of the project and the physical properties of the materials were again measured to determine the changes which had taken place.

The leaching properties of the material investigated included the determination of the chemistry of the leachate under laboratory column leaching and batch extraction (TCLP) conditions (Chapter 3). The leachates from the field lysimeters were also collected and analyzed over a three and a half year period (Chapter 5).

The geotechnical and geochemical properties of the materials are dependent upon complex mineral solution reactions. In an attempt to determine the overall controls on the system, detailed mineralogical determinations were made of the materials (Chapter 2). Also, investigations were made into the state of the thermodynamic data available. A publicly available database and computer program was obtained from the United States Geological Survey and modified for this project (Chapter 6).

Summary of Findings

Geotechnical

Laboratory Results. Ninety-five percent (95%) of the Coolside material passed a 200 mesh sieve (-75 micron) and had a specific gravity of ~2.5. Index properties tests indicated that the Coolside materials were non-plastic and classified as ML (silt) in the Unified Classification System and A-4 under the ASSHTO System.

The Coolside material has the potential to bean excellent engineering material. Specimens compacted to 95% of maximum dry density (-1 120 kg/m^3 or -70 lbs/ft^3) and with optimum moisture (36.5%) were found to develop unconfined compressive strengths of between 1,000 psi and 2,500 psi (-6,900 to -17,200 kPa). These strengths approach some types of concrete and greatly exceed natural soils under comparable conditions. The compacted Coolside materials achieved permeabilities from 4 x 10^{-5} to 3 x 10^{-6} cm/sec (low to very low) in the lab.

The Coolside materials exhibited unusual swell properties. Submerged molded specimens which were unaged and unconditioned had total swell which ranged from 10% to 23%. Aging the samples before submerging and the addition of surcharging greatly reduced the amount of swell to values within the range of typical soils. Swelling could have an impact on the utilization of the materials for some engineering applications.

Field Results. The field lysimeters were filled at three differing levels of compaction. Lysimeter L1 was loose filled (i.e. uncompacted) and had average dry density and moisture content of 706 kg/m^3 (44.1 lbs/ft^3) and 37.5%, respectively. Lysimeter L2 was compacted to the density designed to simulate the compactive efforts of a D9 bulldozer (1 17.3 kPa or -17 psi). Dry density and moisture contents averaged 788 kg/m^3 (49.2 lbs/ft^3) and 38.9% in this lysimeter. The third lysimeter (L-3) was filled with Coolside material compacted near 95% of standard maximum dry density and optimum moisture content. Average

values of dry density and moisture content were 1060 kg/ins (66.2 lbs/ft^3) and 37.0%, respectively.

Upon excavation, after 3.5 years of weathering, the materials were excavated and their geotechnical properties determined. The average strengths of the materials in the three lysimeters were 44.1, 46.4 and 1,629 psi for the L1, L2 and L3 lysimeters respectively. Average permeabilities were 1.55x 10-4, 4.6 xl 0^{-4} and 2.2 x 10"fi for L1, L2, and L3 respectively. Thus, compaction had an overarching effect on the physical properties of the material. Achieving optimum compaction resulted in a fill which had substantial strength (layers of L3 achieved compressive strengths as high as 2,600 psi) and greatly reduced permeability (layers with permeabilities as low as 10"8 to 10"g cm/sec were measured).

Geochemical Results

The Coolside material as received was composed of quartz (SiO$_2$), mullite (Al$_6$Si$_2$O$_{13}$), portlandite (Ca(OH)$_2$)), calcite (CaCO$_3$), hannebachite (CaSO$_3$ 0.5H$_2$O) and minor anhydrite(CaSO$_4$). A glassy phase is also present in the raw Coolside material and typically consists of spherical Si-Al fly ash particles. Upon hydration ettringite (Ca$_6$Al2(SO$_4$)$_3$ OH$_{12}$26 H$_2$O), the principal cementitious mineral in the system rapidly forms,
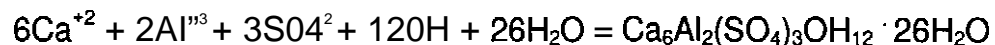
$$6Ca^{+2} + 2Al^{"3} + 3S04^2 + 120H + 26H_2O = Ca_6Al_2(SO_4)_3OH_{12} \cdot 26H_2O$$

The state of compaction of the materials was found to have a strong impact on the chemistry of the leachates. Two distinct patterns emerged over the study. Lysimeters L1 and L2 initially had much higher elemental concentrations compared to L3 which was compacted to optimum density. Sodium, Cl, K and sulfate were all higher in concentration by factors of 3 to 4 and Ca by a factor of

more than 10 in LI and L2 leachates. The longer term elemental release pattern showed a more rapid decline in elemental concentrations in the LI and L2 leachates. For example, Na in LI dropped from an average value of 15,767 ppm--which is approaching the concentration of a brine--the first year, to an average value of 1,637 ppm the second year, and 604 ppm the third. The L3 leachates declined in concentration at a lower rate, with an average of 5,480 ppm the first year followed by averages of 2,302 ppm and 1,436 ppm the second and third year.

The leaching pattern for minor and trace elements did not necessarily show a similar pattern to that of the major elements. For example, Al and Si increased in concentration during the second year of the study in the L1 and L2 leachates as a function of pH of the leachates which increased over time. The average pH of the L1, L2 and L3 leachates was 9.7, 10.4, and 12.3 during the first year of collection. Most transition metals are insoluble under these conditions and were not detected. However, elements which can form oxyanionic complexes such as Mo ($MoO(^2)$), Se (SeO_4^{-2}), As (AsO_4^{-3}) and V (VO_4^{-3}) were found in measurable and sometimes significant concentration (e.g. Mo reached maximum concentrations >100 ppm in several samples the first year).

Carbon dioxide concentrations in the soil gases of the lysimeters were monitored in the second and third year of the study. In general, the highest CO_2 concentrations were reached during the summer and the lowest during mid-winter, as a function of respiration. The highest concentration recorded was 3.2% (32,000 ppm), well above that of atmospheric concentration (-350 ppm). Soil gas profiles gave clear and conclusive evidence of the highly reactive nature of the Coolside materials with respect to CO_2. At pH's above -10 CO_2 reacts directly with hydroxide and forms carbonate ion,

$$CO_2 + 20H" = HCO_3^- = H^+CO_3^{-2}$$

The thermodynamic analysis of the chemical composition of the leachates indicated that they are all supersaturated with respect to calcite and undersaturated with respect to gypsum and hannebachite. This, combined with direct mineralogical evidence, indicates that minerals are both dissolving and precipitating. The most important long term weather reactions include the precipitation of calcium carbonate and the dissolution of sulfites and sulfates, primarily hannebachite in this case, summarized as follows:
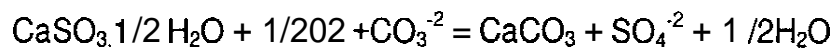
$$CaSO_3.1/2\,H_2O + 1/202 + CO_3^{-2} = CaCO_3 + SO_4^{-2} + 1\,/2H_2O$$

Both the mineralogical and thermodynamic data indicate that ettringite will also break down over time. However this does not appear to proceed until the sulfate is largely exhausted. Thus, in effect, the sulfate acts as a buffer to extend the stability of the ettringite.

Elements of environmental concern which were found in concentrations exceeding RCRA limits included Se (RCRA limit 1 ppm) and As (RCRA limit 5 ppm). Some of the leachates from the L3 lysimeter reached concentrations as high as 19 ppm As during the first year of the study. The average concentration of Se for all of the leachates from the Coolside materials for the first year of study exceeded the 1 ppm limit.

Batch leaching extractions following US EPA protocols were not relatable to elemental concentrations as observed in the field. Long term column leaching experiments produced leachates with elemental concentrations of the same magnitude as produced by the field lysimeters. This included similar As and Se concentrations as found in the field leachates.

CHAPTER 1. INTRODUCTION AND PROJECT BACKGROUND

Description of the Technology and Statement of Objectives

Project Objectives

The primary objective of the study was to produce sufficient chemical and geotechnical information to assure that the disposal of Coolside flue gas desulfurization (FGD) material can be conducted in an environmentally safe manner. More specifically, our objectives were to determine the elemental release or "leaching" characteristics as well as changes in the physical characteristics of the materials over time.

The leaching research included both field lysimeter studies and laboratory research, including standard andcolumn extraction methods. The geotechnical research also included field and laboratory work. The field research focused on the testing of the materials as emplaced in the lysimeter and after 3.5 years of leaching. Thelaboratory workincluded standard methodology toclassify the material's engineering properties, and tests to measure its performance under various conditions of moisture and compaction. Twoareas of special emphasis included the measurement of the swelling characteristics of the material and its mineralogy.

Description of Coo/side Technology

Coolside is a dry flue gas desulfurization (FGD) technology for removal of SO_2 in coal fired power plants. The technology was designed as a retrofit to existing power plants by CONSOL Research and Development.

Coolside is an attractive option for retrofit SO_2 reduction for plants which have limited boiler life or where capital cost or space limitations are important factors. The capital investiture is modest compared to wet scrubbing technologies, as all that is required is ductwork modification and the installation of a reagent delivery system. Because the technology utilizes the existing hardware, it is ideal for installations which have space limitations. The technology operates on the tail end of the power generating system, where malfunctions in the SO_2 scrubber technology are unlikely to cause disruptions of the operation of the power plant. Coolside can be coupled with burner lime injection (BLI) technology to provide higher overall calcium utilization and SO_2 reductions than can be achieved by either alone.

Process Description. Coolside is similar to other dry scrubbing technologies such as Dravo's HALT process (Hydrate Addition at Low Temperatures).[1] In these processes hydrated lime is pneumatically injected dry into the power plant duct work on the "cool side" of the air preheater (Figure 1-1). The flue gas stream is then humidified to within about 20 to 30"F of adiabatic saturation by spraying atomized water. This also reduces the flue gas temperature.

Humidification of the flue gas is critical to the process as it greatly increases SO_2 sulfur capture efficiency by activating the sorbent. Sulfur capture has been shown to increase linearly with relative humidity and to be strongly affected by the presence of water droplets.[2] Humidification enhances the performance of the electrostatic precipitators (ESP) by reducing the resistivity of the ash.

The Coolside process can be operated with the addition of a "promoter", such as NaOH or Na_2CO_3, to the water spray to enhance SO_2 capture efficiency. Increased capture efficiency may be due to several factors including: 1) additional sulfur capture by the promoter itself; 2) the modification of the surface of the sorbent by the promoter; 3) increasing the basicity of the sorbent with the

8
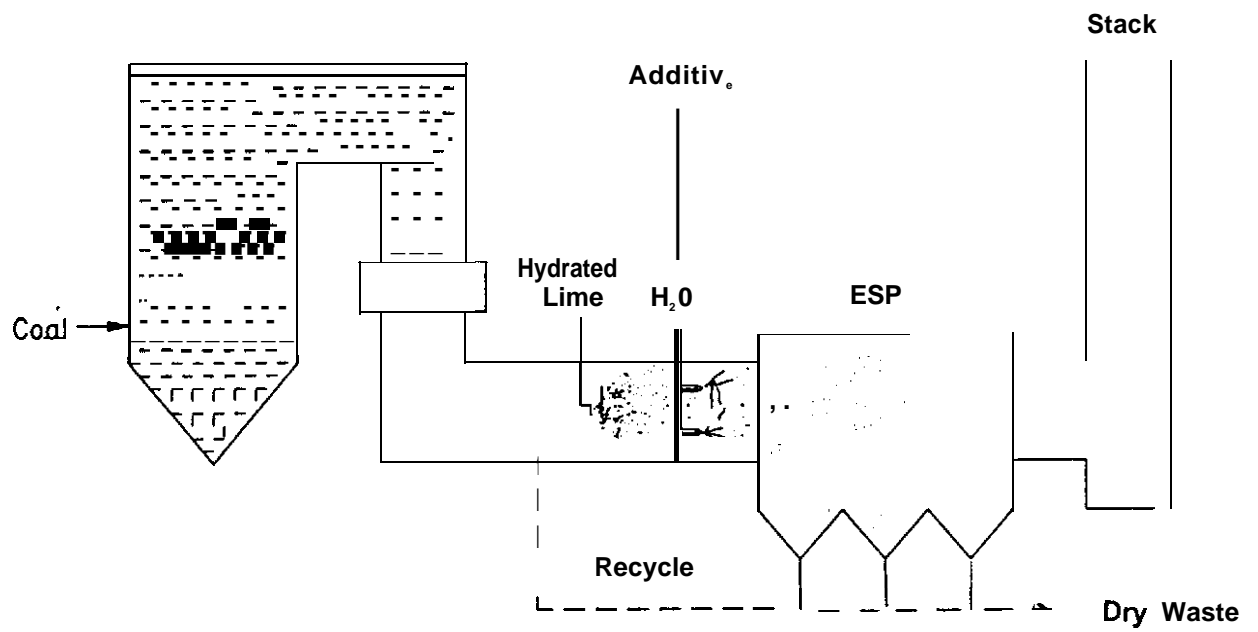
Figure 1-1. Schematic diagram of Coolside process.

promotion of acid-base SO_2 capture reactions, and; 4) increasing or retaining moisture at the sorbent surface, of importance for deliquescent promoters such as NaOH.[3] In general sodium based compounds have been found to be the most effective promoters, although chloride salts have also been shown to be effective if added during lime hydration.

Calcium utilization efficiency can also be increased by recycling the ash from the ESP. The recycled sorbent has been shown to be almost as effective as fresh material in absorbing SO_2. Recycling can increase calcium utilization from approximately 40% to 50% and improve the overall process costs. [4]

Coolside can be combined with lime or limestone injection (BLI) to achieve even greater SO_2 reductions. In combined Coolside-BLI application the sulfated lime, fly ash and unreacted calcined lime from BLI pass through the Coolside humidification zone where a promoter may also be added. This results in sorbent reactivation and further SO_2 reduction. The ash is collected in an ESP and can also be slaked and recycled to the burner for improved calcium utilization. BLI alone results in low calcium utilization, typically about 20%, and sulfur captures of approximately 50%. Humidification results in lime reactivation, increasing the overall SO_2 removal to 65%. The injection of the promoter results in further SO_2 removal, up to about 80%.

The Edgewater Demonstration

A demonstration of the Coolside technology was successfully proposed in 1986 under the first Clean Coal Solicitation. The actual demonstration included the participation of the Ohio Coal Development Office, Babcox and Wilcox Co., Ohio Edison and the Consolidation Coal Co., in addition to the U.S. DoE.

The demonstration was conducted at Ohio Edison's Edgewater Power Plant, located in Lorain, Ohio, on the 105 MW #13 Utility boiler. The test lasted from July of 1989 through February of 1990 and had two primary goals. The first was to achieve overall SO_2 reductions of 30%, 50% and 70%. The second was to achieve reliable process operations at 20 'F and 25 "F, approaching adiabatic saturation. The demonstration was considered successful, as the earlier pilot plant results were reproduced and the suitability to scale-up of the technology was proven.[5] Problems encountered during the tests indicated that improvements in the humidifier design and the ESP and ash removal systems needed to be made.

Coo/side *Waste Sample* Collection. Personnel from the Center for Applied Energy Research of the University of Kentucky spent the last two weeks of the demonstration in residence at the Edgewater Plant collecting solid waste for the process. The sample collection was conducted in response to an invitation by the U.S. DoE. The samples were loaded pneumatically into 55 gallon fiber barrels from the No. 2 ESP (the No. 1 unit was out of service). Each barrel was capped and tightly sealed with duct tape and stored indoors. The samples, totaling 65 tons in weight, were transported to Lexington in covered vans and since that date have been warehoused indoors at a commercial facility. This material serves as the focus for this proposal.

The solid waste produced by the Coolside process is similar to other types of dry scrubber waste, such as that from BLI and LSD (Lime Spray Dryer), in that it is composed primarily of coal fly ash and partially sulfated lime. These solids are very high in calcium compared to conventional fly ash (Table 1-1).[s]

Coolside solids differ from BLI materials in that they are produced at relatively low temperatures, and the residual lime remains hydrated. Coolside waste differs from that of other low temperature scrubbing technologies due to the

Table 1-1 Comparison of elemental composition between Coolside
material and fly ash (FA) used in the field lysimeters.

	Coolside		PCC FA
Element	**Avg**	St. *Dev.*	**Avg**
Wt %			
Al, %	10.56	1.65	17.4
Ca, %	9.39	1.69	0.85
Fe, %	6.29	0.91	7.99
K, %	**1.35**	0.15	2.17
Na, %	1.11	0.18	0.225
Ti, %	**0.38**	0.05	0.88
ppm			
As	219	31	108
Ba	428	190	1805
Br	113	57	142
Cr	**138**	19	176
Cu	79	8	172
F	450	95	68
Ga	36	6	58
Ge	47	8	39
Li	86	27	188
Mn	116	20	136
Mo	29	6	25
Ni	73	10	76
Pb	112	32	93
Rb	97	10	632
Se	12	4	3
Sr	318	32	98
V	186	14	241
Y	62	8	376
Zn	**281**	35	149
Zr	175	29	36
	N=263		N=2

presence of significant quantities of sodium compounds derived from the sorbent activator. In addition to fly ash, the other major compounds present in Coolside waste include $Ca(OH)_2$, $CaSO_3$, $CaSO_4$, with minor amounts of Na_2SO_4, Na_2SO_3 and $CaCO_3$.

The samples for the study were collected by the CAER during the pilot demonstration of the Coolside technology at Ohio Edison's Edgewater Power Station. Three "samples" consisting of a series of barrels during specified intervals were collected. The first and third of these (Coolside No. 1 and No. 3) were utilized in the field work.

An aliquot of each barrel of material was recovered at the sample storage warehouse and was analyzed for total sulfur. This data will be used to identify individual barrels with compositions which are not representative of that feasibly produced under commercial conditions.

The second sample was clearly lower in sulfur than either the first or third. It is not considered to be representative of a material which would be produced by a commercial application and will not be used. The three samples averaged 1.94%, 1.67% and 1.940/. sulfur, respectively (4.8%, 4,2%, 4.8% as SO_2). The samples collected later in the test were also more variable. Standard deviations of 0.23, 0.36 and 0.36 (1 F) were calculated for the three samples, respectively. The sulfur data confirmed the information received from the pilot plant operators. For example, during the final sample collection day the system was not operating effectively early in the afternoon. However when load conditions dropped, system efficiency improved, reaching a peak late at night.

Lysimeter Description and instrumentation

Four concrete lysimeters located at the University of Kentucky's Environmental Field Research Station in Montgomery County, Kentucky were used to study

field behaviors of material generated from the Coolside process. These are compared to a commercially available Class F fly-ash. The four lysimeters surround a central chamber used for leachate collection and instrumentation. Each individual lysimeter is 2.4 m (8 ft) by 2.4 m (8 ft) by 3 m (1 O ft) deep (Figure 1-2). The tops of the lysimeters are flush with the ground surface. The inner walls, adjacent to the central access chamber, are fitted with knock-outs at various depths to allow installation of leachate transport tubes and access to instrumentation.

Pressure cells were mounted in Lysimeter 3 (L-3 in Figure 1-2) at depths of 4 and 6 feet from the surface. A view of one of the pressure cells is shown in Figure 1-3. An additional pressure cell was installed in Lysimeter 4 at the mid-point of the fly ash fill. Before filling, a stainless steel tube was placed in the center of each lysimeter to allow access for a nuclear moisture probe. The probe has been used to monitor changes in moisture under natural weathering conditions. Thermocouples (right cable in Figure 1-3) were placed at various depths in the lysimeters to measure temperature differences which might occur from hydration or mineralogical phase changes. Settlement (swell) platforms were placed at the soil-Coolside interfaces and the soil-fly ash interface to measure vertical movements of the materials.

Filling Operations

The material was transported to the site in barrels, as shown in Figure 1-4. Enough material was mixed with water to construct one lift. Each lift ranged from 10.2 to 15.2 cm (4 to 6 in) in thickness. Usually about five barrels of Coolside residue was sufficient to make one lift. To avoid weighing each individual barrel, a correlation was established to determine the weight. The distance from the top of the barrel to the surface of the Coolside residue was measured for several barrels. The barrels were then weighed on a portable field scale. A correlation
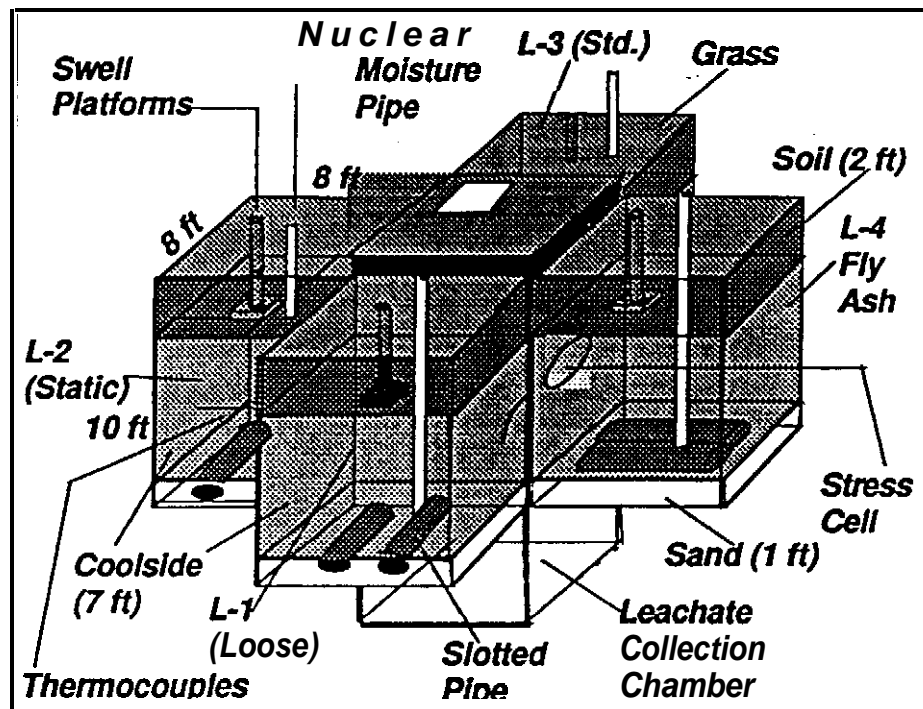
Figure 1-2. Schematic of field lysimeters.
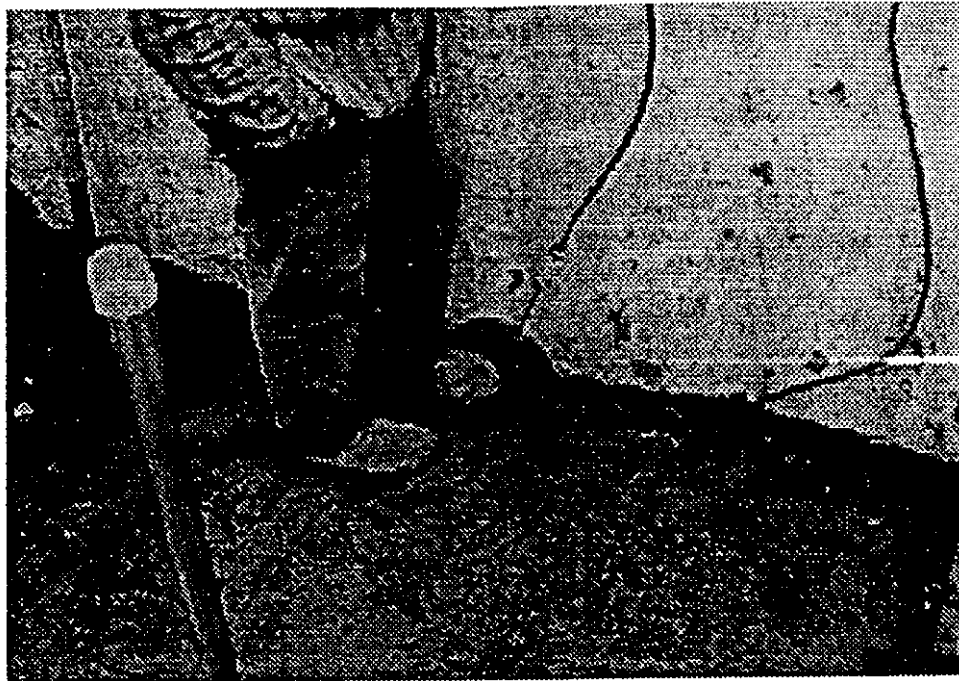
Figure 1-3. View of pressure cell and thermocouple placed in Lysimeter 3.
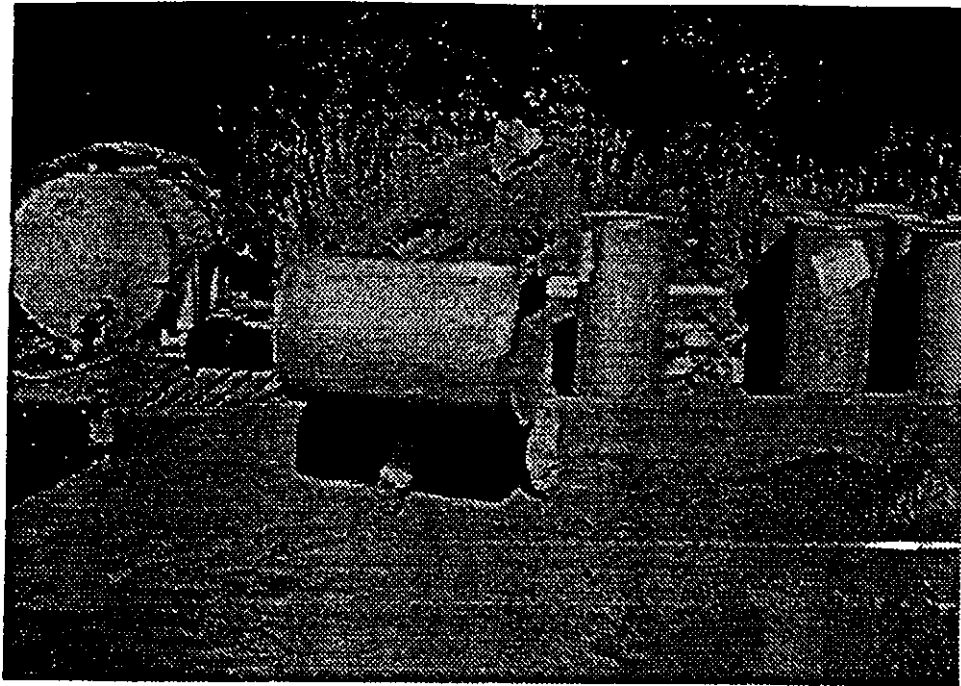
Figure 1-4. **View** of the barrels used to transport the Coolside ash to the lysimeter site and concrete mixing pad.
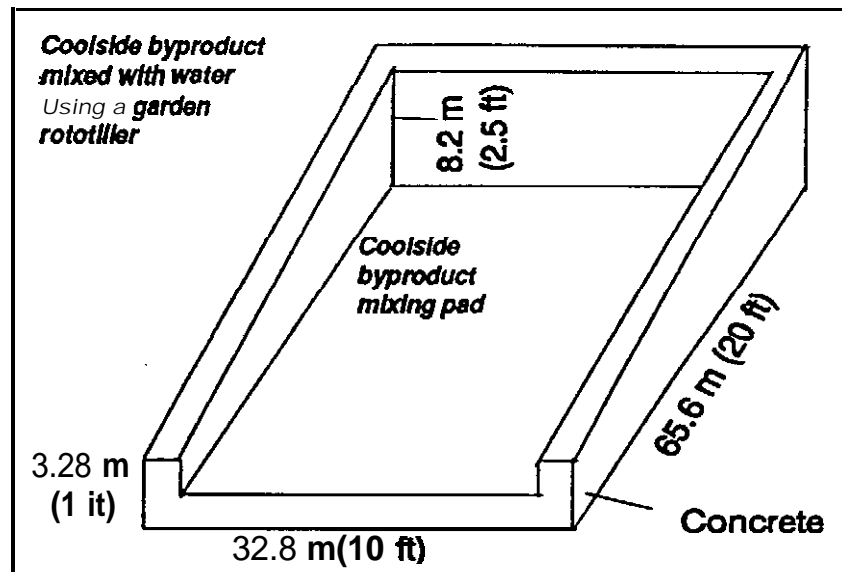
Figure I-5. Configuration and dimensions of Coolside concrete mixing pad. '

was established whereby the weight of the material could be determined by simply measuring the distance from the top of the barrel to the surface of the material. This procedure worked very well in determining the weight of the material because of the *uniform particle size and density of the material.* The average weight of each barrel was approximately 112 kg (250 lbs). The amount of water needed to reach the desired moisture content was then calculated. Each lift consisted of approximately 572 kg (1,250 lbs) of dry Coolside material. The residue was placed on a concrete mixing pad, as shown in Figures 1-5 and 1-6, which was built with three side curbs to contain the materials on the pad while mixing, Water from a calibrated tank, Figure 1-7, was then added to sufficiently moisten the material to control dust. The water for mixing with the Coolside ash was transported to the site using the truck-mounted tank shown in Figure 1-8. The mixture was blended with a rear tine tiller, as shown in Figure 1-6. Water was continually added until the desired moisture content was reached, A front end loader was used to place the mixture into the lysimeter, Figure 1-9. The front end of the concrete pad did not contain a side curb so that the front end loader was free to move onto the pad to load the mixed materials, back out, and place the mixed ash in the lysimeters.

A 30.5 cm (1-ft) layer of Ottawa sand was placed in the bottom of each lysimeter (Figure 1-2) to improve leachate collection. Three leachate transport tubes (Figure 1-1 O) were embedded in the sand. Lysimeters were filled with 2.1 m (7 ft) of Coolside materials. Lysimeter 4 was filled with 2.1 m (7 ft) of fly ash. Leachate collection tubes were also placed at the soil-Coolside interfaces and the fly ash-soil interface and at various depths in the four lysimeters. A native silty clay was loosely placed, to facilitate the downward movement of rainfall, on the residue ash in the top 0.6 m (2 ft) of each lysimeter.

Moisture and density measurements were obtained from drive-tube and sand-cone tests. A nuclear moisture-density gauge was also used. Results obtained from the nuclear gauge were used for comparison and calibration purposes and

Figure 1-6. View of concrete mixing pad, Coolside ash, watering, and rototiller.

Figure 1-7. View of calibrated water tank.

18
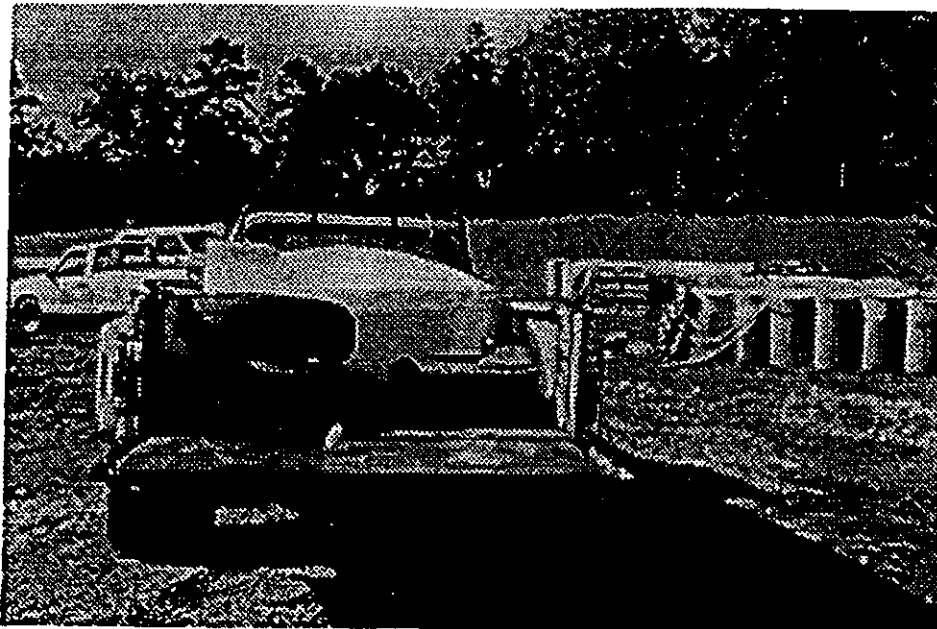
Figure 1-8. View of truck-mounted plastic tank used to transport water to the site.

Figure 1-9. View of front end loader used to transport barrels of Coolside to the mixing pad and to place the Coolside ash mixture into the lysimeters.
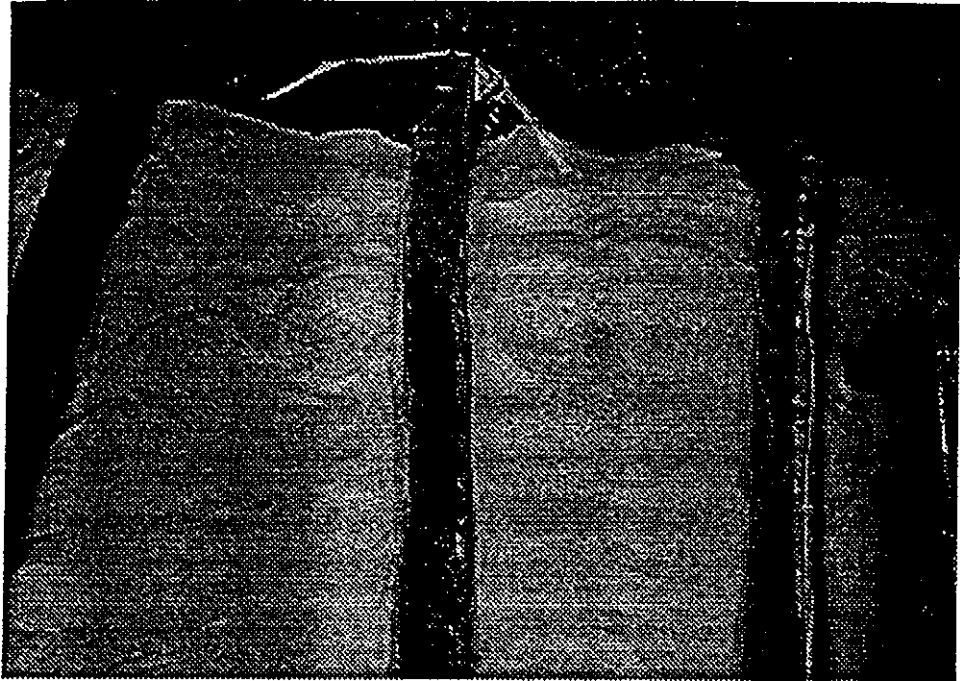
Figure 1-10. View of leachate collection tubes and the Ottawa sand used at the bottom of the lysimeters.

Figure 1-11. Drive sampling tube used to obtain specimens for checking dry density and moisture content of each lift.

were not used to determine actual density and moisture conditions. Because of the fine-grained nature of the materials, the drive-tube sampler (Figure 1-11) technique provided the most reliable means of measuring the dry density and the moisture content of each lift.

Compacting ash and FGD materials conserves landfill space while increasing disposal costs. In placing the materials, different compactive efforts were used in an attempt to simulate different compactive states of the Coolside by-product as it might exist in a landfill.

Laboratory Compaction for Field Emplacement

The filling of the field lysimeters was preceded by extensive laboratory studies. Different laboratory compactive energies were used to examine the effects of increased compactive effort. Laboratory moisture-density tests were performed at modified, standard, and low energy compaction. Compactive energies of these tests were 376,754, 71,885, and 14,430 kg-m/m^3 (56,246, 12,374, and 4,050 ft-lbs/ft^3), respectively. A low energy compaction procedure was devised to examine engineering properties of lightly compacted materials. The testis similar to standard methods, except a lighter (0.835 kg, or 1.84 lbs.) rammer is used. Dry density increased as the compactive effort was increased. Values ranged from 576 kg/m^3 (36 lbs/ft^3) --loose state-- to 1251 kg/m^3 (78.1 lbs/ft^3) -- modified compaction. When the compactive energy was increased above the low energy compactive energy, the dry density increased from 1079 kg/m^3 (65.5 lbs/ft^3) to 1251 kg/m^3 (78.1 lbs/ft^3). The maximum dry densities obtained from standard (ASTM D698) and modified compaction (ASTM D1 557) were only 6.4% and 1 9.2%, respectively, greater than the maximum dry density obtained from the low energy test, although the compactive energies were 3.1 and 13.9 times larger than the low energy compactive effort. Consequently, efforts to compact the Coolside material to a dry density greater than maximum dry density

obtained from standard or low energy compaction would probably be uneconomical. However, the economics would depend on such variables as land cost, equipment cost, and haul distances. Moreover, the economics of environmental impacts would play a major role in formulating a field compaction scheme. Optimum moisture content decreased as compactive energy increased. Optimum moisture contents for low energy, standard, and modified compaction were 45.0, 36.5, and 28.50/., respectively.

References

1. Yoon, H., F.W. Theodore, F.P. Burke, B.J. Koch, 1986, Low Capital Cost, Retrofit SO_2 Control Technologies for High Sulfur Coal Applications. Reprint, Air Pollution Control Association, 79th Annual Meeting, Paper No. 86-47.5, 21 p.

2. Stouffer, M. R., H. Yoon, and F. P. Burke, 1989, An Investigation of the Mechanisms of Flue Gas Desulfurization by In-Duct Dry Sorbent Injection. I&EC Research, 28, p. 20-27.

3. Yoon, H., J.A. Withum, W.A. Rosenhoover and F.P. Burke, 1986, Sorbent Improvement and Computer Modeling Studies for Coolside Desulfurization. Presented at EPA/EPRI Joint Symposium on Dry SO_2 and Simultaneous SO_2/NO_x Control Technologies, Raleigh, N.C., 20p.

4. Withum, J. A., W.A. Rosenhoover and H. Yoon, 1988, A Pilot Plant Study of the Coolside Desulfurization Process With Sorbent Recycle. *Proceedings, 5th Annual Pittsburgh Coal Conference*, Pittsburgh, PA, p. 84-96.

5. Kanary, D. A., R.M. Statnick, H. Yoon, D.C. McCoy, J.A. Withum and G.A. Kudlac, 1990, Coolside Process Demonstration at the Ohio Edison Company Edgewater Plant Unit 4- Boiler 13. *Proceedings,* 1990 *SO$_2$ Control Symposium,* EPRI and U.S. EPA, Session 7A, V 3, New Orleans, LA, 19p.

6. Wu, M. M., and R.A. Winschel, 1988, *Coolside Waste Management Studies-- Fins/ Report.* U.S. DoE Cooperative Agreement No. DE- FC22-87PC79798, *78p.*

CHAPTER 2. MINERALOGIC INVESTIGATION OF THE COOLSIDE MATERIAL

Overview

The mineralogical study of the Coolside material was aimed at a comprehensive understanding of the material's impact on the environment. Of particular importance was the question of how soon after wetting the powderous Coo[side material would turn into a hardened crystalline or semi-crystalline matrix, and whether it would gain concrete-like properties. After solidification of the materials the next stage was to determine how severely the Coolside material would undergo weathering reactions.

The main emphasis of this part of the research program, therefore, included short- and long-term monitoring of the material's overall physical and chemical transformations, both of which are governed by mineral growth, dissolution, precipitation and disintegration reactions. In the beginning, wetting of the Coolside material causes reactions to form hydrated phases, either by crystallographically bonding or physically adsorbing portions of the added moisture. The excess moisture can either be contained as pore fluids, and the pH of the pore fluids controls the formation of new crystals as well as the dissolution of others, or, it contributes to the leachate phase. The excess moisture also plays a major role in the transport of dissolved ions and dissolved carbon dioxide from the atmosphere which mineralize within available pore space. The degree of compaction of the Coo[side materials restricts the accessibility of moisture and controls the leaching characteristics by affecting the rate of fluid migration through the Coolside materials. The ionic strength of the solutions (amount of dissolved ions) affects the precipitation of the solid phases. Hydration reactions are responsible for the bulk of the expansive properties of the materials, including strength gain, and have been found to be affected by the degree of compaction of the materials.

Introduction

To gain a comprehensive understanding of the individual mineral reactions that affect the Coolside material, including permeability, leaching potential and stability, the mineralogical study was sub-divided into four series of investigations with distinct objectives.

Series 1:   Field Lysimeter Study
Series II: Column Lysimeter Study
Series ill: Kinetic Study
Series N: Pelletization of FBC Material

The investigations focused on a field demonstration (Series 1) using field lysimeters to monitor changes in the mineralogy of the Coolside material as a function of different packing densities (degree of static loading) and moisture content, Additional moisture was controlled by the seasonal rain water influx. The field lysimeters were sampled on four different occasions within the field testing period. Results from the field demonstration are then compared to those obtained from controlled laboratory column lysimeter tests (Series II). The laboratory columns received controlled amounts of moisture over the testing period. Top, middle and bottom zones of individual laboratory lysimeters were collected at the end of the test period and subjected to a thorough analysis of new mineral growth or decay.

In order to gain a better understanding of the mineralogical transformations that occur during hydration of the Coolside material, a kinetic study (Series III) was conducted in which the material was submerged in distilled water, within a sealed container, and the crystalline phases were monitored soon after hydration as well as over an extended time period. Although these conditions do not reproduce those in the field lysimeters, the experiments provide information on mineral stability relations in a closed system, and assist in predicting reactions that would occur under other conditions.

Finally, a pelletization study was conducted as part of the Coolside testing program (Series IV). The FBC material was received from Wormser Development Company. The pelletization study aimed at understanding the engineering properties of a selected FBC waste material using a disc pelletizer, controlled moisture content, carefully chosen additives and curing of the materials in a humidified atmosphere at elevated temperatures, The optimum pelletization conditions were determined and discussed by Dr. Milton Wu at Consol. The mineralogical processes involved in the curing, aging and weathering of the pelletized materials were subjected to a thorough testing at CAER as part of the Coolside program and the results are summarized in this report. The mineralogical findings of the pelletization project are expected to aid in the overall understanding of the long-term stability of the materials, but also help determine new applications such as high volume usage.

Analytical Methods

The materials were analyzed using x-ray diffraction (XRD) methods. The XRD methods depend on the measurement of the intensities of suitable x-ray diffraction lines combined with a calibration from a single compound standard. Mineral phases were typically detected, if present, in excess of **5** volume percent within the sample material. The XRD spectra were obtained with a Philips APD 3500 X-ray diffractometer, using CU-K radiation (1.5418 rim), a scan speed of two counts/second, an increment of 0,1° over a 2 range from 7 to 400. Mineral phases that were not abundantly present within the sample materials to be detected with the XRD method could be investigated using a scanning electron microscope (SEM) with energy dispersive x-ray capabilities for chemical determinations. Crystallization of mineral compounds may occur within small voids and can be observed in situ using the SEM application. Additional sample identification was based on crystal morphology. The SEM analyses were conducted using a Hitachi S-2700 SEM (xl 0^4 magnification) after gold-coating of the samples.

Important Mineral Phases

Because the following discussions on the fate of the Coolside material focus on specific mineral phases that are either present in the raw Coolside material or formed as a result of the aging and weathering process, an overview of the dominant phases is presented first. Particular emphasis is placed on the mineral formation/decay process, including the crystal morphologies and XRD profiles.

The predominant mineral phases that are observed in the raw or aged Coolside material include:

Silicon Dioxide:	$SiO2$
Mullite:	$Al6Si2O13$
Portlandite :	$Ca(OH)_2$
Anhydrite:	$CaSO_4$
Ettringite:	$Ca6Al2(SO4)3OH12\ 26\ H2O$
Calcium Carbonate:	$CaCO_3$
Hannebachite:	$CaSO_3\qquad 0.5H_2O$

Glassy Phase. A glassy phase is present in the raw Coolside material and typically consists of spherical Si-Al fly ash particles. The amount of glassy particles diminishes in the aged samples as the amorphous phase partially dissolves and contributes to new mineral growth. SEM investigations indicate that the glassy particles are often frothy in appearance. Their relatively high surface areas promote the occurrence of dissolution at a faster rate compared to a dense glass phase. In contrast to the glassy particles which are part of the raw Coolside material, a Si-Al gel phase as well as a Ca-Si-Al gel phase develops in the aged materials forming a binder between mineral grains. Although the gel phase has not enough symmetry on a molecular level to produce characteristic XRD peaks for identification, the gels are "semi-oriented and have a higher density compared to the frothy glass phase.

Silicon Dioxide. Pure silicon dioxide occurs in the form of hexagonal quartz crystals. Quartz is a chemically very inert substance at ordinary temperatures and behaves as an indifferent material. In the XRD analyses quartz may be viewed as an internal standard. The non-crystalline silicon dioxide (glassy component) is less dense compared to the crystalline modification and readily participates in early hydration reactions. The differences in reactivity are therefore not due to chemical but rather physical conditions based on texture and porosity. Under alkaline conditions which are favored in the hydrated Coolside materials, the volubility of SiO_2 becomes enhanced because of the formation of monomeric and multi meric silicates. The volubility of SiO_2 can be characterized by the following equilibria:

$$SiO_2 \text{ (quartz)} + H_2O = Si(OH)_4 \qquad \log K = -3.70$$
$$SiO_2 \text{ (amorphous silica)} + 2 H_2O = Si(OH)_4 \qquad \log K = -2.70$$
$$Si(OH)_4 = SiO(OH)_3^- + H^+ \qquad \log K = -9,46$$
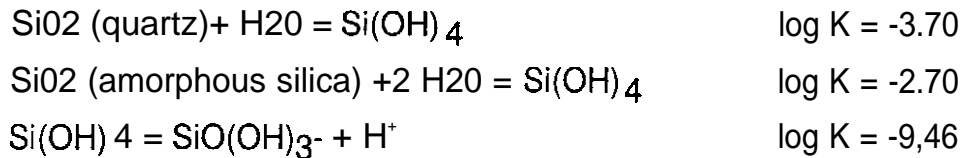
Mullite. Mullite is a stable form of the system $Al_2O_3 SiO_3$. The crystals form from a cooling liquid which controls their composition. Mullite melts congruently at 1850° C. Like crystalline SiO_2, the mullite crystals are very erosion resistant and have only minor affects on the mineral transformations that are important to the Coolside material. The composition of mullite approximates to $3 Al_2O_3 2SiO_2$ with the formula being A16Si2013. The mullite crystals can be identified by their characteristic x-ray peaks, but are also easily recognized by their very distinctive needle-like morphology using SEM applications.

Portlandite. Portlandite is a calcium hydroxy hydrate phase which forms by the hydration of lime by water. If crystallized slowly, as in the hydration of portland cement, it forms large, well developed hexagonal crystals with a typically platy appearance. In the Coolside materials, morphologically well developed portlandite crystals are rare but identification is readily achieved using XRD methods. In the presence of excess water, portlandite reacts with CO_2 to form calcium carbonate.

$$Ca(OH)_2 + CO_2 = CaCO_3 + H_2O$$
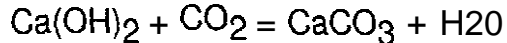
Anhydrite. Anhydrite is a calcium sulfate mineral, $CaSO_4$. Anhydrite occurs in the raw Coolside material as a result of the sulfur removal process. Depending on the temperature of the process, the anhydrite crystals maybe present in a more or less reactive form, distinguishing the soluble and insoluble anhydrite. Upon reaction with water anhydrite is converted to gypsum, $CaSO_4 \cdot 2H_2O$. The transformation is associated with a 60 percent increase in molar volume. The anhydrite crystals do not simply adsorb the water molecules into their structure, thereby forming gypsum. The process involves a dissolution-reprecipitation reaction. Upon dissolution of the anhydrite crystals, Ca and SO_4 ions are liberated. Nucleation and growth of gypsum occurs secondarily.

Gypsum/Hemihydrite. The hydration of anydrite may occur in different steps. The transformation point of gypsum to hemihydrite ($CaSO_4 0.5H_2O$) in water is 97° C, and therefore, the hemihydrite is typically present in temperature cured samples (FBC pellets), rather than in the lysimeters. The hemihydrite occurs as needle-like crystals which can be distinguished from gypsum using XRD application or using SEM based on the pseudo-trigonal symmetry of the needles. Compared to anhydrite, gypsum is much less soluble (at 25° C, 1 atm). For comparison, the equilibrium constants for the anhydrite - gypsum conversion are presented hereof.
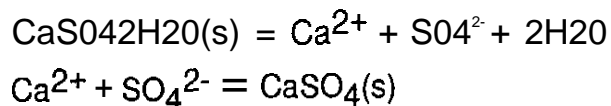
$$CaSO_4 2H_2O(s) = Ca^{2+} + SO_4^{2-} + 2H_2O \qquad Log_{Ks\ gypsum} = -4.60$$
$$Ca^{2+} + SO_4^{2-} = CaSO_4(s) \qquad Log_{Ks\ anhydrite} = +4.38$$
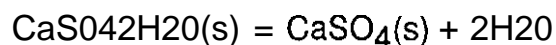
$$CaSO_4 2H_2O(s) = CaSO_4(s) + 2H_2O \qquad Log\ K \qquad = -0.22$$

The gypsum - anhydrite stability fields are temperature dependent. At ordinary temperatures gypsum is more stable compared to anhydrite. Above 42° C anhydrite becomes more stable instead.

Ettringite. Ettringite is both an individual mineral ($Ca_6Al_2(SO_4)_3(OH_{12})$ 26 H_2O), and also a group name for a series of analogous isostructural compounds. Ettringite crystals require a substrate surface to nucleate. They incorporate aluminum from the glass phase, and hydroxyl ions into their lattices, thereby causing portlandite to continue to dissolve. Nucleation occurs on precursor surfaces which need to be enriched in Si, Al, Ca or S. Ideal substrate surfaces in the Coolside materials would be the Si-Al glassy phases, portlandite and anhydrite/gypsum surfaces. Ettringite is commonly observed in the SEM observations to have crystallized on the glassy fly ash spheres. The morphology of the ettringite crystals is that of an elongated hexagonal rod which makes the ettringite appear needle shaped. The needles usually coat the fly ash surfaces giving the impression of spiky billiard balls. The trigonal-hexagonal unit cell of the mineral consists of columns of composition $(Ca_6[Al(OH)_6]_2$ 24 $H_2O)^{6+}$ which are aligned along the crystallographic c-taxis. These columns are accompanied by channels of composition {$(SO_4)_3 2H2^0$}-6. Within that structure the Al ions are octahedrally surrounded by OH ions. The sulfate ion, on the other hand, occurs in tetrahedral orientation. Within the natural and experimental systems, sulfate may be substituted by the sulfite ion. Crystallization of 1 mole of ettringite, theoretically, consumes 6 moles of calcium and 3 moles of sulfate/sulfite while incorporating 26 moles of water.

Calcium Carbonate. Calcium carbonate ($CaCO_3$) precipitates from $Ca(OH)_2$ solution by CO_2. The crystals are typically idiomorphic, which is viewed using SEM applications. Factors that are important in the formation (and dissolution) of calcium carbonate are low supersaturation and poor mechanical agitation. These conditions are preferably present in the field and lab lysimeters. The introduction of atmospheric carbon dioxide into the system could cause portlandite dissolution via the following reactions in which portlandite is a buffer:

$$CO_2 + \mathbf{OH^-} = HCO_3^-$$

$$HCO_3^- = \mathbf{H^+} + CO_3^{2-}$$

$$Ca(OH)_2 = CaOH^+ + OH^-$$

$$CaOH^+ = Ca^{2+} + OH^-$$

Hannebachite. The calcium sulfite hydroxide ($CaSO3.5H2O$) is the major source of sulfite for the formation of ettringite. Hannebachite's volubility causes the $[Ca^{2+}]/[OH^-]$ ratio to increase in the solution. Portlandite which is the most soluble calcium-bearing mineral ($K_{sp}=10^{-5.3}$) continues to dissolve when hannebachite goes into solution ($[Ca^{2+}][SO_3^{2-}] = 10^{-7.0}$; K_{sp} of hannebachite).

Mineralogical Makeup of the "Raw" Coolside Material

The mineralogical composition of the "raw" Coolside material was determined using XRD application. The mineralogical analysis of the bulk "raw" Coolside material indicates the material is composed principally of unreacted $Ca(OH)_2$, crystalline $SiO2$ (quartz), mullite ($A16Si2013$) and x-ray amorphous Al-Si-Fe oxide/hydroxide. No ettringite occurs in the raw mixture. The crystalline sulfate that was identified by XRD was gypsum ($CaSO_4$ $2H2O$) and anhydrite ($CaSO_4$).

Series 1: Field Lysimeter Study

This study comprises the mineralogical findings of the four field lysimeters from the time of sample emplacement (April 1992) till the end of the monitoring period (April 1996). A

summary of the field lysimeter conditions is presented with the results of the corresponding XRD analyses.

The field lysimeters 1-3 contain Coolside material with different degrees of compaction. The changes in mineralogy were monitored as a function of lysimeter depth and compared for lysimeters with different degrees of compaction. At three different time intervals throughout the study, core samples were taken and mineral phases were identified by reference to the JCPDS powder diffraction files. The main objective was to identify how much ettringite and calcium carbonate formed in the lysimeters upon reaction of the Coolside waste with seasonal rain water and to establish a depth profile for the reactions. Ettringite was of importance as it would contribute to the strength development within the materials. Calcium carbonate was studied as a weathering indicator. The drill cores obtained during the first field testing in March of 1994 are summarized first. The profiles of the drill core samples are shown in Figure 2-1. The drill cores, all of which are characterized by a 2" diameter, were taken two feet below the soil interface and extended to four feet depth. Material was collected from the drill cores at two inches apart and subjected to XRD analyses. The results indicated that, independent from the packing densities, the amounts of ettringite present in the core samples increased with increasing lysimeter depth (Figures 2-2; 2-3; 2-4). Ettringite was observed in the SEM study of the materials to have formed both on mineral surfaces and within available pore space (Figure 2-5). The SEM study further indicated that at a greater depth, more pores were infilled by ettringite crystals. The ettringite crystals that formed a dense layer appear more prism-like, while those that nucleated and grew on mineral surfaces and fly ash surfaces were characterized by a more needle-like morphology. These findings suggest that the ettringite morphology may be controlled by the confining pressure (Figure 2-6).

Near the soil interface for all field lysimeters the majority of the mineral transformations could be identified as calcium carbonate reactions. At greater depth, independent of the confining pressure, only very little calcium carbonate was observed in the XRD analyses, suggesting that the migration rates of C02 within the lysimeters is only minor.

DRILL-CORES
Experimental Field Lysimeters
Montgomery County KY

24-26"

2,0-2.5'

2,5- 3.0'

3,0- 3.5'

3,5- 4,0'

L-1

2'0''

2'6''

3'0''

3'6''

L-2A

2'0''

2'6''

3'0''

3'6"

L-2B

2'0''

2'6''

3'0''

L-3
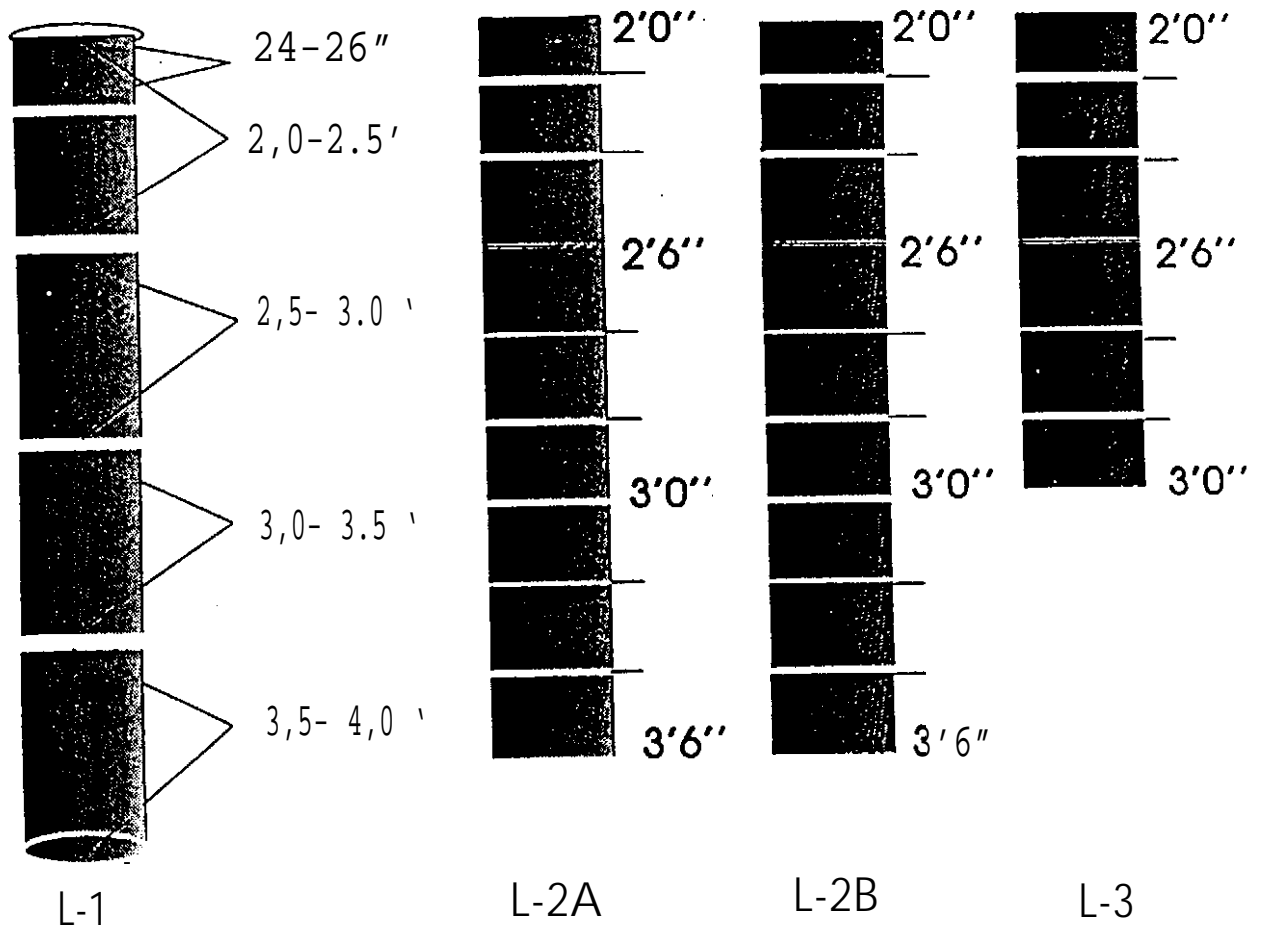
Figure 2-1. Illustrated are drill core profiles for experimental field lysimeters in Montgomery County, KY. L1 represents Lysimeter 1 with the lowest packing density of Coolside material. Samples for XRD analyses were taken at the intervals shown in the figure. Two cores were obtained for Lysimeter 2 which are represented by L-2A and L-2B. The drill core obtained from Lysimeter 3 is represented by L-3 and ranged only to a depth of three feet.

32
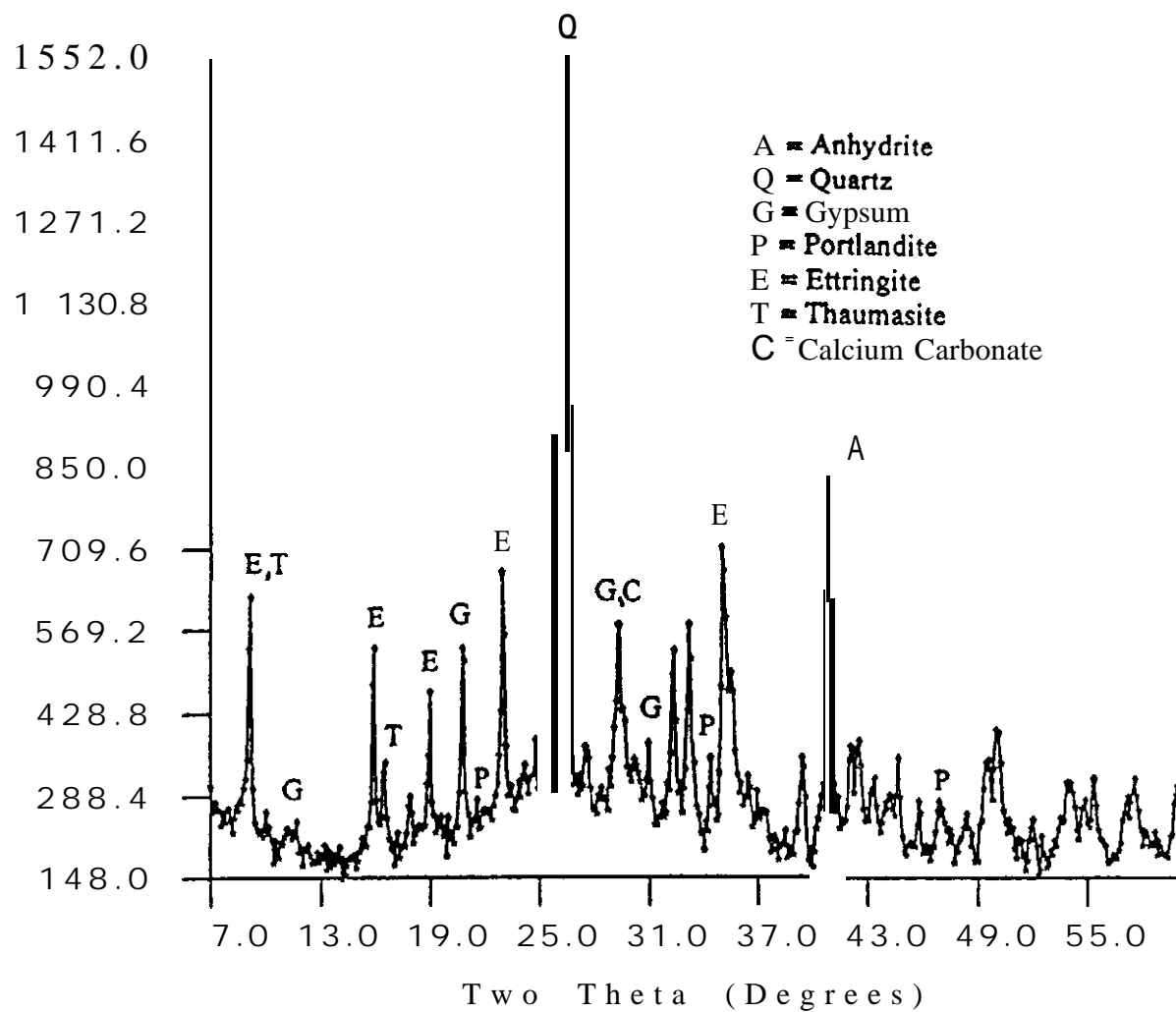
Figure 2-2a. XRD analysis of drill core obtained from Lysimeter 1 at 20-2'2" depth. Major mineral constituents are indicated in the legend and by their corresponding peaks. Ettringite (E) was abundantly present.

Lysimeter 1 3'6''-4'0''

A ≈ Anhydrite
Q = Quartz
G = Gypsum
P = Portlandite
E ≈ Ettringite
T= Thaumasite
C = Calcium Carbonate

Two Theta (Degrees)
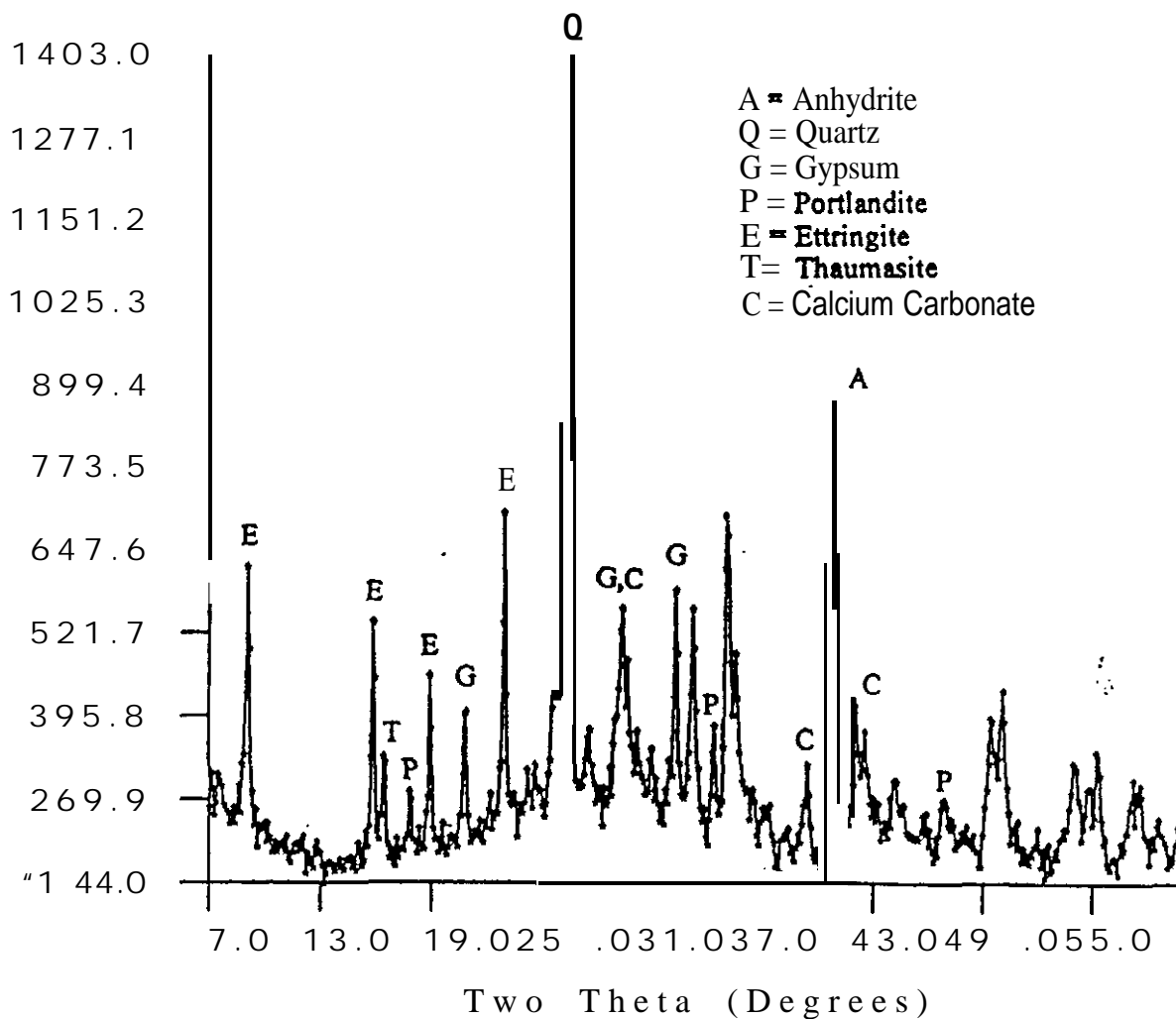
Figure 2-2b. XRD analysis of sample material from same drill core as in 2-2a, but at greater lysimeter depth (36-4'0). Ettringite (E) is abundantly present.

34

Ettringite in Field Lysimeter-1
Depth Profile

■ % Ettringite in L-1 relative to Quartz
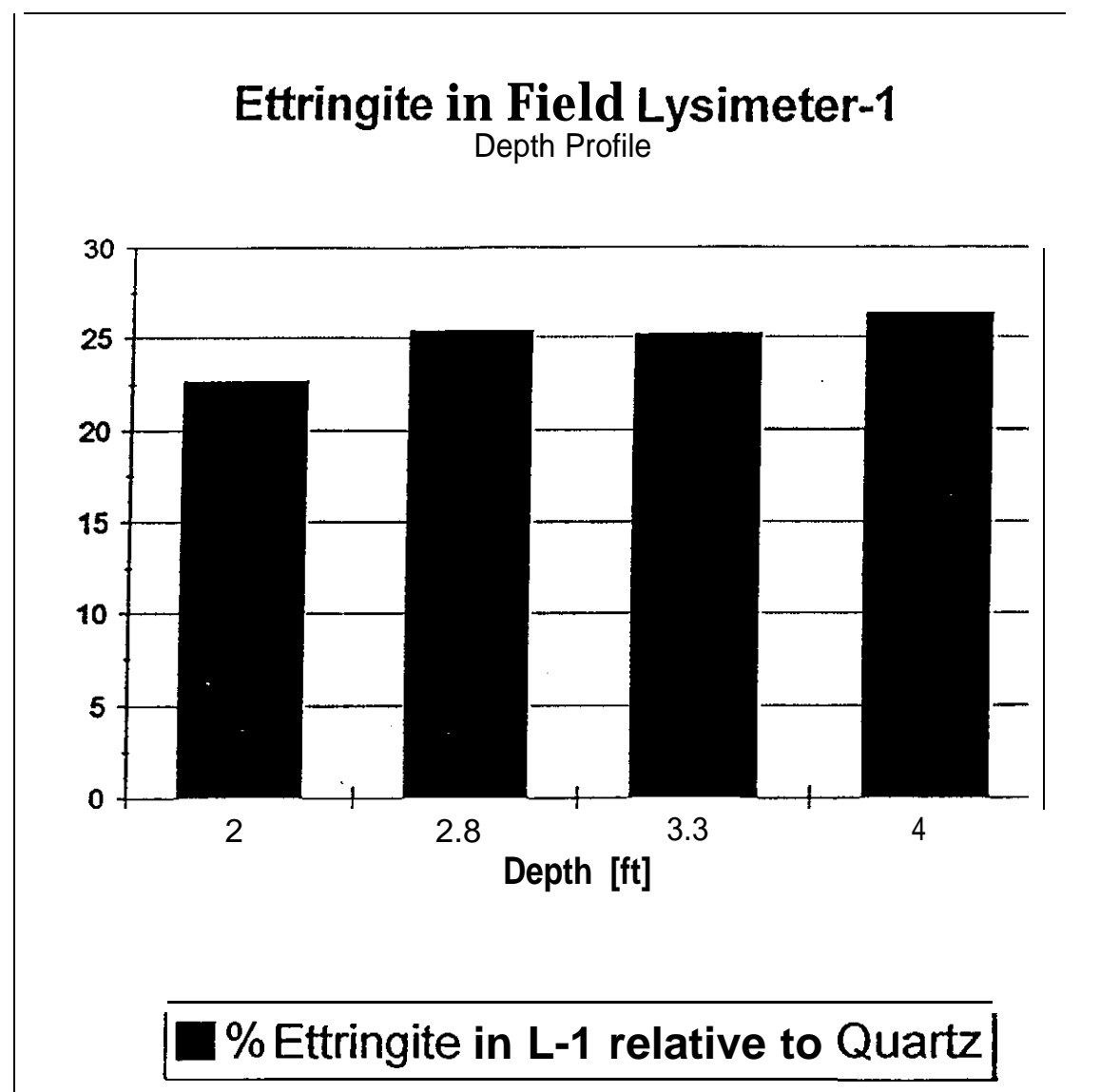
Figure 2-2c. Ettringite abundance relative to Quartz in Field Lysimeter 1 is illustrated for 4 different depth profiles. Ettringite seems to increase with increasing lysimeter depth.
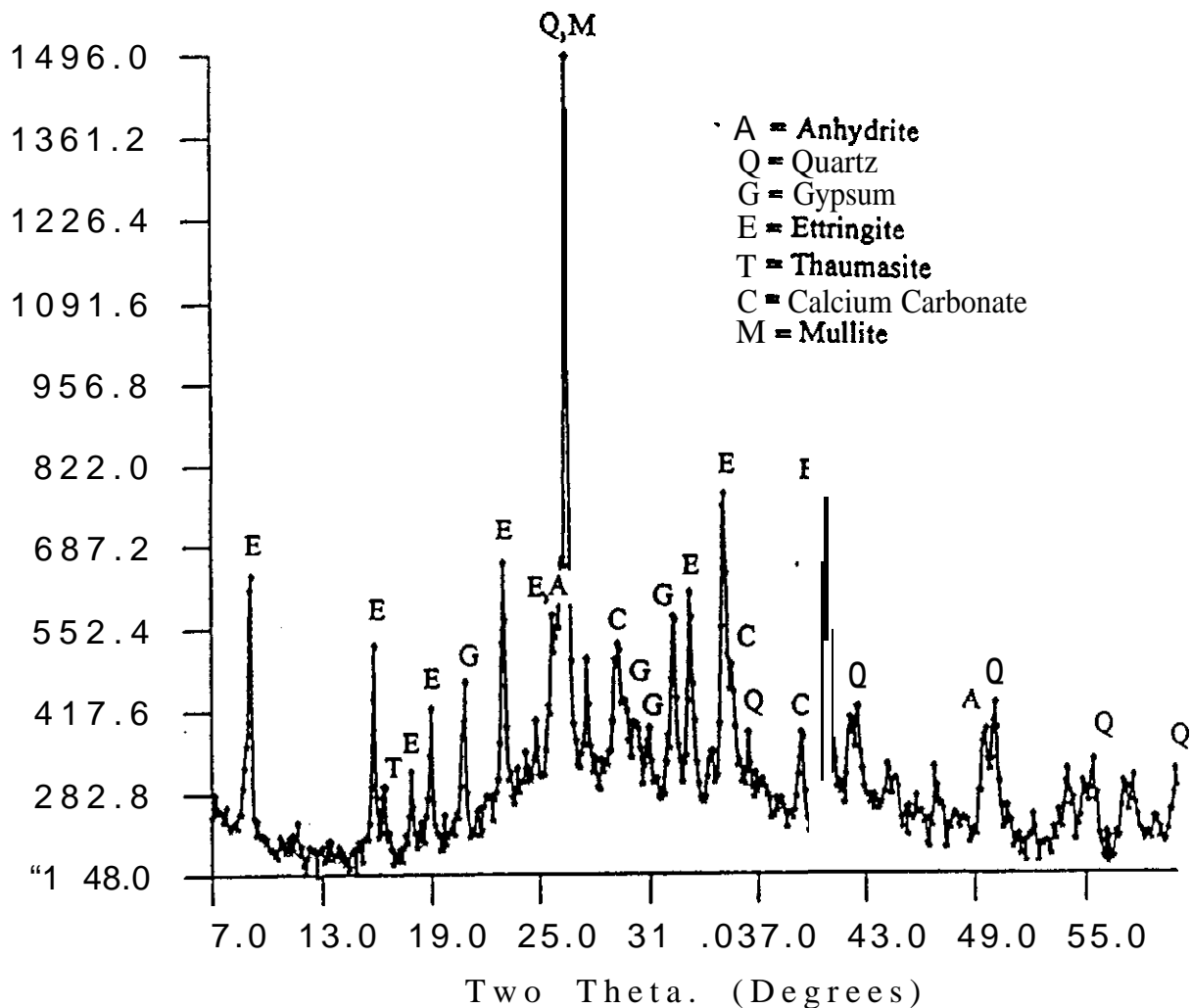
Figure 2-3a. XRDanalyses ofdrill coreobtained from Lysimeter 2Aat2'4 depth. Major mineral constituents are indicated in the legend and by their corresponding peaks. Ettringite (E)was abundantly present.

Lysimeter 2A 3'6"
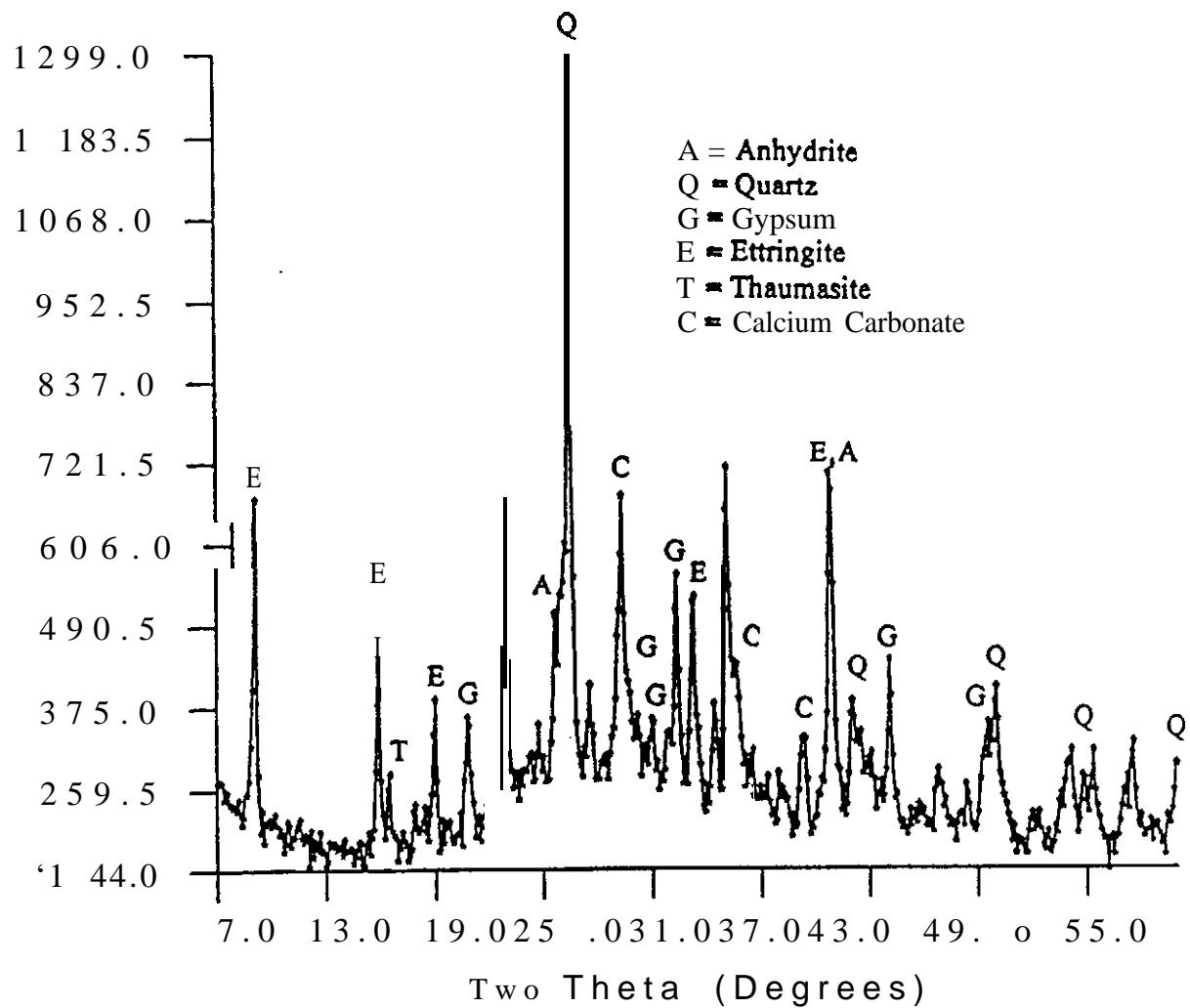
Figure 2-3b. XRD analysis of sample material from same drill core as in 2-3a, but at greater lysimeter depth (3'6). Ettringite (E) is abundantly present.

37

Ettringite in Lysimeter-2A
Depth Profile
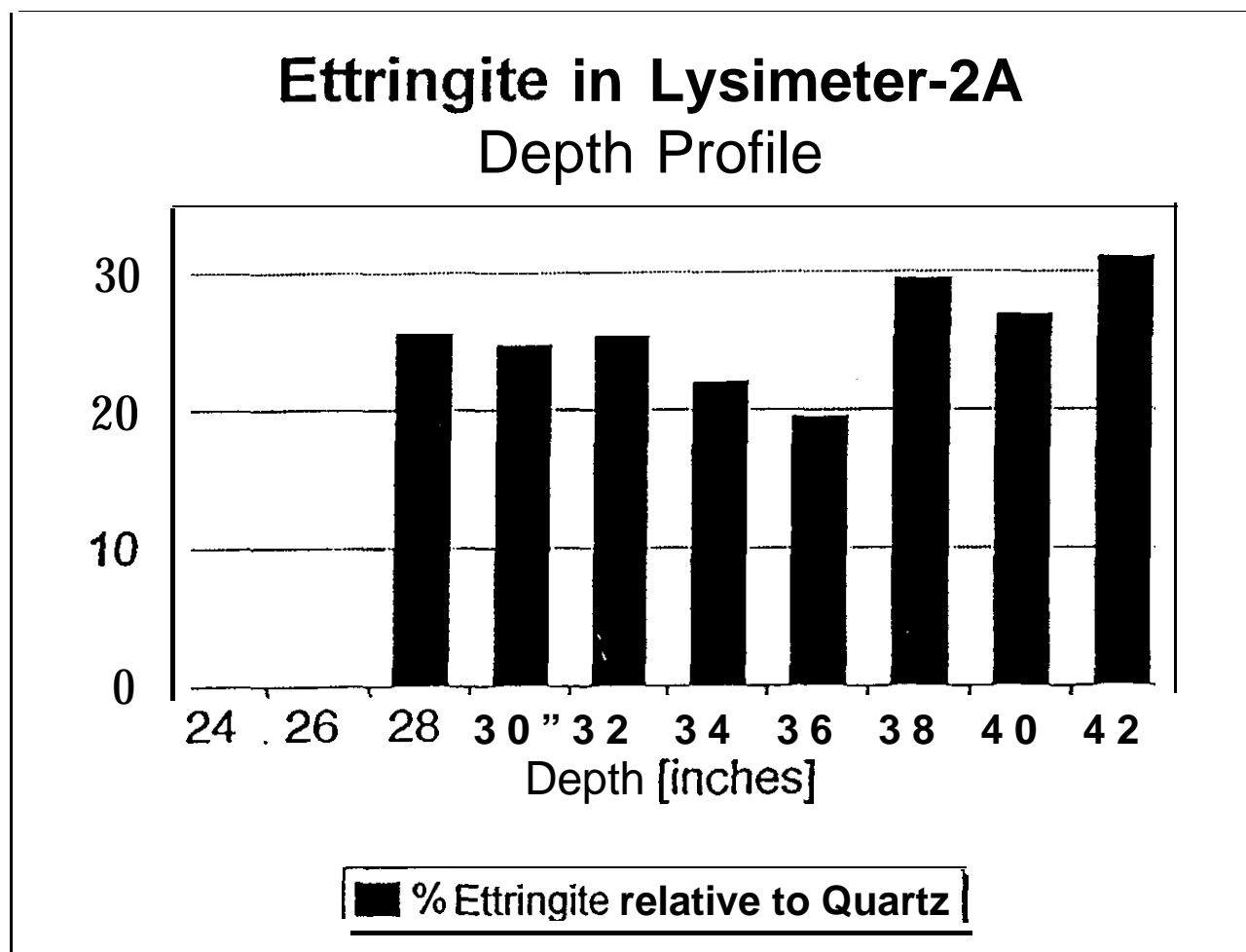
Figure 2-3c. Ettringite abundance relative to quartz in Field Lysimeter 2A is illustrated for 8 different depth profiles. Ettringite abundance fluctuates with increasing lysimeter depth.
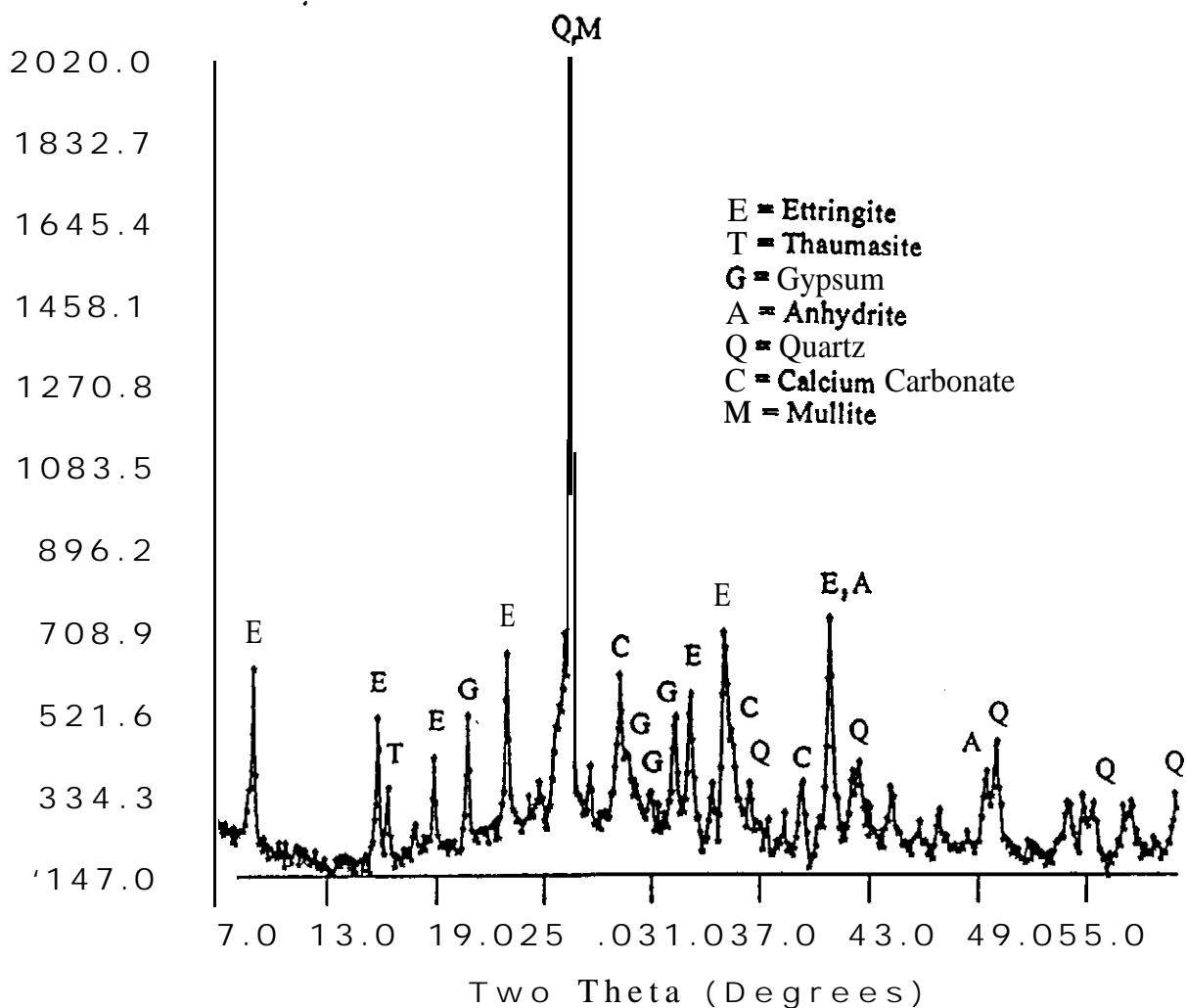
Figure 2-4a. XRD analyses of drill core obtained from Lysimeter 3 at 20" depth. Major mineral constituents are indicated in the legend and by their corresponding peaks. Ettringite (E) was abundantly present.

Lysimeter3 3'0"

E = Ettringite
T = Thaumasite
G = Gypsum
A = Anhydrite
Q = Quartz
C = Calcium Carbonate
M = Mullite

Two Theto (Degrees)
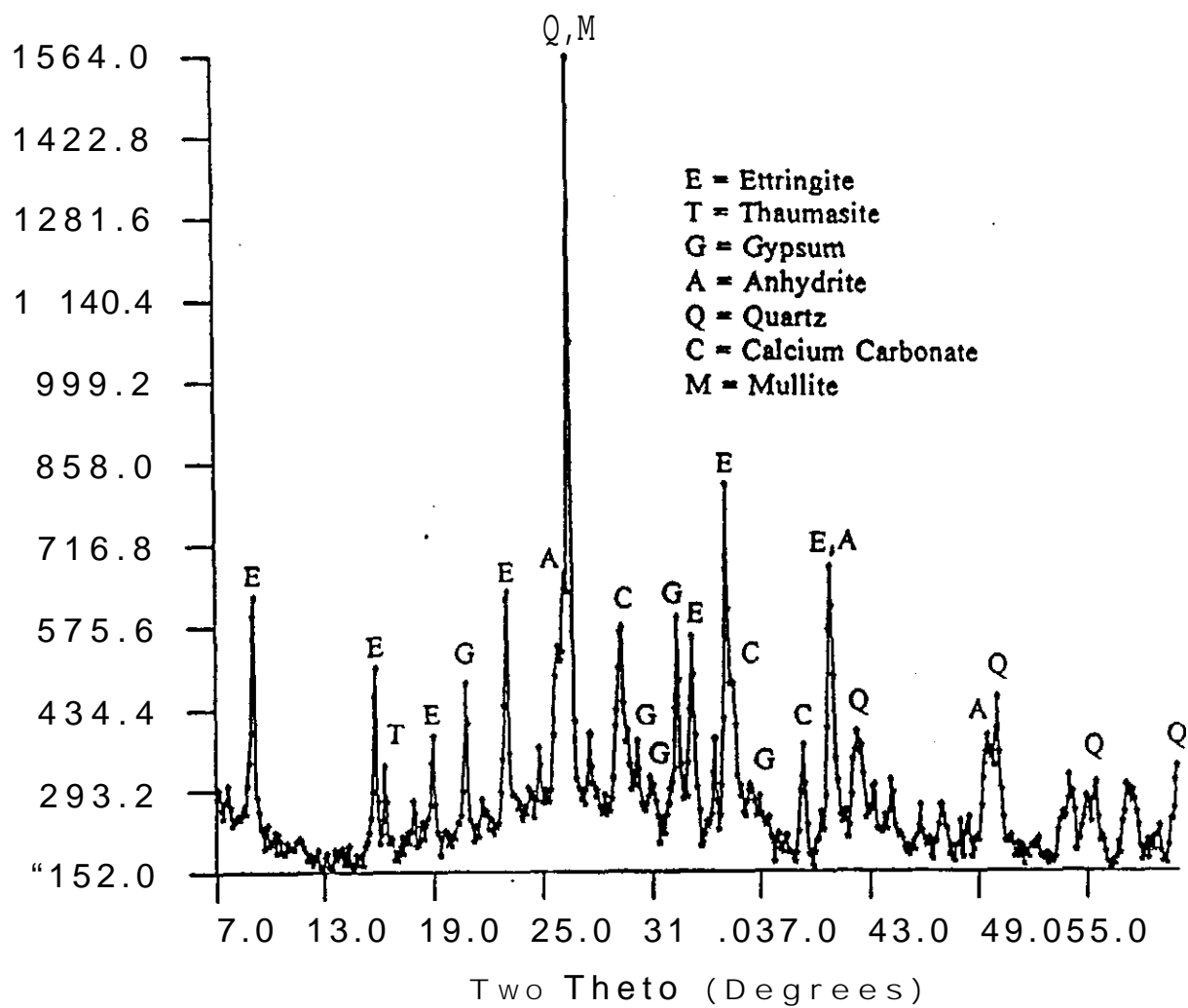
Figure 2-4b. XRD analysis of sample material from same drill core as in 2-4a, but at greater lysimeter depth (3'0"). Ettringite (E)is abundantly present.

Ettringite in Field Lysimeter L-3
Depth Profile

% Ettringite in L-3 rel. to Quartz
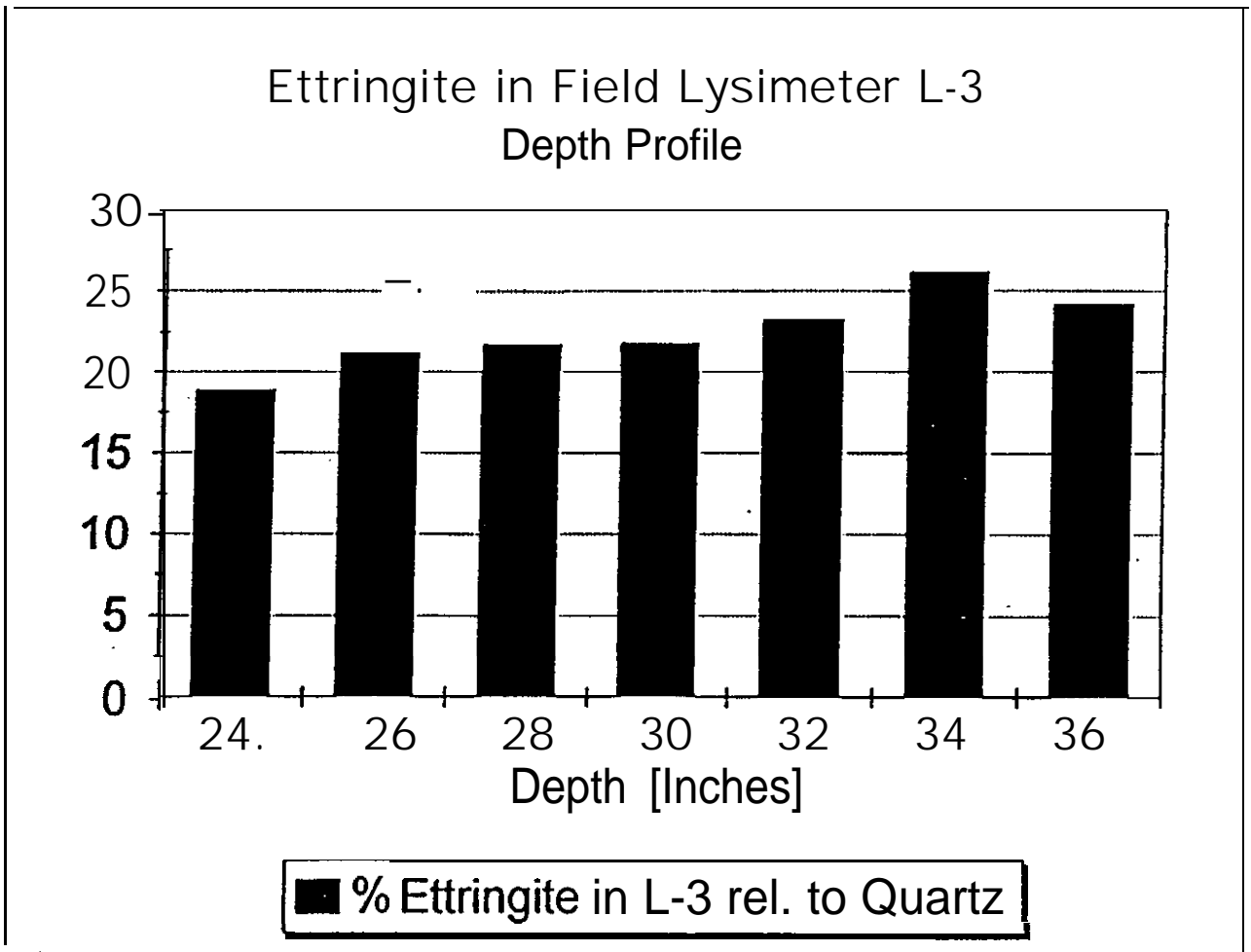
Figure 2-4c. Ettringite abundance relative to quartz in Field Lysimeter 3 is illustrated for 7 different depth profiles. Ettringite abundance appears to increase with increasing lysimeter depth with minor fluctuations at the bottom of the core.
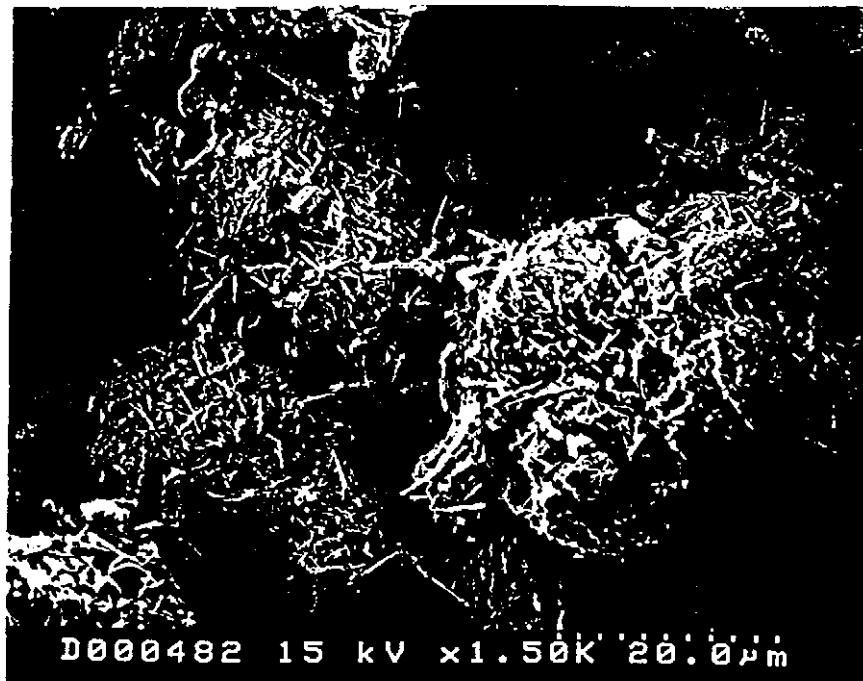
Figure 2-5a. Illustration of ettringite needles overgrowing fly ash surfaces. The ettringite needles form a network of interlinking crystals. Pore space has not yet been infilled by crystal growth.

Figure 2-5b. Dense crystal growth of ettringite needles with only minimal pore space.

42

Figure 2-6. SEM illustration of platy ettringite crystals inside the densely packed Lysimeter 3.

A continuation of the field lysimeter tests occurred during the report period of October 1, 1995- October 31, 1995. Additional data obtained during this sampling period supported earlier results and indicated that mineralogical transformations of the Coolside materials continued in the lysimeters as a function of available moisture, aging and static loading. Ettringite was observed to continue to be the dominant product in all lysimeters (1-3) packed with the Coolside material (Figure 2-7; 2-8; 2-9). Lysimeter 1 with the least compaction showed a recognizable difference in ettringite abundance from top to bottom of the drill cores. Ettringite needles were more abundant in the lower zones (Figure 2-7). In comparison the more densly packed Lysimeters 2 and 3 did not have distinguishable differences in ettringite abundance within the top, middle and bottom zones of the drill cores (Figure 2-8; 2-9). Trends in gypsum availability within the lysimeters suggest that a rapid leaching of gypsum must have taken place at all layers of the lysimeter cores (Figures 2-7; 2-8; 2-9). It is expected that gypsum continues to be present in the deeper zones that were out of reach during drilling.

In lysimeters with higher degrees of static loading (static loading increases in the order of Lysimeter 1 to 3), minerals are forced to grow within available pore space. This minimizes perk and causes leaching rates to slow down. Leaching rates, in turn, control the dissolution/reprecipitation of minerals in the lysimeter zones. Calcium carbonate is a mobile phase and its presence strongly depends on the perk within the systems. Calcium carbonate is enriched in the top layer within the drill core taken from Lysimeter 1 and less abundant in the deeper zones (Figure 2-7). In the denser packed lysimeters (2 and 3), the calcium carbonate abundance was approximately the same for the top, middle and bottom zones of the drill cores obtained (Figure 2-8; 2-9).

The mineralogy obtained during XRD analyses of the second set of drill cores was summarized as follows:

44

Loose compaction in Lysimeter 1 (33 lb/f^3) corresponds to an overall increase in ettringite abundance with lysimeter depth (Figure 2-7) and a significant calcium carbonate enrichment in the top zone.

A compaction of 41 lb/f^3 in Lysimeter 2 corresponds to a minor increase in ettringite abundance with increasing lysimeter depth. Calcium carbonate is preferentially present at the top zone, but the variation with increasing lysimeter depth is less pronounced compared to the loosely packed Lysimeter 1 (Figure 2-8).

This study observed only a minor variation in ettringite and calcium carbonate abundance with increasing depth in Lysimeter 3 with the highest compaction of 66 lb/f^3 (Figure 2-9).

Because the Lysimeter 4 (reference lysimeter) with fly ash has no calcium that could react with C02, the XRD analyses revealed no calcium carbonate or ettringite (Figure 2-1 O).

The results suggest, that mineral growth is strongly controlled by the perk of the solutions downwards. The high degree of compaction restricted perk in Lysimeter 3 and minimized mineral transformations. The depletion of ettringite in the upper zone of the least compacted Lysimeter 1 in conjunction with a calcium carbonate enrichment may be caused by rapid leaching and ion migration through large void spaces and channel ways. Ion migration causes depletion in the upper lysimeter zone of Al and S04. As a result, ettringite becomes more soluble and starts to disintegrate. Recarbonization (formation of calcium carbonate) occurs in areas with high pCO_2 and lower pH regimes. Fluctuations in pH are governed by the influx of rain water. Because calcium hydroxyhydrate is only a minor constituent in the aged lysimeters and gypsum almost entirely restricted to the lower lysimeter zones, ettringite becomes the dominant calcium bearing mineral phase. When dissolved C02 is mixed into the lysimeter zones by means of incoming rain water, the pH drops below the stability of ettringite crystals and calcium carbonate forms by reaction with Ca ions that are provided in the dissolution of ettringite needles. In contrast to the loosely
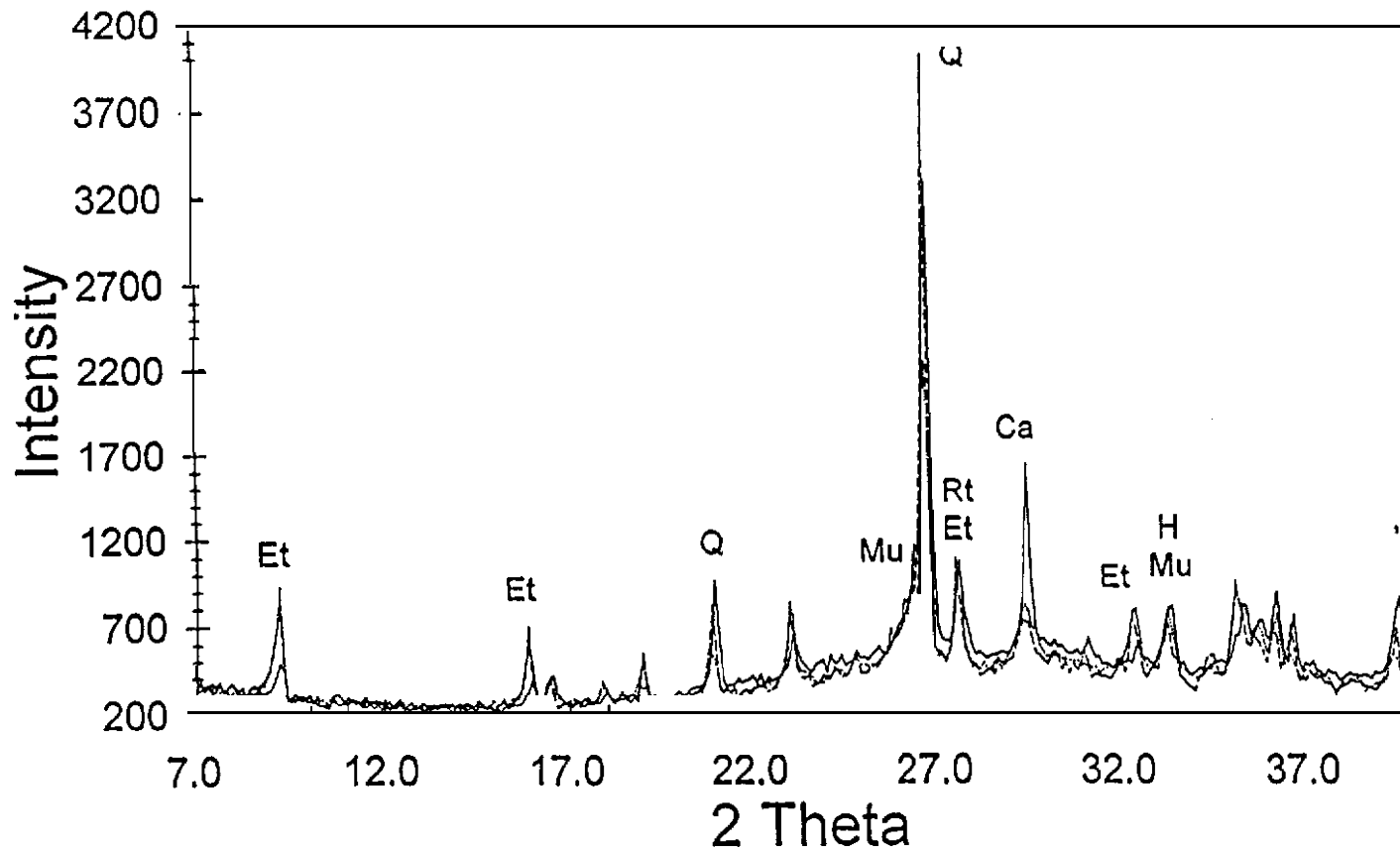
Figure 2-7. XRD analysis of Coolside material from Lysimeter 1 after second drilling. Figure includes data for samples from 3" (top), 6-8", and 18" depths. (Et = ettringite; Q = quartz; Mu = mullite; Rt = rutile (internal standard); Ca = calcium carbonate; H = hematite). Ettringite is abundantly present in the sample.

Lysimeter #2

Figure 2-8. XRD analysis of Coolside material from Lysimeter 2 after second drilling. Figure includes data for samples from 3" (top), 6-8", and 16-18" depths. (Et = ettringite Q = quartz; Mu = mullite; Rt = rutile (internal standard); Ca = calcium carbonate; H = hematite). Ettringite is present in all three layers of the core.
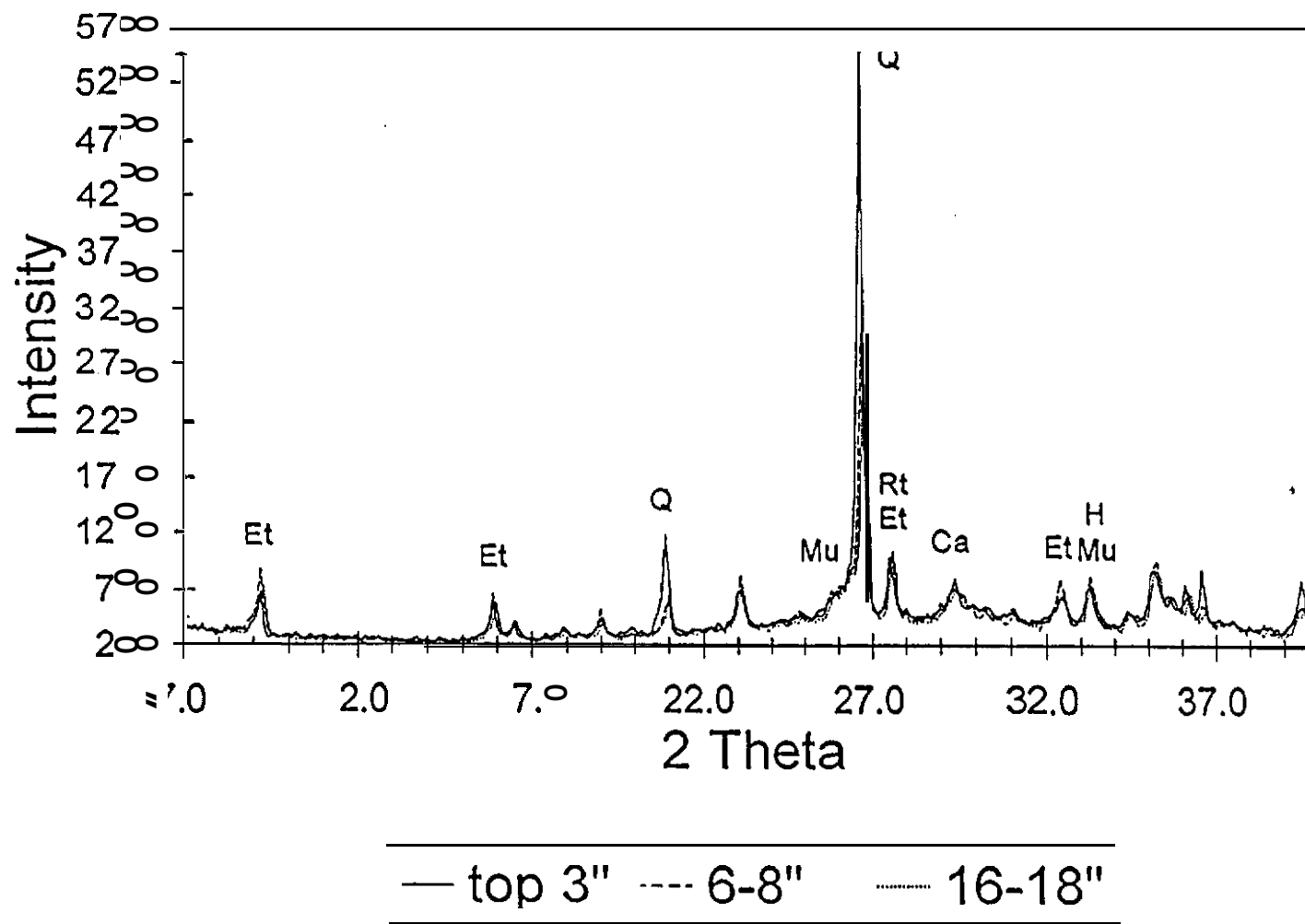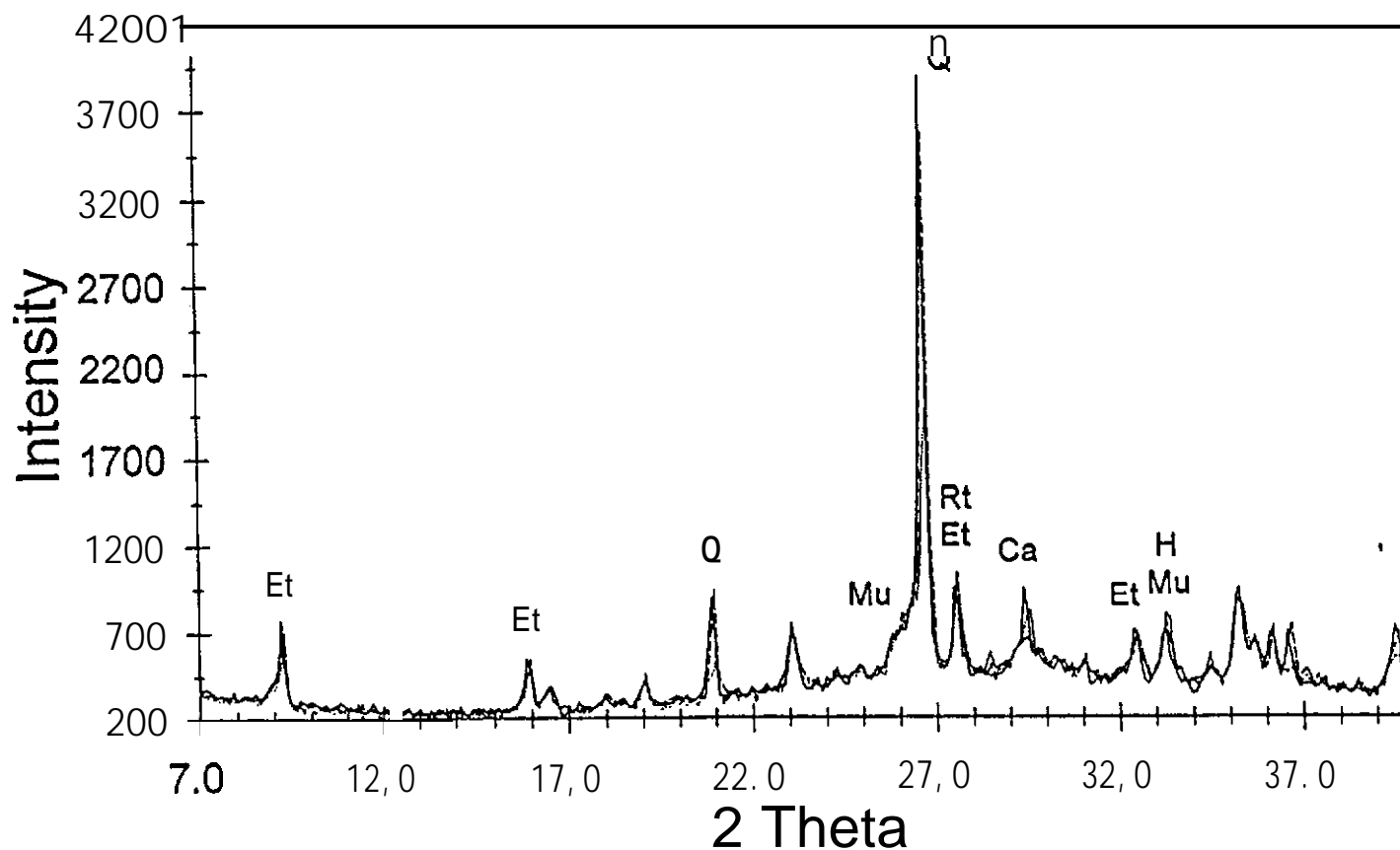
Figure 2-9. XRD analysis of Coolside material from Lysimeter 3 after second drilling. Figure includes data for samples from 3 (top), 6-8, and 18 depth. (Et= ettringite; Q = quartz; Mu = mullite; Rt = rutile (internal standard); Ca = calcium carbonate; H = hematite). Ettringite abundance is identical for the three layers.
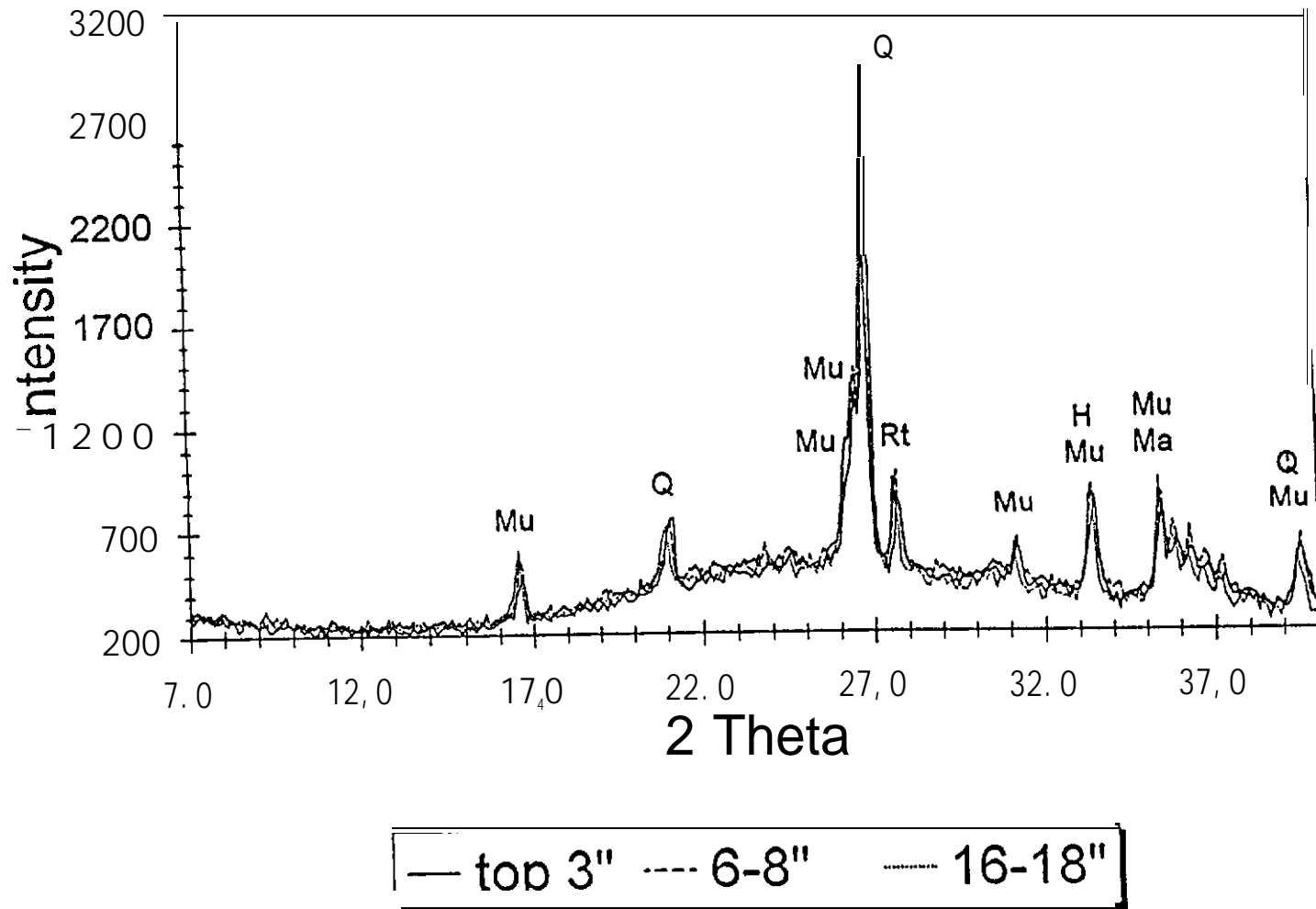
Figure 2-10. XRD analysis of material from the reference Lysimeter 4.

compacted Lysimeter 1, Lysimeters 2 and 3 show minor or no increase in ettringite abundance with lysimeter depth. These findings are in accordance with the earlier suggested mechanism of ion migration by slower flowing fluids through more densly packed lysimeters. The longer residence times of the fluids in voids may lead to mineral precipitation which further enhances the compaction and density of the lysimeters, thereby reducing the mineral migration rates even more.

The third and final core sampling of the field lysimeters occurred in April of 1996. XRD analyses of the cored materials indicated that mineralogical transformations continued in the field lysimeters as a function of available moisture, aging and static loading of the Coolside materials. As indicated in the introduction, one of the major objectives of the Coolside study was to investigate the formation and transformation of minerals during long-term exposure. Throughout the testing period ettringite, gypsum and calcium carbonate are the dominant phases in Lysimeters 1-3, but their abundances vary with time. The XRD results for the final Coolside field samples obtained during the most recently taken lysimeter cores are summarized in Figures 2-11 and 2-12. Results indicate that the ettringite which was still abundantly present in the earlier cores, now is completely leached from the top, middle and bottom parts of the cores. Similar trends are observed for the gypsum distribution within the lysimeters. Calcium carbonate is now the most prominent phase and is present throughout all core samples and in all depth profiles. Within instrumental errors, no differences were observed for Lysimeters 1 and 2. Lysimeter 3 was cored, but only one mixed sample rather than top, middle and bottom samples was available due to difficulties during drilling.

The mineralogical observations indicate that in Lysimeters 1 and 2 essentially all of the sulfate-bearing phases, including ettringite and gypsum had been dissolved out, The XRD pattern for Lysimeter 1 with the least compaction showed no differences for the top, middle and bottom zones. The same results were obtained for the Lysimeter 2 with higher compaction of the Coolside materials. Mullite, quartz, calcium carbonate and hematite are the minerals that correspond to the XRD peaks in Figures 2-11 and 2-12 for all zones of
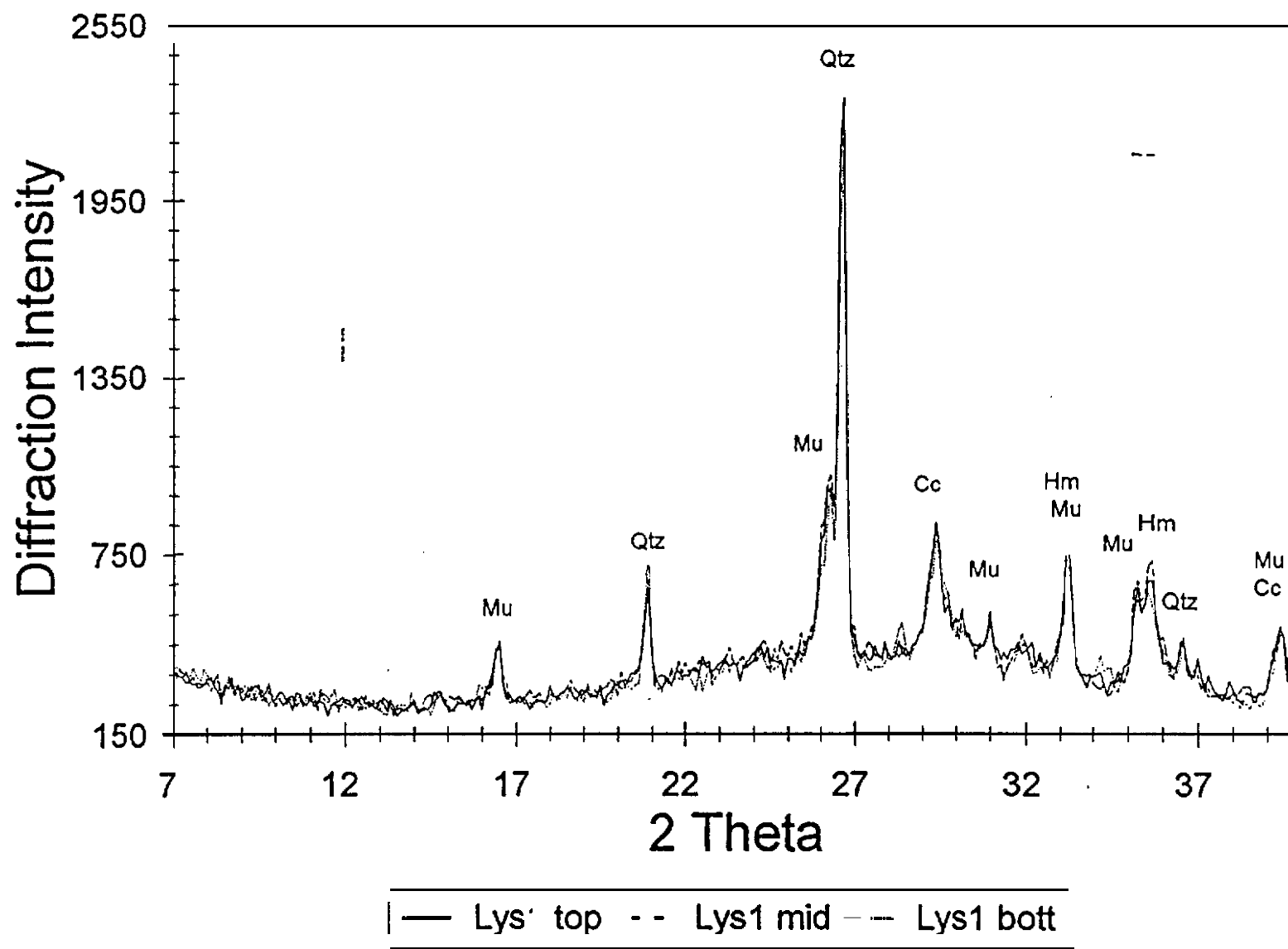
Figure 2-1 . XRD analysis of final drilling material obtained from Lysimeter 1.
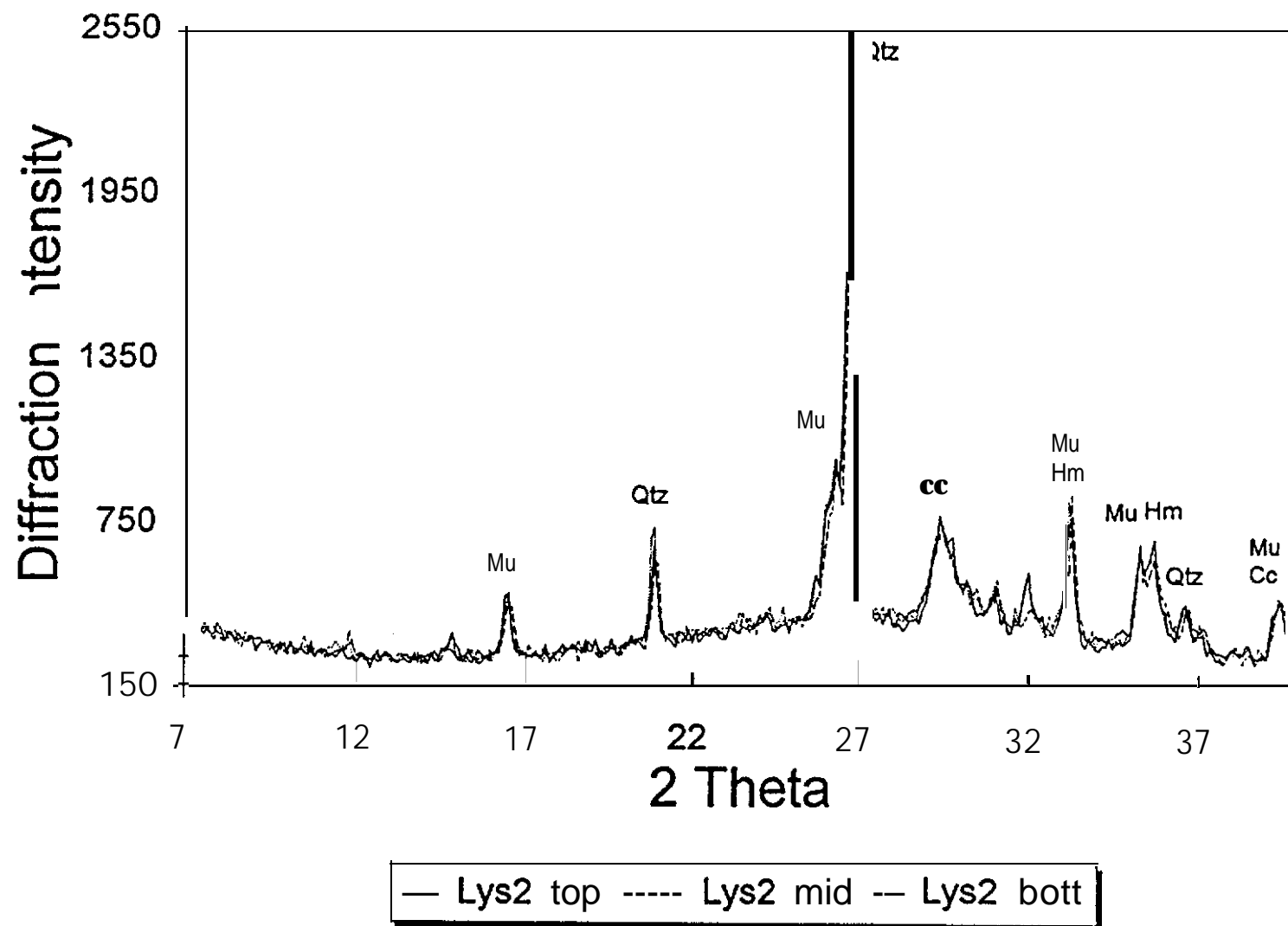
Figure 2-12. XRD analysis of final drilling material obtained from Lysimeter 2.

the Lysimeters 1 and 2. Differences in packing densities affected mineralogical changes while leaching progressed. When the final drilling was performed, leaching in Lysimeters 1 and 2 had progressed to what may be considered a steady state mineral composition. Minerals include those with very low solubilities such as quartz and mullite. Calcium carbonate, which is less soluble than gypsum under the conditions in the lysimeters, formed at the expense of gypsum and ettringite. The decrease in sulfate concentration in the lysimeters is concomitant with an increase in carbonate concentration. Although ettringite was found to be relatively stable within the weathering lysimeter zones as indicated by the results of the second drill core analyses, long-term leaching causes ettringite disintegration and massive recarbonization.

Series II: Laboratory Lysimeter Study

The laboratory lysimeter study was aimed at investigating the elemental release characteristics of the Coolside materials. A preliminary study using a variety of lysimeter conditions, packing densities, and fluid throughput, set the stage for the final testing phase. Although the earlier study supplied information on mineral transformations and dissolution patterns, particluarly the early formation of ettringite throughout the lysimeter columns, the leaching rates were extremely slow in the compacted columns and, therefore, leaching characteristics did not resemble closely enough the flow patterns in the field lysimeters where incoming seasonal rainwater was briskly transported to lower lysimeter zones.

The final testing phase is described in detail in Chapter IV: Laboratory-Lysimeter Studies. This section of the Coolside study focuses on the mineralogical changes within the top, middle and bottom zones of the laboratory lysimeters to better understand the effects of fluid migration on new mineral growth.

The laboratory columns that were sampled for the XRD study of the aged Coolside material are listed in Table 2-1. A discussion of the lysimeter characteristics is presented in great detail in Chapter IV.

Table 2-1

SAMPLE ID	RUN #	% CO_2	MOISTURE	COMPACTION	XRD Analyses
LC1	CS Run #3	o %	Fixed Feed	Loose	Figure 2-13
LC2	CS Run #3	2.5 %	Fixed Feed	Loose	Figure 2-14
LC3	CS Run #3	070	Rain Simulation	Loose	Figure 2-15
LC4	CS Run #3	2.5 %	Rain Simulation	Loose	Figure 2-16
LC5	CS Run #3	o %	Fixed Feed	Proctor	Figure 2-17
LC6	CS Run #3	2.5 %	Fixed Feed	Proctor	Figure 2-18
LC7	1000 Series	2.570	Fixed Feed	Loose	Figure 2-19
LC8	CS Run #1	2.5 %	Fixed Feed	Loose	Figure 2-20

A comparison of the XRD analyses of top, middle and bottom samples from LCI with O % C02, fixed feed and loose compaction (Figure 2-13) showed no significant differences for any minerals within the aged materials. In contrast, samples obtained from LC2 with 2.5 % C02 addition had removed ettringite from the top layer, enriched gypsum in the middle zone and formed significant amounts of calcium carbonate in all layers, with the top layer showing the highest concentration (Figure 2-1 4),

A comparison of the XRD data for Coolside Run #3 with rain simulation for samples LC3 which had loose compaction and O % C02 indicates that ettringite abundance increased downwards in the column lysimeter while gypsum appeared to be preferentially present in the top zone of the lysimeter (Figure 2-15). Calcium carbonate was predominantly observed in the top layer, suggesting C02 uptake from the atmosphere.

Figure 2-13. XRD analysis of Coolside Run #3 after 0% C02 was added to a fixed feed through the loose compacted Column LC1. The ettringite peak is present at the top, middle and bottom samples (9.2 2 theta).

Figure 2-14. XRD analysis of Coolside Run #3 after 2.5% C02 was added to a fixed feed through the loose compacted Column LC2. The ettringite peak is present at the bottom sample (9.2 2 theta).

LC3; CS Run#3; 0% C02
Rain Simulation; Loose Compaction

Figure 2-15. XRD analysis of Coolside Run #3 after O% C02 was added to a rain simulation through the loose compacted Column LC3. The ettringite peak is present at the top, middle and bottom samples (9.2 2 theta) and is most prominent at the bottom layer.

Sample LC4, which had the same conditions as LC3 with the exception of a 2.5 % addition of C02 indicated minor differences in the XRD patterns obtained. Addition of C02 caused ettringite in the top layer to be completely removed. The amount of gypsum in all zones of LC4 was significantly less in the sample without C02 addition (Figure 2-16).

Samples with proctor rather than loose compaction for the Coolside Run #3 material showed no recognizable differences for the materials that had O % (LC5; Figure 2-17) or 2.5 % (LC6; Figure 2-18) C02 additions. A comparison of the top, middle and bottom zones for both columns LC5 and LC6 suggest that ettringite was not removed from the top layer as was the case for all loosely compacted columns. Gypsum was absent from all layers in both LC5 and LC6 columns. The relative amounts of calcium carbonate in the compacted columns did not vary significantly for top, middle and bottom zones.

Coolside material from the 1000 Series was placed in column LC7 using 2.5% C02 additions, fixed feed and loose compaction. A comparison of the XRD results for top, middle and bottom zones for LC7 indicated that ettringite had been removed from the top layer while calcium carbonate was preferentially enriched in the top layer (Figure 2-19).

Cooside material from Run #1 was placed in column LC8 using 2.5% C02 additions, fixed feed and loose compaction. The most striking variation in mineral composition between top, middle and bottom zones was the presence of gypsum in the top layer of the column while no gypsum was recognized in the XRD patterns for either middle or bottom zones of LC8 (Figure 2-20). Calcium carbonate was preferentially present in the top zone which is similar in all columns that had additions of CO_2.

Series Ill: Kinetic Study

In order to gain a better understanding of the mineralogical transformations that occur during hydration of the Coolside FGD material, a laboratory study was completed in which the material was submerged in distilled water, within a sealed container, and the crystalline

LC4; CS Run#3; 2. 5% CO2
Rain Simulation; Loose Compaction
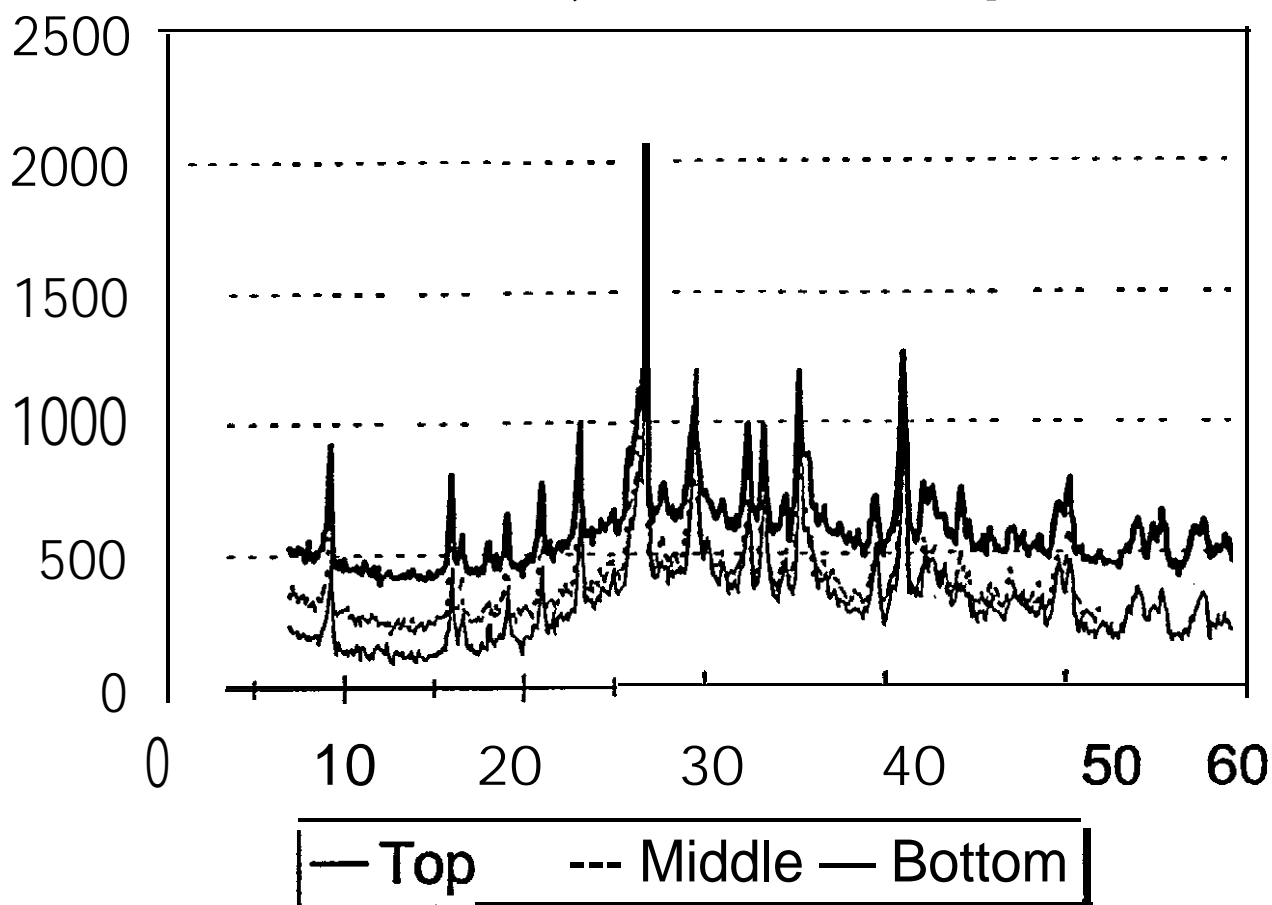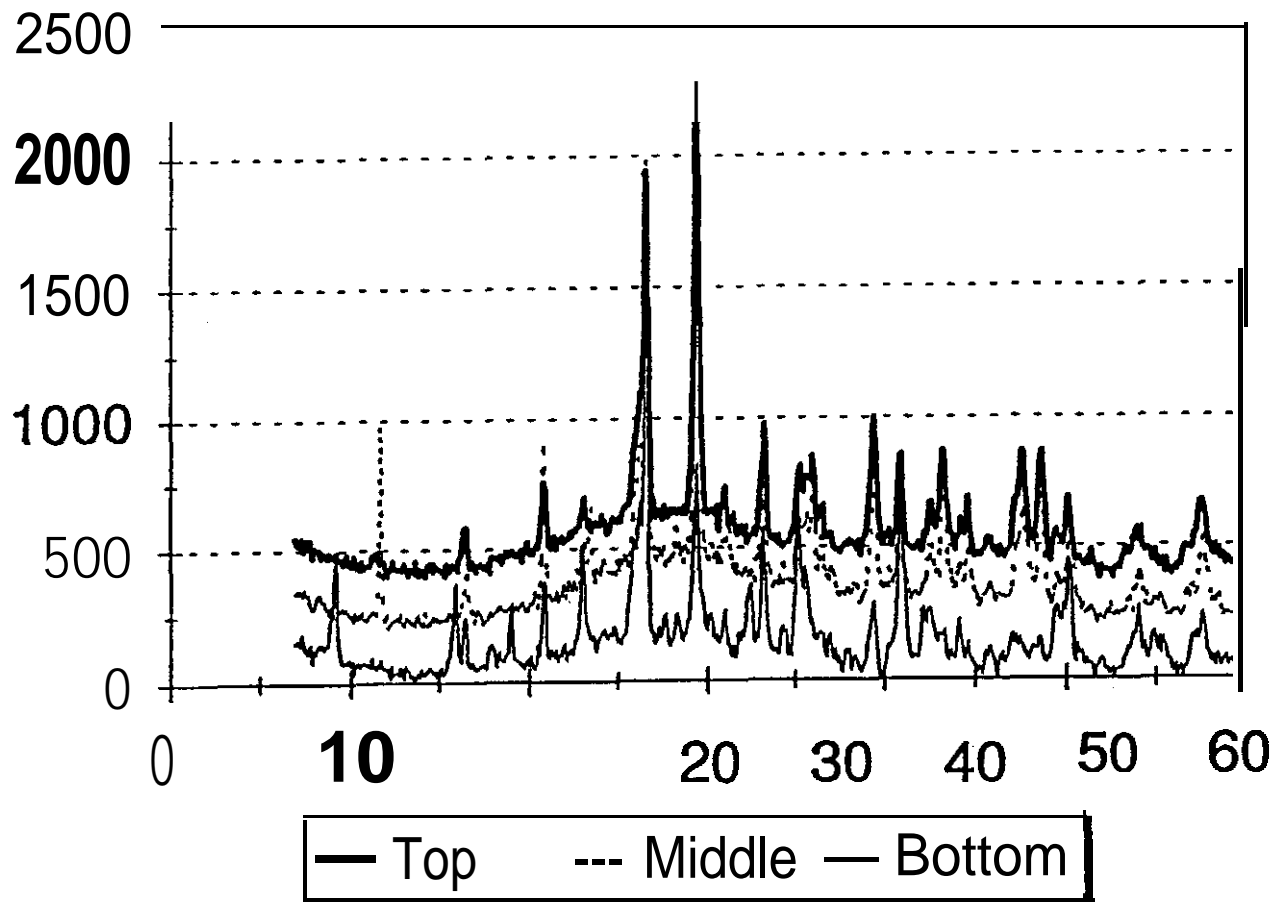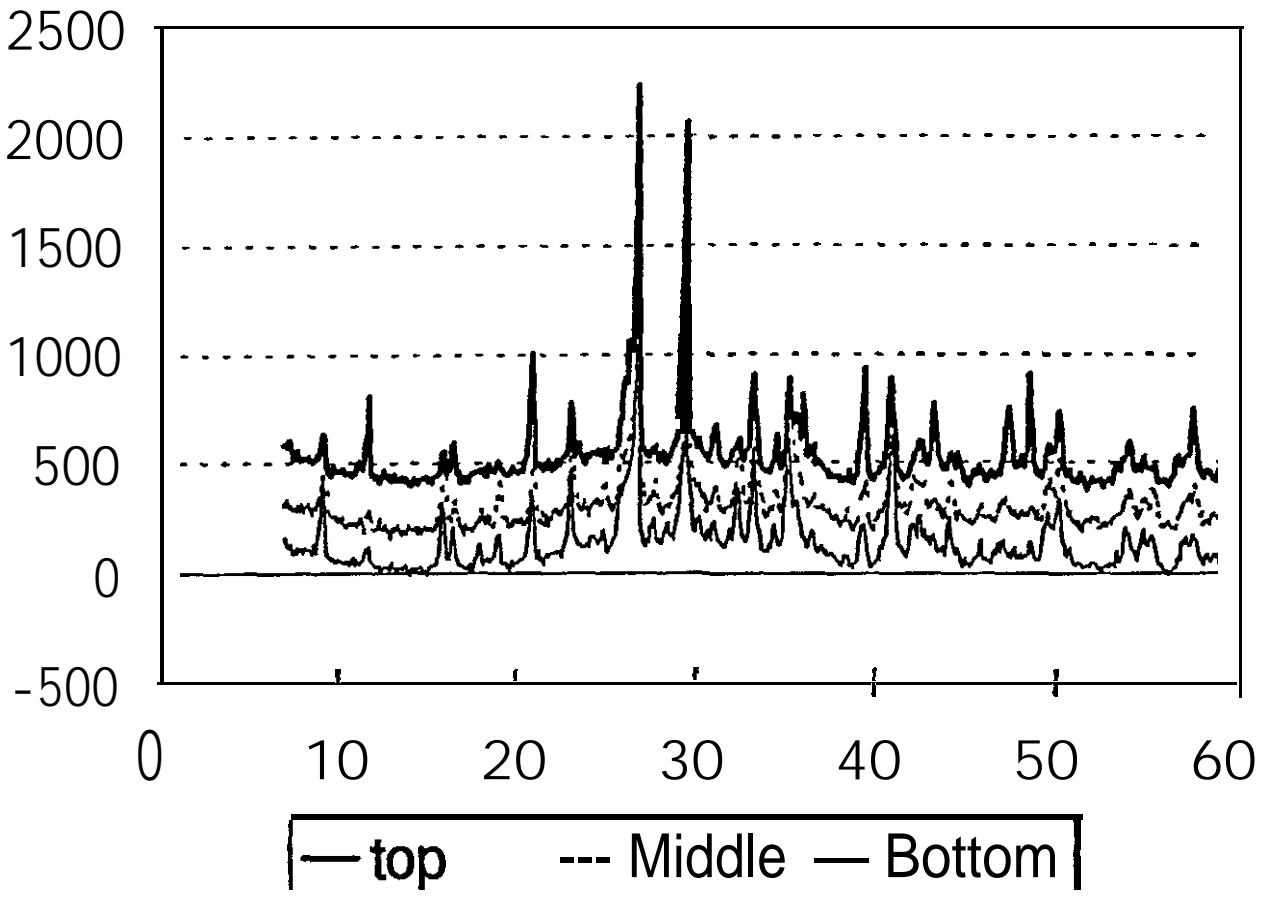
— top   - - - Middle — Bottom
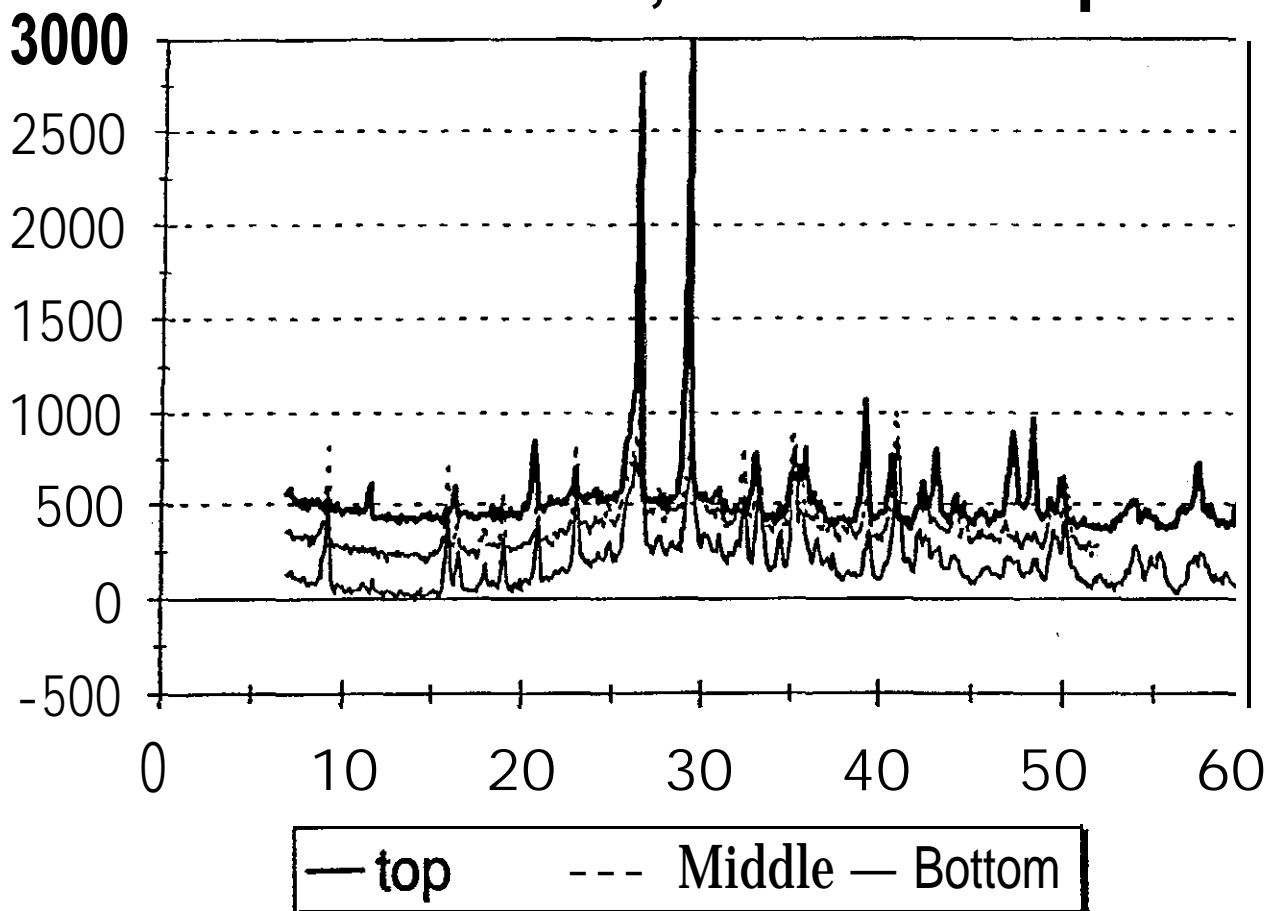
Figure 2-16. XRD analysis of Coolside Run #3 after 2.5% C02 was added to a rain simulation through the loose compacted Column LC4. The ettringite peak is present at the middle and bottom samples (9.2 2 theta), but was more intense for the bottom layer.

LC5; CS Run#3; 0% CO2
Fixed Feed; Proctor Compaction

Figure 2-17. XRD analysis of Coolside Run #3 after 0% C02 was added to a fixed feed through the proctor compacted Column LC5. The ettringite peak is present at the top, middle and bottom samples (9.2 2 theta) at very similar intensities.

Figure 2-18. XRD analysis of Coolside Run #3 after 2.5% C02 was added to a fixed feed through the proctor compacted Column LC6. The ettringite peak is present at the top, middle and bottom samples (9.2 2 theta) at very similar intensities.

LC7; 1000 SERIES; 2.5% C02
Fixed feed; Loose Compaction

— Top   --- Middle   — Bottom --- Drk Bnd

Figure 2-19. XRD analysis of Coolside 1000 Series after 2.5% C02 was added to a fixed feed through the loose compacted Column LC7. The ettringite peak is present at the top, middle and bottom samples (9.2 2 theta).

LC8; CS Run#I; 2.5% CO2
Fixed feed; Loose Compaction

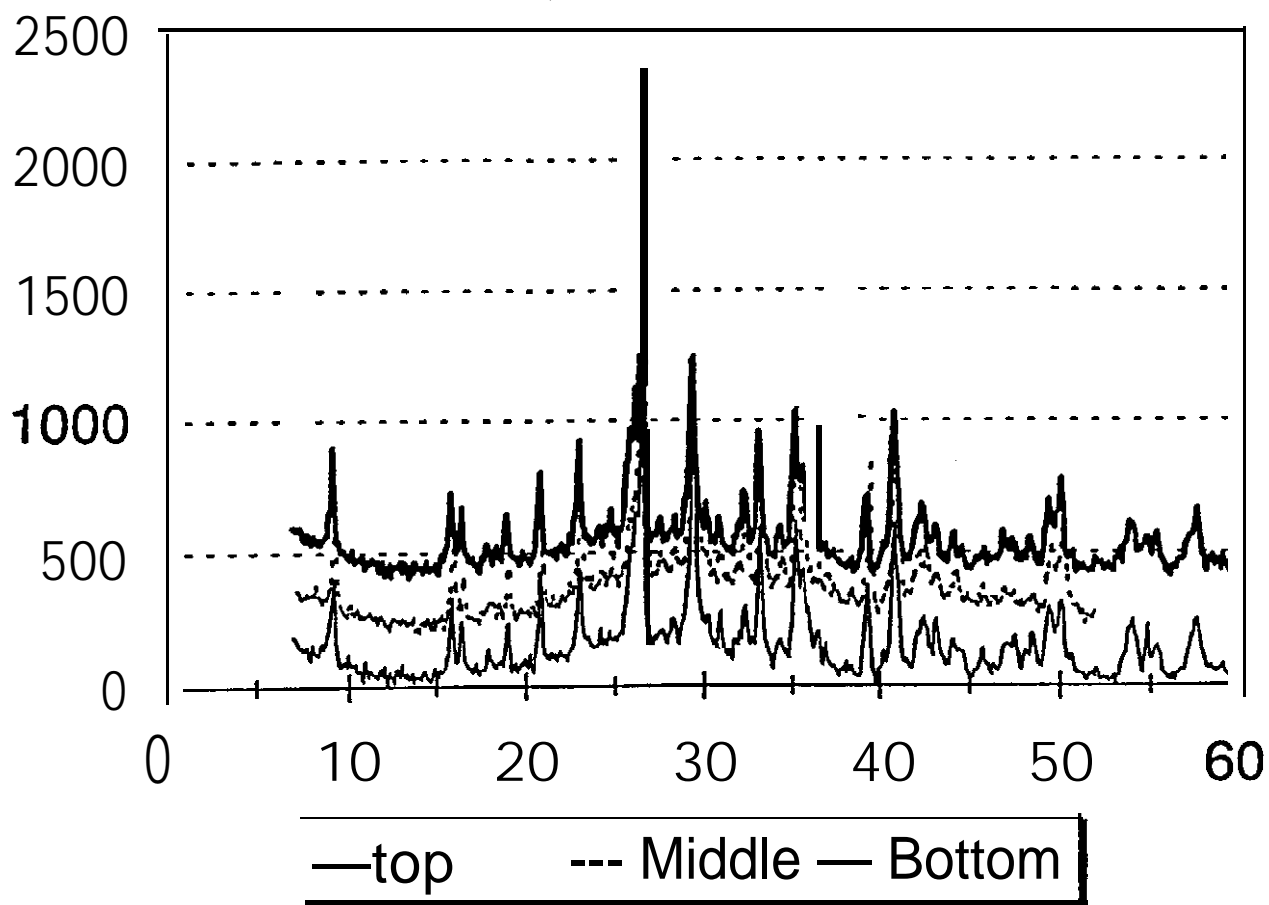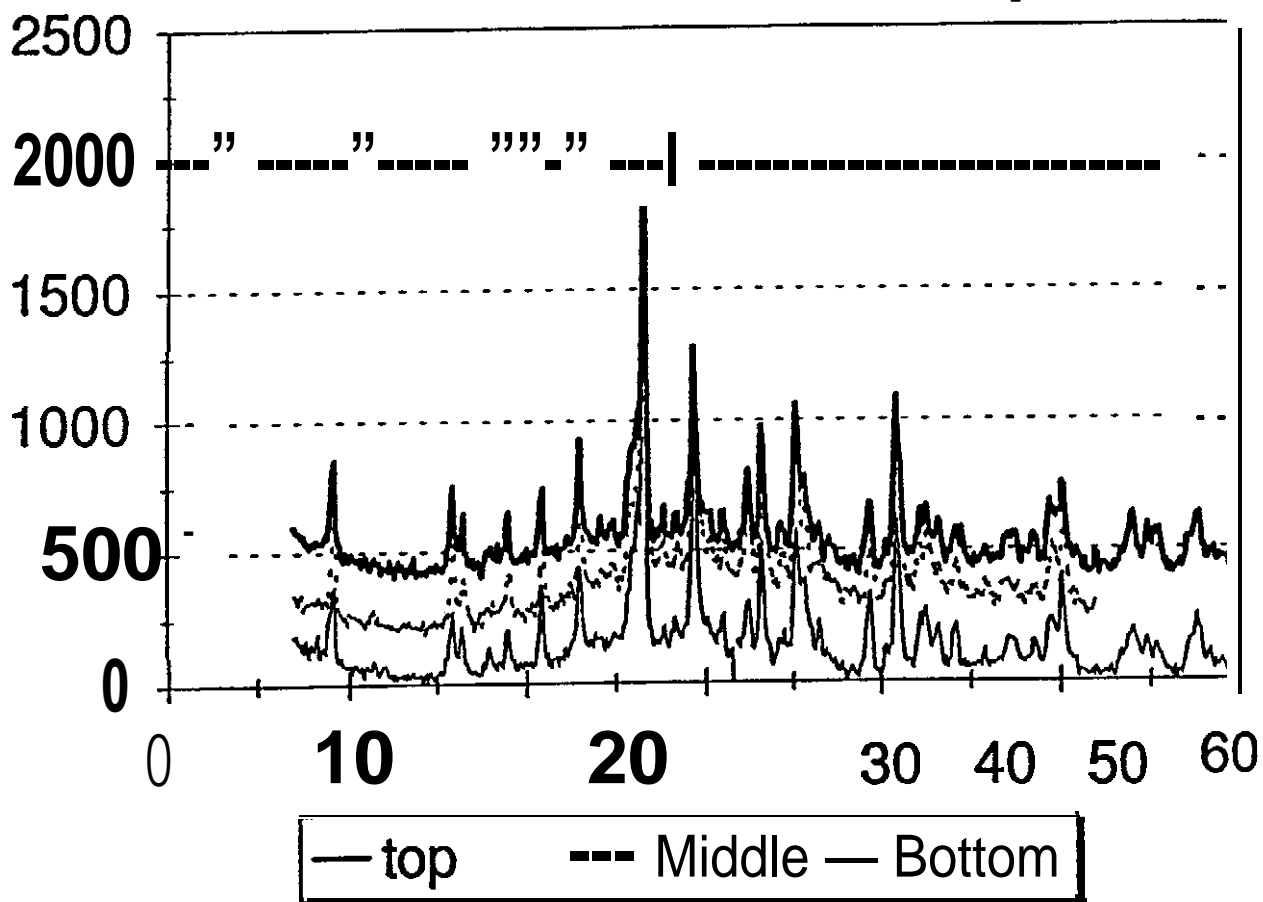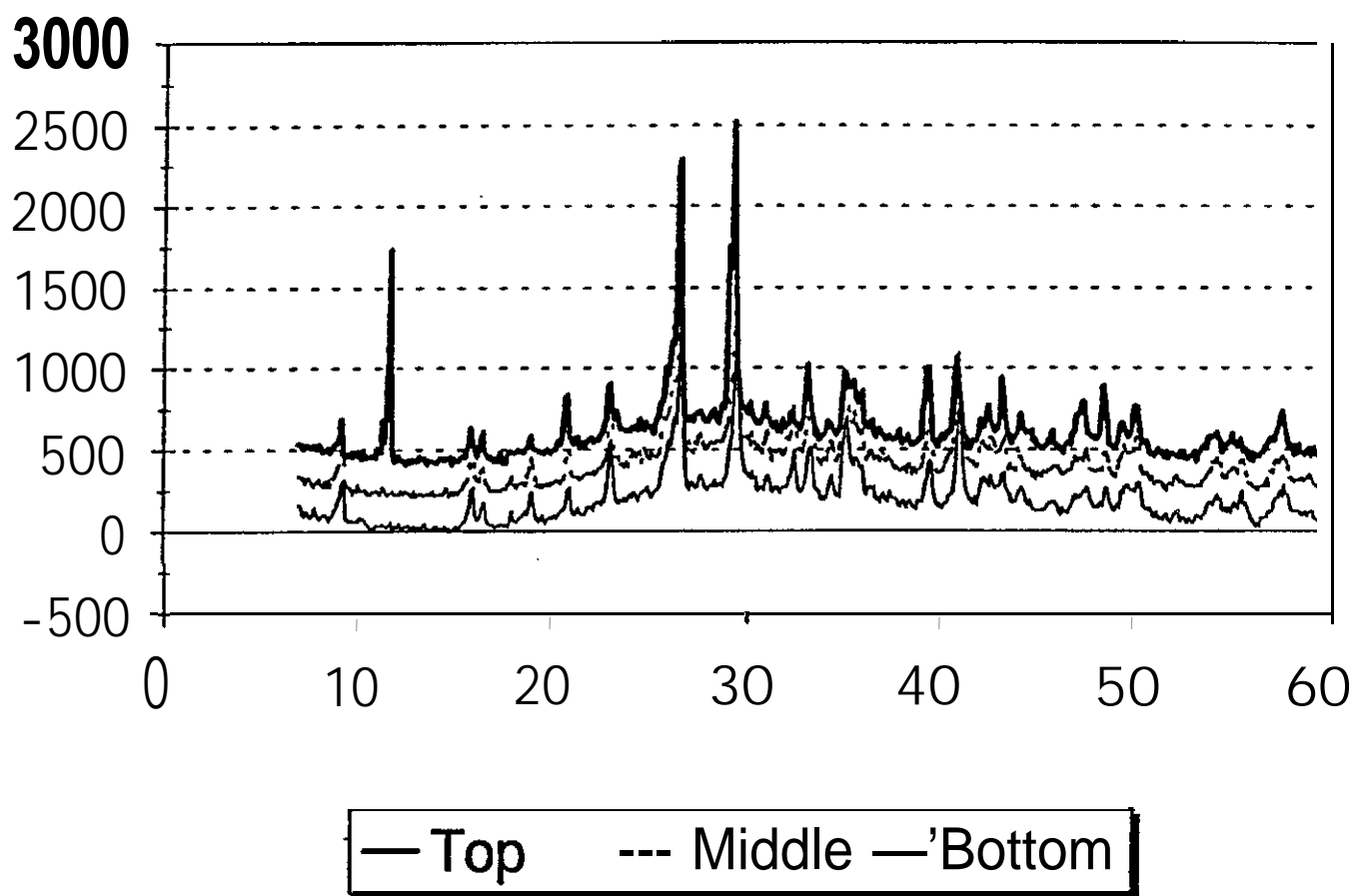Figure **2-20.** XRD analysis of Coolside Coolside Run #1 after 2.5% C02 was added to a fixed feed through the loose compacted Column LC8. The ettringite peak is present at the top, middle and bottom samples (9.2 2-theta). The gypsum peak is only present at the top layer (1 1.4 2-theta).

phases monitored over an extended time period. Although these conditions do not reproduce those in the field lysimeters, this experiment does provide information on mineral stability relations in a closed system, and assists in predicting reactions that would occur under other conditions,

In this study, Coolside Run #2 material was mixed with water to a moisture content of 31 %, and placed into small (1 in. by 1.5 in.) PVC cylinders that were open at each end. Approximately 15 g of wet material was used per cylinder. Each sample was placed in a polypropylene jar, 50 ml of distilled/de-ionized water added (sufficient to cover the sample), and a plastic lid (screw type) was secured tightly to the jar to seal its contents from the atmosphere. The equilibrium temperature of the solutions was $20^{\circ}C$.

At specific intervals, over a period of 300 days, a sample was removed from the water bath and the FGD material extracted from the PVC cylinder. In many of the jars, a small amount of calcium carbonate was observed on the water surface, probably from uptake of CO_2; these deposits were not included in the XRD analysis. The sample was ground thoroughly with a mortar and pestle, and approximately 2 grams acquired for XRD analysis, which was conducted using CU-K radiation, from 7-40° 2theta, at an increment of O.1°, and the spectra compared to that from the dry, parent material.

The solutions were decanted through a Whatman No. 4 paper filter, and the pH measured at 20°C.

Figure 2-21 shows XRD spectra for the samples. The dry material comprised mainly hannebachite ($CaSO_3$ 0.5 H_2O), portlandite ($Ca(OH)_2$), calcium carbonate, quartz, mullite, and hematite. Over the course of 300 days, calcium carbonate (Figure 2-22), hannebachite (Figure 2-23), and quartz (Figure 2-25) abundance changed a negligible amount, as did mullite and hematite (Figure 2-21). The calcium carbonate abundance was controlled in the closed system of the sealed containers. Ettringite formation (Figure 2-24) commenced within the first day of the study and increased to an equilibrium amount after
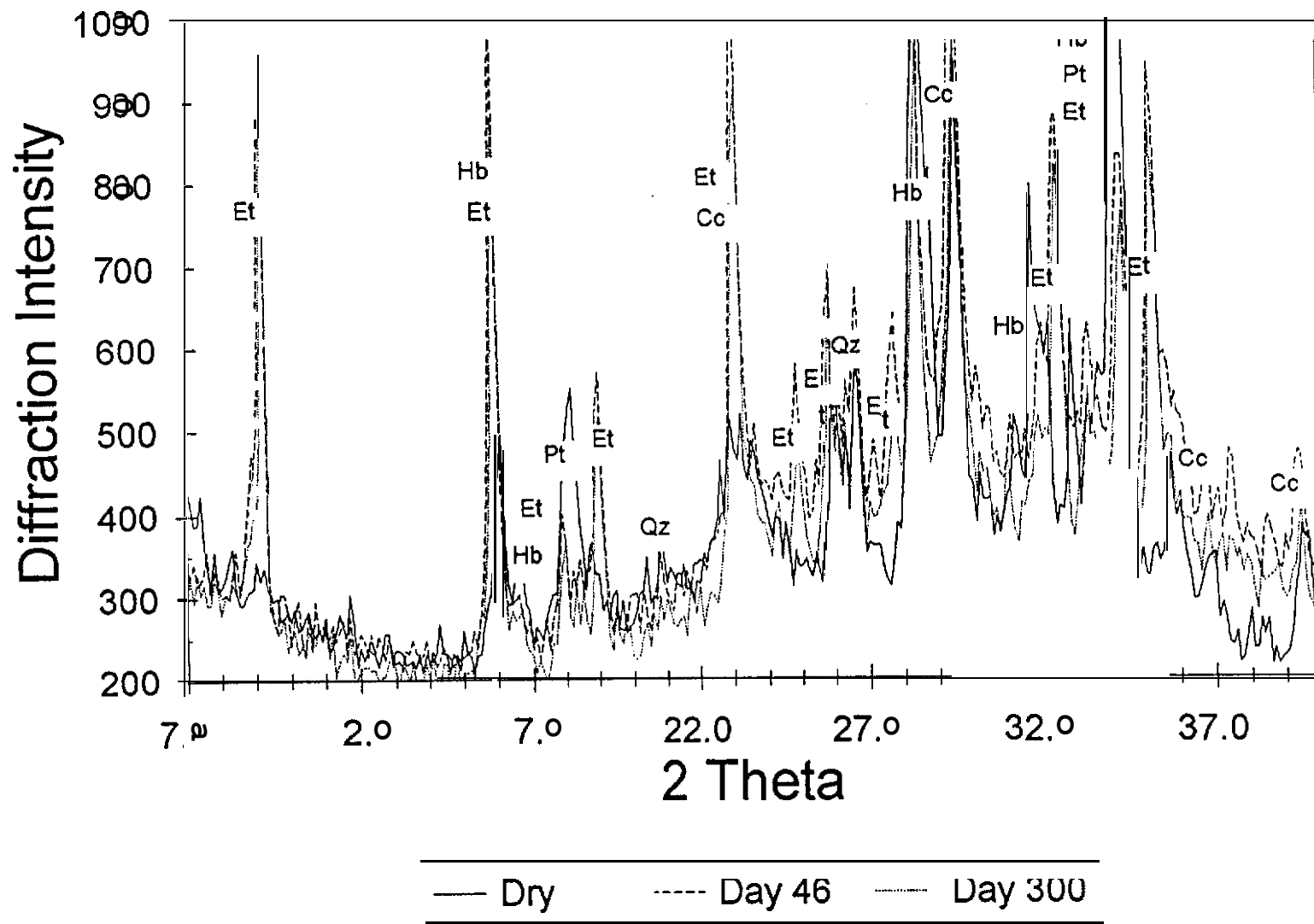
Figure 2-21. XRD spectra for Coolside material from Run #2 used in the kinetic study. Illustrated are XRD results for the dry material compared with material aged for 46 days and for 300 days. (Et = ettringite; Hb = hannebachite; Pt = portandite; Qt = quartz; Cc = calcium carbonate). Ettringite was not present in the dry material, but significant amounts of crystals in the aged materials.

Figure 2-22. **Illustration of the relative amounts of calcium carbonate** in the kinetic study as a function of sample age.

Figure 2-23. Illustration of the relative amounts of hannebachite in the kinetic study as a function of sample age.
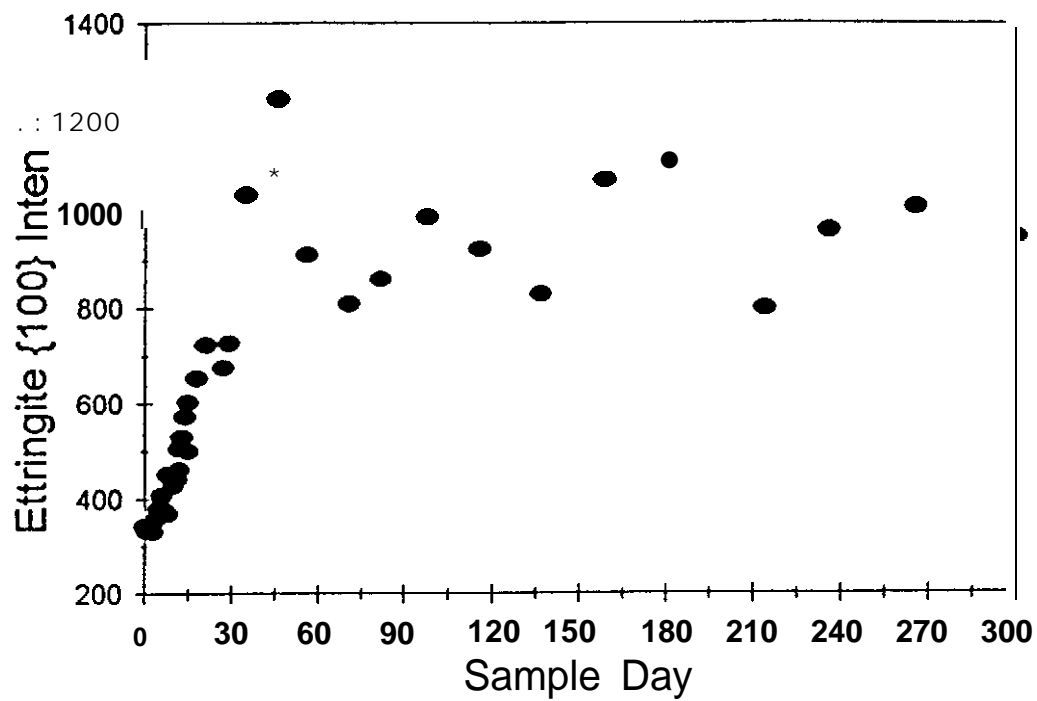
Figure 2-24. Illustration of the relative amounts of ettringite in the kinetic study as a function of sample age.
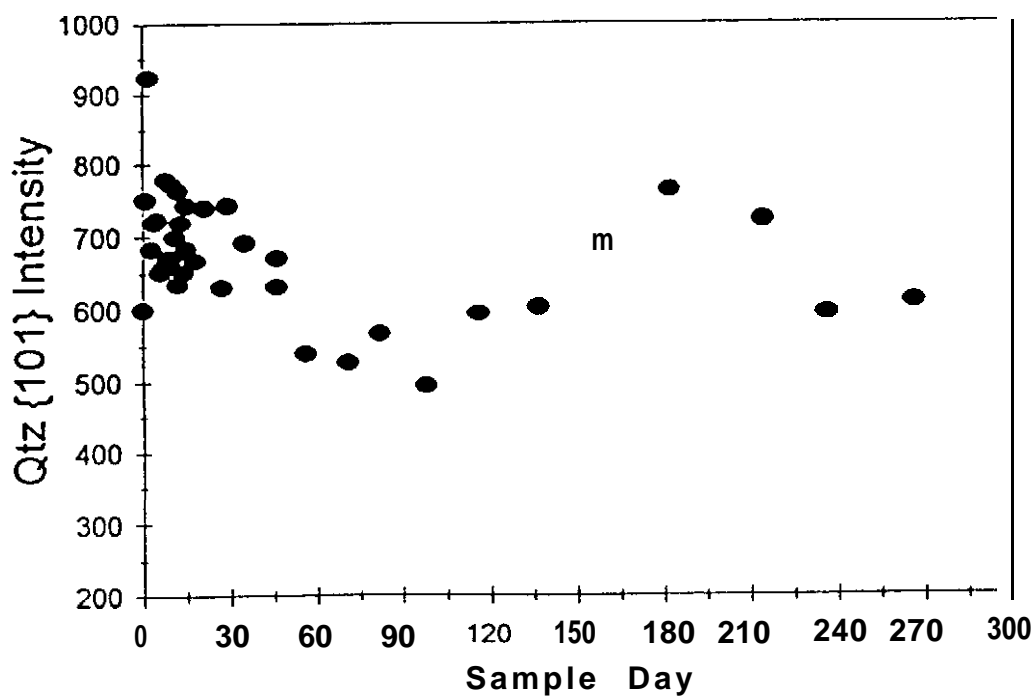
Figure 2-25. Illustration of the relative amounts of quartz in the kinetic study as a function of sample age.

67

approximately 45 days; from 45 days to 300 days, the diffraction intensity fluctuated about a mean value. All of the mineral diffractions exhibited considerable variation in intensity over the course of the study, due to instrument variation and sample heterogeneity. However, a sufficient number of samples were analyzed to elucidate general trends.

Portlandite abundance decreased with aging to a minimum at approximately 45 days, as is shown in Figure 2-26. Because of overlap of the {101] peak with that from hannebachite, the minimum intensity of about 700-750 counts mainly represents the constant abundance of hannebachite. Gypsum formed within the first day of the experiment and increased in abundance up to approximately day 10 (with considerable variation in reflection intensity) whereupon it exhibited a marked decrease and was more-or-less absent by day 15 (Figure 2-27). Ettringite formation is the likely cause of the gypsum and portlandite decrease, which is discussed below.

The solution pH remained constant at approximately 12.5 until day 45-55, upon which it monotonically declined to about 8.5 (Figure 2-28), a value approaching that of bicarbonate buffer in equilibrium with atmospheric C02. This suggests the occurrence of a small leak in the lid-container seal, although the system was nominally closed to the atmosphere. In fact, the surfaces of the solutions contained small amounts of calcite, although the deposits did not increase consistently over the course of the experiment, and there was negligible evaporation of the solution). However, the pH in the solution was possibly higher than the measured value because ettringites are reportedly unstable at a $pH < 11$, and the constant intensity of the ettringite XRD reflections in the solid material over time suggest that the mineral was not dissolving.

The introduction of atmospheric carbon dioxide into the system could cause portlandite dissolution via the following reactions in which portlandite is a buffer:

$$C02 + OH^- = HCO_3^-$$
$$HCO_3^- = H^+ + C03^{2-}$$

68
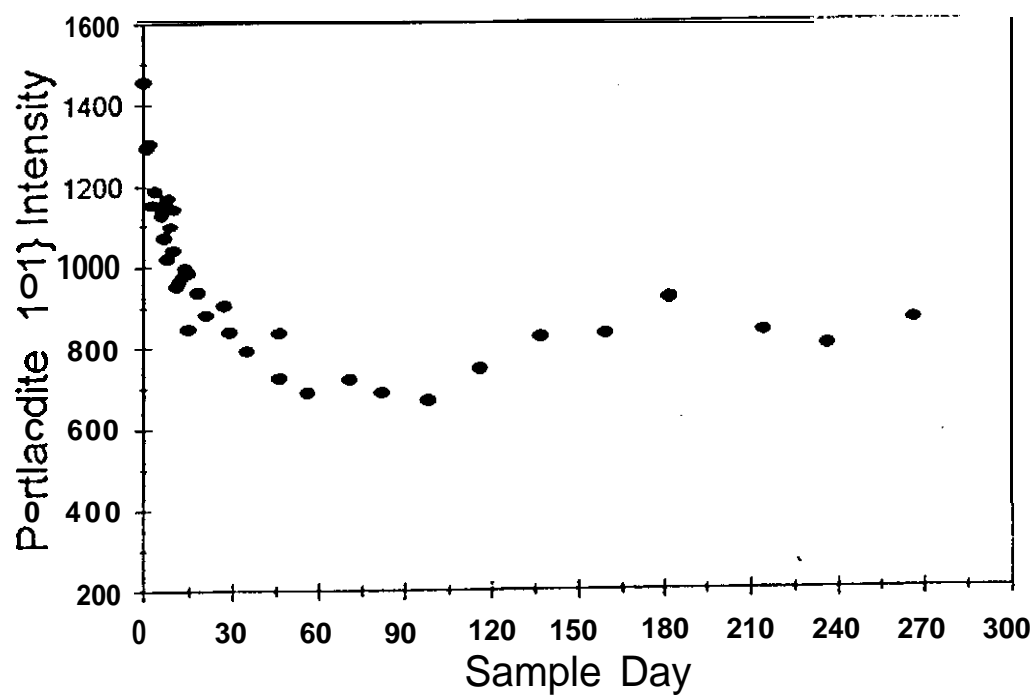
Figure 2-26. **Illustration of** the **relative amounts** of portlandite in the kinetic study as a function of sample **age.**
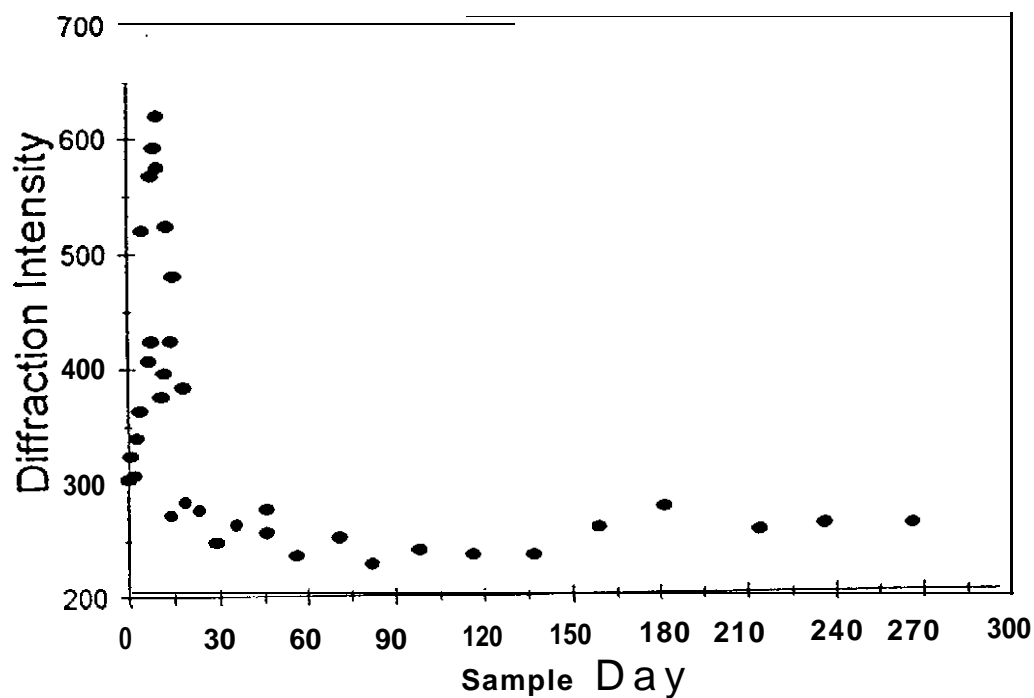
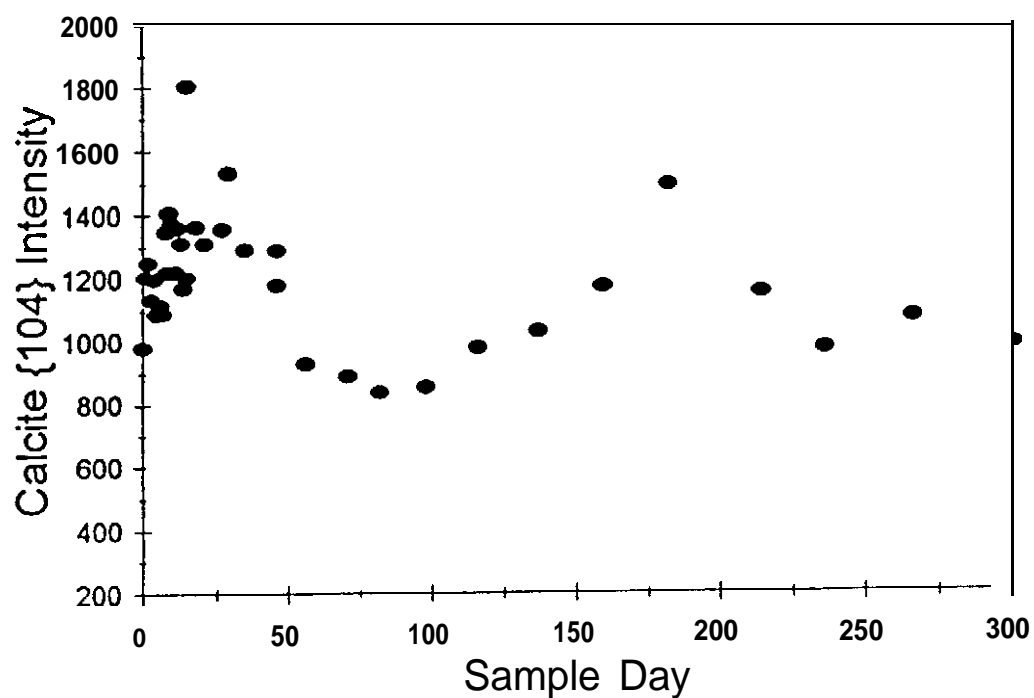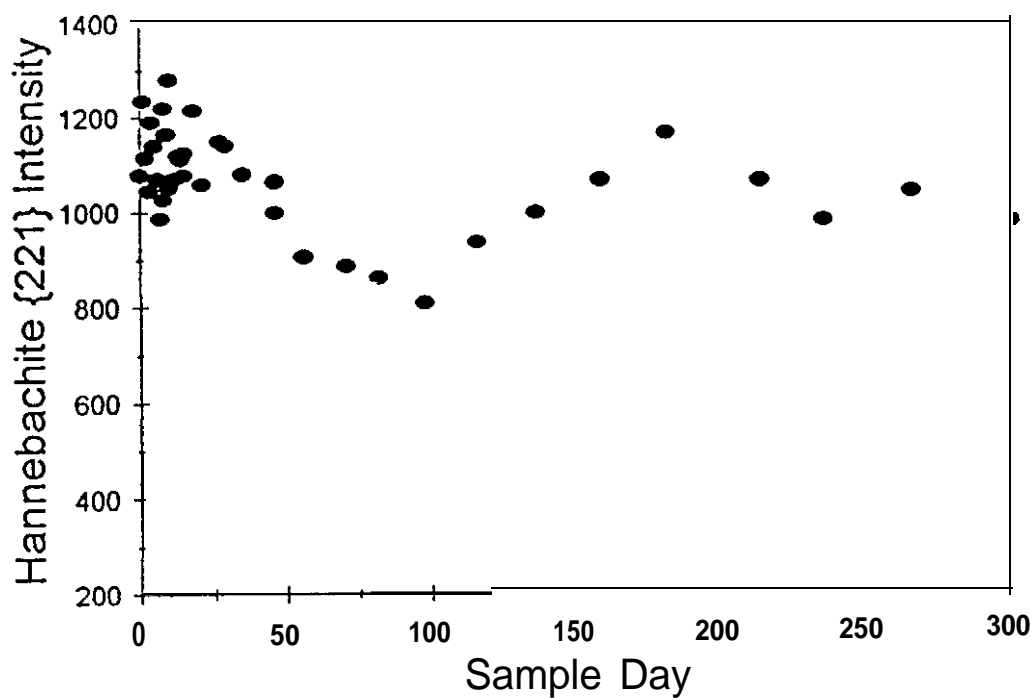**Figure 2-27. Illustration of the relative amounts of gypsum** in the kinetic study as a function of sample age.
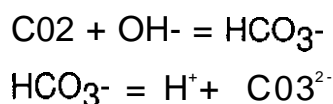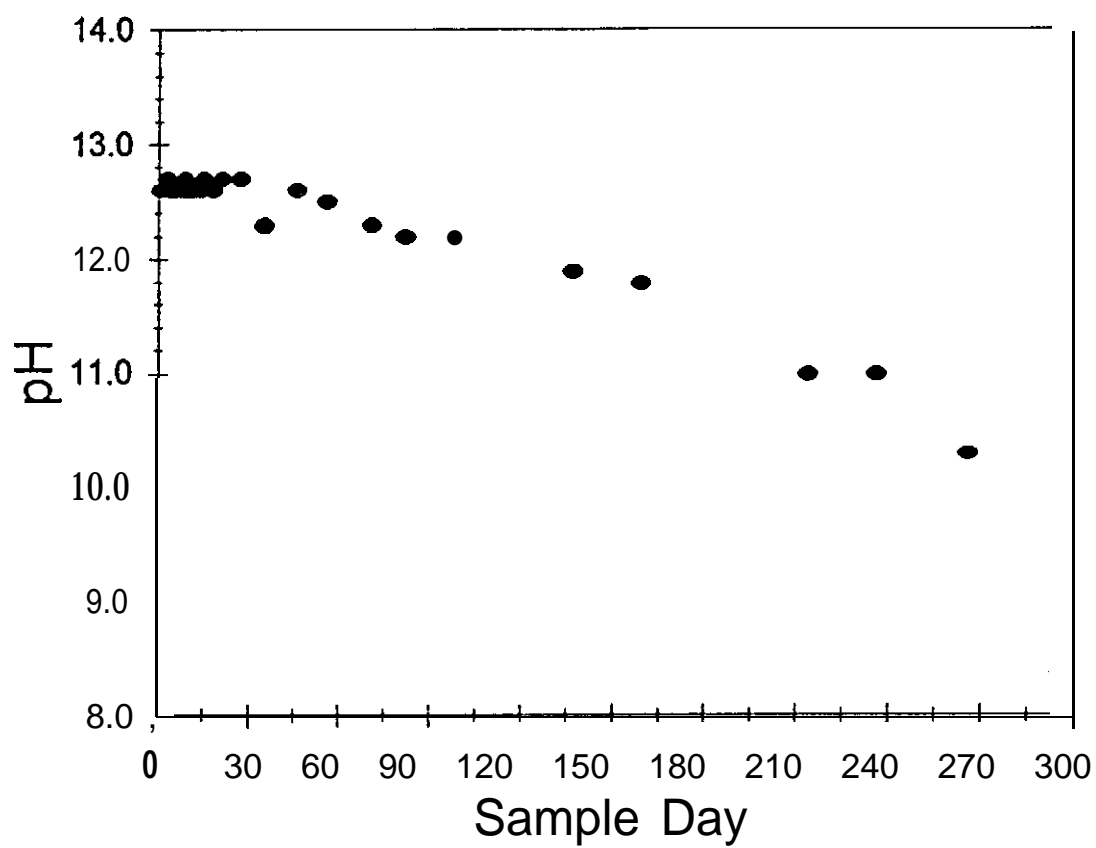
Figure 2-28. Monitoring of the solution pH in the Coolside samples throughout the kinetic experiments.

$$Ca(OH)_2 = CaOH^+ + OH-$$
$$CaOH^+ = Ca^{2+} + OH-$$

The solution pH would eventually decrease when all of the portlandite was depleted.

The formation of ettringite in the solid can cause dissolution of portlandite, for several reasons. Crystallization of 1 mole of ettringite, theoretically, consumes 6 moles of calcium and 3 moles of sulfate, whereas dissolution of hannebachite produces 1 mole each of calcium and sulfite ion. Assuming hannebachite to be the major source of sulfite, after gypsum-derived sulfate is depleted, then ettringite formation would cause the $[Ca^{2+}]/[SO_3^{2-}]$ ratio to decrease in the solution. In order to maintain equilibrium of hannebachite with the solution, which is suggested by the XRD data, then the activity of calcium in solution needs to increase such that $[Ca^{2+}][SO_3^{2-}] = 10^{-7.0}$ (the K_{SP} of hannebachite). In this system, since portlandite is the most soluble calcium-bearing mineral ($K_{SP}=10^{-5.3}$), it dissolves. Furthermore, as the glass component dissolves, aluminum is released and forms $Al(OH)_4-$ at the high pH of this solution. Ettringite is commonly observed crystallizing on the glass fly ash spheres, incorporating aluminum from the glass, and hydroxyl ions into its lattice, thereby causing portlandite to dissolve.

The formation of ettringite is, therefore, likely to be the primary cause of the portlandite dissolution, mainly in the first 45 days, with ancillary effects from calcite formation, It is predicted that if, under these conditions, the experiment had continued over a prolonged period, portlandite would be depleted, the pH would decrease to approximately 8.0, and ettringite would dissolve incongruently (precipitating a non-crystalline, aluminum-rich gel). If the system were kept completely sealed from the atmosphere, then portlandite and ettringite, in addition to the other crystalline phases, would coexist indefinitely within the material.

Series IV: Pelletization of FBC Material

The main objective of this part of the Coolside project was to investigate the importance of different mineral components and their relative abundances in the pellet precursor materials (FBC ash versus spray dryer ash) to understand the contributions of mineralogical transformations upon hydration and aging on the overall pellet stability.

The FBC ash (Wormser) that was utilized in the preparation of pellets was X-rayed after receiving the raw mixture. The XRD results indicate the presence of portlandite, slow reacting anhydrite, and quartz, as well as amorphous SiO_2, small amounts of gypsum (possibly formed from a reactive anhydrite within the raw mixture through contact with surface moisture), and small amounts of mullite.

The spray dryer ash has very similar mineral constituents compared to the FBC ash described above, however, the anhydrite fraction present consists predominantly of reactive anhydrite which readily reacts with moisture to form gypsum.

The data obtained during the entire reporting period supports the conjecture that detrimental swell associated with continued pellet aging upon exposure to humidified air or upon exposure to water is principally a function of calcium sulfate hydration reactions. The main difference between the FBC pellets and the spray dryer pellets produced by CONSOL, are summarized hereof:

Anhydrite crystals in the FBC pellets, upon exposure to moisture, undergo a dissolution-reprecipitation reaction that results in the nucleation and growth of gypsum crystals. The reaction is extremely delayed (slow reaction kinetics) since the anhydrite crystals were produced under high temperature conditions such as occurring in a fluidized bed reactor (the expression "dead burned" anhydrite maybe used to describe the degree of crystallinity of the anhydrite crystals formed at elevated temperatures in an FBC unit). The mineralogical transformation is delayed because of the dense crystal structure of the anhydrite grains causing early formed cementitious bonds to rupture, and, overall, leads to poor pellet strength. The performance of the FBC pellets under weathering conditions

72

(reported in laboratory and field testing by Dr. Milton Wu at Consol) was unsatisfactory and, based on this study, was attributed to the slow mineralogical transformation from anhydrite to gypsum which takes place long after initial solidification of the material. The transformation, which is associated with a 60 percent volume increase, causes detrimental crack and fracture formation in the pelletized FBC materials. In contrast, spray dryer materials are lacking "dead burned" anhydrite crystals. Therefore, the anhydrite to gypsum transformation in the spray dryer pellets occurs prior to the solidification of the material and, hence, avoids the detrimental swell.

The mineralogic analyses of the two different kinds of ash, FBC ash versus spray dryer ash, used in the pelletization study illustrate the differences in the mineralogical makeup of the pellet precursor materials. Chemical characterization of the FBC pellets indicates that the main mineral components are anhydrite ($CaSO_4$), portlandite ($Ca(OH)_2$), free lime (CaO), minor calcium carbonate ($CaCO_3$), minor mullite($A[6Si2013$) and, of course, quartz. During early curing the anhydrite did not hydrate to spontaneously form gypsum but rather resulted in the early hydration products portlandite and ettringite as evidenced by XRD and SEM investigations of the materials. Although ettringite needles form early bonds between mineral grains, subsequent hydration of anhydrite leads to extremely large gypsum crystals that form in voids and fractures, causing the complete disrupture of mineral bonds after 160 days curing period.

In the spry dryer material, the main mineral components after hydration are: hannebachite, ettringite, and calcite, with only minor amounts of gypsum. Mullite, rutile and quartz are present in both the starting and hydrated spray dryer pellets. The XRD peaks for the spray dryer material are typically indicative of the presence of a substantial amount of glassy phase. The glass diffraction "ramp" is centered approximatelyat29-302 theta and is relatively broad, indicative of a high CaO component within the glassy phase. Figure 4 compares the XRD results obtained for the spray dryer ash (SDA-F) with the pelletized material (SDA-P). It is evident from the XRD data that hannebachite (CaS030.5H20) is the most important mineral participating in the "spray dryer ash" transformation reactions.

The aged spray dryer pellets have abundant hannebachite present as well as ettringite needles, both of which contribute to mineral bonding and early strength gain of the materials. In contrast, gypsum crystals which comprise the bulk of newly formed minerals in the FBC pellets, are only a minor component in the spray dryer pellets, suggesting, that gypsum crystals easily reprecipitate in the FBC material from the Ca and SO_4 supersaturated pore waters, while in the spray dryer materials oxidation of SO_3 to SO_4 is the rate limiting step in the reaction forming gypsum. Based on the results of this study it appears that ettringite crystals, which also require the sulfate ion, are more readily formed in an S04 starved environment compared to gypsum crystals. One of the prerequisites for the ettringite crystals to form is the presence of aluminum ions, which, in the pore solutions of the spray dryer pellets are most likely supplied by the mullite phase available in the starting material.

In summary the present results suggest that the spray dryer ash constitutes a better precursor material for pelletization work than FBC ash. The results are based on XRD and SEM observations that indicate a lesser effect of mineral transformations and swell causing mineral growth in the spray dryer pellets compared to that of the FBC ash pellets.

CHAPTER 3: THE PHYSICAL AND GEOTECHNICAL CHARACTERISTICS OF THE COOLSIDE MATERIALS

The Characteristics of the Coolside Materials as Emplaced in the Field

Geotechnical Characteristics of the Materials As Emplaced

Density and Moisture Content. Coolside material was placed in Lysimeter 1 with no compactive effort. The material was mixed to a target moisture content of **37'?.** before placement, No target density was established because the material was placed loosely. The average dry density and moisture content of the 16 loosely placed lifts were 706 kg/m^3 (44.1 lbs/ft^3) and 37.5%, respectively. Average lift thickness was approximately 13.5 cm (5.3 in). Values of dry density and optimum moisture obtained for each lift are shown in Figures 3-1 and 3-2, respectively.

Coolside materials placed in the second lysimeter (L-2) were compacted to target dry density and moisture content values of 794 kg/m^3 (49.6 lbs/ft^3) and 41.2 o/., respectively. These values were obtained from moisture-density tests designed to simulate the compactive efforts of a D9 bulldozer. This test was performed by applying a static pressure of 117.3 kPa (17 psi--the stress exerted by the track of a D9 bulldozer) to the Coolside by-product, which was placed in one lift in a standard 10.16-cm (4-inch) diameter Proctor mold. The material was then compacted at various moisture contents. The pressure was applied until the maximum load was reached. It was then held for 1 minute and released. The moisture-density curve was similar to those established in standard moisture-density tests. Field compaction was performed with a hand-held plate compactor. The dry density and moisture content obtained for 17 lifts averaged 788 kg/m^3 (49.2 lbs/ft^3) and 38.9 O/., respectively. The average lift thickness was about 12.4 cm (4.9 in). Values of dry density and moisture content obtained for each lift of Lysimeter 2 are shown in Figures 3-3 and 3-4, respectivley.

Figure *3-1.* Dry densities measurements of each lift in Lysimeter 1
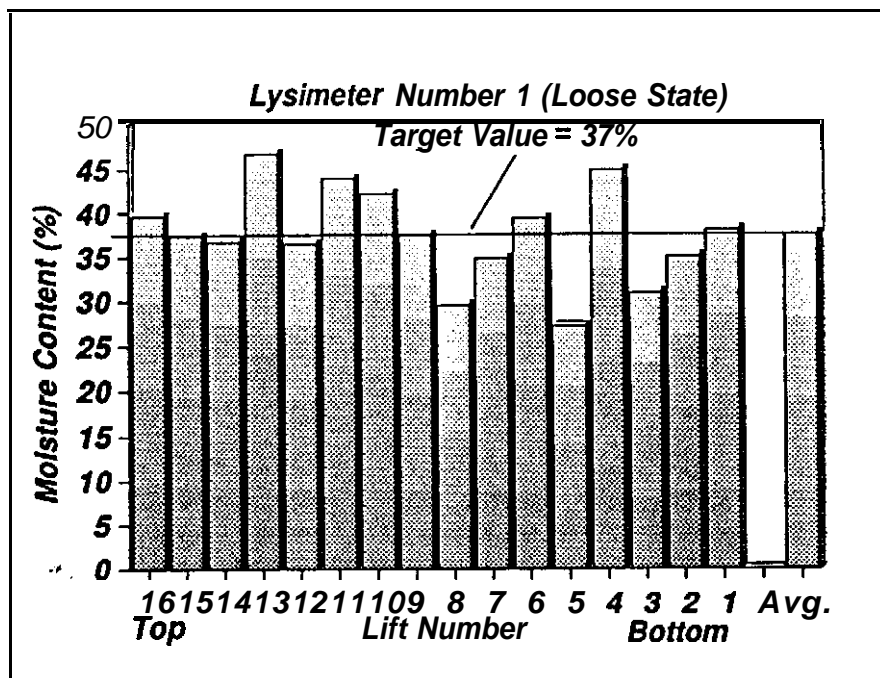
Figure 3-2. Moisture contents of each lift of Lysimeter 1

Figure 3-3. Dry density measurements of each lift of Lysimeter 2
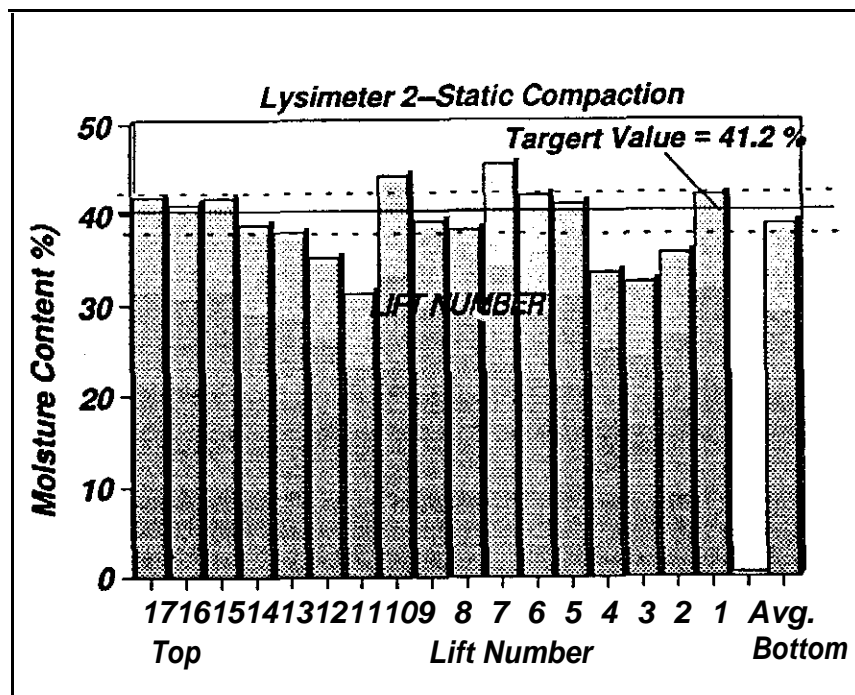
Figure 3-4. Moisture content of each lift of Lysimeter 2

77

The third lysimeter (L-3) was filled with Coolside material compacted near 95% of standard maximum dry density and optimum moisture content. Target values for density and moisture were 1065 kg/m^3 (66.5 lbs/ft^3--95 percent of standard compaction) and 37.0 %, respectively. Maximum dry density and optimum moisture content obtained from standard moisture-density tests were 1121 kg/ins (70.0 lbs/ft^3) and 36.5 %, respectively. Dry densities and moisture contents obtained for each lift of Lysimeter 3 are compared in Figures 3-5 and 3-6, respectively. The material was compacted with hand-held gasoline-powered compactors. Vibratory plate and static (jumping jack) compactors were used. Target density was easily obtained with the static compactor; therefore, it was used more frequently. Average values of dry density and moisture content obtained for 23 lifts of compacted Coolside material were 1060 kg/m^3 (66.2 lbs/ft^3) and 37.07., respectively. Dry density and moisture content measurements of each lift are shown in Figures 3-5 and 3-6, respectively. Moisture content exceeded optimum moisture content by more than 2% in a few lifts. Liquefaction occurred in these few lifts because of the excess moisture and the silt-sized particles.

A commercial fly ash was placed in the fourth lysimeter (L-4). Fly ash was used as a control material for leachate monitoring. The fly ash was purchased and transported to the field site in seventy pound bags. Approximately 803 kg (1750 lbs--25 bags) of material was used for each lift. The material was lightly compacted with a hand compactor near 90% of standard maximum dry density, 2% below optimum moisture content. Maximum dry density and a moisture content that was about optimum moisture content for the fly ash were 1374 kg/m^3 (85.8 lbs/ft^3) and 22%. Target density and moisture content were 1236 kg/m^3 (77.2 lbs/ft^3--(90% of standard density) and 20% percent moisture, as shown in Figure 3-7. The average density and moisture content values obtained for nineteen lifts were 76.4 lbs/ft^3 and 20.5%, respectively. Dry density and moisture content of each lift are shown in Figures 3-8 and 3-9, respectively. Target and actual values of dry density and moisture content obtained for each
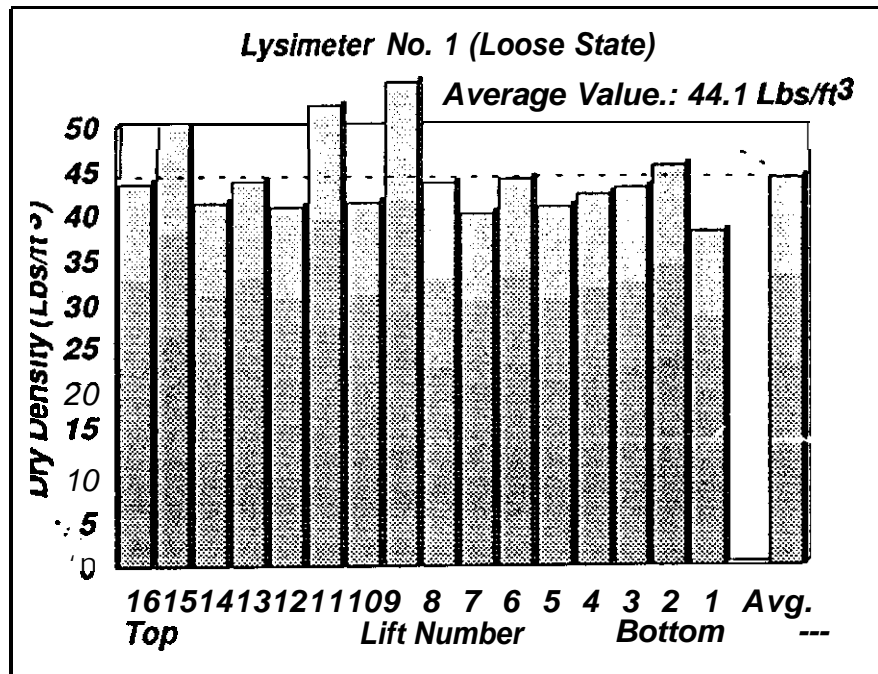
78
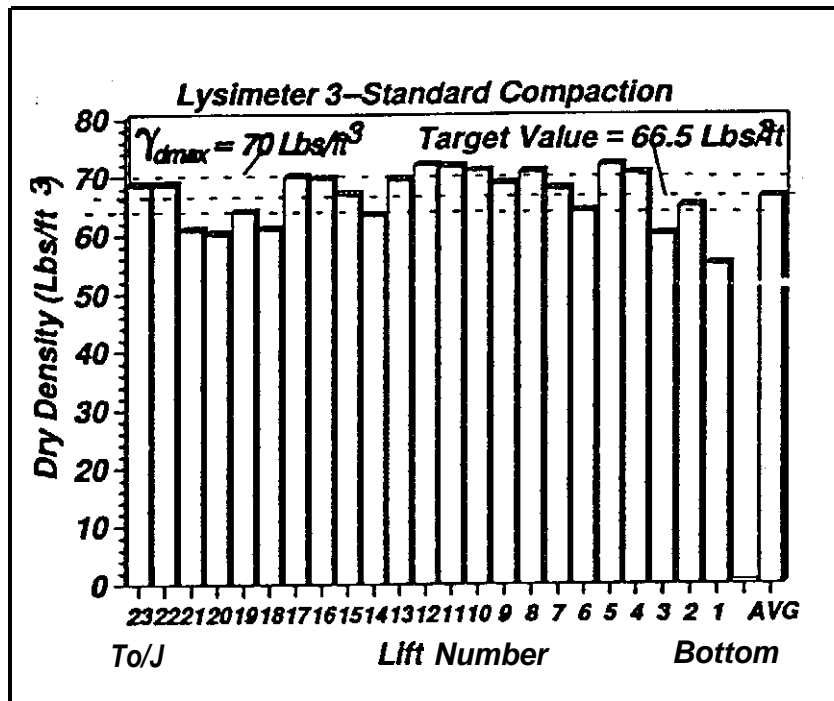
Figure *3-5.* Dry density measurements of each lift of Lysimeter 3
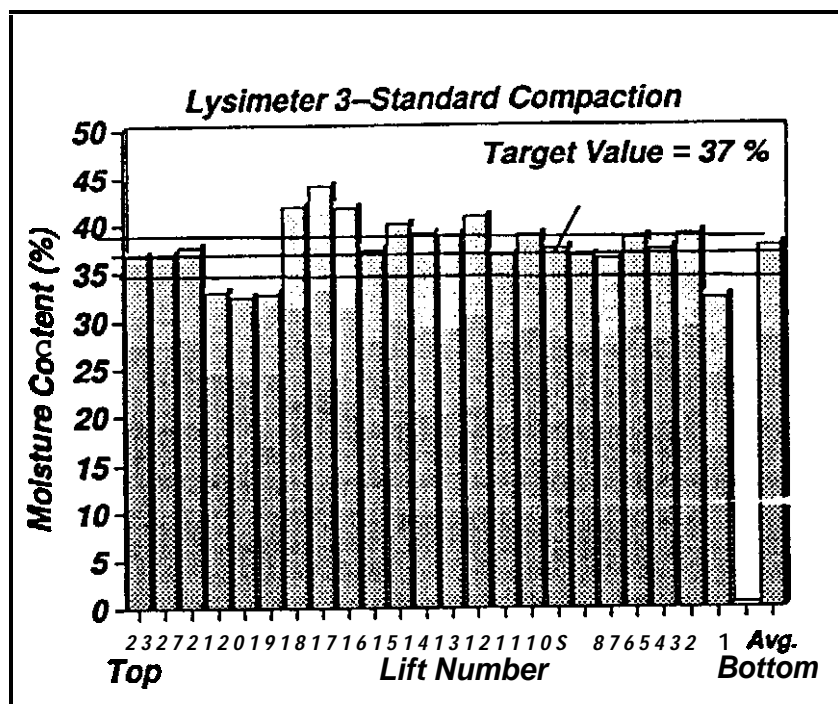
Figure 3-6. Moisture content of each lift of Lysimeter 3

79

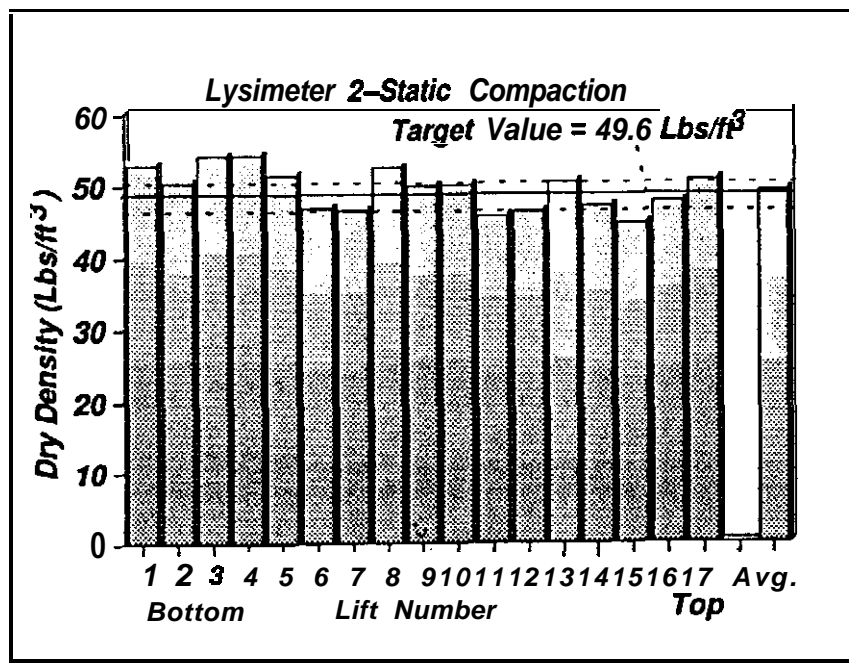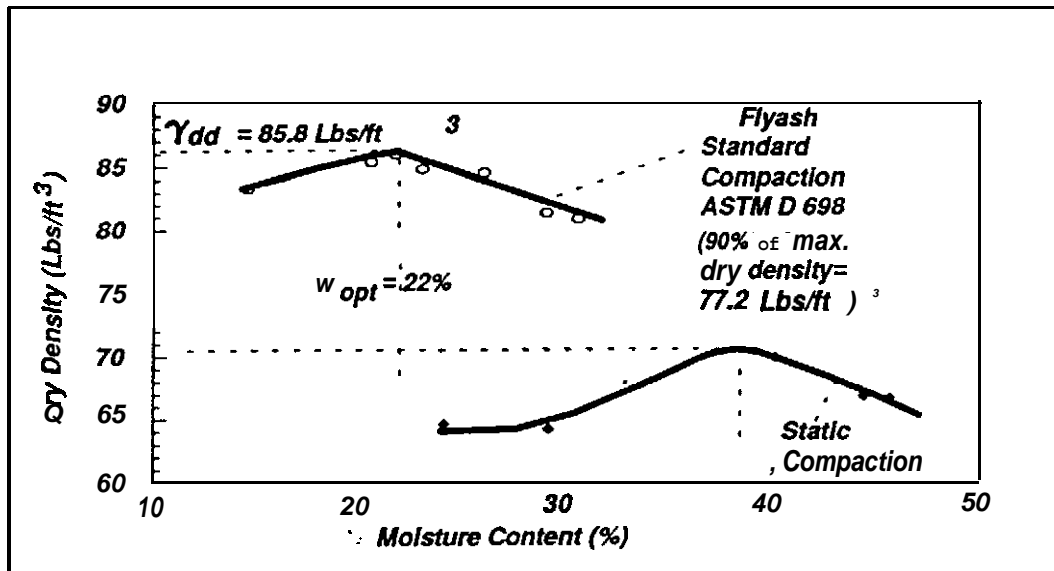Figure 3-7. Dry density-moisture content relationships for the fly ash used in Lysimeter 4
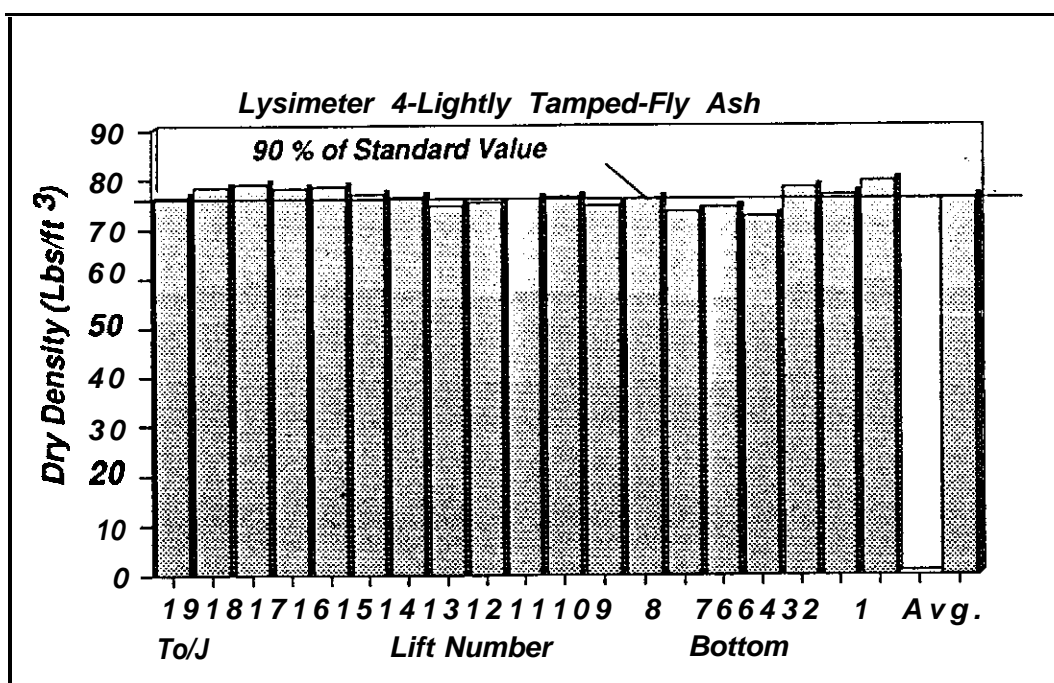
Figure 3-8. Dry density measurements of each lift of Lysimeter 4

80
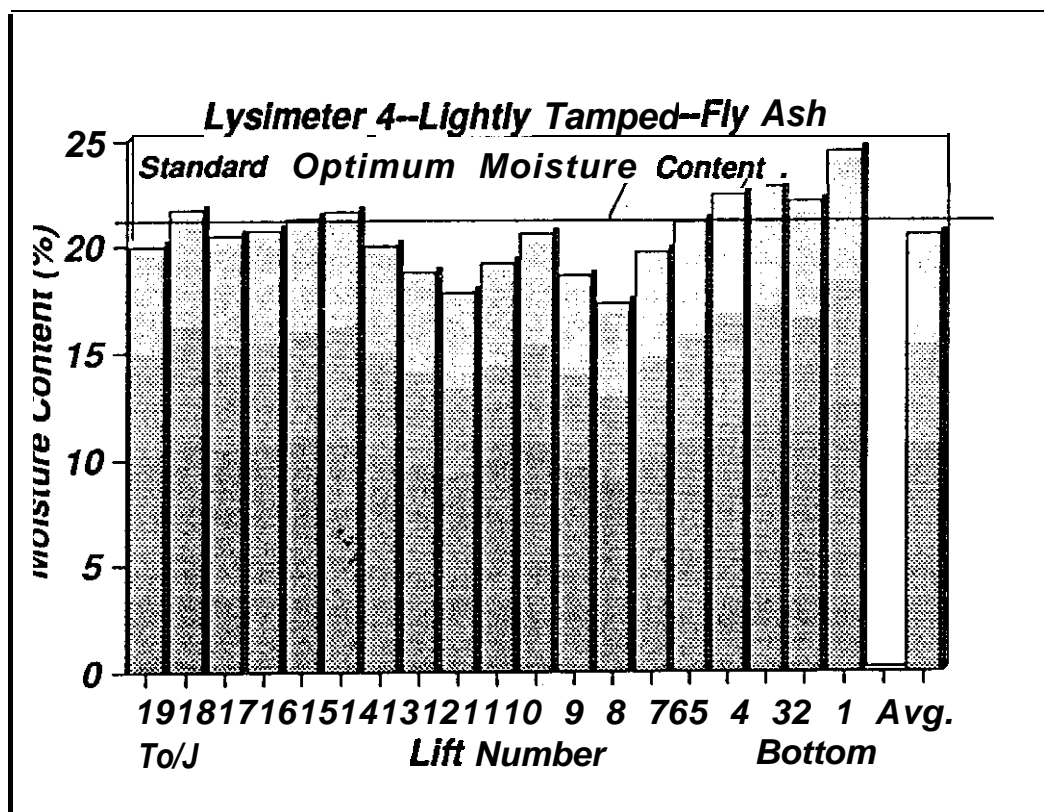
Figure *3-9.* Moisture contents of each lift of Lysimeter 4
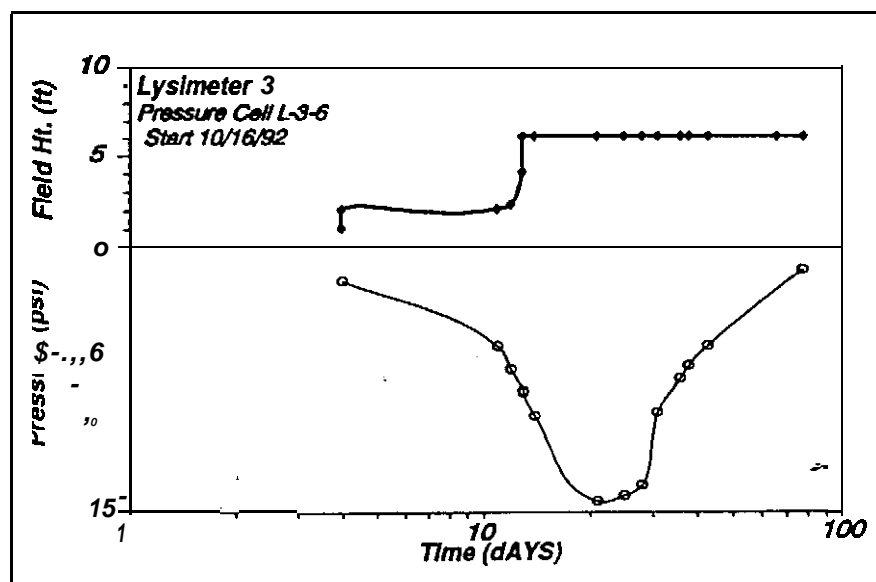
Figure 3-10. Observed side pressures in Lysimeter 3 during loading and chemical reactions

81

lysimeter are compared in Table 3-1.

Table 3-1. *Summary of Dry Density and Moisture Content Measurements.*

Lysimeter	Average Dry Density (lbs/ft^3)	Target Dry Density (lbs/ft^3)	Average Moisture Content (%)	Target Moisture Content (%)	Number of Lifts
1	44.1	N/A	37.5	37.0	16
2	49.2	49.6	38.9	41.2	17
3	66.2	66.5	37.0	37.0	23
4	76.4	77.2	20.5	20.0	19

Pressure, Temperature, and Swell Measurements. Pressure at a depth of 6 feet in Lysimeter 3 increased slightly as fill was placed. A maximum pressure of 103.4 kPa (15 psi) was reached a few days after filling operations were completed, Variation of the pressure on the side wall, during loading and shortly after completion of loading, in Lysimeter 3 with increasing time is shown in Figure 3-10. The pressure eventually returned near to zero. Pressure at 4 feet increased to about 103.4 kPa (15 psi) and returned near to zero (Figure 3-11). A pressure increase in the lysimeter containing fly ash was less than 13.78 kPa (2 psi), as shown in Figure 3-12. In the three lysimeters containing Coolside materials, the moisture accumulated near the top of the materials, initially, and gradually moved downward in the materials with increasing time. Moisture from precipitation in Lysimeter 4 initially increased at the bottom of the fly ash and gradually increased upward to the top of the material.
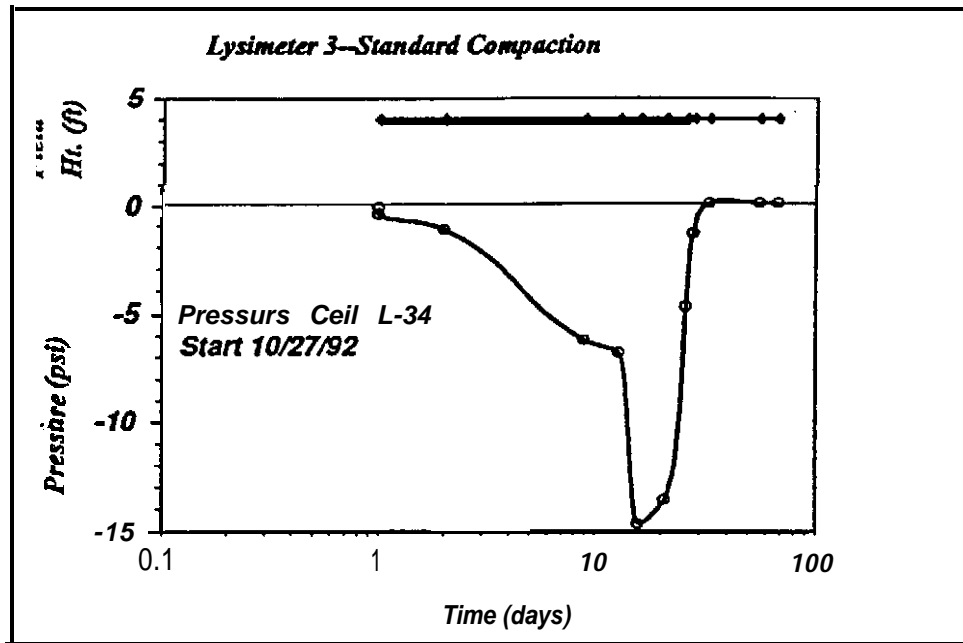
Figure 3-11. Observed side-wall pressure at a four foot depth in Lysimeter 3
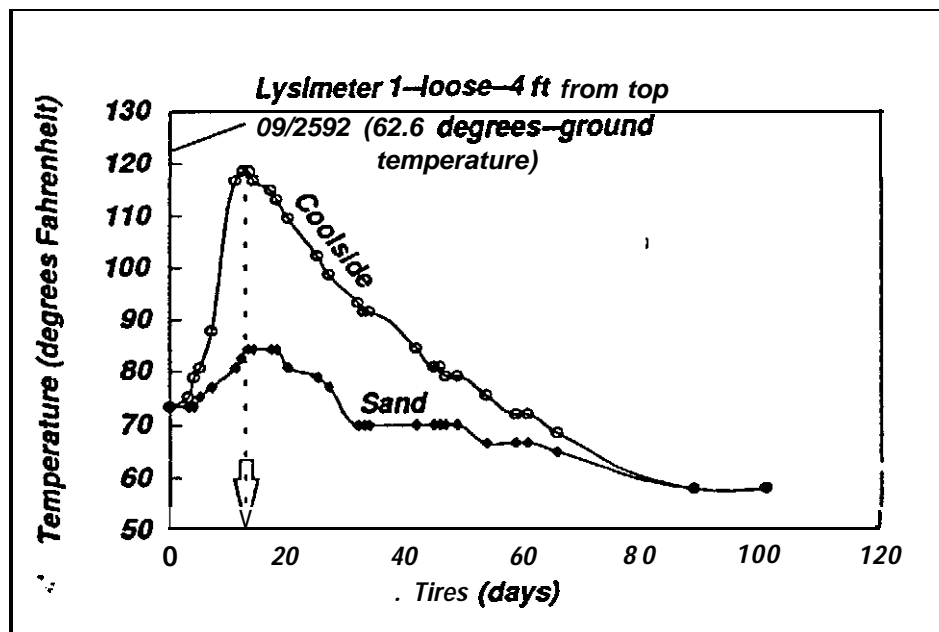
Figure 3-12. Temperatures observed in Lysimeter 1 during the filling operation

Lysimeters containing Coolside materials increased in temperature, as shown in Figure 3-12, and reached a maximum value of 48.9°C (120 degrees Fahrenheit) about two weeks after placement of the Coolside residue. Subsequently, the temperature decreased, Thermocouples installed in the lysimeter containing fly ash showed no increase in temperature (see Figure 3-13). Temperatures at the interface between the fly ash and bottom of the soil layer and the interface between the bottom of the fly ash and sand during the first two months after filling are shown in Figure 3-14. At both interfaces, the temperatures decrease and appear to reach some constant values. During the 3.5-year study period, no significant swell (or consolidation) occurred in the Coolside or fly ash materials,

Collection and Testing of Specimens. Immediate y after the Coolside ash had been compacted in Lysimeter 3, thin-walled tube samples were collected. The Coolside ash in this lysimeter had been compacted to 95% of standard density. Unconfined compressive strength tests were performed on these specimens. The specimens were allowed to age for various times before testing. The strengths of the field specimens are compared in Figure 3-15 to laboratory strengths of specimens remolded near 95% of standard maximum dry density. Strength tests on lysimeter samples were performed after permeability tests were conducted. Unconfined strength of the lysimeter specimens ranged from 8.27 kPa (1.2 psi) at a 1-day aging time to approximately 1295.51kPa (188 psi) at a 7-day aging time. As seen in Figure 3-15, the unconfined compressive strengths of the field lysimeter samples correlated well with unconfined compressive strengths of the laboratory specimens.

Permeability tests were performed on selected samples obtained from Lysimeters 3 and 4. The coefficients of permeability (k) for the lysimeter samples are shown as a function of void ratio (the volume of voids divided by the volume of solids) and compared to permeability coefficients of remolded laboratory samples in Figure 3-16. The coefficient of permeability of the Coolside materials increases as the void ratio
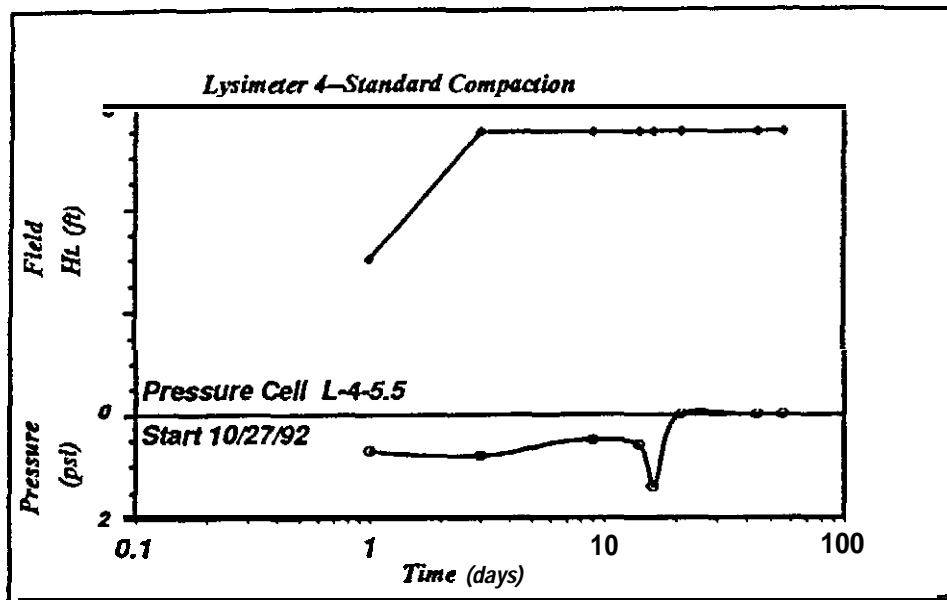
Figure 3-13. Observed side-wall pressure in Lysimeter 4
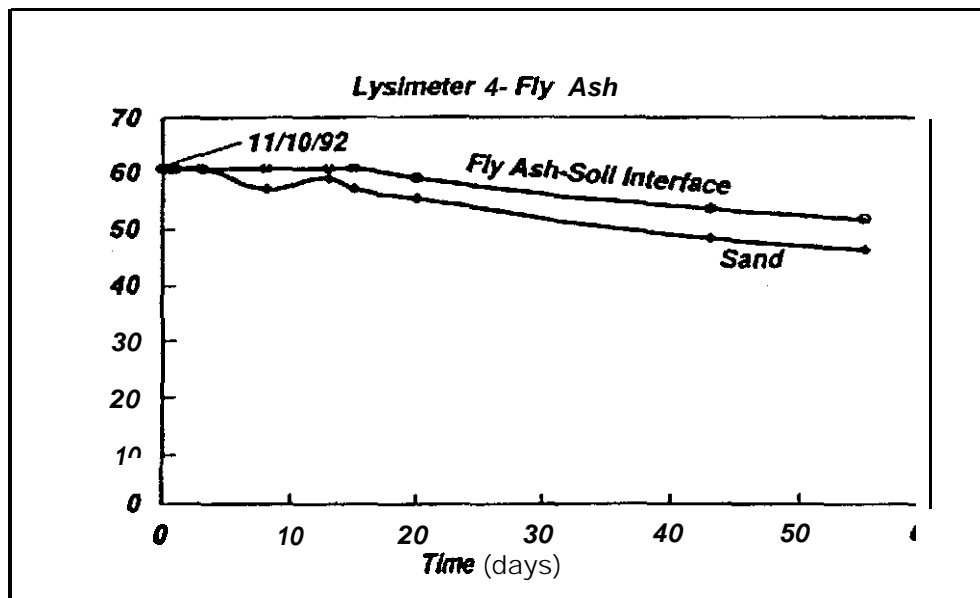
Figure 3-14. Observed temperatures at fly ash-soil and fly ash-sand interfaces

85
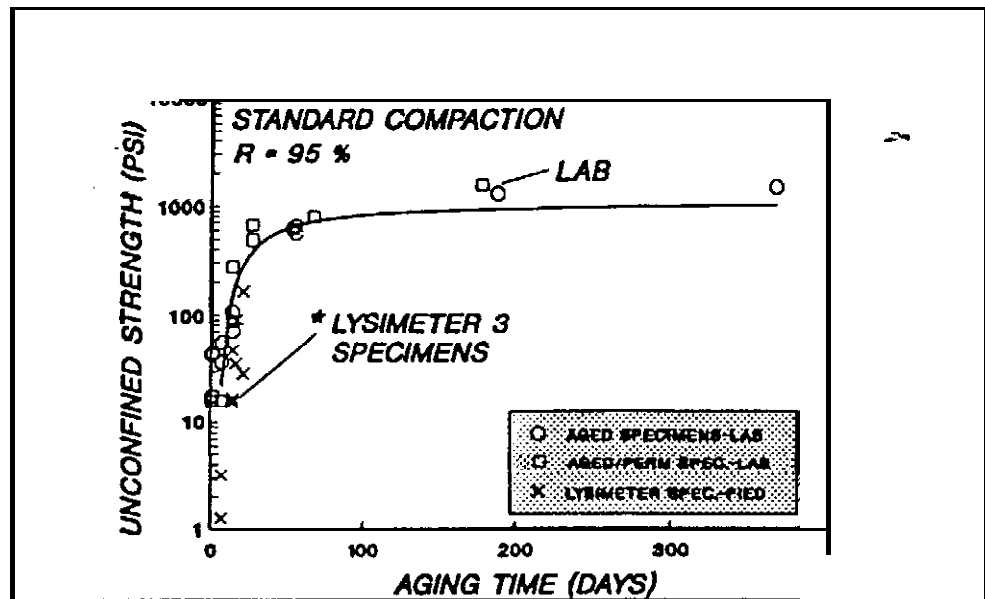
Figure 3-15. Unconfined. compressive strength of laboratory and lysimeter samples
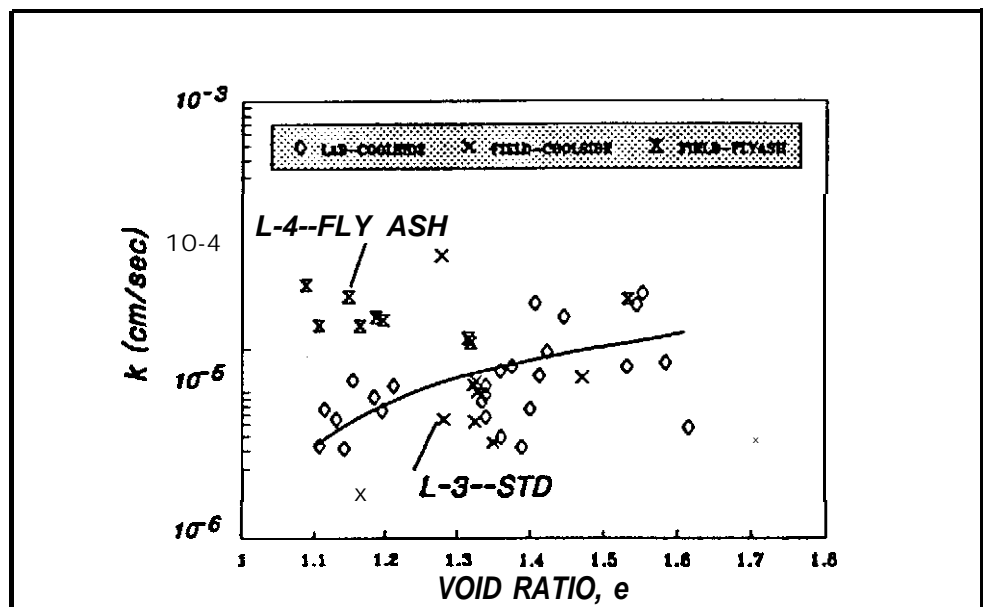
Figure 3-16. Permeability coefficient as a function of void ratio

increases. The tests were performed in a pressurized cell using a back saturation technique and falling head, rising tailwater method.

Field and Laboratory Tests on Specimens Collected after 3.5 Years

About 3.5 years after the Coolside ash had been placed, standard penetration tests (SPT) were performed continuously in Lysimeters 1 (loose state) and 2 (simulated static compaction of 117.2 kPa, or 17 psi). Thin-walled tube samples (7.1- cm, or 2.8-in diameter) were obtained at 0.61-m (2-ft) intervals in those lysimeters. Samples obtained from SPT tests were submitted to the University of Kentucky Center for Applied Energy Research (CAER) for a calibration of the neutron moisture gauges and mineralogical characterization. In Lysimeter 3 (the Coolside material had been compacted to 95% of maximum dry density and optimum moisture content), standard penetration tests were attempted. However, the tests had to be ended when the blows per 0.1 5-m (0.5-ft) interval exceeded 50 at the 0.91 to 1.07-m (3.0 to 3.5 ft) interval. Subsequently, core samples were obtained. Portions of the core sample were submitted to the CAER for mineralogical characterization. Results of standard penetration tests are shown in Table 3-2.

Table 3-2. Results of standard penetration tests

Lysimeter Number	Depth (feet)	*Blows per 0.5 foot	Types of Material	Standard Penetration Resistance (blows per foot)
1	0.0-2.0 2.0- 4.0 4.0-6.0 6.0-8.0 8.0-10.0	0/2/3 5/10/11/11 10/8/1 1/1 4 7/6/6/1 6 715/3/3	Soil Coolside Coolside Coolside Sand	2 11 12 11 **3**
2	0.0-2.0 2.0- 4.0 4.0-6.0 6 . 0 - 8 . 0 8.0-10.0	0/1/1/5 16/19/16/17/ 12/1 7/19/16 10/15/15/11/ 8/7/4/4	Soil Coolside Coolside Coolside Sand	3 16 18 13 4
3	0.0-2.0 2.0-4.0 #0.33(4 in.) Foot penetration	10101112 25/38/50#	Soil Coolside	1 Refusal

One **blow is a 140-pound weight free falling 30 inches.**
 # Test terminated-50 blows for less than 0.5 foot penetration is considered refusal during SPT testing.

In Lysimeter 4 (fly ash), attempts were made to obtain thin-walled tube samples. These efforts were unsuccessful because there was not enough cohesion between the fly ash and the sampling tube to retain the sample in the tube. Due to the soft nature of the fly ash, Dutch cone penetration tests were performed to obtain strength parameters. Efforts to perform cone penetration in Lysimeters 1, 2, and 3 were unsuccessful because the Coolside material *was too hard.* Results of field and laboratory tests performed on the in situ material and field specimens are summarized in Tables 3-3, 3-4, and 3-5, respectively, for Lysimeters 1, 2, and 3. Dutch cone results for Lysimeter 4 are summarized in Table 3-6.

Table 3-3. Field and laboratory results of tests performed on Coolside material in Lysimeter 1.

Depth (feet)	Moisture Content (percent)	Dry Density (lbs/ft^3)	Permeability (crn/see)	Unconfined Strength (psi)
2.0- 2.5	72.42			
2.5'- 3.5'	70.08			
3.5' - 4.0'	82.96			
4.0- 5.0	99.72			
5.0-5.5'	97.37	44.60	4.05 x 10"4	7.1
5.5-6.0'	64.80		3.96 x 10"5	
6.75'-7.25'	81.04	53.04	2.12 X10"^{5}	41.1
● Average	81.20	48.82	1 .55x 10"4	24.1

The average moisture content and dry density of Coo/side material in Lysimeter 1 at the time of filling was 37.5 percent moisture and 44.1 lbs/ft^3, respectively.

Unconfined strengths of specimens obtained from Lysimeters 1, 2, and 3 are compared in Figure 3-17. While the unconfined strength of the material in Lysimeter 1 only averaged about 542.6 kPa (24 lbs/in^2), the strength of specimens from Lysimeter 2 averaged about 1116.3 kPa (162 lbs/in^2), or almost seven times larger than strengths of Lysimeter 1 specimens.
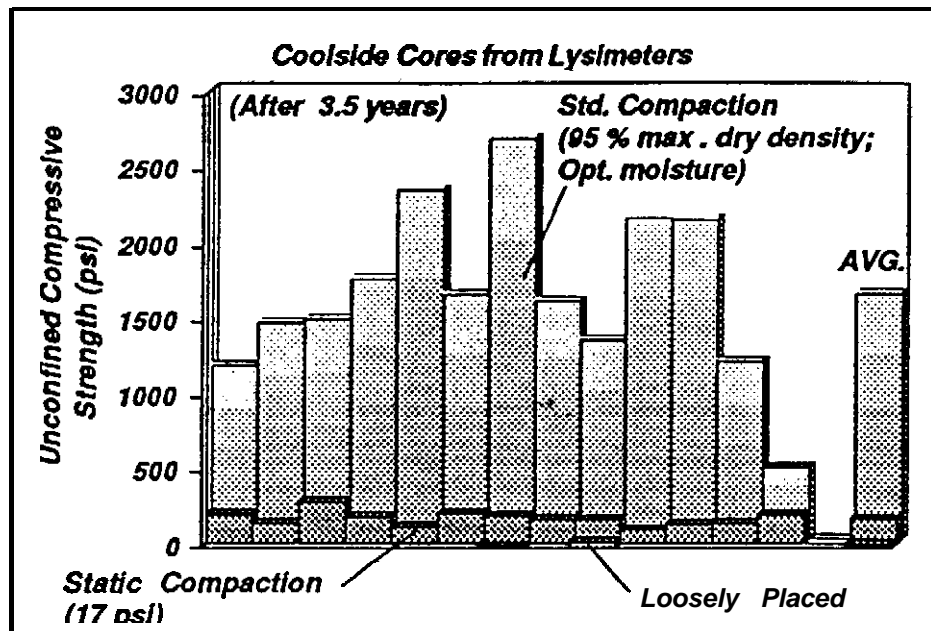
Figure 3-17. Comparisons of unconfined compressive strengths of cored specimens from Lysimeters 1,2, and 3
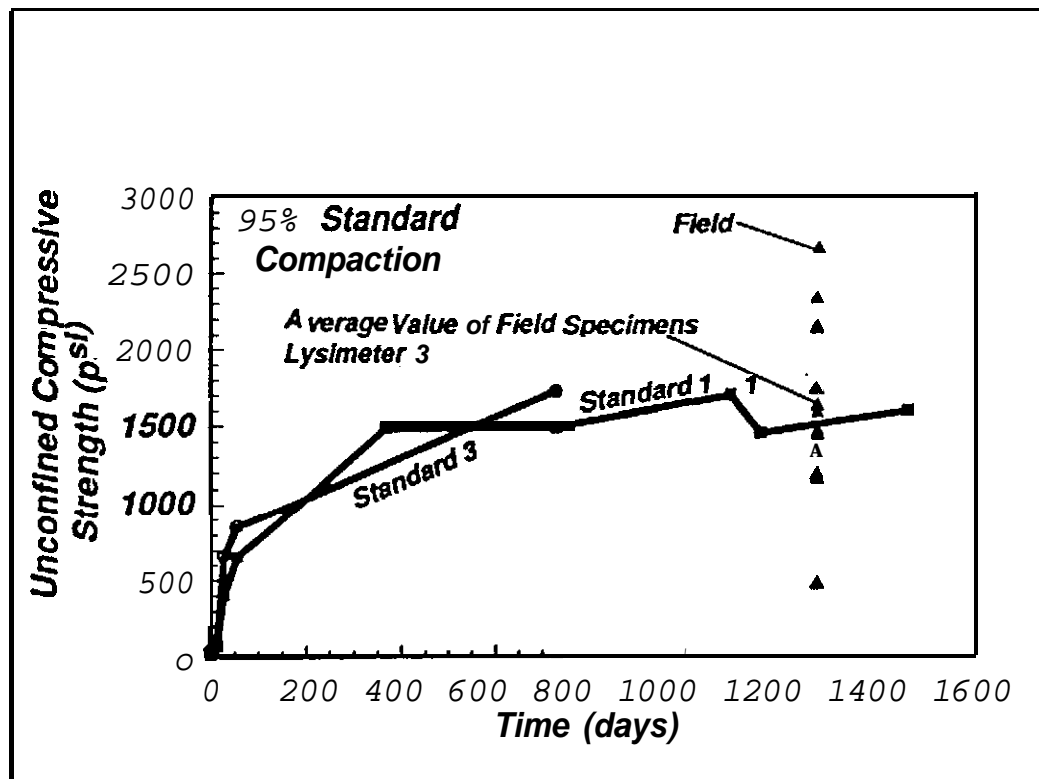
Figure 3-18. Comparisons of the coefficients of permeability of cored specimens of Lysimeters 1, 2, and 3

Table 3-4. Field and laboratory results of tests performed on Coolside material of Lysimeter 2.

Depth (in.)	Moisture Content (percent)	Dry Density. (lbs/ft^3)	Permeability (cm/sec)	Unconfined Strength (psi)
24-29	60.99	53.60	2.22×10^4	192.0
29-34	86.75	45.01	5.67×10^{-4}	130.9
34-39	74.13	50.55	2.35×10^{-4}	274.0
39-44	89.01	45.13	3.63×10^{-4}	175.4
44-48	104.05	41.06	3.75×10^{-4}	109.5
48-56	98.32	44.06	$1,19 \times 10^{-4}$	194.1
56-63	86.13	47.42	3.25×10^{-4}	180.9
78-86	76.16	49.70	1.88×10^{-4}	157.6
86-92	84.35	44.79	1.70×103	154.2
92-97	94.46	43.57	5.22×10^{-4}	91.1
97-103	97.99	44.80	2.63×10^4	123.6
103-108	97.17	43.85	4.20×10^{-4}	129.5
108-114	76.83	49.89	6.89×10^4	188.9
Average	86.64	46.42	4.61×10^4	161.7

Sample from 63 to 78 inches was not recovered.
The average moisture content and dry density of Coolside material in Lysimeter 2 at the time of filling was 38.9 percent moisture and 49.2 lbs.ft^3, respectively.

Table 3-5. Field and laboratory results of tests performed on Coolside material of Lysimeter 3.

Depth (in.)	Moisture Content (percent)	Dry Density (lbs/ft^3)	Permeability (cm/see).........(psi)	Unconfined Strength
24-29	48.90	69.51	9.16×10^{-8}	1153.6
47-53	46.18	68.85	7.91×10^{-6}	1436,0
55-59	64.46	60.34	4.76×10^{-6}	1457.6
59-63	47.34	68.09	1.56×10^{-7}	1728.4
63-69	42.05	73.44	8.23×10^{-8}	2319.6
69-73	43.20	72.61	$1,98 \times 10^{-7}$	1619.4
84-88	41.24	74.47	7.86×10^{9}	2654.8
88-90	56.25	65.69	7.66×10^{-7}	1578,9
91-94	52.48	67.41	2.18×10^{-6}	1319.5
94-97	49.15	69.21	$4.34 \times 10{-7}$	2138.4
97-101	39,63	74.54	7.39×10^{9}	2130.0
101-105	59.16	62.97	4.89×10^{-7}	1179.0
109-113	75.96	54.66	1.17×10^{-5}	467.0
'Average	51.23	67.83	2.20×10^{-6}	1629.4

*The average moisture content and dry density of Coo/side material in Lysimeter 3 at the time of filling was 37.0 percent moisture and 66.2 lbs.ft^3, respectively.

Table 3-6. Results obtained from Dutch Cone Penetration Testing of the Fly Ash in Lysimeter 4.

Depth (m)	Cone (Kg/cm^2)	Cone + Sleeve (Kg/cm^2)	
0.0- 0.1	4.5	5.0	
0.1 -0.2	4.5	5.0	
0.2- 0.3	3.0	8.0	SOIL
0.3- 0.4	4,0	6.0	
0.4- 0.5	2.5		
0.5- 0.6	7.0	12.0	
0.6- 0.7	8.5	13.0	
0.7- 0.8	7.0	11.0	
0.8- 0,9	5.5	7.0	
0.9- 1.0	6.0	9.0	
1,0- 1.1	8.0	12.0	
1.1 -1.2	6.0	9.0	
1.2- 1.3	4.0	8.0	
1.3- 1.4	4.0	9.5	
1.4- 1.5	3,5	5.0	FLY ASH
1.5- 1.6	4.0	5.5	
1.6- 1,7	5,5	6.5	
1.7- 1.8	2.5	4.0	
1.8- 1.9	1.0	3.0	
1.9- 2.0	0.5	1.5	
2.0- 2.1	0.5	1.0	
2.1 -2.2	0.5	1.0	
2.2- 2.3	1.0	1.5	
2.3- 2.4	0.5	0.5	
2.4- 2.5	2.0		
2.5- 2.6	4.0	7.0	
2.6- 2.7	13.0	18.0	SAND

However, the average strength of the specimens from Lysimeter 3 was 11 ,225.5kPa (1629 lbs/in^2), or a strength that was about ten times the average strength obtained for the specimens from Lysimeter 2. Hence, compacting the Coolside to 95% of maximum

dry density (ASTM D 698) produced strengths that were much larger than strengths that would be produced from a tracked dozer. The strengths of the Lysimeter 3 specimens are similar to those that would be obtained from a low-strength concretes.

Unconfined strengths obtained for laboratory specimens compacted to 95% of maximum dry density and optimum moisture content obtained from standard compaction (ASTM D 698) are compared in Figure 3-18 to the unconfined strengths of the field specimens from Lysimeter 3. Although the unconfined strengths of the specimens from lysimeter ranged from 3,218.1 kPa to 18,294 kPa (467 to 2654.8 lbs/in^2), the average value was about 11,225 kPa (1629 lbs/in^2). This strength was very similar to laboratory specimens remolded in the laboratory to the same conditions.

Coefficients of permeability of Coolside specimens from Lysimeters 1, 2, and 3 are shown in Figure 3-19 as a function of dry density. As the dry density increases, the coefficient of permeability decreases. A good correlation exists between the permeability coefficient and dry density. As the compactive effort approaches that used in standard compaction, the coefficient of permeability approaches a value of 1 xl 0^{-7} cm/sec.

Coefficients of permeability of the field specimens and laboratory specimens are compared and shown as a function of dry density in Figure 3-20. In both instances, the coefficients of both types of specimens decrease as the dry density increases. The coefficients of permeability of the field and laboratory specimens are very similar. As shown in Figure 3-21, the coefficient of permeability of the cored field specimens increases as the void ratio increases. The coefficient approaches a value of 1 x 10^{-7} cm/sec when the void ratio approaches a value of approximately 0.8.
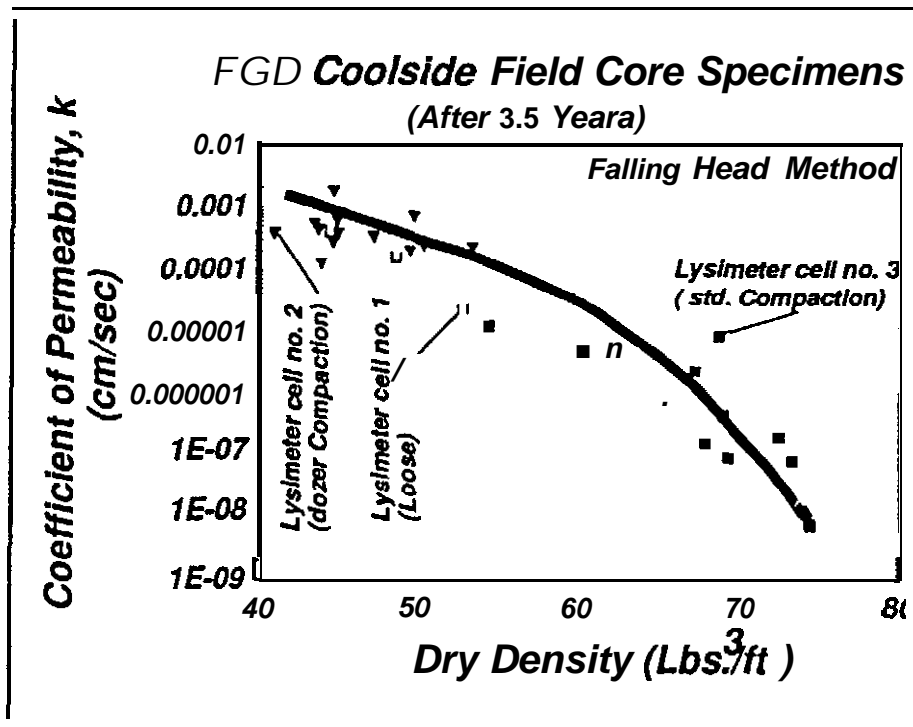
Figure *3-19.* Comparisons of the coefficients of permeability of cored specimens of Lysimeters 1, 2, and 3
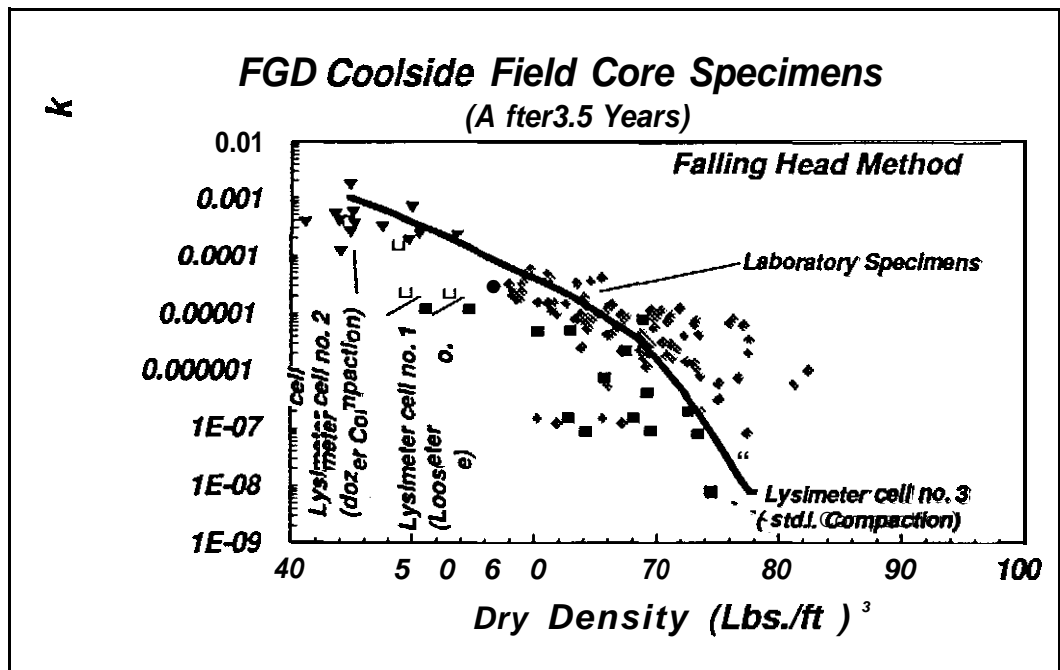
Figure 3-20. Comparison of the relationship between the coefficients of permeability of core specimens from Lysimeters 1, 2, and 3 and laboratory specimens and dry density
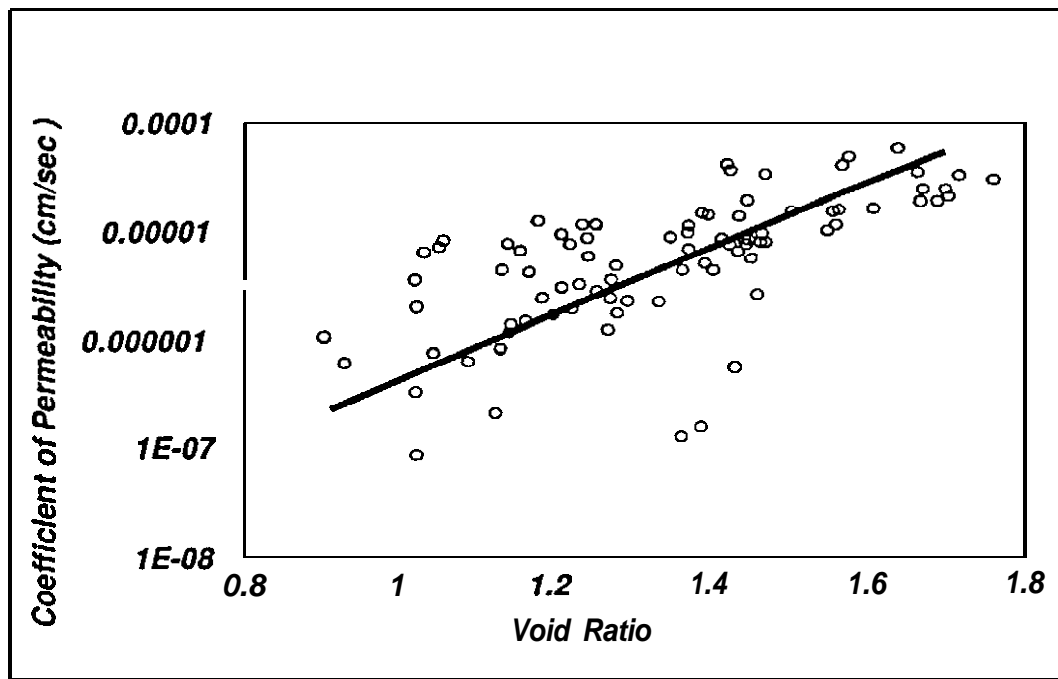
Figure *3-21.* Coefficients of permeability of cored specimens from Lysimeters 1, 2, and 3 as a function of void ratio
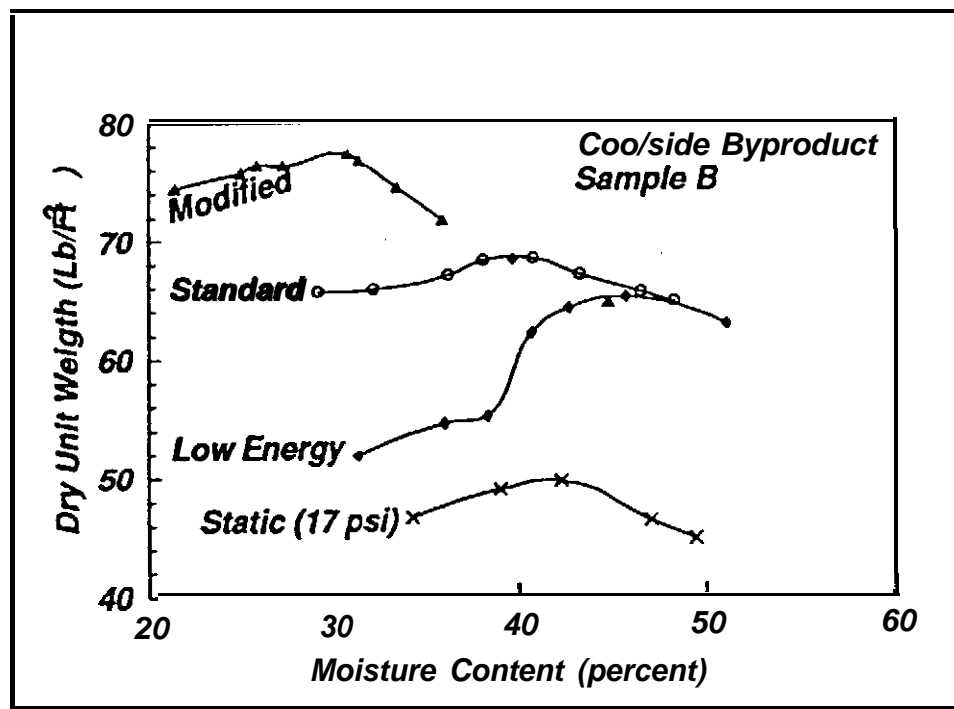
Figure 3-22. Moisture-density relations for different compactive energies

Geotechnical Laboratory Test Program

Index Properties and Classification

Geotechnical index and classification tests were performed in accordance with ASTM procedures. These tests were performed to characterize and classify the Coolside material. ASTM test designations are summarized in Table 3-7. The index tests consisted of sample preparation, moisture content, moisture-density relationships, liquid and plastic limits, particle size analysis, specific gravity, and classification. The Coolside material was also classified according to the Association of American State Highway Transportation Officials (AASHTO).

Index properties and classifications of the Coolside byproduct are shown in Table 3-8. Samples identified as CS-I 040, CS-1 050, CS-388, and CS-397 were obtained from runs 1 and 3 at the Ohio Edison coal-fired power plant at Lorain, Ohio. A sample identified as CS-2 was obtained from CONSOL's Coolside pilot plant at their research facility in Library, Pennsylvania. The different samples had essentially the same properties, All of the specimens were nonplastic (NP). That is, none of the materials, when initially wetted, exhibited cohesion. All the materials passed the U.S. 200 sieve and 95 percent of the materials were finer (by weight) than the U.S. sieve number 200. Specific gravity of the materials ranged from 2.51 to 2.55. Based on the Unified Classification System, the Coolside materials were classified as ML (silt). According to the ASSHTO Classification System, the materials were classified as A-4.

Moisture-Density Relations

Laboratory compaction tests were performed at different compaction energies to examine the relationships between dry density and compaction effort, and optimum moisture content and compaction energy. These tests were performed at modified

w METHOD	TEST PROCEDURE
SAMPLE PREPARATION	ASTM D 421
MOISTURE CONTENT	AS7M D 2216
MOISTURE-DENSITY RELATIONHIPS	
MODIFIED	ASTM D 1557
STANDARD	ASTM D 698
LOWENERGY	(1.S44.8 HAMMER; 1-17 DROP; 3 LAYERS/15 BLOWS PER LAYER
ATTERBERG :	
LIQUID LIMIT	ASTM D 4318
PLASTIC LIMIT	ASTM D 4318
PARTICLE SIZE:	
SIEVE ANALYSIS	ASTM D422
HYDROMETER ANALYSIS	ASTM D 422
SPECIFIC GRAVITY	ASTM ASTM D 854
CLASSIFICATION	ASTM D2487- S5

Table 3-7. Index properties test procedures

SAMPLE NUMBER	LIQUID LIMIT (%)	PLASTIC LIMIT (%)	GRAIN-SIZE ANALYSIS % FINER THAN: NO. 10	NO. 200	SPECIFIC GRAVITY	CLASSIFICATION UNIFIED	AASHTO
CS-2	NP	NP	100	95	"254	ML	A-4(0)
CS-388	NP	NP	100	95	251	ML	A-4(0)
CS-397	NP	NP	100	95	252	ML	A-4(0)
CS-104O	NP	NP	100	95	255	ML	ii-I(o)
CS-105J3	NP	NP	100	95	251	ML	A-4(0)

Table 3-8. Index properties and geotechnical classification of the Cool side byproduct

compaction (ASTM D 1557), standard compaction (ASTM D 698), and a low energy compaction method (Hopkins, 1988). Compaction energies were 326,754, 71,885, and 14,450 m-kg/m^3 (or 56,246, 12,374, and 2,025 ft-lb/ft^3). Besides the three dynamic compaction energies, compaction tests were performed using static compaction. These tests were performed to simulate the compaction action of the tracks of a Caterpillar7D9L track-type tractor (Caterpillar Performance Handbook, 1981). The static compaction tests were performed at a stress of 117 kPa (17 psi) --the contact stress of the tracks of this equipment. Specimens were molded statically in a testing machine using this stress.

Typical compaction test results obtained for the Coolside byproduct, identified as CS-3, are illustrated in Figure 3-22. Sample CS-3 was a composite sample from the Run number 3 series of the Edgewater plant in Lorain, Ohio. Identical results --not shown-- were obtained for a Coolside byproduct identified as sample CS-I. As the compaction energy increases, the maximum dry density increases and the optimum moisture content decreases. The maximum dry density ranges from 7.79 kN/m^3 (49.5 lbs/ft^3) at static compaction to 12.10 kN/m^3 (76.5 lbs/ft^3) at modified compaction. The dry density of the Coolside material in a loose state is 5.72 kN/m^3 (36.5 lbs/ft^3). Consequently, the maximum dry density obtained from the static compaction is only about 36% greater than the loose state dry density.

Variation of the maximum dry density of sample CS-3 with compaction energy is illustrated in Figure 3-23. The maximum dry density (10.80 kN/m^3) of the Coolside material is about 1.9 times the dry density of the material in a loose state. However, the maximum dry density at modified compaction is only about 1.12 times the maximum dry density obtained from standard compaction. Therefore, for a fourfold increase in compaction energy above the standard compaction energy, the dry density increases only about 120/.. Consequently, efforts to compact the Coolside material to a dry density greater than the maximum dry density obtained from standard compaction
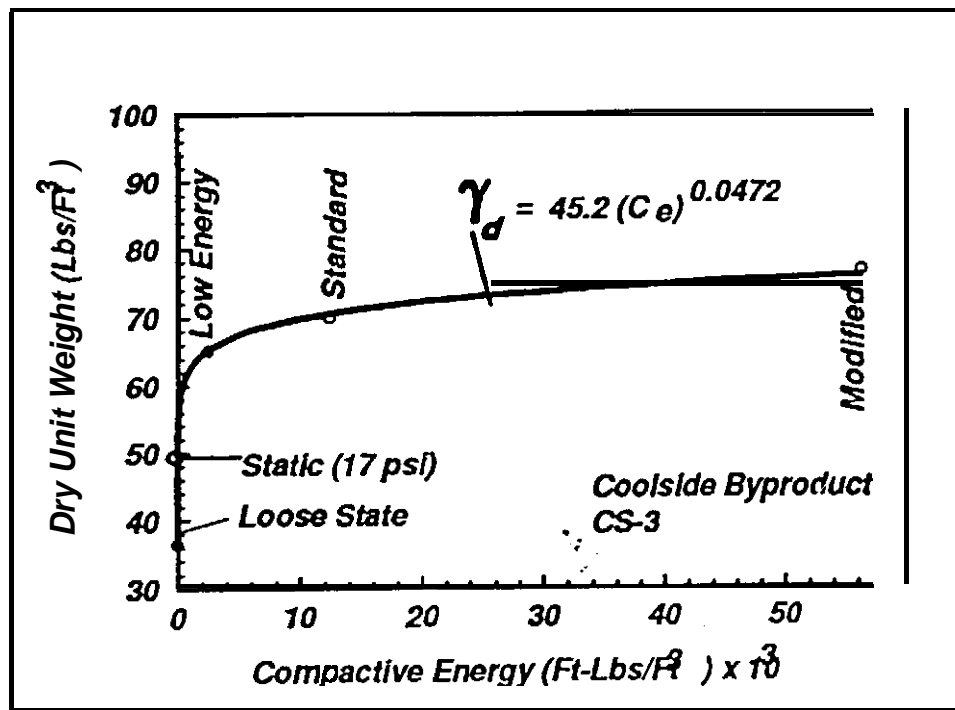
Figure 3-23. Variation of the maximum dry density with compactive energy
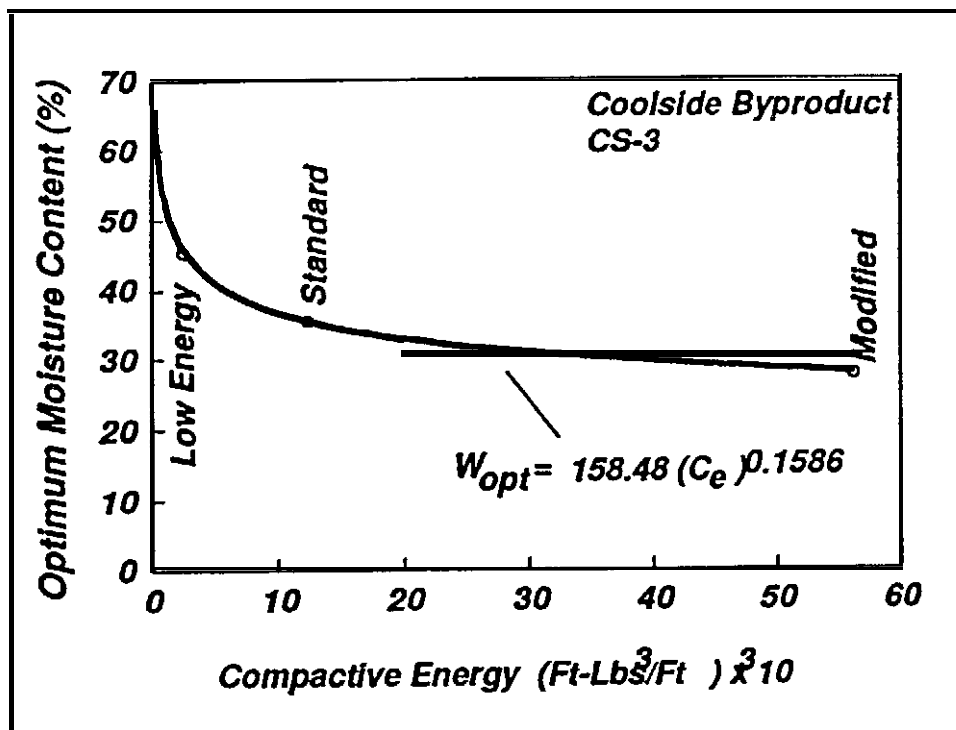
Figure 3-24. Variation of optimum moisture content with compactive energy

100

would probably be uneconomical. However, the compaction energy selected would depend on the specific site variables, such as land cost, cost of compaction equipment and operation, haul distances, and availability of land for disposal. Economic evaluation of those factors would be required at a given site to select the most economical compaction energy.

Variation of optimum moisture content and compaction energy for sample CS-3 is illustrated in Figure 3-24. At standard compaction, the optimum moisture content is about 36.5?4.. Compaction of the Coolside material could pose a problem when the water content is greater than the optimum moisture content. Because the Coolside byproduct contains a large silt content, the material may liquefy under compaction stresses when the moisture content is greater than optimum moisture content.

Recommendations

Based on the results of index tests, *95* to 1007. of maximum dry density obtained from standard compaction tests may be achieved using sheep foot rollers. Compacted lift thickness should be about 15.24 cm (6 in) and 4 to 6 passes of the compaction rollers may be required to achieve a specified compactive state. Foot contact stress should range between 1380 and 2760 kPa (200 to 400 psi). A self-propelled Sheep foot roller with a blade may be desirable so that the material could be spread and compacted simultaneously. Alternatively, rubber tire rollers may be used. Here, the lift thickness of 25.4 cm (1 O in) is indicated. About 4 to 6 passes of the rollers are required. Large size tires with inflation pressures ranging from 276 to 345 kPa are desirable to avoid shearing and rutting failures. Field trials at a given site should be performed to ensure the proper selection of compaction equipment and to decide desired field density states. If standard compaction is selected as the compactive state, the moisture content should generally not exceed the optimum moisture. Otherwise, the silty material may liquefy under the stress imposed by construction and compaction

equipment. A short curing period of the compacted material will improve the bearing capacity of the material since the material gains strength with increasing time. However, the total strength gain depends partly on the energy used to compact the material.

Structural Properties Tests

Remolding Procedure. In the design of untreated and chemically treated subgrades, geotechnical laboratory tests, such as triaxial tests and permeability tests, should be performed on specimens of the materials that closely simulate the compactive state of the materials as they may exist in an engineered subgrade or landfill. The laboratory compaction test (Hopkins et al, 1988 and Hopkins and Beckham, 1993) should produce specimens for physical properties tests that duplicate the anticipated, or specified, field dry density and moisture content. For example, if field compaction specifications require that a subgrade be compacted to 95 percent of maximum dry density and 2 percent of optimum moisture content (ASTM D 698), then the laboratory compaction procedure should produce specimens that duplicate, as practically as possible, those target values of dry density and moisture content.

Moreover, since the maximum dry density and optimum moisture content of a soil may change as a chemical admixture is added, then it is essential that the remolding procedure account for such a change. Otherwise, the physical properties as measured from laboratory tests may differ significantly from those that may exist in the completed engineered subgrade. Additionally, when chemical admixtures are used, a method is needed to decide the most economical amount, or percentage, of a chemical admixture to add to the soil subgrade to obtain some desired strength. The procedures developed during this study for compacting specimens that conform to specified values of dry density and optimum content and for determining the optimum percentage of a chemical admixture are described below. The procedure is applicable to a variety of

fine-grained materials, such as soils, byproducts, and mixtures of byproducts and soils and chemical admixtures and soils.

Equations. Equations used in the proposed procedure to compact specimens to selected, or target, values of dry density and moisture content are described below. When byproducts, or other chemical admixtures, are added to soils, the matrix of the mixture consists of air, water, soil particles, and admixture particles. To determine the weights of soil solids (W_s), water (W_w), and a chemical admixture (W_p), that must be mixed to form a specimen of a known volume (V), dry density (γ_d), and moisture content (w_t), the phase diagram of Figure 3-9, maybe used in formulating the necessary equations.

By definition, the total density ((t), is

$$\gamma_t = WN = (W_w + W_s + W_p)/V. \tag{1}$$

The target moisture content, w_t, is, by definition

$$w_t = W_w/(W_s + W_p). \tag{2}$$

By definition, the dry weight of an admixture is expressed as a percentage, P, of the dry weight of soil particles, or

$$W_p = PW_s. \tag{3}$$

Solving for W_w in Equation 2 and inserting this quantity, and the quantity given by Equation 3, into Equation 1, then the dry weight of soil, W_s, is

$$W_s = \gamma_t V/(1+w_t)(1+P). \tag{4}$$

The air-dried weight, W_{ad}, is related to the oven-dried weight, W_s, (or weight of soil solids) by the expression:

$$W_{ad} = W_s (1+w_{hs}), \tag{5}$$

103

where w_{hs} is the (hydroscopic) moisture content existing in the soil at the time of mixing. The total density is related to the dry density by the expression,

$$\gamma_t = \gamma_d(1 + w_t).$$ (6)

Substituting Equations 4 and 6 into Equation 5, then

$$W_{ad} = (_dV(1+w_{hs})/(1+P)$$ (7)

Equation 7 gives the weight of air-dried soil that must be added to form the specimen of a known volume, V, dry density, $_d$, and moisture content, w_I. The air-dried weight, W_{pad}, of chemical admixture maybe computed from the following expression.

$$W_{pad} = W_p(1 + w_{hp}) = PW_s(1+w_{hp}),$$ (8)

where w_{hp} is the hydroscopic moisture content of the air-dried (or moisture content at the time of mixing) admixture. Equation 8 gives the weight of an air-dried admixture that must be added to the mixture.

The amount of water (W_{wadd}), which must be added to the mixture depends on the amounts of moisture (or hydroscopic moisture content) existing in the soil and admixture at the time of mixing. If the materials have been air-dried, then the materials may contain only hydroscopic moisture. Hydroscopic moisture content (w_{hs}), of the soil, and w_{hp}, of the admixture must be determined from laboratory tests. The total amount of water required to mix the materials and form the specimen of a known volume and selected dry density may be determined from Equations 1 and 2, or,

$$W_w = w_t W_s(1+P).$$ (9)

From the phase diagram, Figure 3-25, the amount of water existing in the soil before mixing (by definition) is,

104
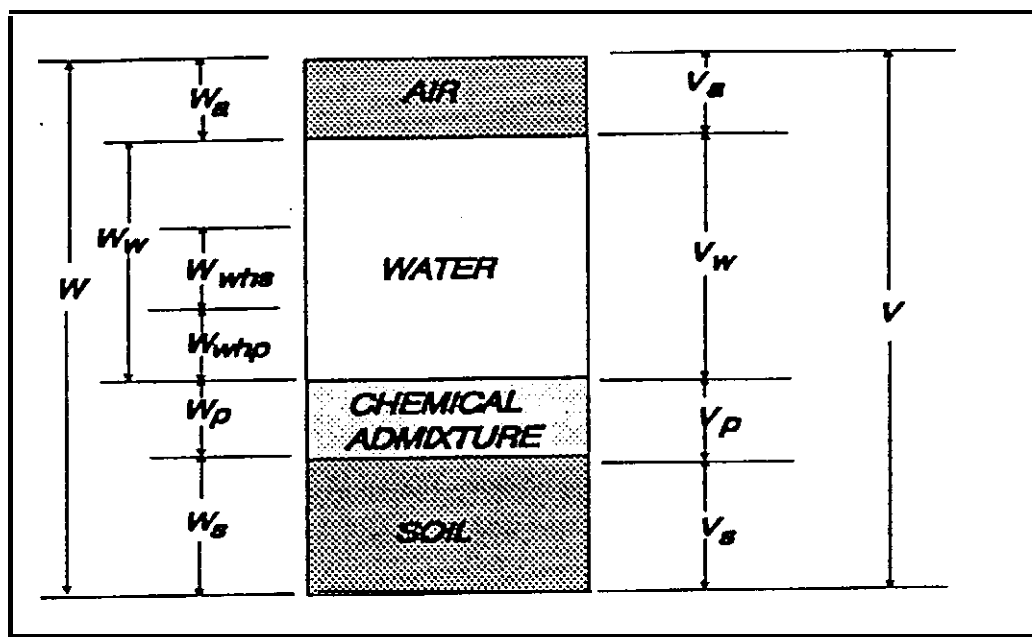
Figure **3-25.** Phase diagram
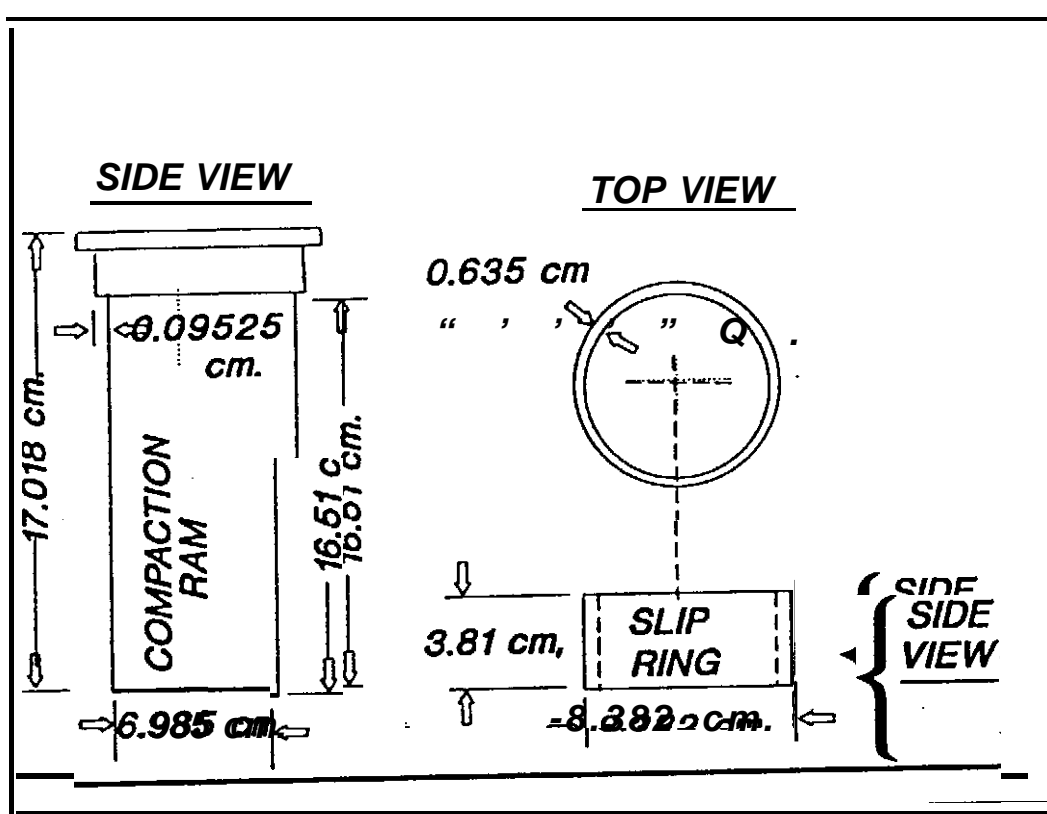
Figure **3-26.** Schematic of the ram and slip rings used to compact specimens

$$W_{whs} = w_{hs}W_s,$$ **(lo)**

and in the admixture,

$$W_{whp} = w_{hp}W_p = w_{hp}PW_s.$$ (11)

The amount of water to be added at the time of mixing (Figure 3-25) is

$$W_{wadd} = W_w - W_{whs} - W_{whp}.$$ **(12)**

Substituting the expressions given by Equations 8, 9, and 10 into Equation 11, then

$$W_{wadd} = W_s [P(w_t\text{-}w_{hp})+w_t\text{-}w_{hs}].$$ (13)

A spreadsheet computer program was developed to compute the weights of air-dried soil, water, and admixture needed to compact a specimen of a known volume and selected values of dry density and moisture content.

Compaction Equipment and Method. Equipment required to compact a specimen includes some type of apparatus, or other means, for mixing the specimen, an electronic scale with a resolution of 0.01 grams, a split-type mold, and specially-designed ram and slip rings. Although the split-type mold for compacting the specimens may be designed for any selected dimensions, a type of mold that is convenient for forming specimens for triaxial or permeability testing measures 20.32 cm (8 in height and 7.11 cm (2.8 in) in diameter. Specimens are compacted to a height of 15.24 cm (6 inches). The inside diameter of this mold is the same as the diameter (7. 11 cm) of a commonly-used, thin-walled, field sampling tube. Another suitable size of a split-type mold for laboratory compaction purposes measures 15.24 cm in height and 5.08 cm (2 inches) in diameter. Specimens are compacted to a height of 11.43 (4.5 inches). By using a split-type mold, the specimen maybe removed from the mold conveniently, the need to extrude the compacted specimen from the mold is avoided, and sample disturbance after compaction is reduced,

The function of the ram and rings, which slip over the ram, is to control the height of each layer of the compacted specimen. In the compaction standard, ASTM D 698, the specimen height is 11.6434 cm (4.584 inches); the specimen is compacted in three layers and each layer is 3.879 cm (1.527 inches) in height. In the proposed compaction procedure, each layer of the specimen is compacted to approximately the same height, or 3.81 cm (1.5 inches). For example, specimens measuring 15.24 cm in height are compacted in four layers but each layer is 3.81 cm in height. A schematic of the ram and slip rings used to compact specimens measuring 15.24 cm in height and 7.11 cm in diameter is illustrated in Figure 3-26. Views of the split mold, rings, and ram are shown in Figure 3-27.

Procedure. The purpose of the compaction procedure is to produce a specimen that has a dry density and a moisture content that are near prescribed, or target, values of dry density and moisture content. For example, if field specifications dictate that a given material must be compacted to 95 percent (or another choice) of maximum dry density obtained from a standard laboratory test, such as ASTM D698, then the target values for remolding the laboratory specimen would be selected according to the field specifications. After developing the specified moisture-dry density curve, target values of dry density and moisture content are selected. When only one material is involved $(P=0)$, Equations 45 and 41 are used to calculate the weight of air-dried material and the volume of water that must be used to remold a specimen of a known (or selected) volume. However, the material does not necessarily have to be air-dried. The only requirement here is that the existing moisture content, w_{hs}, in the material at the time of sampling, must be equal to or less than the selected, target moisture content. After a small sample is obtained to find the existing moisture content of the material, the material may immediately be placed and sealed in a zip-lock plastic bag to prevent any further loss of moisture, The material remains sealed until the time of mixing. Sealing the material in a plastic bag is not necessary when the material is air dried. To mix the sample, the material is placed in a mixing bowl and the amount of water, as determined

from Equation 51, is added to the material. When the specimen to be formed is 15.24 cm in height and 7.11 cm in diameter, the mixed material is divided into four parts of equal weight and stored in zip-lock bags. It is imperative that care is exercised in this portion of the procedure to avoid the loss of material when the material is weighed and transferred to the plastic bags. Normally, the material remains sealed in the plastic bags for about 24 hours before remolding to allow an even distribution of moisture.

After the mellowing period, the specimen is compacted as illustrated in Figure 3-28. The contents of the first bag are placed in the split mold and the ram is hammered down until the collar of the ram rests against the top of the mold. When the collar touches the top of the mold, the first compacted layer is exactly 3.81 cm (1.5 inches) in height, The top of the first layer is scarified and the second bag of material is added to the mold. The first slip ring is slipped over the ram and the second layer is compacted. When the bottom of the first ring touches the top of the mold, the second layer is exactly 3.81 cm. The procedure is repeated for the third and fourth layers, as shown in Figure 3-29, respectively. When the last layer is compacted, the specimen is exactly 15.24 cm in height. During the compaction procedure, the number of blows does not have to be counted because the exact amounts of materials and water are used to form the specimen of a selected dry density, water content, and known volume.

When admixtures, such as a byproduct (Coolside, FBC, etc.) or hydrated lime, are added to soil, chemical reactions may occur. Maximum dry density and optimum moisture content derived from a given type of compaction test depend on the percent of an admixture used in the mix. If this percent of an admixture is known (or assumed), then the maximum dry density and optimum moisture content may be determined using the known percentage. However, if the objective of the testing program is to determine the optimum percent of an admixture, then the testing procedure must be altered because the maximum dry density and optimum moisture content vary with increasing percentage of an admixture. These variations are illustrated, for example, in Figures 3-
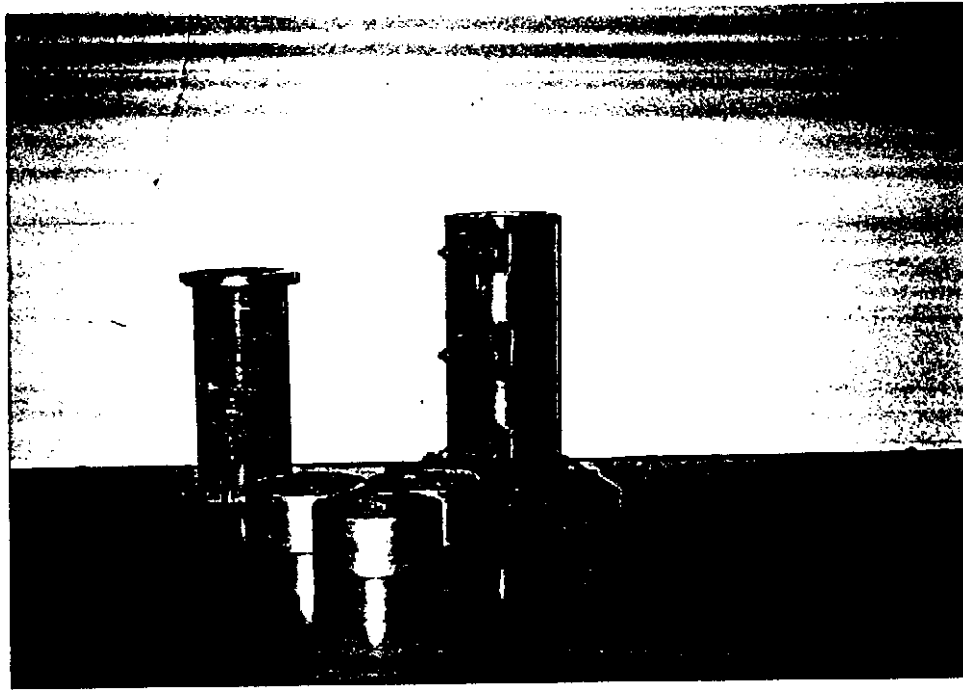
Figure *3-27.* View of the split mold, rings, and ram
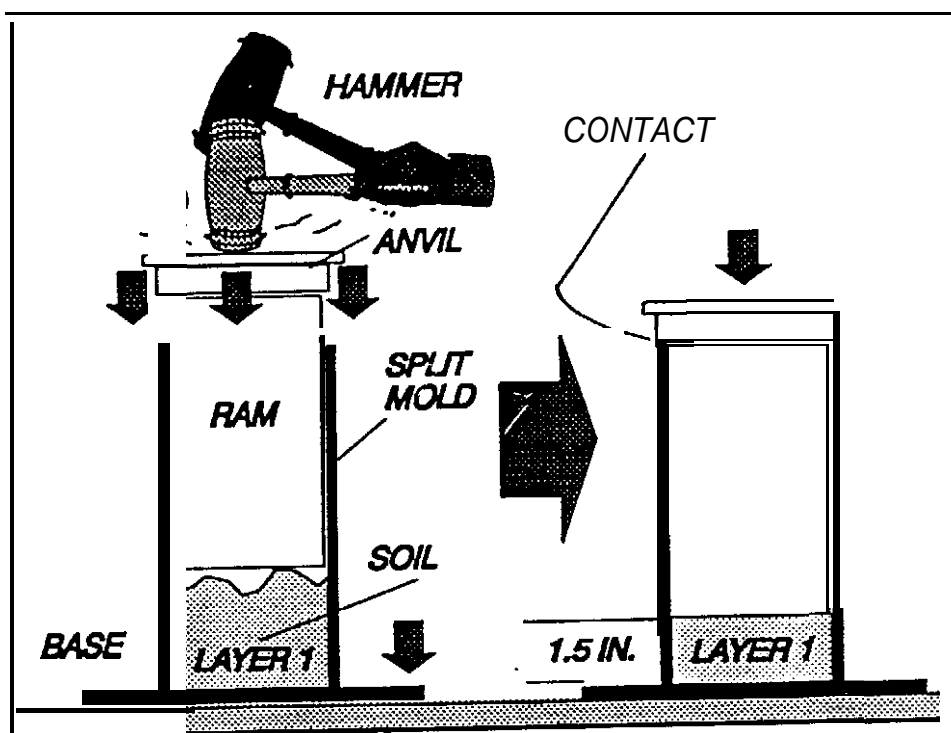
Figure *3-28.* Compaction of a specimen
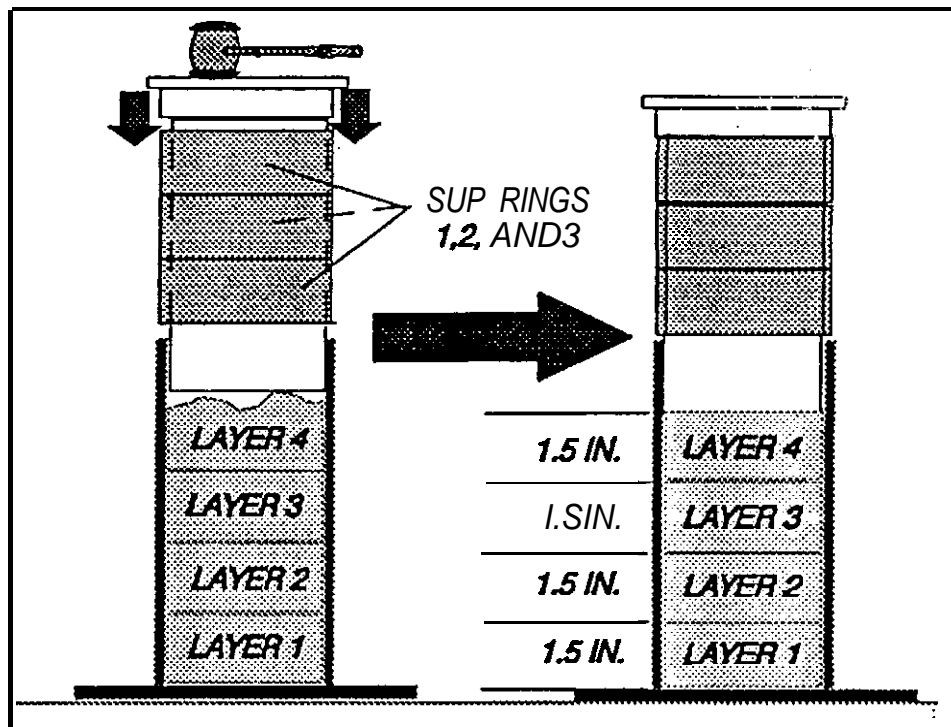
Figure *3-29.* Compaction procedure is repeated for four layers
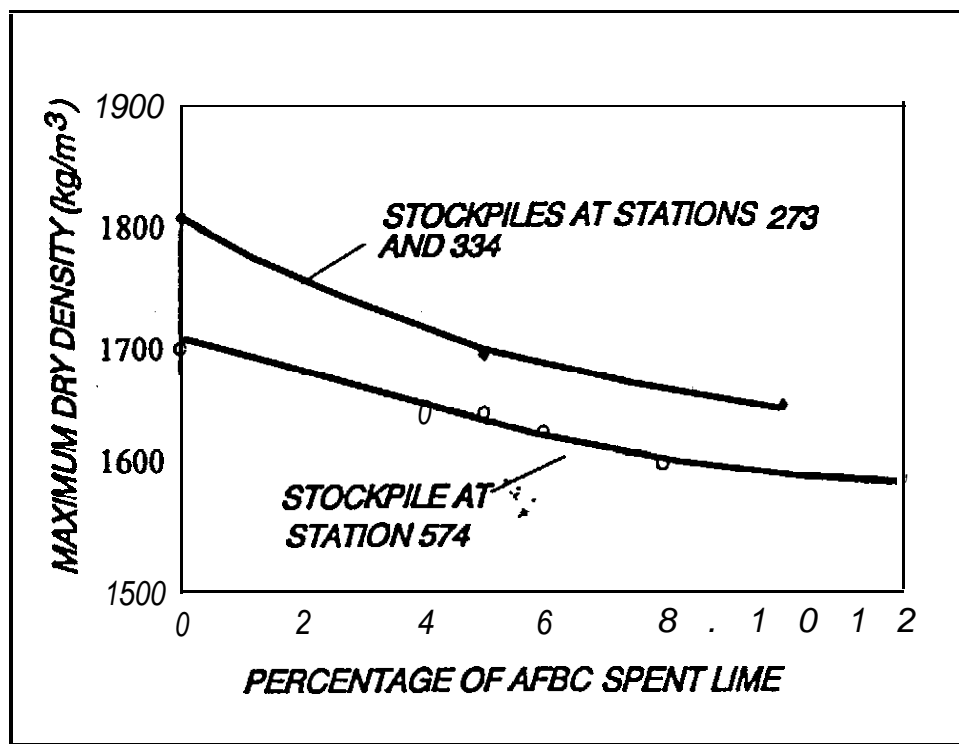
Figure 3-30. Variation of the maximum dry density with the percentage of AFBC spent lime
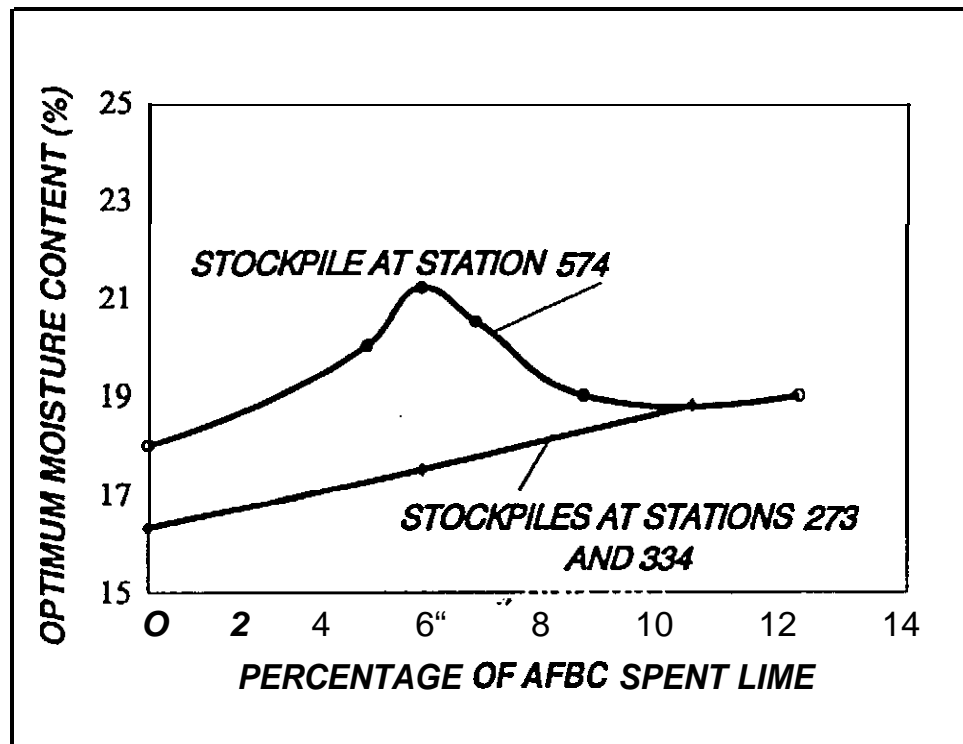
Figure 3-31. Variation of optimum moisture content with the percentage of AFBC spent lime
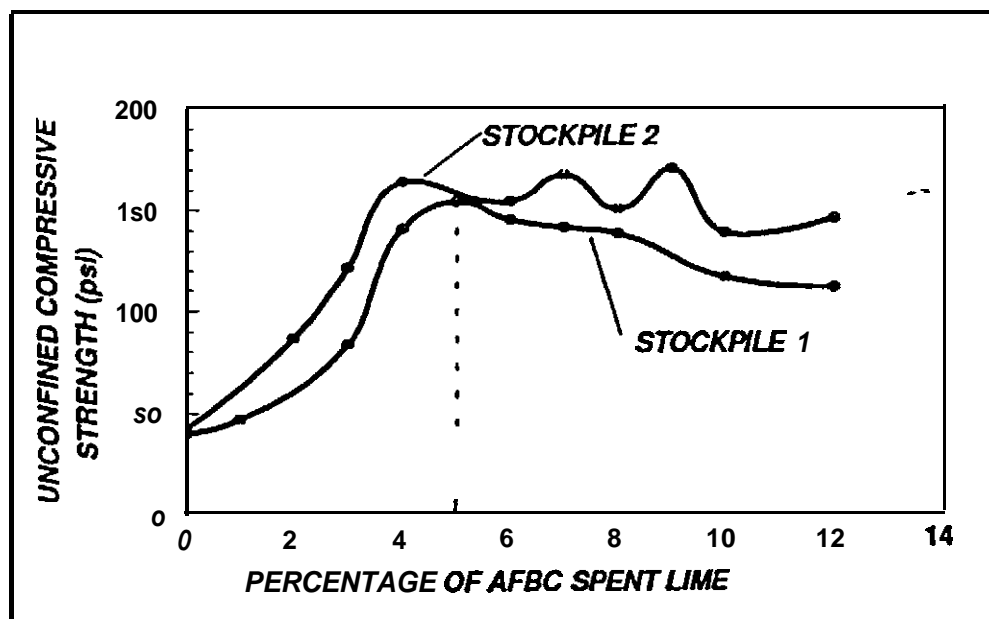
Figure 3-32. Results of unconfined compressive strength tests performed on different remolded specimens of AFBC byproduct-soil mixtures

30 and 3-31. This example involves mixtures of an AFBC byproduct (or admixtures) and a clayey soil. As the percent of AFBC byproduct increases, the maximum dry density decreases and the optimum moisture content increases. Therefore, to account for these variations, three to five compaction tests may need to be performed on the soil-admixture mixtures using different, selected percentages.

The percent of admixture is ranged from a low percent to a high percent. Since the objective of this testing program was to determine the maximum strength (unconfined compressive strength) and corresponding optimum percent of an AFBC byproduct, several compaction tests were performed on mixtures containing different percentages. Unconfined compressive tests were performed on specimens remolded to selected percentages of the AFBC byproduct. For a selected percent of an AFBC byproduct, the maximum dry density (γ_d) and optimum moisture contents were selected from the curves shown in Figures 3-30 and 3-31. Equations 7 through 13 are used to calculate the amounts of admixture, soil, and water that must be mixed to form a specimen of a known dry density, moisture content, and volume. Figure 3-32 shows the results of unconfined compressive tests performed on different remolded specimens of AFBC byproduct-soil mixtures. As these data show, the maximum strength occurred at 5 percent.

Statistical Analysis. To determine the reliability of the remolding procedure, actual dry densities and moisture contents obtained from the proposed compaction procedure were compared statistically to target values of dry densities and moisture contents. Seventy cases, which represented a variety of fine-grained soils, and different values of relative compaction, were analyzed. Deviation of the average dry density, or the difference between the actual dry density of the compacted specimen and target dry density, was MI.011 kN/m^3 (0.07 lb/ft^3). Standard deviation wasM.121 kN/m^3 (0.77 lb/ft^3). Deviation of the average moisture content, or the difference between the actual moisture content of the compacted specimen and the target moisture content, was

-0.31 percent. Standard deviation was ± 0.88 percent.

Triaxial Strength **Properties**

The short-and long-term stabilities of geotechnical facilities constructed with, or on, the Coolside byproduct will depend on the shear strength of the Coolside material at different times of aging, since the material has pozzolanic properties. Since construction equipment must operate on the material during construction or during land filling of the material, the initial bearing, or shear strength, is important to insure mobility and efficient operation of construction traffic. A knowledge of the long-term shear strength of the material is vital to maintaining stable structures throughout their useful lives. Results of triaxial and bearing tests are described below. The triaxial testing program consisted of performing, unconsolidated-undrained (UU) triaxial compression tests and unconfined triaxial compression tests (UC). All specimens were remolded to 950/. of standard maximum dry density and optimum moisture content (ASTM D 698). The specimens were aged in sealed containers at room temperature (about $21^{\circ}C$, or $70^{\circ}F$).

Unconsolidated-Undrained (UU) Triaxial Compression Tests. A minimum of three UU-tests (ASTM D 2850) was performed at different cell pressures at a selected curing period. The tests were performed on unsaturated, aged specimens of the Coolside byproduct to observe the effects of aging, or curing, on the total stress parameters, the angle of internal friction, ϕ_u, and cohesion, c.. Generally, confining pressures of 138, 276, and 414 kPa (20, 40, and 60 psi) were used for a given series at a selected aging time. Since the strength changes with aging time--as observed in the first initial testing of the remolded Coolside material--each specimen of a test series (38, 276, and 414 kPa) was tested precisely at the end of the selected aging time. Otherwise, data fits to determine the strength parameters would not have been valid. Variations of the

strength parameters, ϕ_u and c_u, with aging time are shown in Figures 3-33 and 3-34. The strength parameter, c_u, increased from about 62 kPa (one-day aging time) to 466 kPa (21-day aging time). The strength parameter, ϕ_u, increased from about 29.3° (1 - day aging time) to 32.9° (21-day aging time).

Variations of the ϕ- and c-values at each selected curing time are shown in Figures 3-33 and 3-34. In curing and testing the triaxial specimens, each specimen was tested exactly at the end of the selected curing period. Otherwise, the tests of a set would not be valid, since each specimen continued to gain strength as it cured. As shown in Figure 3-33, the internal angle of friction, ϕ, increased slightly as the curing period increased. The $-value increases from about 29 degrees at one day of curing to about 33 degrees when the compacted specimens were cured for 21 days. The relationship between the cohesive component, c, and aging time is shown in Figure 3-34. The c-component increases from about 60 kPa at one day of curing to about 465 kPa at 21 days of curing. Apparently, the cohesive component continues to increase with curing time after 21 days. Specimens could not be tested for longer curing periods because the strengths exceeded the capacity of the triaxial equipment.

Unconfined Compression Tests. Unconfined compression tests (ASTM D 2850) were performed on remolded specimens, which were compacted to different compactive states, to examine the effects of aging on strength. Specimens were compacted to 90, 95, and 100 percent of maximum dry density obtained from a low-energy compaction method, standard compaction, and modified compaction. In each case, the specimens were compacted to optimum moisture content obtained from each compaction method, respectively. Moreover, the unconfined compression tests were performed on specimens that been aged to different curing periods. Each specimen, after remolding, was wrapped in Saran® wrap and stored in PVC cylinders that measured about 6.5 inches (16,5 cm) in height and about 3 inches (7.62 cm) in diameter. Rubber (Shelby-tube) caps were placed on each end of the cylinder and taped. This insured that the

114
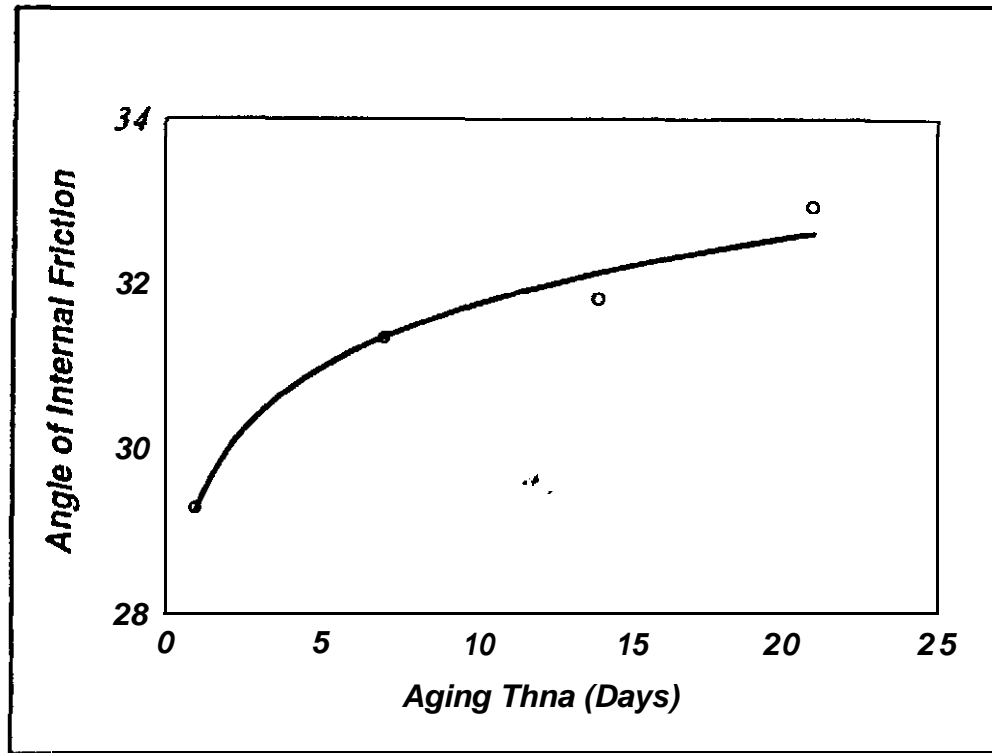
Figure *3-33.* Variation of the angle of internal friction, φ, with aging time
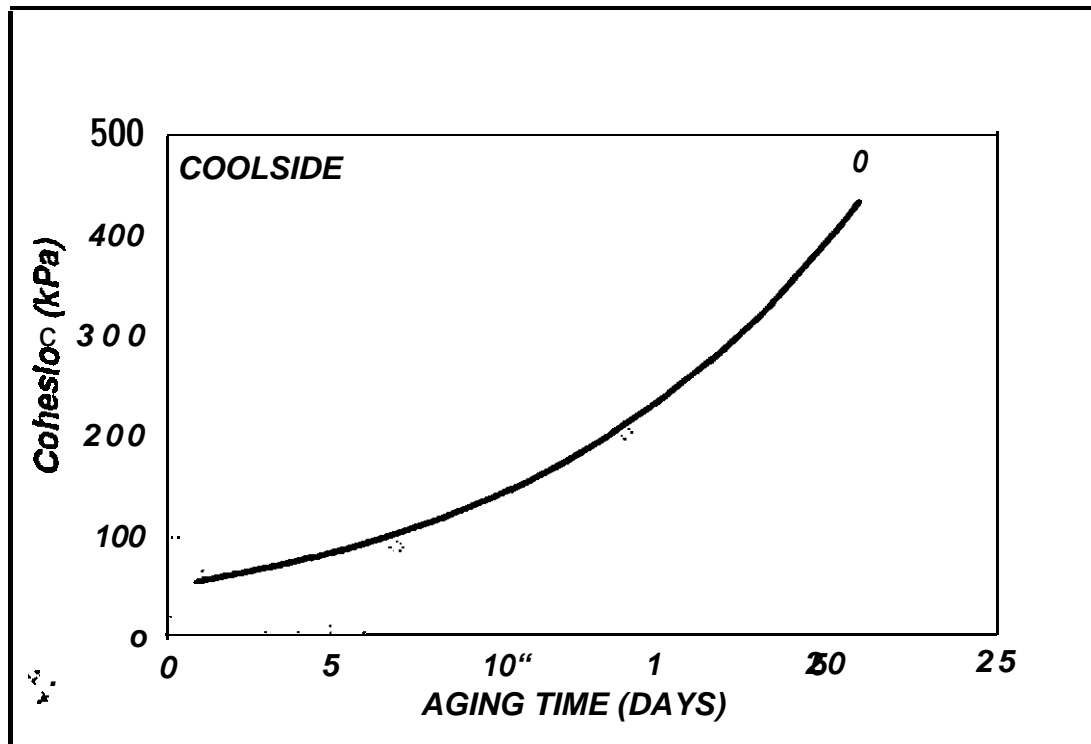
Figure 3-34. Variation of cohesion, c_u, with aging time

115

specimens did not lose moisture doing storage. The specimens were cured, or aged, to different periods. Some specimens were aged for 3.5 years. The specimens were aged in sealed containers at room temperature (about 21°C). Two series of tests were performed. The first series consisted of performing the unconfined compressive tests at different aging times in an unsaturated state. The second series consisted of performing tests on specimens saturated during permeability testing.

Results of the unconfined compression tests are shown as a function of curing time in Figures 3-35, 3-36, and 3-37. Unconfined strengths of the specimens compacted to 90% of maximum dry density obtained from low energy, standard, and modified compaction methods increased rapidly in the first 90 days. The low energy specimens obtained a strength of about 540 psi (3721 kPa) in the first 90 days while the specimens compacted to standard compaction increased to 660 psi (4548 kPa). The specimens that were compacted using modified energy reached a strength of 1150 psi (7925 kPa) in the first 90-day period. [n each of the three cases, the strengths decreased after peaking at 540, 1850, and 1850 days, respectively (to values of about 1028, 542, and 1374 psi (7084, 3735, and 9468 kPa), respectively). As shown in Figure 3-30, the peak unconfined strengths of specimens compacted to 100% of maximum dry density obtained from low energy, standard, and modified were 1922, 2488, and 2610 psi (13,245, 17,145, and 17,985kPa), respectively. However, the strengths of the standard and modified specimens decreased with increasing curing time after the peak strengths had been reached at curing times of 365 and 730 days, respectively.

California Bearing Ratio

Both short-term and long-term California Bearing Ratio (CBR) tests were performed on compacted specimens of the Coolside material. Results of the short-term tests are shown in Figure 3-38. All specimens were compacted to 95% of maximum dry density
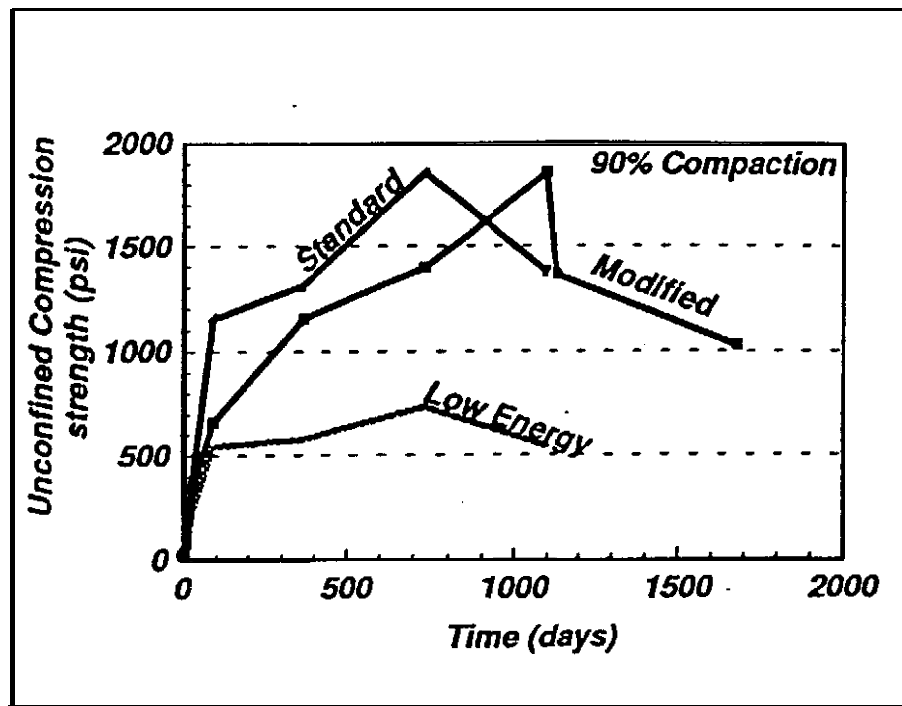
Figure 3-35. Unconfined compressive strength as a function of curing time for Coolside specimens compacted to 90% of low energy, standard, and modified compaction
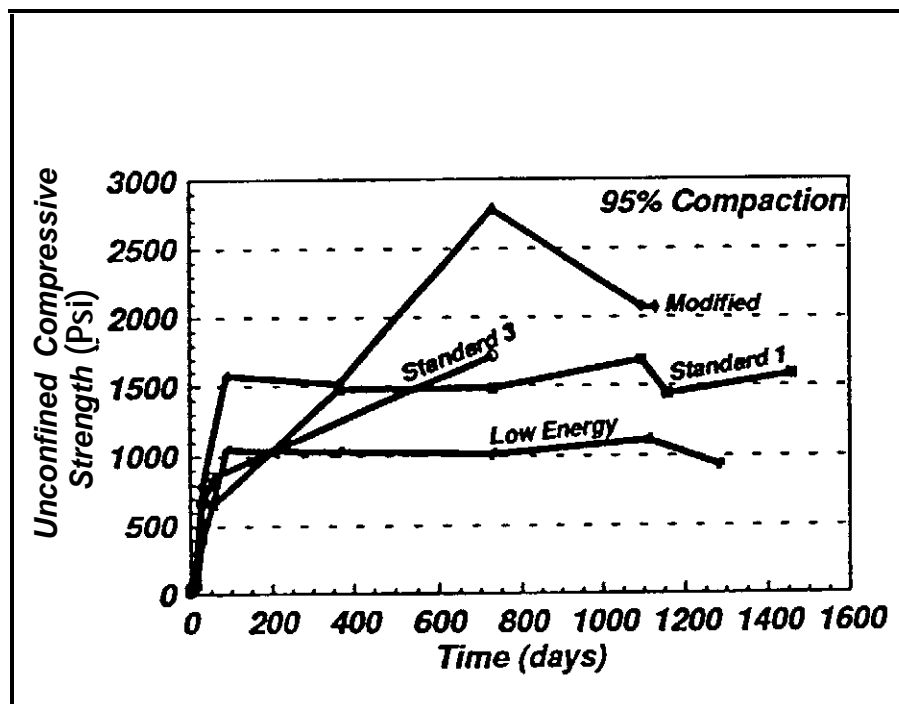
Figure 3-36. Unconfined compressive strength as a function of time for Coolside specimens compacted to 95% of low energy, standard, and modified compaction

117
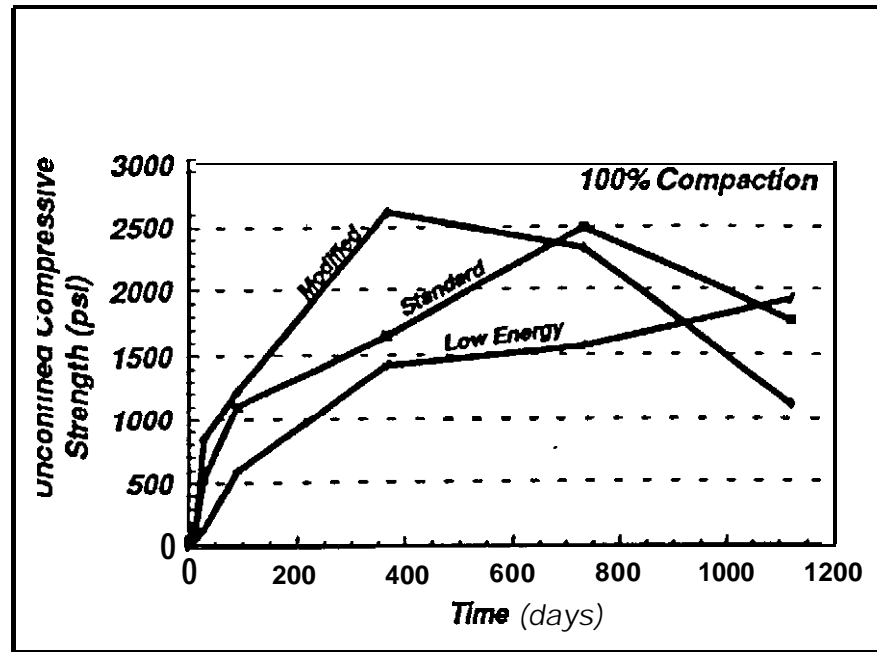
Figure 3-37. Unconfined compressive strengths as a function of time for specimens compacted to maximum dry density obtained from low energy, standard, and modified compaction
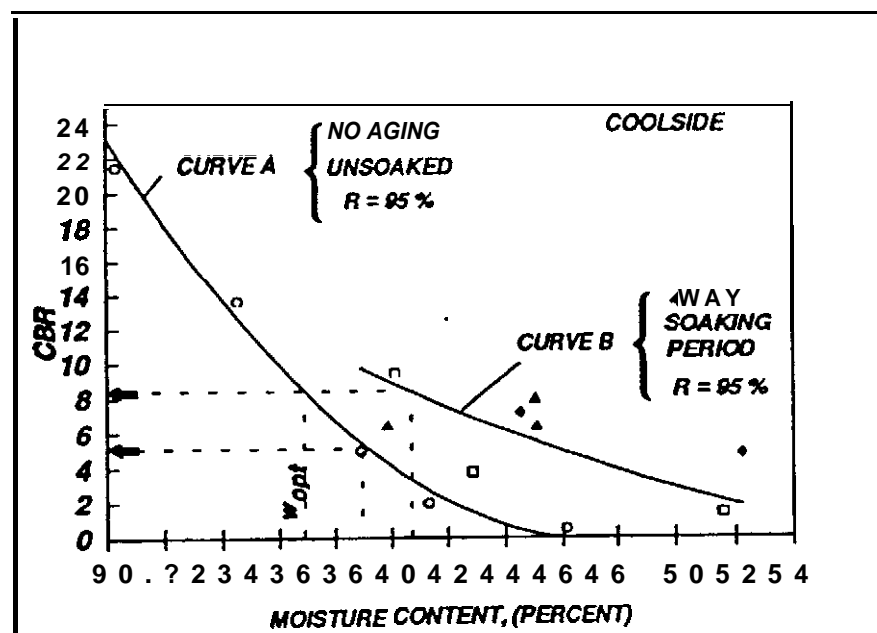
Figure 3-38. California Bearing Ratio (CBR) test values as a function of molding moisture content

118

obtained from ASTM D 698. The purpose of those tests was to characterize the bearing strengths of the Coolside material during construction handling. The relationship between CBR and compaction moisture content is represented by curve A in Figure 3-38. Here, none of the specimens were aged or soaked before the CBR test was performed. The tests were performed immediately after compaction. The intent of these tests was to simulate the field bearing strengths of the Coolside material during construction. As the moisture content of the specimens increases, the CBR value decreases. When the moisture content increases above the optimum moisture content (w_{opt}), the CBR strengths decrease rapidly to small values. At two percent above optimum moisture content, the CBR value is only about 5.

Curve Bin Figure 3-38 represents the relationship between CBR and moisture content of specimens cured and soaked in water for 4 days. The tests were performed after the specimens had been soaked for four days. Although the moisture contents of the soaked specimens were greater than the moisture contents of specimens represented by Curve A, the CBR strengths were comparable to those values represented by Curve B. For example, at a moisture content of 41%, the CBR of the 4-day soaked specimens (Curve B) was 8. At a CBR of 8, the moisture content of the unsoaked specimen (Curve A) is about 37%. Consequently, during the soaking period, the compacted Coolside material gained strength. Apparently, pozzolanic reactions occurred during the soaking, or curing period.

Long-term CBR strength of the Coolside ash was also examined. Specimens of the ash were remolded in CBR molds (Figure 3-39) to 95% of maximum dry density and optimum moisture content. Results obtained from the CBR tests are shown in Figure 3-40. In these tests, the CBR specimens of the Coolside ash were allowed to swell until secondary swell was reached, or essentially most of the swelling had occurred before the CBR test penetration was performed. Time to complete swell ranged from about 2.6 to almost 6 months. The soaked values of CBR always exceeded 100--exceedingly
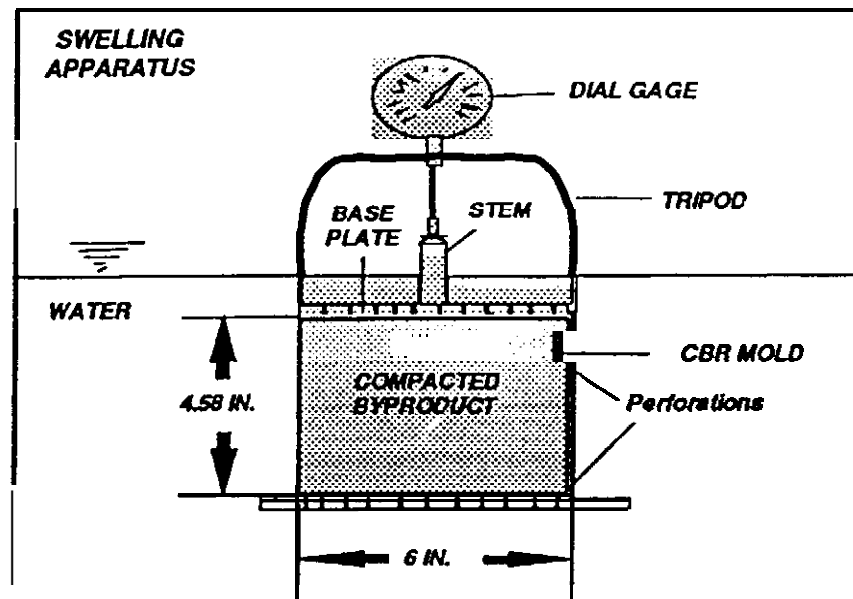
Figure 3-39. CBR mold
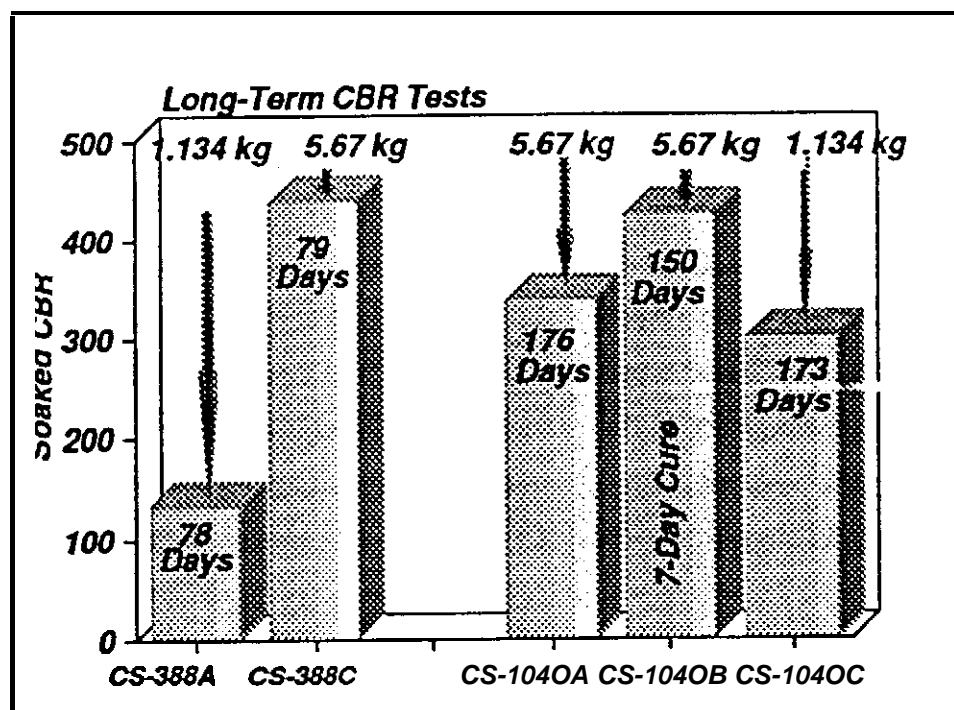
Figure 3-40. Long-term, soaked CBR values of the Coolside ash

large values.

Permeability

Permeability, or hydraulic conductivity, is the ability of a material to transmit fluid. Hydraulic conductivity depends on the unit weight, pore spacing, and degree of saturation of the material. The coefficient of permeability, k, is an important parameter used in engineering applications to decide the rate and quantity of flow through a material. Permeability tests were performed on specimens remolded to different densities and different aging times. The specimens were remolded to 90,95, and 100% of maximum dry densities obtained from low-energy, standard, and modified compaction. Optimum moisture contents obtained from the respective compaction methods were used in remolding the specimens. The tests were performed using a back saturation technique and falling head method in triaxial cells. Equations for calculating the coefficient of permeability have been described by Daniel (1989).

The coefficient of permeability, k, as a function of aging, or curing time, is shown in Figures 3-41, 3-42, and 3-43. Analysis shows that aging does not significantly affect the coefficient of permeability. The values decreased only slightly as the curing time increased, The coefficient of permeability ranges from about 4 x 105 cm/sec to 3 x 10^{-6} cm/sec. The permeability of the compacted specimens of the Coolside by-product may be described as low, or very low. However, the material in a compacted state is permeable, since the coefficient of permeability is not smaller than 10^{-7} cm/sec.

Variation of the coefficients of permeability with dry density and void ratio (volume of voids divided by the volume of solids) is shown in Figures 3-44 and 3-45. As the dry density increases, the coefficient of permeability decreases and approaches 1 x 10^{-7} cm/sec^2 as the dry density approaches a value of the maximum dry density obtained from modified compaction. The coefficient of permeability increases as the void ratio

121
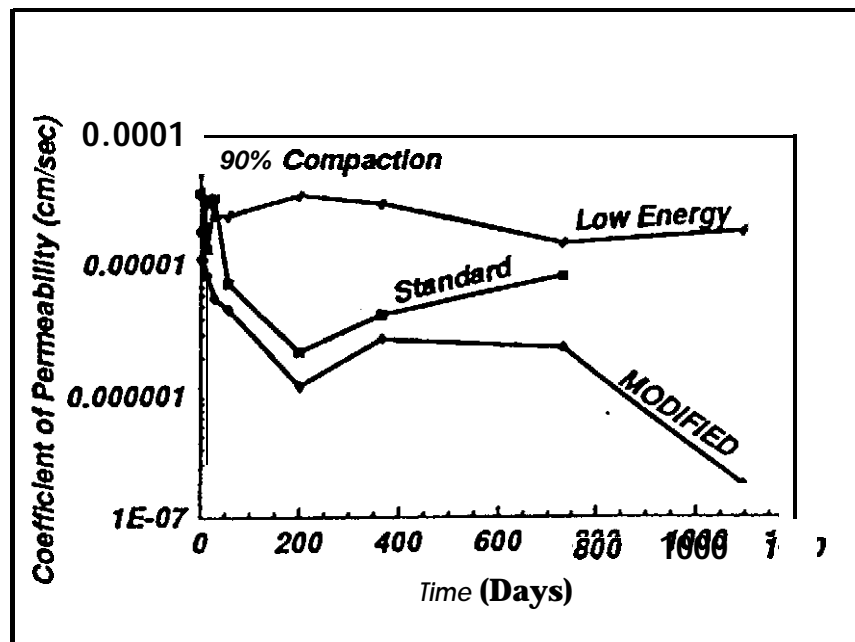
Figure 3-41. Coefficient of permeability as a function of time for specimens remolded to 90% of maximum dry density
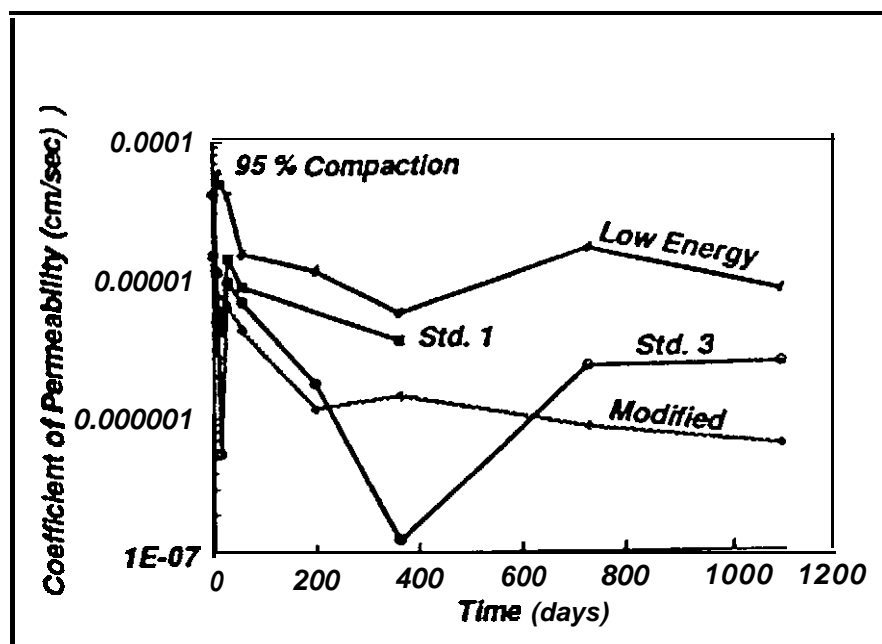
Figure 3-42. Coefficient of permeability as a function of time for specimens compacted to 95% of maximum dry density
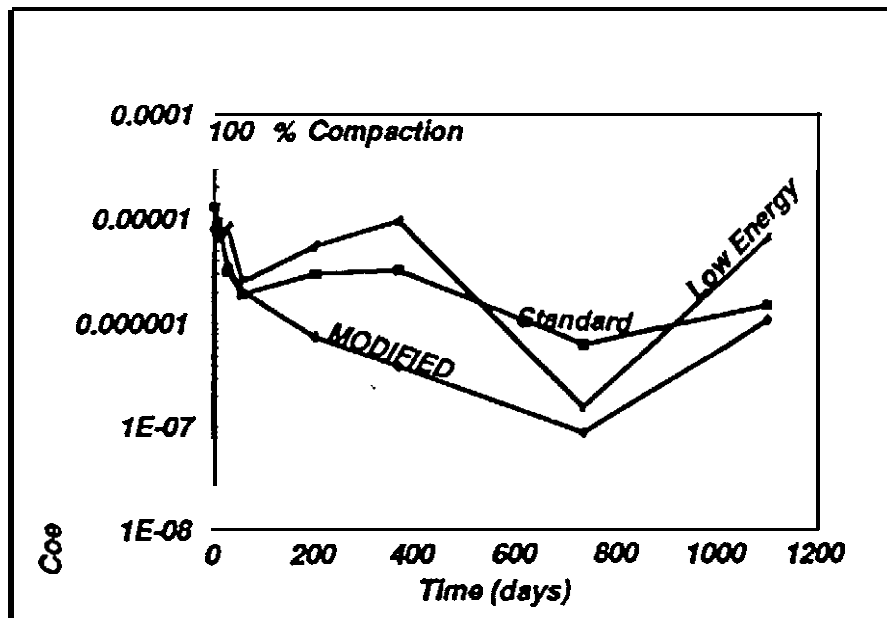
Figure 3-43. Coefficient of permeability as a function of time for specimens remolded to 100% of maximum dry density
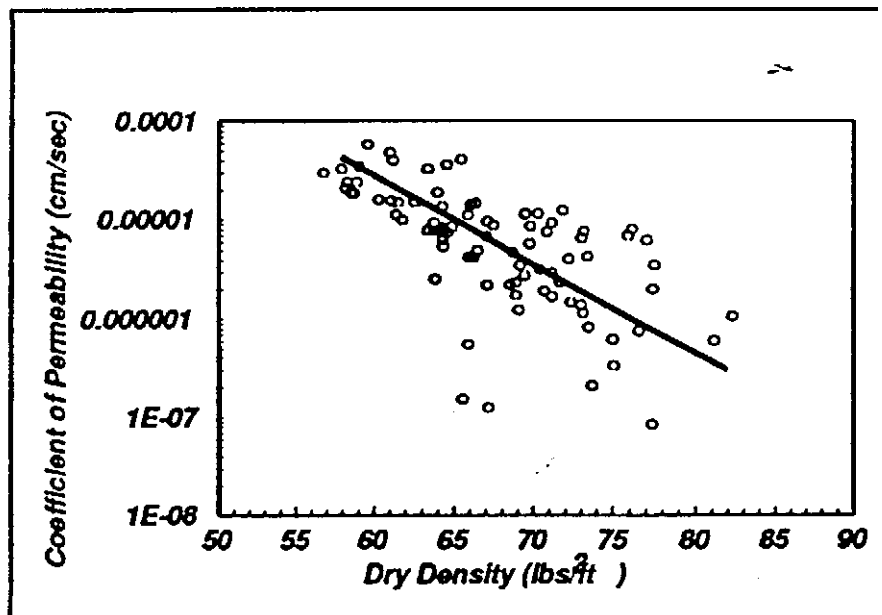
Figure 3-44. Coefficient of permeability as a function of dry density
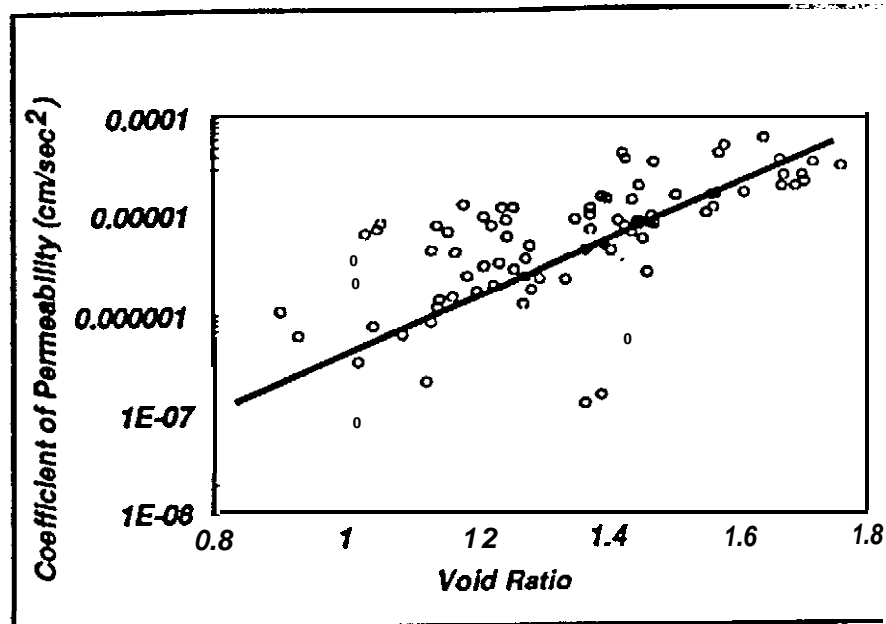
Figure 3-45. Variation of the coefficient of permeability and void ratio
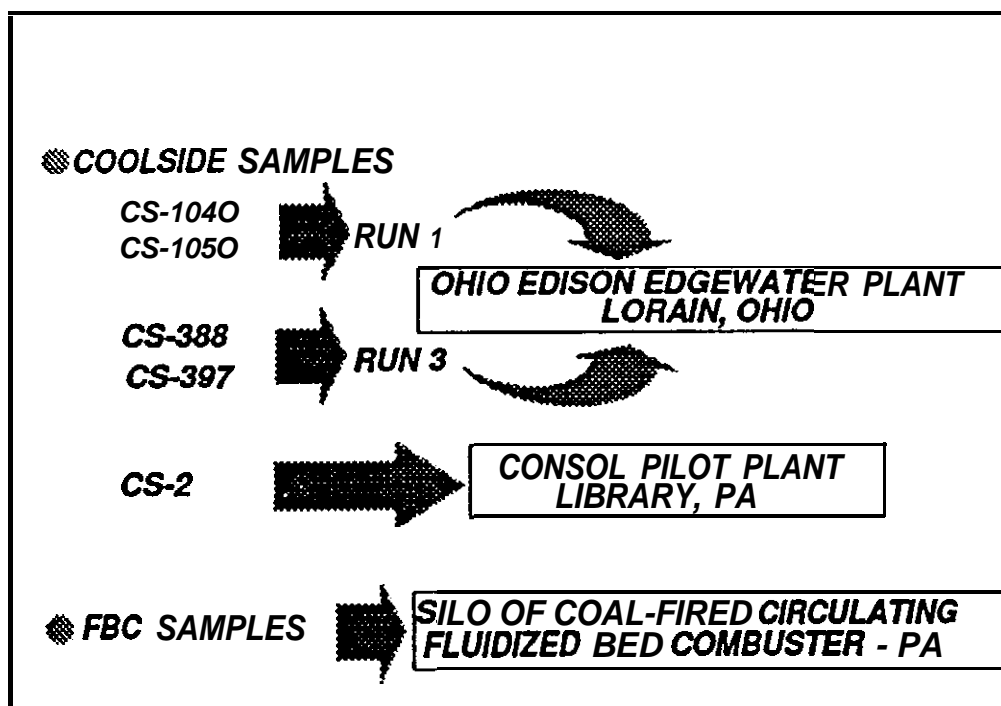
Figure 3-46. Sources of Coolside materials and an FBC material

124

increases.

Swelling Characteristics Of the Coo/side Ash

As described above, the Coolside and other FGD byproducts could be used in a number of highway applications. However, to qualify as viable materials in the highway industry, swelling of these materials must be predictable. Typically, many soils used to construct subgrades of pavements swell some zero to 20 percent. Pavements on clayey subgrades, which exhibit swelling magnitudes of 5%, or greater, generally have performed poorly. When the swelling exceeds about 10%, pavements have performed extremely poorly. When the swelling percentage becomes larger than about four or five, the bearing strength decreases. If swelling of the Coolside and FGD byproducts is severe, then the physical and geochemical mechanisms that may cause swelling must be understood and means to control swelling must be devised. The intent here was to examine and evaluate the swelling characteristics of these materials.

Sources Of Materials For Swelling Tests And Index Properties. Long-term swelling characteristics of dry flue gas desulfurization (FGD) byproducts obtained from a successful demonstration of Coolside technology and a Coolside pilot plant operation were examined and compared to the swelling properties of two typical clayey soils, an FBC ash, and an atmospheric fluidized bed combustion (AFBC) spent lime-clay mixture.

Coolside byproducts were obtained from the Ohio Edison Edgewater Station at Lorain, Ohio and the CONSOL Coolside pilot plant in Pennsylvania. Three series (numbers 1, 2, and 3) of Coolside byproduct samples (Figure 3-46) were collected from the ESP hopper (Figure _3-47)_ of the Edgewater Station in February of 1988 during the Coolside demonstration program, Samples identified herein as CS-388 and CS-1 050 were two bulk samples obtained from Edgewater sample series run numbers 1 and 3,
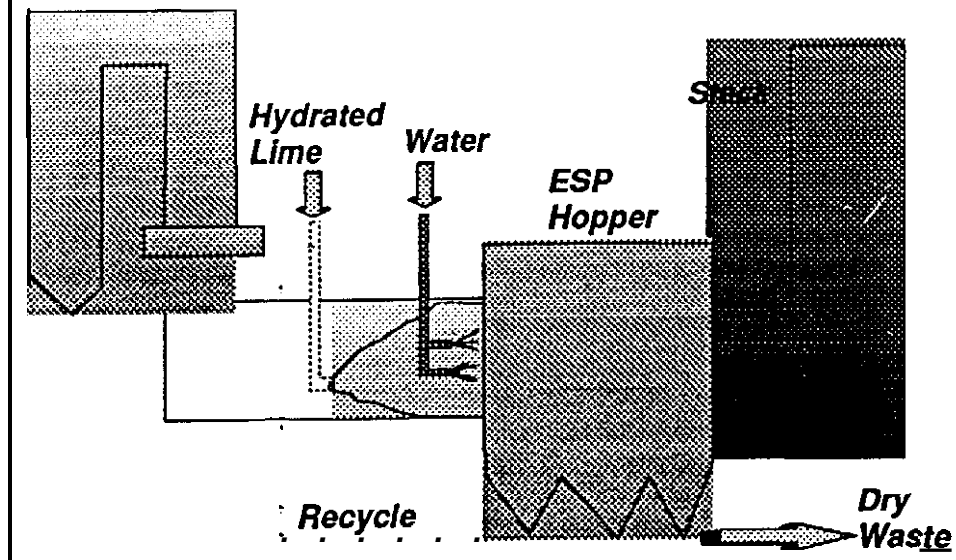
Figure 3-47. Coolside process
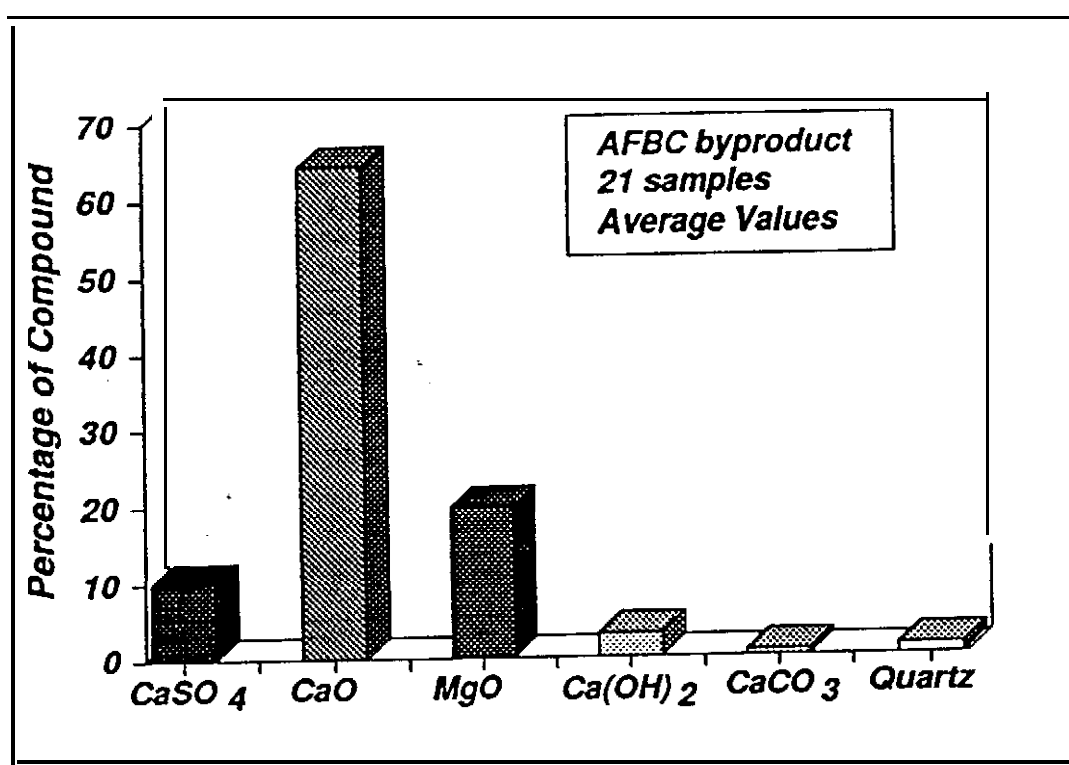
Figure 3-48. Chemical analysis of an AFBC ash

Sample Number	Liquid Limit (%)	Plasticity Index (%)	Grain-Size Percent Finer than: No. 10 (%)	No. 200 (%)	Classification Unified	AASHTO
Coolaide	NP	NP	100	95	ML	A-4(0)
FBC "ash	NP	NP	100	51	SM	A-4(0)
Silty Clay	36	11	90	70	ML	A-6(8)
Plastic Clay	71	3'7	99	93	ML	A-7-5(44)
AFBC(7%)-Soil Mixture	49	14	91	49	ML	A-7-5(5)

Table 3-9. Index properties

respectively. Samples identified as CS-104O and CS-1050 were two samples from Edgewater sample series number 1. Samples identified as CS-I were a composite sample from run number 1 (also, identified as Sample A). Samples identified as CS-3 were a composite sample from run number 3.

Samples identified as CS-2 were obtained from the CONSOL Coolside pilot plant operating in the recycling mode. These samples were produced at conditions that simulate operation of the Coolside process installed on a unit burning medium-sulfur (2.5%) Ohio coal. The sulfur content of CS-2 was about 8 percent. Edgewater Coolside samples contained about 2 percent of sulfur. Samples of an FBC ash were obtained from a silo of a coal-fired circulating fluidized bed combuster in a coal-fired co-generating plant in Pennsylvania on February 18, 1992. The FBC byproduct was hydrated by CONSOL. However, nonhydrated samples of the FBC ash were also received for testing. The AFBC spent lime (nonhydrated) was obtained from an oil refinery in 1987 and is a byproduct of an AFBC process used in cracking crude oil. TWO typical soils were obtained in Kentucky. Index properties of the materials are compared in Table 3-9. This AFBC material contains some 10% of calcium sulfate and about 65% of calcium oxide, as shown in Figure 3-48.

Swell Testing Procedures. Swelling characteristics of the Coolside byproducts and the other materials selected for comparative purposes were determined by submerging compacted specimens in water in confined CBR molds and oedometers (consolidometers). Two series of tests were performed in oedometers, which commonly are used to perform consolidation tests. The third series of tests was performed in CBR molds. A schematic of the arrangement of specimens in CBR molds was illustrated previously in Figure 3-39. Diameter and height of the CBR-size specimens were 6 in (15.24 cm) and 4.58 in (11.63 cm). Consolidometer specimens measured 2.5 in (6.35 cm) in diameter and 1 in (2.54 cm) in height. All specimens were compacted to about 95 percent of maximum dry density and optimum moisture content

128

was obtained from standard compaction (ASTM D 698) following a procedure described above and elsewhere (Hopkins and Beckham, 1993). This compactive state was used because field specifications of many agencies require those compaction criteria.

Swelling periods for tests conducted in the oedometer apparatus usually ranged from 18 to 21 days. Swelling periods of tests performed in the CBR molds ranged from 64 to 79 days. In the first series of oedometer tests, the Coolside material was compacted immediately after mixing. After compaction, the tests were started by submerging the specimens (and mold) in water. In the second series of tests, the Coolside material was compacted and the specimens were allowed to age, *or* cure, for seven days in a sealed container at room temperature (about $21^{\circ}C$). In the third series, the swelling tests were started after the CBR specimens had aged O, 7, and 14 days. Laboratory bearing ratio tests were performed on some of the larger specimens as a means of evaluating bearing strength properties after swell.

 Test Results and Analysis. Swelling of FGD byproducts due to the absorption of water (and chemical reactions) may affect the structural integrity of the disposed material at the disposal site and the potential uses of the byproduct in structural applications, such a base material for pavements or chemical admixture for pavements subgrade. For example, swelling of a compacted byproduct, used as a base course, may do little structural damage to the pavement if it occurs very rapidly and before placement of the pavement, although the magnitude of swelling maybe very large. Although the time rate of swelling may be very slow, taking many years to complete, little damage may occur if the magnitude is small. Bearing strength is directly related to the magnitude of swell, as illustrated in Figure 3-49. As the total magnitude of swell increases, the bearing decreases.

Based on previous work by Hopkins (1994, 1995), the minimum CBR strength of subgrades to sustain tire stresses of 552 kPa (80 psi) should be 6.5 (for a factor of
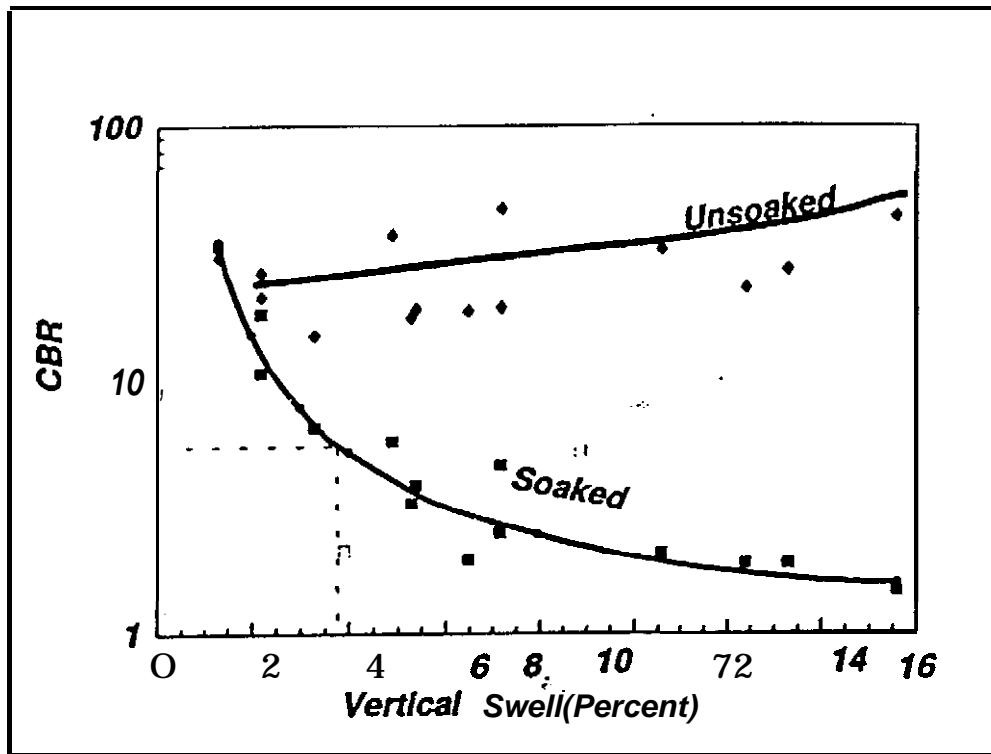
Figure *3-49.* Decreases in CBR strengths as the total swell of compacted soils increases
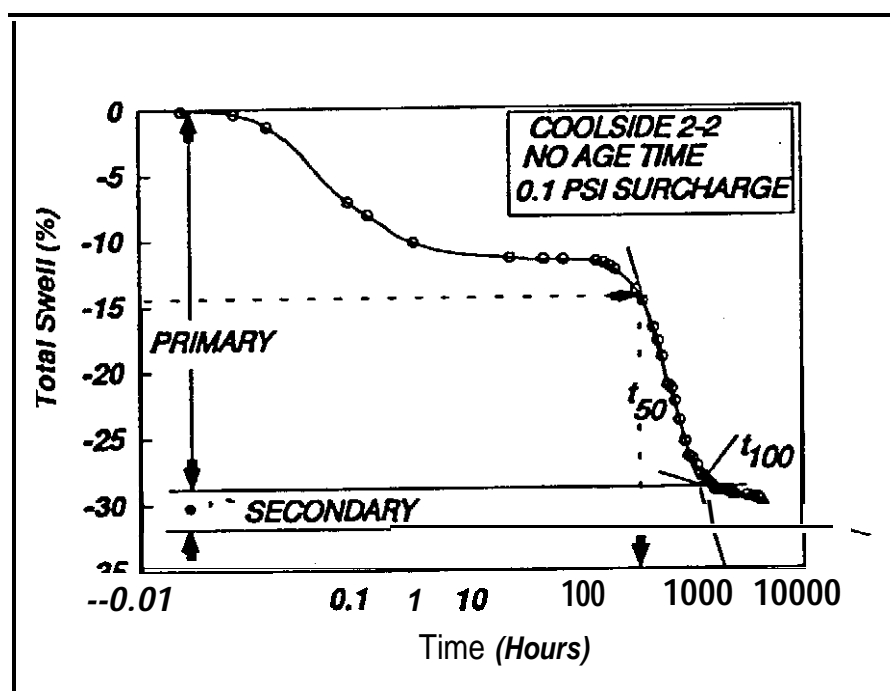
Figure 3-50. Vertical swell of Coolside specimen number 2

130

safety equal to one). As shown in Figure 3-49, the magnitude of swelling should be below about 4 percent for the CBR strength to be above 6.5. Atypical swelling-time curve of a compacted specimen of the Coolside material (CS-2) is shown in Figure 3-50. Typical swelling curves obtained for Edgewater runs 1 and 3 (CS-388 and CS-1040) are shown in Figure 3-51.

Swelling may be divided into two parts: primary and secondary swelling. Usually, primary swelling represents a large portion of the total magnitude of swelling. Secondary swelling is linear when the vertical swelling is plotted as a function of the logarithm of time. All specimens of the Coolside material behaved as shown in Figure 3-50. Hence, coefficients of primary swelling and secondary swelling maybe computed using principles proposed by Terzaghi (1947) and fitting methods proposed by Casagrande (1 936) --logarithmic-of-time-- and Taylor (1 945) --square-root-of-time-- since swelling due to the absorption of water is consolidation in reverse. The swelling rate increases with an increasing coefficient of swell at any time. These principles may be used to forecast the time rate of swelling for a given field problem. The magnitude of primary swelling (of thin layers) may be estimated by the vertical strain observed from a laboratory test. Values of coefficients of primary and secondary coefficients are summarized in Table 3-10. These values were determined from a computer program developed by McNulty, et al (1978).

In the first series of oedometer tests, where no aging was permitted and no surcharge pressures were used, the total swell of the four specimens ranged from 10 to 23%. Primary swell ranged from 8 to 16%. Secondary swell ranged from 0.206 .57.. In comparison, total values of swell of two typical, compacted clays were 4.6 and 12.57.. Two typical swelling curves of the Coolside material are compared in Figure 3-52 to swelling curves of two typical clay soils and an atmospheric fluidized bed combustion material--AFBC-- (from an oil refinery). Primary values of swell were 4.1 and 11 .6%, respectively, as shown at the bottom of Table 3-10.
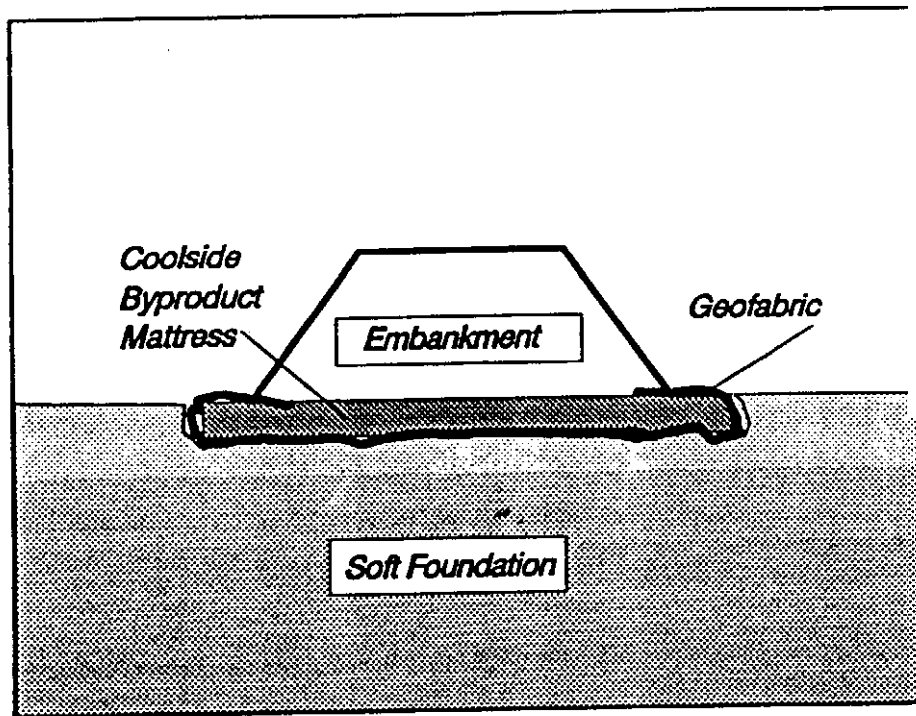
Figure 3-51. Use of the Coolside material to construct a mattress reinforced with geofabric to support an embankment on a soft foundation
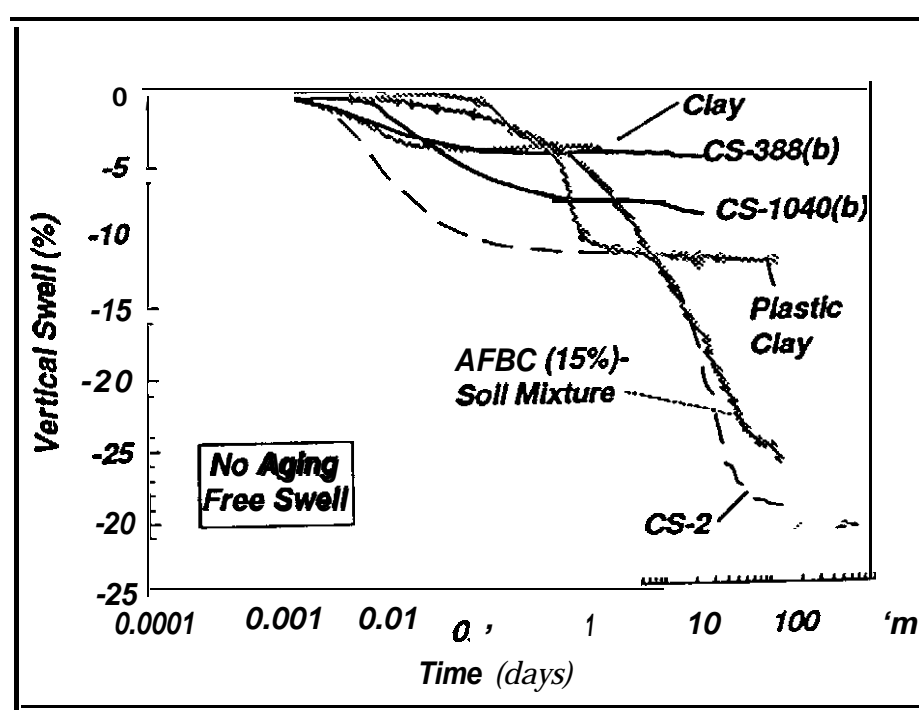
Figure *3-52.* Comparisons of the swelling curves of AFBC- and FGD-type byproducts and two natural clays

| specimen Number | Curing Period (days) | Fitting Methods | | | | Coefficient of Secondary Swell Cds | Primary Swell (%) | t_{100} (min.) | Total Swell (%) |
| | | Square-Root-of-Time | | Logarithmic-of-Time | | | | | |
		t_{90} (Min.)	Coefficient of Primary Swell (cm2/day)	t_{50} (Min.)	Coefficient of Primary Swell (cm2/day)				
CS-388[a]	0	18.5	1022	43	1022	0.0	6.0	25.1	22.5
CS-397[a]	0	38.05	1.8	14.7	31.1	0.0009	15.4	56.2	15.6
CS-1040[a]	0	177.8	11.1	13.0	352	0.0040	14.s	316.2	15.1
CS-1050[a]	0	28.7	38.7	5.6	81.7	0.00	8.0	46.4	9.9
CS-388[a]	7	13,200	0.15	3,600	0.13	0.0	4.9	18,000	4.9
CS-397[a]	7	7,200	027	2,700	0.17	0.0	2.1	10,020	2.1
CS-1040[a]	7	7,800	025	3,300	0.14	0.0011	0.9	10,998	1.0
CS-1050[a]	7	6,600	0.30	4,200	0.11	0.0021	2.1	15,840	2.2
CS-388A[b]	O	9045	8.0	21	458.0	0.0041	4.1	132.8	5.1
CS-1040B[b]	O	1,050	39.4	300	32.1	0.0092	7.4	1,286	9.0
CS-388C[b]	O	180	2462	39	229.5	0.0010	1.3	170.0	1.6
CS-1040D[b]	O	300	137.5	45	213.7	0.0007	1.4	180.0	1.6
CS-1040E[b]	7	17,404	2.4	4,200	23	0.0	0.2	24,000	0.2
CS-388F	14	15,000	11.3'.	3,900	9.8	0.0	0.1	18,000	0.1
AFBC-Soil[b]	o	67,500	0.5	17,160	0.4	0.0776	24.2	120,000	262
Silty Clay [a]	o	2,700	02	90	03	0.0025	4.1	3,600	4.6
Plastic Clay[a]	o	2,800	14.4	39Q	24.6	0.065	11.6	4,s00	12.5

Notes: (a), Specimen mold = oedometer; (b). Specimen mold= CBR; the third series of tests were performed on CBR-size specimens. Four (specimen numbers 388A, 1040B, 388C, and 1040D) of the six specimens were not agad prior to soaking.

Table 3-10. Swelling characteristics of compacted specimens of Coolside byproduct

Magnitudes of primary swelling are shown in Figure 3-53. Numbers (O, 7, and 14) shown at the bottom of each bar refer to the aging time (in days) of each specimen in sealed containers before submerging in water. Numbers at the top of each bar represent a small surcharge pressure (O, 0.69 kPa [0.1 psi], and 3.44 kPa [0.5 psi]) applied to each specimen. A pressure of 3.44 kPa is about equivalent to the pressure exerted by a 15.24-cm (6-in) layer of pavement. When the aging and the applied surcharge pressure were zero, the magnitude of primary swell of specimens CS-388, 397, 1040, and 1050 ranged from 8 to 16 percent.

The amount of primary swelling decreased as the surcharge pressure was increased. For example, when the surcharge pressure of CS-388 and CS-1040 was increased from zero to 3.44 kPa (0.5 psi), the amount of swelling decreased from about 150/. to 2%. Swelling of CS-2 was reduced from 29% to 15'7. when the surcharge was increased from 0.69 kPa to 3.44 kPa (0.1 to 0.5 psi). A similar trend was observed for the other specimens. Additionally, the amount of swelling decreased when the specimens were allowed to age prior to soaking. For instance, the amount of swelling of CS-388 decreased from about 16% at no aging time to about 5% at a 7-day aging period. Primary swelling of the two soils were about 5 to 12%, respectively. Primary swelling of the AFBC-soil mixture was about 25%. Primary swelling of the Coolside specimens that had been aged for seven days prior to soaking and surcharged to 3.44 kPa (0.5 psi) was less than 5%--a value equal to or less than values of primary swelling observed for the two typical soils. The higher sulfur content of CS-2 may have played an important role in producing a swelling magnitude that was greater than those observed for the other Coolside samples.

Coefficients of primary swelling are compared in Figure 3-54. This coefficient is calculated by the equation shown in Figure 3-55. Specimen aging generally had a significant effect on the observed values. For example, coefficients of primary swelling
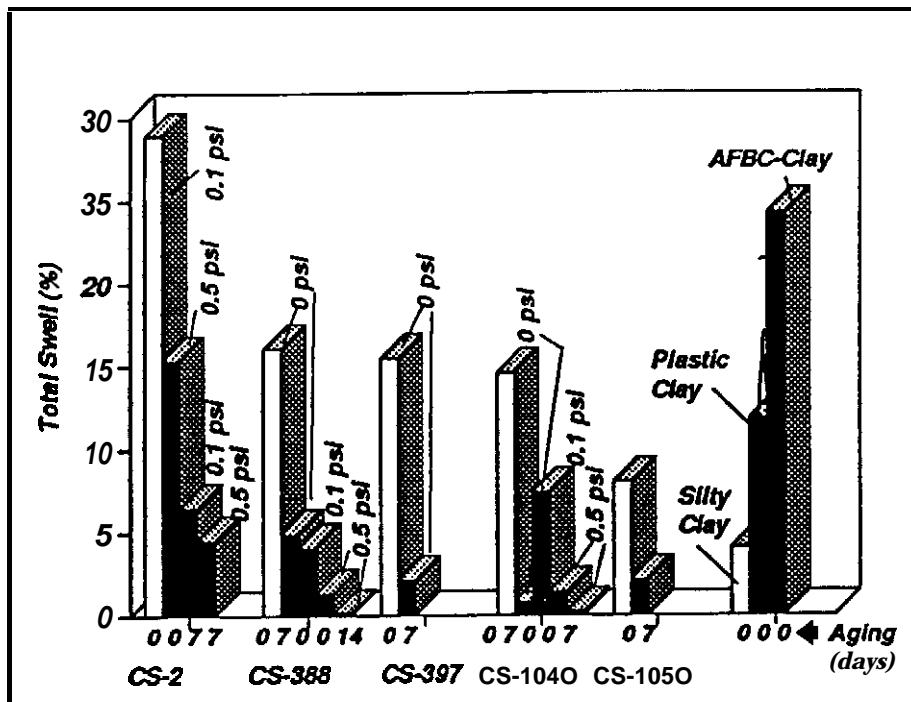
Figure 3-53. Comparison of total magnitudes of swelling
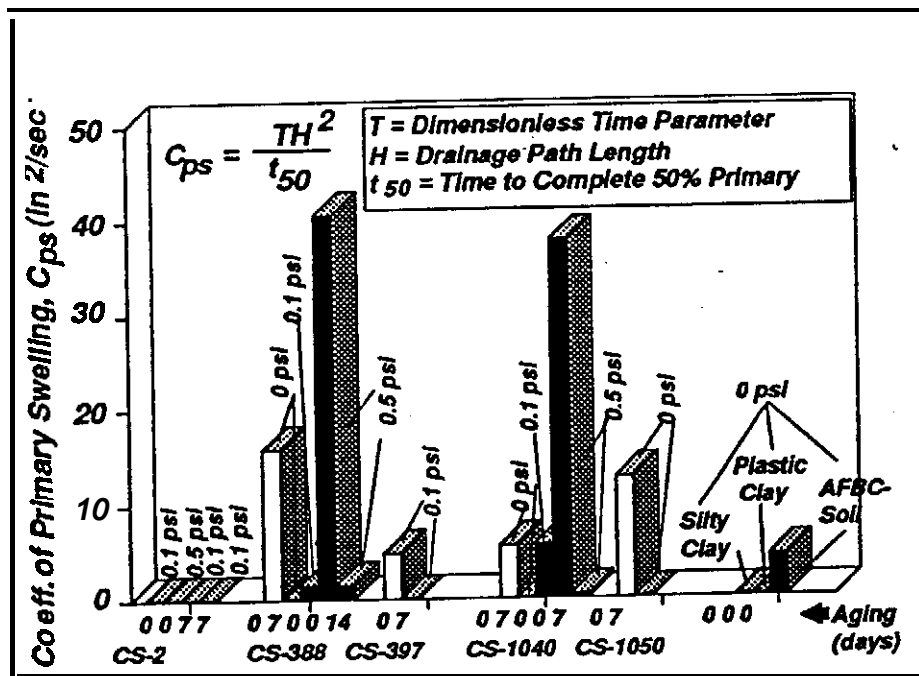
Figure *3-54.* Primary swelling coefficients
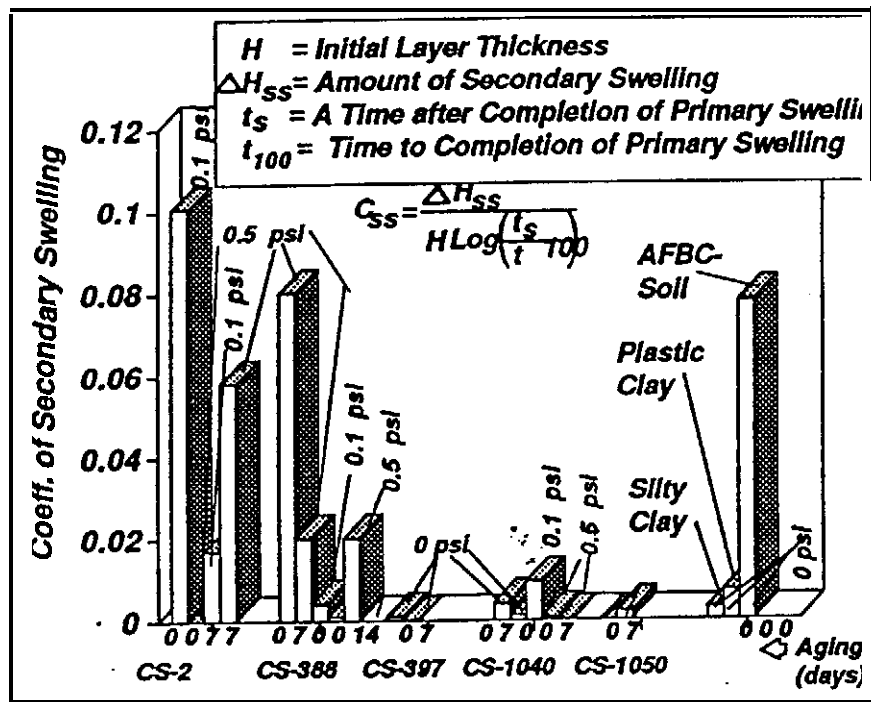
Figure 3-55. Secondary swelling coefficients
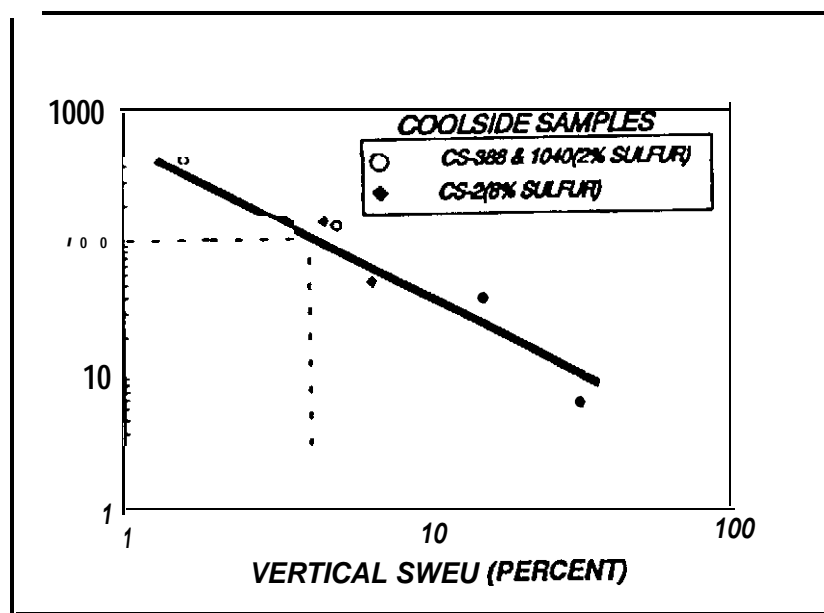
Figure 3-56. Variation of CBR strength and total magnitude of swell of compacted Coolside specimens

of specimens, CS-388, CS-397, CS-1040, and CS-1 050 at zero aging time ranged from 14.2 to 40.1 cm^2 per day (5.6 to 15.8 in^2 per day). Coefficients of the same Coolside samples that had been aged ranged from only 0.04 to 3.9 cm^2 per day (0,017 to 1.52 in^2 per day). Primary coefficients of those specimens increased when the surcharge pressure was increased from zero to 3.44 kPa (0.5 psi). Coefficients of primary swelling of the AFBC spent lime-soil mixture, the silty clay, and the plastic clay were 0.18, 0.13, 11.0 cm^2 per day (0.07, 0.053, and 4.35 in^2 per day), respectively. Changing the aging period, or increasing the surcharge pressure did not appear to cause significant changes in the coefficient of primary swell of CS-2. Values ranged from 0.13 to 0.20 cm^2 per day (0.05 to 0.08 in' per day).

Generally, coefficients of secondary swelling of CS-2 specimens (Figure 3-55) were slightly larger than the secondary coefficients of CS-388, CS-397, CS-1040 and CS-1050. The equation shown in Figure 3-55 was used to calculate the secondary coefficients. Coefficients of secondary swelling of all Coolside specimens ranged from zero to 0.1. Secondary coefficients of CS-2, CS-388, and CS-397 that had not been aged appeared slightly larger than coefficients of specimens that had been aged for seven to 14 days. However, secondary coefficients of specimens surcharged 0.69 kPa (0.1 psi) were generally slightly smaller than those of specimens that were not surcharged.

CBR strengths of Coolside byproducts after swelling ranged from 133 to 430-- exceptionally high values. However, as shown in Figure 3-56, the CBR strengths decrease rapidly as the magnitude of swell increases. Whereas CBR values of natural soils compacted to values of about 95% of maximum dry density and optimum moisture content are only about 6 at a magnitude of swell of about 3.5%, the CBR values of Coolside specimens, compacted to the same conditions, are greater than 100. In fact, at a swell magnitude of about 30%, the CBR value of the Coolside material is about 7. This implies that the Coolside material could go through an expansion period and still

retain considerable strength.

Prehydrating FGD byproducts before use has been suggested for eliminating, or minimizing, the large magnitudes of swelling observed in these materials. To check this common assumption, two series of swelling tests were performed using an FGD byproduct in two different states. In contrast to slaking the byproduct, which involves combining water with the calcium oxide of the byproduct so that a slurry is formed, the byproduct was hydrated. In the hydration process, 990/. of the water is chemically combined as hydroxide to produce a dry, finely powdered, hydrated lime. In hydration, less water is used than when the slaking process is involved. The byproduct selected for testing was an FBC ash obtained from a power plant in Pennsylvania. Some material was prehydrated by CONSOL, Inc. Additionally, FBC ash specimens were received that had not been hydrated.

Swell tests were performed on both the hydrated and nonhydrated material. These tests were performed on specimens compacted to 950/. of standard compaction and optimum moisture content. Values of maximum dry density and optimum moisture content used to remold the swell specimens were obtained from compaction tests performed on both the hydrated samples and the nonhydrated samples (Figure 3-57). Swelling (expressed as a percentage), as a function of the logarithm-of-time for the hydrated and nonhydrated FBC ash specimens is shown in Figures 3-58 and 3-59. The swelling tests were conducted for different specimens aged to two different conditions and different surcharge pressures. Two specimens were not aged while two specimens were aged for 7 days before submerging the specimens in water. Surcharge pressures of 0.69 kPa (0.1 psi) --which corresponds to a weight of about 1.08 kg (2.4 lbs)-- and 3.45 kPa (0.5 psi)-- which corresponds to a weight of 5.8 kg (12.8 lbs)--were used. In both cases, the nonhydrated and prehydrated specimens are still in a primary swelling state. The nonhydrated specimens have been in primary swelling for some 1292 days--3.5 years--and have not reached a secondary swelling
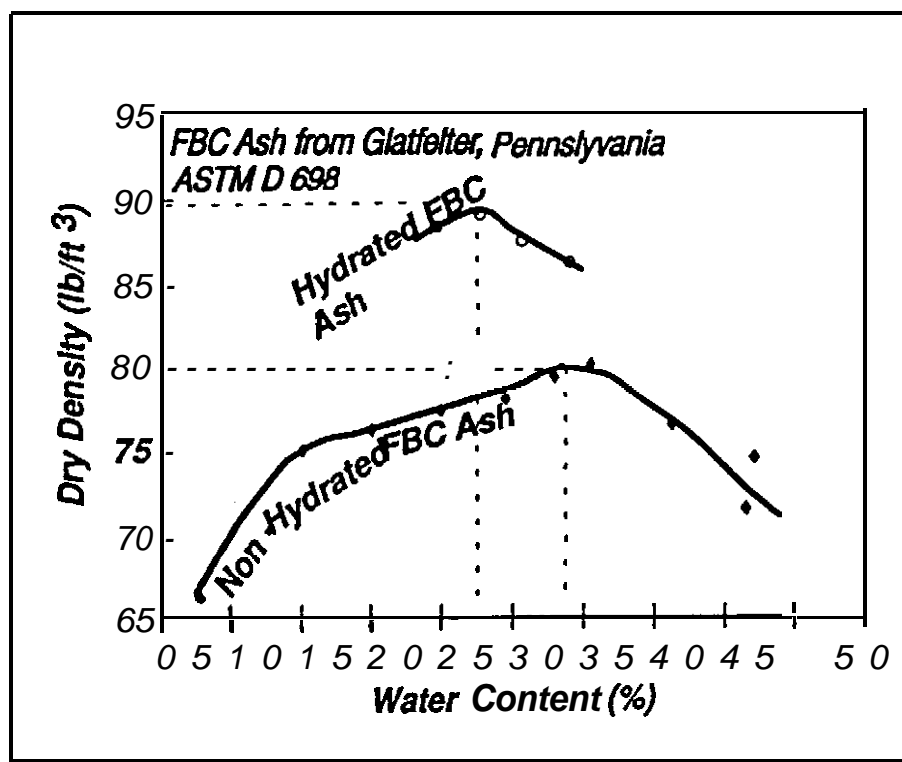
Figure *3-57.* Dry density-moisture content relationships of an FBC ash from Pennsylvania
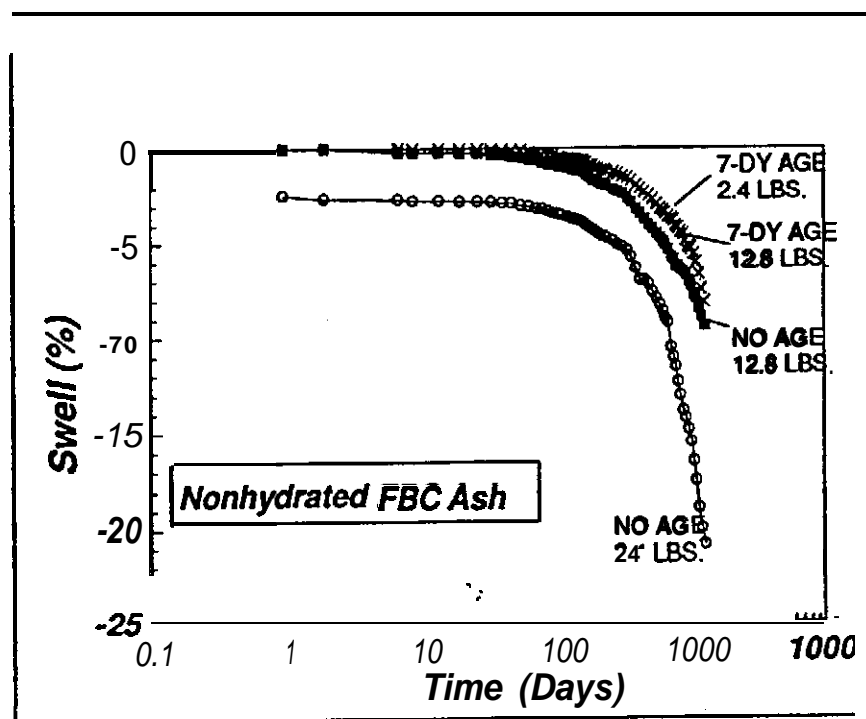
Figure 3-58. Swell curves for the nonhydrated FBC ash from Pennsylvania

139
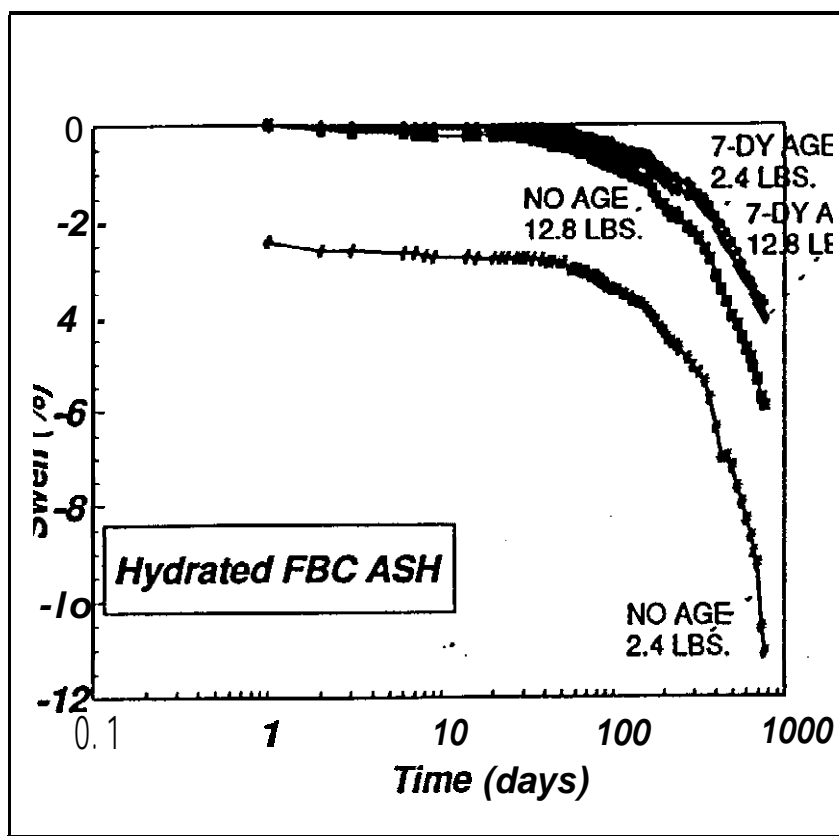
Figure 3-59. Swell curves for an FBC (prehydrated) ash from Pennsylvania
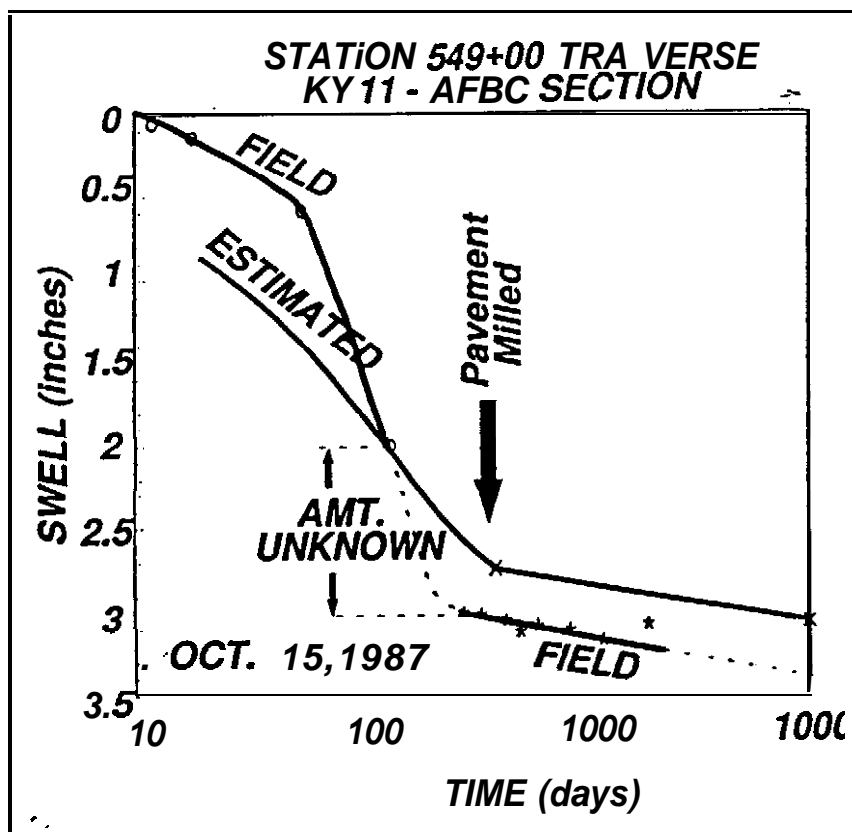
Figure 3-60. Comparison of predicted and observed swelling of the AFBC-clayey subgrades of the KY 11 Route

140

condition. Similarly, the preydrated specimens, as shown in Figure 3-59, have been swelling for some 766 days, or 2.1 years, and have not reached the secondary swelling state. As shown in Figures 3-58 and 3-59, the magnitudes of swelling for aged specimens were much more than specimens that had not been aged. Moreover, the magnitudes of swelling of specimens with larger surcharge pressures are less than specimens with smaller surcharge pressures. The swelling of the prehydrated specimens ranged from about 4 to 11 o/. after some 2.1 years (Figure 3-59). The swelling amounts for the nonhydrated specimens range from about 8 to 21 % after some 3.5 years. For the same time as the period of the non hydrated specimens (2.1 years), the swelling magnitudes of the prehydrated specimens range from about 3.8 to 11%. So, only small differences in the magnitudes of swelling of prehydrated and nonhydrated specimens are suggested by the results of these tests. However, observations must continue to confirm this finding. Swelling trends of the FBC byproduct are similar to those observed for the Coolside specimens. However, the Coolside specimens reached the secondary swelling state much faster.

CASE STUDY

FGD by-products have the potential to be used to stabilize clayey subgrades of highway pavements. For example, a by-product obtained from an AFBC process of an oil refinery was mixed with a clayey subgrade of a highway route in Kentucky (Hopkins, et al., 1987; 1993). Combined length of the two highway subgrade sections was about 4.0 km (2.5 miles). The pavement section consisted of 21.6 cm (8.5 inches) of asphaltic concrete, 12.7 cm (5 inches) of crushed limestone aggregate, and a 30.5-cm (12-inch) compacted mixture of the AFBC spent lime (7 percent) and clayey soil (93 percent). The AFBC-soil subgrades were allowed to cure for seven days. Approximately two months after placement of the asphaltic base courses and a rainy period, noticeable "humps", running perpendicular to the centerline, formed on the pavement surface.

Many points were immediately established on the surface of the sections and optical surveys were performed periodically. Placement of the asphaltic surface course was delayed for several months. Magnitudes of pavement heaving as large as 8.9 cm (3.5 in) were measured during a 5-month period. Additional laboratory swelling tests were performed. Based on laboratory coefficients of primary and secondary swell, the magnitude and time rate of swelling were estimated. Time required to complete 95 percent of primary swell was estimated to be about 1.1 years after completion of the subgrades. About 10 months after observed differential heaving, the pavement was milled to remove "humps" and the surface course was placed. Survey points were reestablished. These points have been monitored for about 5 years. Observed swelling at one location is compared to the estimated swelling in Figure 3-60. Five years after placement of the surface course, only about 0.5 cm (0.2 in) of swelling has occurred. Based on the projected linear relationship of swelling and the logarithm of time, an additional 0.5 cm (0.2 in) will occur over the next 22 years.

In situ CBR tests performed often on top of the AFBC spent lime over a 6-year period show that the bearing strength decreased slightly after construction. However, CBR strengths during this period generally exceed 10 and range as high as 40. Pavement rutting, 5 years after placement of the surface pavement, is nominal and generally does not exceed about 0.33 cm (0.13 in). If the 30.5-cm (12-in) layer had been constructed of Coolside material of a nature similar to CS-2, the magnitude of swelling, based on the results in Figure 3-60 could, potentially, range from 8.9 cm (3.5 in)--no surcharge pressure--to about 1.5 cm (0.6 in)--with some surcharge pressure. Considering that a six-inch layer of a pavement provides a surcharge loading of about 0.5 psi, the magnitude of swell is estimated to be about 4.8 cm (1.9 in). However, based on the coefficient of primary swelling 0.13 cm^2/day (0.05 in^2/day), a time of about 2.1 years would be required to complete 95 percent of primary swelling. Moreover, based on a coefficient of secondary swelling, approximately 2.0 cm (0.8 in) of secondary swelling

would occur between the approximate end of primary swelling and 27.4 years after construction. Total estimated swell would be about 6.9 cm (2.7 in). This amount of swelling would probably adversely affect the structural integrity of the pavement. However, field trials and more study would be required to determine the exact swelling behavior of the Coolside byproduct.

If a 30.5-cm (12-in) layer of plastic clay was used as the subgrade, then the magnitude of primary swelling is estimated to be about 3.6 cm (1.4 in). Time required to complete 95 percent of primary swelling is estimated to be about 1.6 years. Estimated secondary swelling that would occur between the end of primary swelling and 27.4 years is 0.25 cm (0.1 in). Total swelling is 4.3 cm (1.7 in). If the silty clay is used to construct the 30.5-cm (12-in) subgrade layer, then estimated primary swelling is about 1.3 cm (0.5 in) and about 1.3 years would be required for this amount of swelling to occur. Secondary swelling is estimated to be 0.13 cm (0.05 in). Total swelling is less than 1.5 cm (0.6 in). Hence, swelling of the two typical clayey soils ranges from 1.5 to 4.3 cm (0.6 to 1.7 in), while estimated swelling of the CS-2 is 6.9 cm (2.7 in).

Although by-products produced from FGD technology, such as the Coolside and FBC by-products, have potential applications in the highway industry, the physical and geochemical processes that lead to swelling of these materials need to be fully understood. Means of controlling the swelling of these materials need to be devised. The physical swelling characteristics of materials from the Coolside technology and an FBC byproduct were examined briefly. Results of swelling tests performed on compacted specimens indicated that primary swelling decreased as the surcharge pressure was increased. Aging the materials before inundating them also appeared to reduce the amount of primary swelling. Coolside byproducts that contained less sulfur, or were aged, swelled less.

The Utilization of Coolside and Other FGD Materials in Highway Embankments

Byproducts produced from flue gas desulfurization (FGD) technology, such as the Coolside technology, for the removal of SO_2 in coal-fired power plants have potential applications in the highway construction industry. As shown previously, the shear and bearing strengths of compacted specimens of byproducts obtained from the Coolside (and fluidized bed combustion --FBC) processes are substantially greater than the strengths of compacted specimens of natural soils. For example, because of the pozzolanic reactions, unconfined compressive strengths of Coolside specimens compacted to 95% of the maximum dry density and optimum moisture content of standard compaction approach values of 6981 kPa (1000 psi) to 17,228 kPa (2500 psi). Unconfined compressive strengths of naturally occurring soils compacted to the same conditions are only about 69 kPa (10 psi) to 414 kPa (60 psi). These strengths approach those of some concretes. The strengths of the compacted Coolside specimens are some 120 to 700 times greater than compacted specimens of soils.

Because of the presence of substantial quantities of calcium oxide (CaO), in the Coolside, as well as other FGD byproducts, the materials could be used in a number of potential applications. For instance, as shown in Figure 3-61, the materials could be used as a chemical admixture to construct base courses of highway pavements. Moreover, byproducts containing high percentages of CaO or $Ca(OH)_2$ could be used to mix, stabilize, and improve the bearing strengths of clayey subgrades (Figure 3-62).

Another application of byproducts similar to the Coolside material could be in the construction of embankments with very steep slopes. Normally, clayey, or silty clays, used to construct highway embankments are constructed on a slope of about two horizontal to one vertical, or about 26.5 degrees. Because of the large strengths of the Coolside material, when compacted, embankments constructed with the Coolside material could be constructed at much steeper angles. By constructing embankments

144
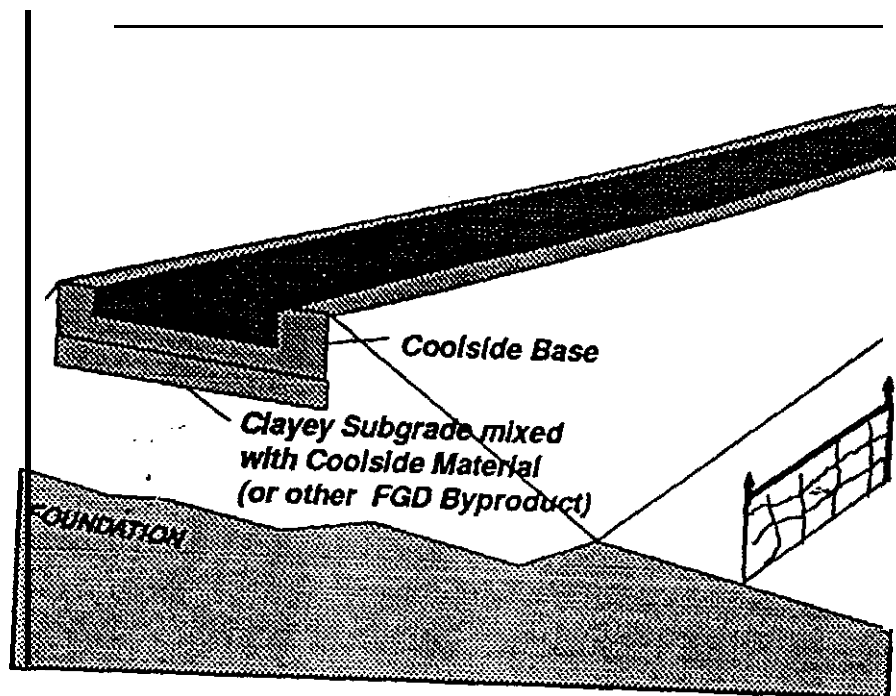
Figure 3-61. Two potential applications of the Coolside byproduct and other FGD byproducts
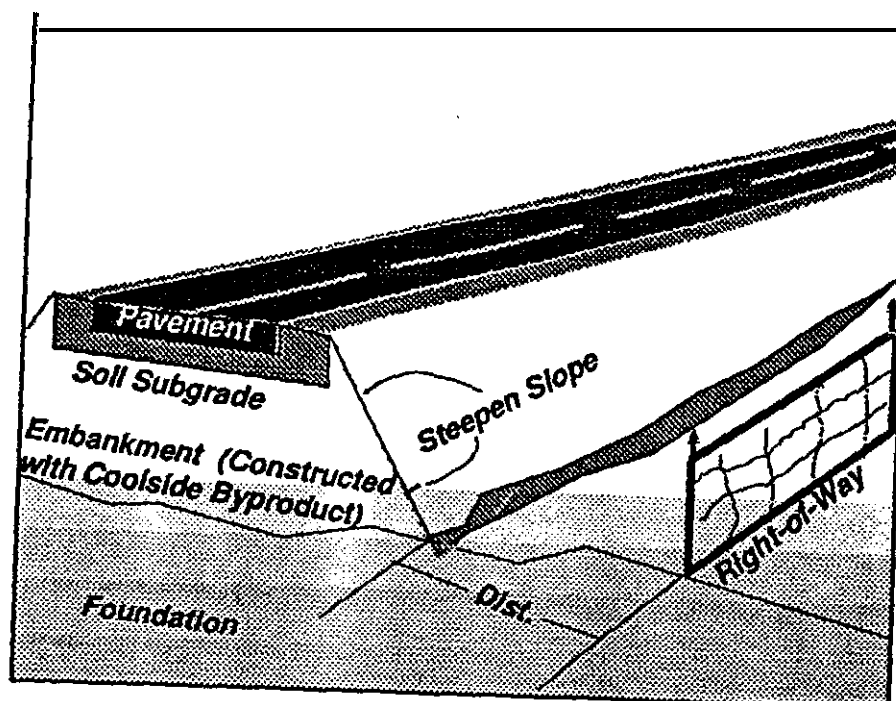
Figure 3-62. Use of Coolside byproduct to construct embankments with a ..Steepen Slope
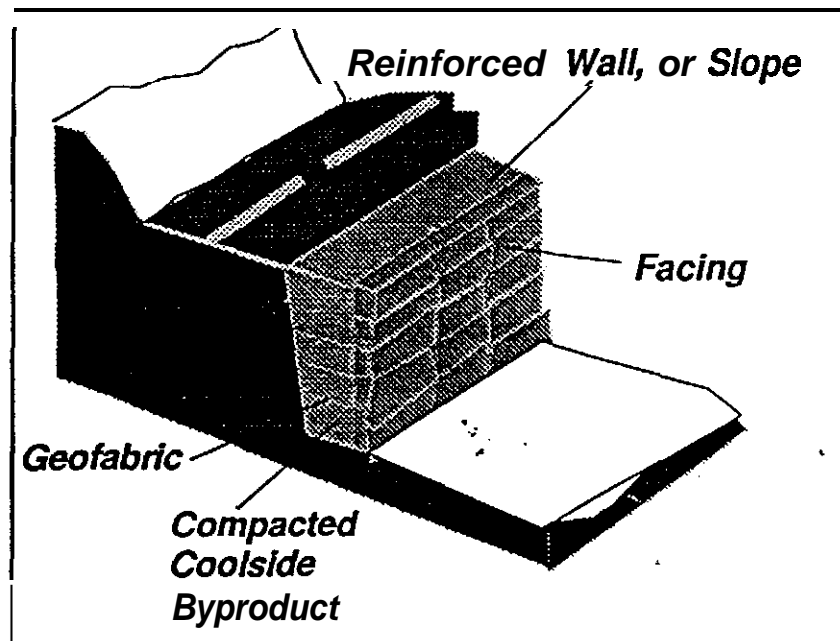
Figure 3-63. Reinforced wall, or slope, constructed with Coolside byproduct

with steep angles, less land is required to construct a highway and a large savings could be realized, especially in urban areas where land may cost several thousands of dollars per acre. In certain instances, the Coolside material could be used with geofabrics to construct vertical walls, as illustrated in Figure 3-63. Because of the large strength of the material, when compacted to standard conditions, the Coolside material could be potentially used to support an embankment on a soft foundation. Geofabric could be used to reinforced the Coolside material, as shown in Figure 3-51.

References

AASHTO; (1995). **Standard Specifications for Transportation Materials and Methods of Sampling and Testing,** Part 11, Seventeenth Edition, Published by the American Association of State Highway and Transportation Officials, Washington, D.C.

ASTM; (1996). **Annual Book of Standards, Soil and Rock (I): D 420-D4914, Section 4 (Construction),** American Society for Testing and Materials, West Conshohocken, PA.

Beckham, T. L. and Hopkins, T. C.; (September 1993). **"Techniques Used in the Placement of Coolside By-Product in Field Lysimeters,"** Proceedings, Tenth Annual International Pittsburgh Coal Conference, Pittsburgh, Pennsylvania.

Casagrande, A., and Fadum, R. E.; (1 940). **Notes on Soil Testing for Engineering Purposes,** Harvard University Graduate School Engineering Publication 8.

Caterpillar Tractor Co.; (October1981). **Caterpillar Performance Handbook,** 1981 Revised Edition, U.S.A.

Daniel, D. E.; (December 1989). "A **Note on Falling Headwater and Rising Tail Water Permeability Tests,"** Geotechnical Testing Journal GTJODJ, Volume 12, Number 4.

147

Graham, U. M., Wu, M. M., Robl, T. L., and Hopkins, T. C.; (Sept. 1993); *"Miners/ogica/ Transformation of Ettringite in Concrete Derived From Dry FGD Byproducts, "* Proceedings, Tenth Annual International Pittsburgh Coal Conference, Pittsburgh, Pennsylvania.

Hopkins, T. C.; (January 1980), *"Shear Strength of Compacted Shales,"* University of Kentucky Transportation Center, Research Report 88-1, College of Engineering, Lexington, KY.

Hopkins, T. C., Hunsucker, D., and Sharpe, G. W.; (October 1988) *"Highway Field Trials of Chemically Stabilized Soil Subgrades,"* Proceedings, ORVSS XIX, Ohio River Valley Soils Seminar, Lexington, Kentucky.

Hopkins, T. C., *"Bearing Capacity Analysis of Pavements,"* Research Report KTC-91-8, University of Kentucky Transportation Center, College of Engineering, Lexington, Kentucky, June 1991.

Hopkins, T. C., and Beckham, T. L.; (September 1993) *"Proposed Procedure for Compacting Laboratory Specimens for Physical Properties Testing,"* Proceedings, Tenth Annual International Pittsburgh Coal Conference, Pittsburgh, Pennsylvania.

Hopkins, T. C.; Hunsucker, D. Q.; and Beckham, T. L.; (October 1993). *"Residue By-product from an Atmospheric Bed Combustion Process Used in Highway Subgrade Modification,"* Syposium Proceedings, Recovery and Effective Reuse of Discarded Materials and By-Products for Construction of Highway Facilities, Sponsored by the Federal Highway Administration and the Environmental Protection Agency.

Hopkins, T. C.; Wu, M. M.; Winschel, R. A.; and Robl, T. L., (January 1993), "The *Ohio Coal Development Office Coo/side Waste Management Demonstration Project,"* Proceedings: Tenth International Ash Use Symposium, Vol.2: Ash Use R&D and Clean Coal By-Products, American Coal Ash Association, Orlando, Florida.

Hopkins, T. C.; Beckham, T. AL.; and Hunsucker, D. Q.; (June 1994). *"Modification of Highway Soil Subgrades,"* Research ReportKTC-94-11, University of Kentucky Transportation Center, College of Engineering, Lexington, Kentucky.

Hopkins, T. C.; (July 1994a), *"Minimum Bearing Strength of Soil Subgrades Required to Construct Flexible Pavements,"* Proceedings, The 4th International Conference on the Bearing Capacity of Roads and Airfields, Vol.1, Minneapolis, Minnesota.

Hopkins, T. C.; (July 1994b), *"Case Studies of Flexible Pavement Failures During Construction,"* Proceedings, The 4th International Conference on the Bearing Capacity of Roads and Airfields, Vol.1, Minneapolis, Minnesota.

McNulty, E. G.; Hopkins, T. C.; and Gorman, C. T.; (1978). *"Analysis of Time-Dependent Consolidation Data,"* Preprint 3280, ASCE Spring Convention and Exhibit.

Terzaghi, K.; (1943), *"Theoretical Soil Mechanics,"* John Wiley and Sons, Inc., New York.

Taylor, D. W.; (1948). *Fundamentals of Soil Mechanics,* John Wiley& Sons, New York, New York.

CHAPTER 4. LABORATORY-LYSIMETER STUDIES

ma

Twenty-two laboratory lysimeters were packed with dry flue-gas desulfurization wastes generated during tests of the Coolside duct-injection Technology. Included in the test matrix were FGD materials from Ohio Edison's 1990 demonstration runs conducted at its Edgewater power plant near Loraine, OH as well as materials derived from runs conducted in CONSOL's Coolside pilot plant in Library, PA. In an effort to characterize the leaching behavior of these materials, water was systematically added to the laboratory lysimeters with the resulting leachate being collected and analyzed on a weekly basis. The primary objective of the study was to generate predictive information on leaching behavior following disposal of Coolside wastes. In addition to the primary objective, the test matrix was designed to examine the impact of various experimental conditions on leaching behavior including 1) lysimeter packing density, 2) use of a constant versus a rain simulation method of water addition, 3) variation in the extent of prehydration of the wastes prior to loading, and 4) exposure to elevated levels of CO_2 in the lysimeter headspace. Following 12 months of leaching, cores were removed from the top, middle, and bottom of each lysimeter for XRD and SEM analyses.

TCLP extractions conducted independently of the leaching study indicated the maximum concentration of extractable hazardous elements to be well below the limits specified by the Federal Resource Conservation and Recovery Act (RCRA) for non-hazardous wastes and often below the analytical detection limits. Leaching results were congruent with the TCLP extractions in that the maximum concentration of hazardous elements in the leachate waters were also well below these same li mits.

The major impact of variations in packing density as well as the level of prehydration was on flow rate (permeability) through the columns which in turn had a significant impact on leaching kinetics. Variation of CO_2 concentrations in the headspace above each column altered the mineralogy of the packed beds and in turn the leachate chemistry. The largest effects of exposure to CO_2 were a decrease in leachate pH, elimination of ettringite, and formation of calcite and gypsum. When the leachate data were examined in terms of total water flow through the column, only minor differences were noted for those columns in which water was added at a fixed weekly volume versus those in which water was added in a manner to simulate regional rainfall.

Due to the massive amount of data generated over a 12-month interval from 22 lysimeters, only those data that are deemed significant or relevant are discussed in this report.

Background

Various scenarios for the use or disposal of the solid wastes generated by the Coolside or similar dry-FGD technologies have been contemplated including landfilling, use as a sub-base for road construction, as soil additive, or light weight aggregate following pelletization. However, none of these strategies maybe realized until it has been demonstrated that the leachates generated from such materials can meet RCRA standards for non-hazardous wastes and that the long-term leaching characteristics are clearly not detrimental to the environment. As discussed elsewhere in this report, the concentrations of hazardous elements extracted from the Coolside wastes are well below RCRA limits as determined by TCLP. However, while useful for determining compliance with RCRA, TCLP does not simulate landfill conditions, nor does it provide information on long term leaching characteristics and/or mineralogic transitions that may occur over prolonged periods. In addition, while actual field studies are the most realistic simulator of landfill conditions, capital costs coupled with sample-size and manpower requirements make it cost prohibitive

to conduct an extensive matrix study of the impact of various packing/leaching parameters or conditions. According y, the laboratory-l ysi meter study was devised with the objective of complimenting a larger-scale concurrent field-lysimeter study by confirming the field results while providing basic information on the impact of leaching parameters unavailable from the larger field study due to cost considerations. To meet these objectives, a total of six Coolside-based samples were loaded to 22 laboratory lysimeters in an effort to monitor long-term leaching behavior and changes in mineralogy.

The lysimeter variables investigated in the study include the solid-waste packing density, the concentration of CO_2 in the column headspace, constant versus rain simulation methods of water addition, and sample prehydration. Due to space limitations, only those results which are deemed significant and/or relevant are discussed. These discussions focus on the impact of packing density, CO_2, and prehydration and for the most part are limited to one sample generated in the Coolside pilot plant (PP run #2) and one sample from the larger scale demonstration-plant runs (Demo run #3).

Experience gained from a preliminary round of lysimeter tests was used to select the conditions and methods employed for a final series of laboratory lysimeters. One of the more significant departures from field conditions is that nearly all the laboratory columns were packed at a relatively low density (loose/static packing) of 49 lb/ft^3. Three of the columns were packed at a more moderate density (proctor-65 lb/ft^3) and none of the columns were packed at the high density level (modified-69 lb/ft^3) included in the preliminary series. Low density packing was emphasized due to problems encountered with low porosity and consequent low flow rates in columns packed at higher density, often precluding the collection of sufficient leachate for analysis. A second significant modification is that, with the exception of the rain-simulation columns, the majority of the columns received a fixed amount of water each week (46.5 or 93.0 mL) as opposed to maintaining fully saturated conditions with a standing column of water over the packed

beds. In this approach, the water added to each column made a single pass through the packed bed then collected in a reservoir at the bottom where it was drained weekly. Two implications of this approach were that water samples were not available for analysis until breakthrough occurred several weeks into the study and this setup provides for the wetting and partial drying of the waste materials during the study, both of which are more similar to prevailing conditions in the field lysimeters. In addition, in an effort to evaluate the impact of high levels of dissolved CO_2 in groundwaters, several of the laboratory columns were blanketed with enriched CO_2 atmospheres (2.5 and 5.0 vol%). The packing and leaching procedures along with the test matrix are detailed in the following sections.

Experimental Design

Samples

A total of 6 waste samples were placed into 22 laboratory I ysimeters. Table 4-1 shows the sample identification, lysimeter number, sample weight, the weight of water addad to the sample prior to packing (prehydration water); packing height, and dry-sample density for each of the lysimeters. The samples identified as Coolside Run #1 and #3 (LC #1 -8) represent FGD wastes from the Edgewater plant demonstration runs 1 and 3, respectively. These materials were comprised of Class F fly ash mixed with $CaSO_4$, $CaSO_3$, $Ca(OH)_2$, and NaOH. The materials loaded to the lysimeters represented blends of material taken from several of the barrels of waste collected during each run. These sample blends had been retained in sealed 5-gallon plastic buckets from the time they were blended until they were loaded to the lysimeters. The samples identified as PP #1 -4 (LC9-1 6, 25-26, and 33-36) represent FGD wastes from the four Coolside pilot-plant tests. These samples were taken from 5-gallon plastic buckets that had remained sealed since early stages of the project.

LC #	SAMPLE ID	Compaction	Fixed Feed	Rain simulation	Fixed Feed-double	CO2 (vol%)	Dry wt (lb)	Prehydration Water (% dry basis)	Column height (in)	Packing Density (lb/cu ft)
1	DEMO RUN 3	loose	x			0	2.138	40.4	24.0	49.0
2	DEMO RUN 3	loose	x			5.0	2.138	40.4	24.0	49.0
3	DEMO RUN 3	loose		X		0	2.138	40.4	24.0	49.0
4	DEMO RUN 3	loose		X		2.5	2.138	40.4	24.0	49.0
5	DEMO RUN 3	moderate	x			0	2.138	40.4	18.0	65.3
6	DEMO RUN 3	moderate	x			2.5	2.138	40.4	18.0	65.3
7	DEMO RUN 1	loose	x			2.5	1.473	40.4	16.5	49.1
8	DEMO RUN 1	loose	x			2.5	1.473	40.4	16.5	49.1
9	PP1	loose	x			2.5	2.138	41.1	24.0	49.0
10	PP2	loose	x			0	2.138	40.4	24.0	49.0
11	PP2	loose	x			2.5	2.138	40.4	24.0	49.0
12	PP2	loose	x			5.0	2.138	40.4	24.0	49.0
13	PP3	loose		x		0	2.138	40.6	24.0	49.0
14	PP3	loose		x		2.5	2.138	40.6	24.0	49.0
15	PP3	moderate		x		0	2.138	40.6	18.0	65.3
16	PP4	loose	x			2.5	2.138	40.4	24.0	49.0
25	PP2		x				2.138	0.0	23.5	50.0
26	PP2		x				2.138	50.0	14.5	81.1
33	PP2	loose			X	0	2.138	0.0	24.0	49.0
34	PP2	loose			X	0	2.138	15.0	24.0	49.0
35	PP2	looso			X	0	2.138	30.0	24.0	49.0
36	PP2	moderate			X	0	2.138	45.0	18.0	65.3

Table 4-1   Test matrix.

Laboratory-Lysimeter Description

A schematic of the laboratory leaching columns fabricated for this study is shown in Figure 4-1. They were constructed from clear-acrylic cylinders, 39 (1 m) in length, 2 (5 cm) inner diameter, and -1/4 (0.6 cm) wall thickness. A plexiglass frit, overlain with one inch of glass wool followed by one inch of Ottawa sand, was sealed in the bottom of each column within a PVC sleeve. The sleeve was in turn connected to a PVC reducing connector and plastic valve that was maintained in the closed position except during leachate collection.

There was an approximate 100 mL void volume between the bottom of the waste bed and the cut-off valve, sufficient for leachate waters passing through the column to collect beneath the waste bed until drained and weighed. This single-pass flow, as opposed to full y-saturated-conditions, was selected since it is believed to more closely simulate conditions encountered within a landfill.

Lysimeter Packing Procedures

Packing the laboratory lysimeters entailed weighing approximately 2.1 lb (-1-kg) of dry sample to a 2-L stainless-steel mixing bowl to which was added a targeted amount of distilled water (prehydration water). The sample and water were then blended with a Kitchen-Aide Classic™ mixer at low speed for approximately five minutes (or until the prehydrated sample had a homogeneous granular appearance). The bowl with prehydrated sample was then placed onto a top-loading balance from where the targeted weight of sample was transferred to a preassembled lysimeter. Each lysimeter was then held vertically and tamped until the targeted column height was attained.

For samples that were loaded to more than one lysimeter, a series of mixtures were prepared as described above with each mixture being split equally among the lysimeters
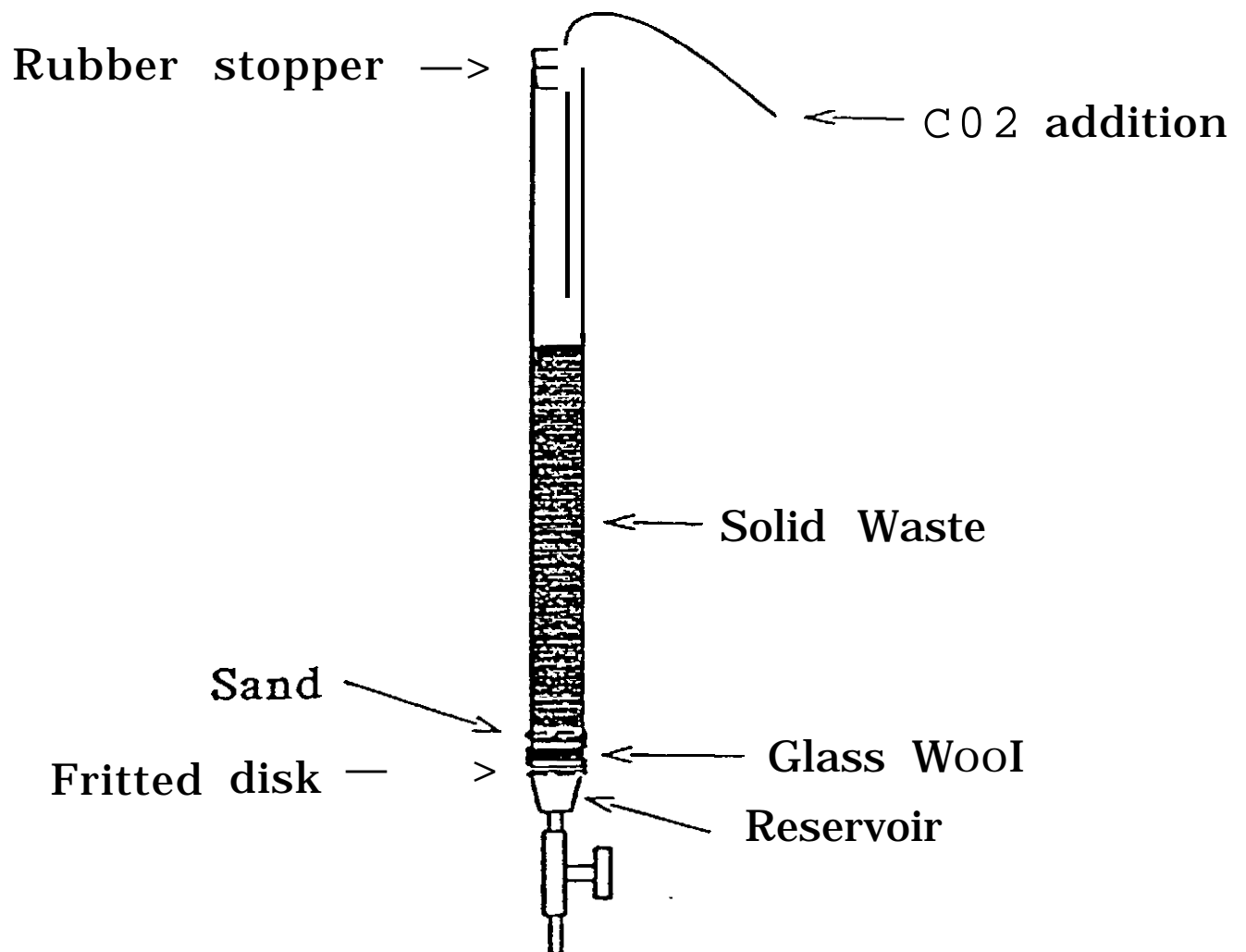
Figure 4-1. Schematic of a laboratory leaching column.

being loaded with that particular sample. Since each mixture contained just enough sample to load one lysimeter, the number of such mixtures prepared corresponded to the number of lysimeters being loaded with that sample. This approach was used to ensure sample homogeneity between different lysimeters containing the same sample.

The exceptions to the packing procedure described above were for lysimeters #7-8 (Demo Run #1), and lysimeters 25,26,33, and 36 (PP #2). For #7 and 8, there was an insufficient amount of sample to pack two columns to a height of 24" at loose density. Instead, the available sample was split between two columns and was intended to serve as a measure of method reproducibility (duplicate conditions). However, as discussed in more detail later, flow problems in LC8 (no flow) prevented the gathering of comparative data for these two columns. The packing of LC25, LC26, LC33, and LC36 varied from the normal procedure because the degree of prehydration was chosen as a test variable for these columns. For LC25 and LC33, the targeted amount of dry sample was loaded to the column without prior water addition (prehydration). For LC26 and LC36, an excess of prehydration water was blended with the sample before loading. The 'mudlike' consistency of these latter high-water-content samples precluded adjusting packing height, i.e. dry density.

All columns were capped with rubber stoppers. With the exception of the rain-simulated columns and those columns exposed to CO_2, these were solid stoppers which served to suppress evaporation. The rain-simulated columns were capped with two-hole stoppers in order to permit some evaporation while restricting the exchange of room air with the headspace atmosphere. Those samples exposed to elevated levels of CO_2 were also capped with two-hole stoppers. For these columns, CO_2-containing gases were delivered through one of the holes and permitted to exit through the other. This approach also permitted evaporation. The use of rubber plugs, as well as the manner in which CO_2 is added, is described more fully in the next section.

Test Matrix

The conditions to which each lysimeter was subjected are shown in Table 4-1.. The same weight of material was targeted for each column with the exception of LC7 and LC8 (Demo run #1). As previously discussed, the limited amount of sample was split evenly between these two columns then the packing height was adjusted to attain the targeted packing density (Table 4-1).

The column headings in Table 4-1 are defined as follows:

<u>*Compaction.*</u> Refers to the packing density of the study samples and is expressed on a dry-sample basis. All columns were packed at either a low-energy compaction of 49 lb/ft^3 (static) or at 65 lb/ft^3 (proctor). These are the packing densities previously determined to correspond to a low-energy static compaction or to that which would result from the pressure applied by the tracks of a Caterpillar D9L track-type tractor using samples from demonstration runs 1 and 3.'

<u>*Fixed Feed and Rain Simulation*</u>. Weekly additions of distilled water were made to each column in one of three manners. For the rain-simulated columns, water additions matched the cumulative weekly rainfall measured at a weather station located approximately 15 miles from the field lysimeters (Farmers-Stanton station). The starting date for rainfall measurements was the week of November 19, 1991. This interval was selected since 1) the 12 month cumulative rainfall measured from this date (46.94 in) matches within one inch the average annual rainfall for this site (46.1) and 2) the field lysimeters were uncovered and exposed to the elements during November of 1992; thus, seasonal wet and dry periods were in rough correspondence for the laboratory and field lysimeters. Weather-

station measurements and water additions to the rain-simulation columns are shown in Table 4-2.

The annual rainfall (46.94) measured from November 19, 1991 through November 18, 1992 at the Farmers-Stanton Station equates to the addition of 46.5 mL of water%.veek to a 2" diameter column. Thus, 46.5 mL of distilled water were added to each of the fixed-feed columns as designated under the *fixed water feed* heading of Table 4-1. By virtue of this approach, both the rain-simulated and fixed-feed columns received equivalent amounts of water over the 12-month study interval. Water was added in a similar matter to those lysimeters as indicated in the *fixed feed-double* heading (LC33-36), only the volume of added water was doubled to 93.0 ml/week. These latter columns were included in the study six weeks after water feed had been initiated to the other lysimeters. The objective for these columns was to expand the examination of prehydration, particularly with respect to the impact on flow rates. They were not intended for a full 12-month study since other columns (LC25-26), in which prehydration water was also a test variable, were already in place for that purpose. Thus, a doubling of the feed rate served to accelerate this phase of the study, permit the study to be completed on schedule, and provide additional information on the impact of prehydration.

The rain-simulated and fixed-feed columns also differ in that water added to the rain-simulated columns was permitted to evaporate and exit the column through a two-hole rubber stopper used to cap these columns. Thus, it is anticipated that some drying of the upper portions of the packed solids will occur during the study, particularly during dry periods (low or no water additions during dryer periods). This was also the case for the fixed-feed and rain-simulation columns which were continuously purged with a blend of N_2 and CO_2 as described in the next paragraph. The remaining fixed feed columns were capped with solid rubber stoppers for the duration of the study to suppress evaporation.

Week number of test	Rain measurement week (1991)	Weather station rainfall	Date H2O added to columns	mL H2C added to columns		Week number of test	Rain measurement weak (1991)	Weather station rainfall	Date H20 added to columns	mL H2C added to columns
1	25-Nov	1.71	24-Jan	66.03		27	27-May	0.04	25-Jul	2.94
2	02-Dec	1.32	31-Jan	67.96		28	03-Jun	1.25	01-Aug	64.35
3	09-Dec	3.08	07-Feb	158.56		29	1 0-Jun	0	08-Aug	0
4	16-D9C	1.32	14-Feb	67.96		30	17-Jun	0.18	15-Aug	9.27
5	23-Dec	0.62	21-Feb	31.92		31	24-Jun	0,67	22-Aug	44.79
6	30-Deo	1.14	28-Feb	66.69		32	01-Jul	1.03	29-Aug	53.03
7	07-Jan	1.26	07-Mar	64.67		33	08-Jul	0.5	05-Sep	25.74
8	14-Jan	0.64	14-Mar	32.95		34	15-Jul	2.44	12-Sep	125.5
9	21-Jan	0.23	21-Mar	11.s4		35	22-Jul	1.97	19-Sep	101.5
10	28 Jan	0.22	28-Mar	11.33		36	29-Jul	0.51	26-Sep	26.26
11	04-Feb	0.23	04-Apr	11.64		37	05-Aug	0.01	03-Oct	0.51
12	11-Feb	1.14	11-Apr	58.69		36	12-Aug	2.16	1 0-Oct	1112
13	18-Feb	1.66	18-Apr	66.49		39	19-Aug	0,46	17-Oct	24.71
14	25-Feb	0.56	25-Apr	29.66		40	26-Aug	0,39	24-Oct	20.08
15	04-Mar	0.61	02-May	41.7		41	02-Sep	0.03	31-Oct	1,54
16	1 I-Mar	0,51	09-May	26.26		42	09-Sep	1.06	07-Nov	54,57
17	18-Mar	1.46	1 6-May	75.16		43	16-Sep	1.25	14-Nov	64.35
18	25-Mar	2.65	23-May	146.72		44	23-Sep	0.17	21-NW	6.75
19	01 -Apr	1.22	30-May	62.61		45	30-Sep	2,38	28-Nov	'122.53
20	08-Apr	0.4	06-Jun	20.S9		46	07-Oct	0.68	05-Dec	35.01
21	15-Apr	2.37	13-Jun	122.01		47	14-Oct	0.01	12-Dec	0,51
22	22-Apr	0.56	20-Jun	26.S3		48	21-Oct	0.21	19-oOc	10.61
23	29-Apr	1.03	27-Jun	53.03		49	28-Ott	0,77	26-Dec	39.64
24	06-May	0.26	04-Jul	13.39		50	04-Nov	0,01	02-Jan	0.51
25	13-May	1.15	11-Jul	59.2		51	11 -Nov	0.01	09-Jan	0.51
26	23-May	0.49	18-Jul	25.23		52	18-Nov	0.25	16-Jan	12.87

	Weather station rainfall	mL H2C added to columns
total	46.94	2416.5
average	0.90	46,47

Table 4-2. Weekly rainfall measurements from the Farmers-Stanton weather station and equivalent water additions to the rain-simulation lysimeters.

%_CO2._ CO_2 concentrations in the lysimeter headspace were maintained at either ≤ 0.03 (atmospheric abundance), 2.5, or 5.6 vol% (Table 4-I). The CO_2-containing gas streams were continuous y routed in parallel to the appropriate columns at a rate of 10-15 cm^3/min/column for the duration of the study. These gases were dispensed from compressed gas cylinders via l/8-id. x 1/4"-o.d. tygon tubes through a two-hole rubber stopper used to cap the CO_2-purged columns. The ends of the delivery tubes were positioned approximately 12" down into the void space above each packed bed. The 1/4" exit holes of each of the rubber stoppers were constricted with 1/8" x 1/1 6"-o.d. plastic reducing unions which served to suppress exchange of void-space gases with room air as well as to provide a more uniform distribution of the CO_2-containing gas stream among the columns. This parameter was selected for study since groundwaters typically contain CO_2 levels well in excess of atmospheric abundance and it is believed that the carbonate anions present in such waters may have a significant impact on the leachate pH, leaching kinetics, and waste mineralogy.[2]

Prehydration Wafer. After encountering problems with heating, swell, and loss of porosity in an initial series of tests, a decision was made to prehydrate the Coolside samples prior to loading, with the exception of LC25 and LC33 which were loaded dry. The values shown for prehydration water are expressed as a percentage of the dry sample weight and indicate the amount of distilled water blended with the sample prior to loading. Except for LC25, 26, and 33-36 in which prehydration was a test variable, a moisture content of 42% was targeted (proctor moisture) since this level provided a granular consistency that was conducive to water flow. Addition of excess water to LC26 and LC36 resulted in a 'mudlike' consistency and precluded adjusting packing density. Immediately after loading, the dry-packed column could only be tamped to a height of 26-27" without risk of breaking the column. However, these columns settled slowly for several days to a final height of 23.5 and 24" for LC25 and LC33, respectively, following the first water addition.

<u>*Dry Weight.*</u> The weight of dry sample loaded to each column.

Flow Problems

As previously mentioned, LC7 and LC8 were packed as duplicate columns and were included as a means to evaluate reproducibility. However, while LC7 flowed freely, LC8 did not. Since this rendered the data from LC8 meaningless, these data will not be presented or discussed in this report. Data on total ion elution from LC7 is presented in Table 4-3 to serve as a comparison to other Coolside samples. LC8 was dissected at the conclusion of the study and the problem was diagnosed as an insufficient amount of glass wool in the bottom of the column. This permitted the overfying sand to block the drain holes in the fritted disk thereby preventing flow through the column.

In addition to the flow problems encountered with LC8, problems with low flow rates were also encountered in LC15, 16, 25, 26, 33, and 36. These low flow rates were apparently due to the level of prehydration selected for LC25, 26,33, and 36 as discussed in the results section. However, for LC1 4-16, the reasons for the unacceptably low flow rates are unknown. Elemental release from these latter columns appeared to be dictated by total flow rendering comparisons between these lysimeters and the free-flowing lysimeters invalid. For this reason, discussion of leaching data for LCI 5-16 is also omitted. In addition, discussion of the data fromLC13 and LC14, which were coupled wfth LC15 in the matrix study, will be limited.

Leachate Analysis

Each weekly collection of leachate waters was analyzed for pH, alkalinity, conductivity, anions (SO_4, SO_3, Cl, NOS., Br), and cations/metals (Ag, Al, As, B, Ba, Be, Ca, Cd, Co, Cr, Cu, Fe, K, Mg, Mn, Mo, Na, Ni, P, Pb, Se, Si, Ti, V, Zn). Splits of each leachate were

	LC1	LC2	LC3	LC4	LC5	LC6	LC7	LC9	LC10	Lysim # LC11	LC12	LC13	LC14	LC25	LC33	LC34	LC35
	Dem3	Dem3	Dem3	Dem3	Dem3	Dem3	Dem1	PP1	PP2	PP2	PP2	PP3	PP3	PP2	PP2	PP2	PP2
Water Feed	Fixed	Fixed	Rain	Rain	Fixed	Fixed	Fixed	Fixed	Fixed	Fixed	Fixed	Rain	Rain	Fixed	Double	Double	Double
C02	0	5	0	2.5	o	2,5	2.5	2.5	0	2,5	5	0	2.5	0	0	0	0
compaction	Loose	Loose	Loose	Loose	Proctor	Proctor	Loose	Loose	Loose	Loose	Loose	Loose	Loose	Loose	Loose	Loose	Loose
Water added-mL	2442	2442	2435	2435	2442	2442	2347,7	2207	2442	2442	2442	2337	2334	2207	1635	4228	4228
Recovery (%)	91,5	77.9	81.0	89,5	87.8	02,4	85,0	34.8	02.2	94.7	87.8	89,3	S1,8	61,9	27.8	02,7	81,0
Ag (mg)	0,00	0.00	0.00	0.00	0.00	0,00	0	0,00	0,00	0.00	0,00	0,00	0.00	0,00	0.006	0.00	0.00
Al (mg)	8,84	9.95	8.84	1,43	36.66	24,85	5,38	7,47	25.32	11,56	8.40	0.53	0.22	24.36	5,30	96.7	64.9
As (mg)	2.14	1.66	2,17	2.85	4.19	4.38	2.22	0,083	0.5S	0.69	0.61	0.00S3	0,12	1.18	1,11	1,55	2.40
B (ma)	7.57	90,3	5.40	20.0	5.48	7.13	5.09	0.42	0.89	1.37	11.39	0,37	0.28	2.04	2,10	4.09	4,57
Ba (mg)	0.056	0.022	0,041	0.021	0.01 e	0,012	0,021	0,0s0	0.023	0.185	0.309	0.069	0.048	0,040	0.023	0,032	0.027
Ca (mg)	142,7	858.9	11S,3	94.5	30.7	33,0	73,2	39,0	69.9	188.0	699.5	134,$	82.3	79.5	40,4	89.0	81.7
Cd (mg)	0,000	0,000	0,000	0.000	0.00	0,00	0,00	0.000	0,000	0.000	0.000	0.000	0.000	0.005	0,000	0.0004	0,0010
Cr (mg)	0.0003	0,000	0.0011	0,000	0.000	0.0007	0,0000	0,0015	0.004	0,0081	0,000	0.000	0,0690	0,0273	0,0004	0,0005	0.0000
K (mg)	3302	1834	2841	3315	2520	2830	2053	2845	till	134s	1202	1243	830	1850	1120	1978	1813
Mg (mg)	0.063	1.97	0.070	0.071	0,045	0.058	0.067	0.061	0,084	0,062	1.73	0.119	0.087	0,031	0.018	0.10	0.12
Na (mg)	10632	8404	8617	11181	8269	87.92	5846	16694	9669	12497	12702	824	374	21072	12835	17565	18837
Ni (mg)	0,00	0.00	0,00	0,00	0.00	0.00	0,00	0,00	0,00	0.00	0,00	0,00	0,00	0.014	0.000	0.001	0,0010
Pb (mg)	0.011	0,001	0,013	0,000	0.001	0,000	0,000	0,000	0,000	0.000	0,000	0.000	0,0060	0,000	0,000	0,000	0.000
Se (mg)	1,23	1.14	1.17	1,40	1.02	1.25	1,01	0.14	0.12	0,23	0.15	0,005	0,00	0.13	0;12	0,25	0,21
cl (mg)	10601	4208	8078	10568	0326	10516	4041	666	591	629	935	13.5	74	772	738	1509	1449
Br (mg)					1031	<678,2	756.9	1159	1073	1345.8				2502	1941	5437	5474
S04 (mg)	11747	1,0413	10032	1 0631	3454	4790	6399	30421	18231	22209	24663	27S5	1864	42.589	33100	34538	32644
Alkalinity	2070	1948	20S4	2678	5311	4850	2031	17078	4963	4418	3.589	496		3778		7106	8076
Ave pH	11,73	10.76	11,00	11.76	12.22	12.15	11.65	12.81	12.14	11,92	10.97	0,87	9.42	11.82	1<.81	11.93	11.82
Ave Conductivity	21.77	18.07	21.04	22.64	20,89	21,79	14,48	46.66	17.46	20.36	21.34	4.18	3.81	34.87	69.31	16.51	17.38

Table 4-3. Total eluted weights for selected ions calculated as the product of the
leachate water weight and ion concentrations summed over the full study interval.

treated with acid immediately after collection to stabilize the samples prior to metals (cation) analysis. All analyses were conducted as soon as practical following leachate collection, particularly for PH and anions (usually same day).

Anions were determined by EPA Method 300.0, *The Determination of Inorganic Anions in Water by Ion Chromatography.* Conductivity and pH were determined using classical electrometric techniques. An Orion Microprocessor Ionanalyzer/901 was used to measure pH and a YSI Model 32 conductance meter to measure conductivity. EPA Method 1620, *Metals by Inductively Coup/cd Plasma Atomic Emission Spectroscopy,* was followed for major and trace elements with a Spectrametrics ICP-AES coupled with a CETAC U-5000 ultrasonic nebulizer.

At the end of the 12-month study period, 1/2 mres were removed one inch from the top, one inch from the bottom, and from the middle of each packed bed. XRD spectra were obtained on each core sample with a Philips APD 3500 X-ray diffractometer, using CU-K radiation (=1 .5418 rim), scan speed of two counts/second, and an increment of O.1° over a 2q range from7to600.

Results

The presentation of the laboratory-lysimeter results that follow is divided into sections. In the first section, total ion elution from the majority of the lysimeters, including information on RCRA elements, is shown. This is followed by discussion of the lysimeter results in subsets. That is, LC1 -6 are treated separately as they were designed to examine the impact of the method of water addition, packing density, and an enriched CO_2 atmosphere on materials from Demonstration Run #3. Likewise, LC1 O-12 examines the impact of CO_2-enriched atmospheres on material from PP2 and LC33-36 will be used to demonstrate the impact of differences in prehydration on leaching behavior, also on material from PP2.

Total Ion Elution

Table 4-3 shows the total weight of selected ions that was eluted from each laboratory lysimeter over the course of the study. These values were obtained by multiplying the weight of leachate water collected each week by the coinciding ion concentrations then summing over the full study interval. The total leachate weights listed in Table 4-3 represent a 52 week interval with the exception of LC7 (50 wks), LC9 (47 wks), LC25 (47 wks), and LC33-35 (45 wks). Since not all columns exhibited free flow, Table 4-3 also shows the weight of water added to each column on an absolute basis as well as the amount of water collected, expressed as a percentage of the weight of added water. As discussed in the experimental section, low flow rates were a particular problem in lysimeters LC8 (660 mL recovered),LCl5(173 mL), LC1 6 (1 85 mL), LC25 (1 364 mL), LC26 (2 mL), LC33 (438 mL), and LC36 (O mL). For LC 25,26,33, and 36, the low flow rates were due to the level of prehydration water added to the samples prior to packing. The reason for flow problems in LC8 was found to be blockage of the drain holes in the fritted disk underlying the sample bed and the same problem is suspected forLC15 and LC16. Since the low flow rates in these latter columns precluded valid comparisons with the other columns that exhibited good flow characteristics, leaching data for several of these lysimeters are omitted from Table 4-3.

Scrutiny of the data of Table 4-3 shows the leachates from LC9 (PP1) exhibited the highest average pH and total alkalinity values. Leachates from LC1 3-14 (PP3) exhibited the lowest pH, alkalinity, and conductivity. LCl -7 (demonstration runs 1 and 3) exhibited the greatest release of Se, As, and Cl. The remaining lysimeters (PP2) were unremarkable with the exception of relatively high SO_4 release. Unfortunately, LCl 6 which was packed with the remaining Coolside sample (PP4), did not flow. Due to the voluminous amount of data in

Table 4-3, additional discussion of the leaching results is deferred to subsequent sections which examine the column data in a less cumbersome form.

TCLP Extraction Data

Results from TCLP extractions for the six Coolside samples are shown in Table 4-4. Also shown are the RCRA hazardous element limits which are used in defining hazardous versus non-hazardous wastes for disposal purposes. Materials from Demonstration runs 1 and 3 were blended prior to conducting this analysis. As can be seen, all of the RCRA elements were either below detection limits or well below limits specified by RCRA. However, pH values for both pilot plant #3 and #4 exceeded the RCRA limit of 12.5 in this analysis. This is somewhat surprising in that it was pilot plant tests 1 and 2 to which a sodium promoter was added and the presence of elevated Na would be expected to lead to greater release of NaOH which in turn yields pH levels higher than those from $Ca(OH)_2$.

The top half of Table 4-5 shows the maximum concentrations of the RCRA elements along With maximum pH values that were measured in the column leachates over the course of the study.' Ag and Cd were below detection limits in all leachates while Pb was below detection limits in all of the pilot plant samples and at trace levels in the remainder. For the lysimeters packed with pilot plant materials, only arsenic in LC33 exceeded RCRA limits as defined for TCLP extraction. In contrast, all of the lysimeters packed with demonstration run materials exceeded the TCLP-defined limits for Se and all but two (LCI and LC7) exceeded the limit for As. Though detected, none of the remaining hazardous elements exceeded RCRA limits in any of the lysimeters.

---

*Note that ion concentrations and pH values for the leachate waters are not required to met RCRA limits. The data is presented in this format for comparative purposes only.

	κCκA Limit (ppm)	ppm				
		Demonstration Runs #1 + #3	Pilot Plant Run #1	Pilot Plant Run #2	Pilot Plant Run #3	Pilot Plant Run #4
Ag	5.0	<0.01	<0.01	<0.01	<0.01	<0.01
As	5.0	0.70	<0.03	<0.03	<0.03	<0.03
Cd	1.0	<0.001	<0.001	<0.001	<0.001	<0.001
Cr	5.0	0.002	0.018	0.023	0.033	0.019
Hg	0.2	<0.0005	<0.0005	<0.0005	<0.0005	<0.0005
Ba	100.0	0.095	0.114	0.151	0.236	0.235
Pb	5.0	<0.02	<0.02	<0.02	<0.02	<0.02
Se	1.0	0.12	<0.03	<0.03	<0.03	<0.03
pH	12.5	12.07	12.44	12.45	12.59	12.58

Table 4-4. TCLP extraction data.

	RCRA Limit (ppm)	Max mum Measured Concentrations (ppm)												
		Dem3	Dem3	Dem3	Dem3	Dem3	Dem3	Dem1	PP1	PP2	PP2	PP2	PP3	PP3	PP2
		LC1	LC2	LC3	LC4	LC5	LC6	LC7	LC9	Lc10	LC11	LC12	LC13	LC14	LC33
Ag	5.0	<.01	<0.01	.0.01	<0.01	<0.01	.0,01	<0.01	<0.01	<0.01	<0.01	.0.01	<0.01	<0.01	.0,01
As	5.0	2.9	5.75	6.5	5.2	8.75	5.0	2.55	0.50	4.1	2.8	3.0	0.35	4.1	6.6
Cd	1.0	<0.001	.0.001	<0.01	<0.01	<0.01	<0.01	<0.01	<0.01	<0.01	.0.01	.0.01	0.01	<0.01	<0.01
Cr	5.0	.018	.0.001	0.017	<0.001	0.01	<0.001	<0.001	0.055	0.037	0.038	.0.001	<0.001	0.007	0.075
Ba	100.0	.165	0.12	0.121	0.0.42	0,091	0.065	0.083	0.145	0.079	1.10	1.75	0.08	0.064	0,16
Pb	5.0	0.13	0.14	0.15	<0.02	0.15	<0.02	80.02	<0.02	<0.02	<0.02	<0.02	<0.02	.0.02	.0.02
Se	1.0	3.5	2.80	3.2	2.7	3.6	3.2	4.0	0.50	0.58	0.80	0.45	0.40	<0.03	0.9
pH	12.5	11.96	12.19	12.15	11.99	12.81	12.49	12.08	13.02	12,53	12.77	12.73	10.43	10.7	12.15
		Samples In excess of RCRA limit (# of weeks)													
Ag		o	0	0	o	0	0	0	0	0	0	0	0	0	0
As		o	1	2	1	6	1	0	0	0	0	0	0	0	3
Cd		o	0	0	0	0	0	0	0	0	0	0	0	0	0
Cr		o	0	0	0	0	0	0	0	0	0	0	0	0	0
Ba		o	0	0	0	0	0	0	0	0	0	0	0	0	0
Pb		o	0	0	0	0	0	0	0	0	0	0	0	0	0
se		8	11	10	9	10	9	5	0	0	0	0	0	0	0
pH		0	0	0	0	3	0	0	34	1	2	2	0	0	0

Table 4-5. Maximum concentrations of RCRA elements and pH measured in the leachate waters from the lysimeters packed with Coolside wastes.

The pH limit of 12.5 was exceeded in one or more of the leachate collections in LC5 and in LC9-LC12, particularly in LC9 (PP1) which remained above 12.5 for most of the study, These high pH values from LC9 likely reflects the use of sodium promoter in this run with the sodium eluting as NaOH which tends to increase pH above the 12.5 limit. Sodium promoter was also used in pilot plant #2 tests but the use of sorbent recycle in this run may have effectively had a dilution effect on the Na. Despite pH values being in excess of 12.5 by TCLP for the pilot plant 3 sample, such was not the case for the leachate from the lysimeters packed with this sample(LC13-LC15).

The bottom portion of Table 4-5 shows the number of collected leachate samples in which the RCRA limits were exceeded. For the most part, those lysimeters that exceeded RCRA limits did so in only 1-3 samples during the study, again with the exception of pH in LC 9 (34 samples), As in LC5 (6 samples), and Se in all the lysimeters packed with demonstration run materials (LC1-LC7). It is interesting to note that the only difference in LC1 and LC5 was that LC5 was packed at a higher density yet LC5 was the only lysimeter packed with demonstration run materials that exceeded the 12.5 pH limit, doing so on three different occasions. This compares to zero samples above the pH limit from the other six lysimeters.

Demonstration *Run* #3. The test matrix for the six columns packed with wastes from demonstration run #3 (LC 1 -6) was devised to examine the impact of packing density, the method of water addition, and variation of gaseous CO_2 concentrations in the column headspace (Table 4-1). In this study, the fixed-feed (LC1 -2) and rain-simulation columns (LC3-4) exhibited free flow from about week 5 onward, i.e., collection rates essentially tracked water addition rates (Figure 4-2). LC5 and LC6, packed at higher densities, did not exhibit free flow until about week 18 at which time a large 'slug' of water passed from each column, followed by free flow for the remainder of the study. Despite differences in packing density and the manner of water addition, pH values were relatively constant and similar for
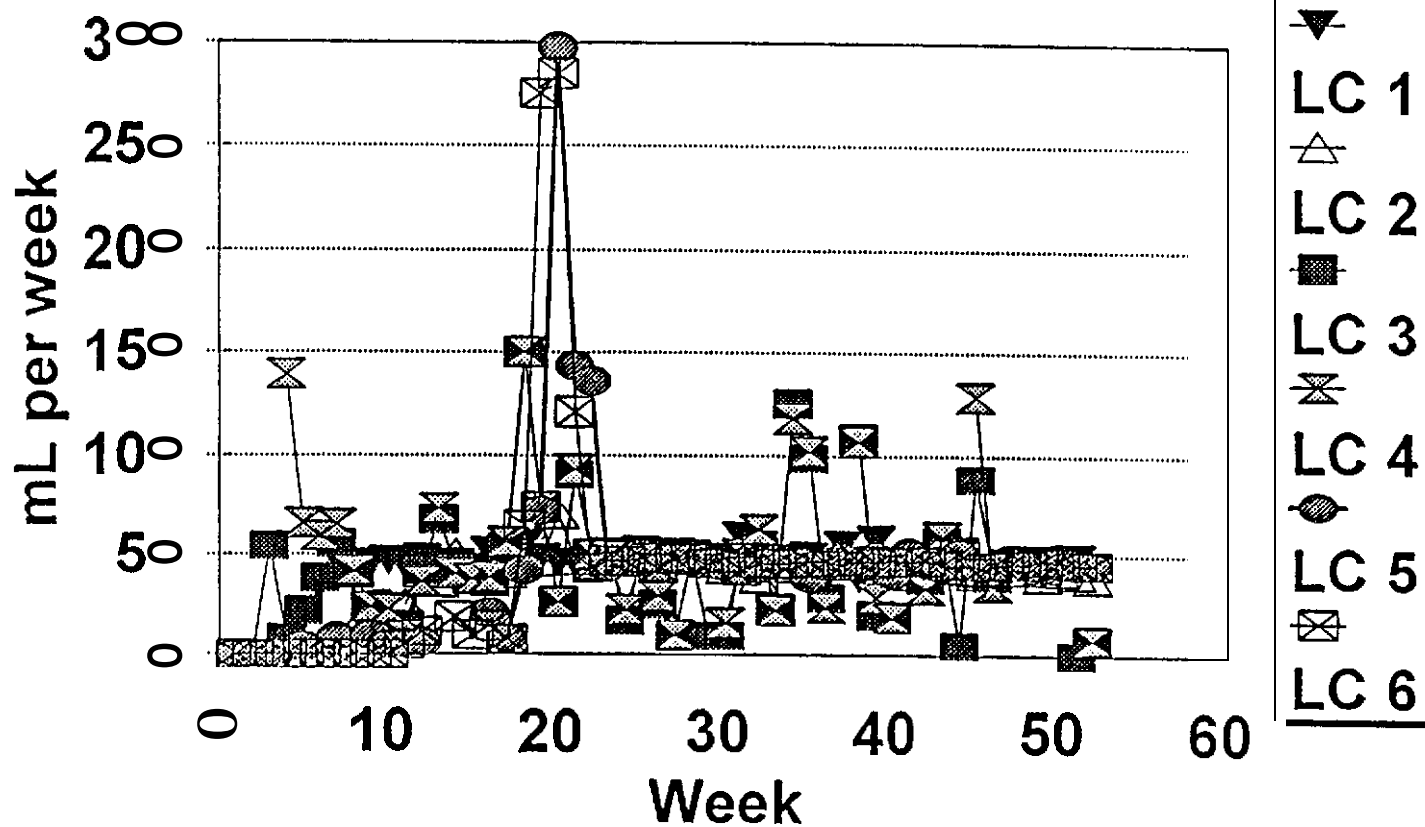
Figure 4-2. Water collections from LC1-LC6.

LC1, LC3, and LC5 which were blanketed with room air (Figure 4-3). In contrast, pH values for LC2 (5.0% CO_2) declined midway through the study to the 9-11 range, indicative of CO_2 uptake and ensuing carbonate buffering. For LC4 (rain simulation/2.50/0 CO_2), PH remained around 12.0 until near the end of the study at which time PH values also dropped to the 9-11 range for the latter three measurements (six weeks of collections). The pH for LC6 (higher density/2.5% CO_2) was initially at approximately 11.5 then increased to near 12.0 and remained at that level for the remainder of the study. Thus, LC2 which was blanketed with the highest level of CO_2 exhibited the largest pH drop followed by LC4 blanketed with 2.5% CO_2 and loosely compacted. LC6, packed at a greater density, was relatively unaffected by the presence of elevated levels of CO_2 in the column headspace despite exhibiting total flows similar to those of LC2 and LC4.

Elemental release patterns for LC1 -6 can roughly be divided into three patterns. The first, represented by the plots of Figure 4-4, appears to include highly soluble ions that were rapidly depleted as a function of flow rate. Thus, the rain-simulated columns (LC3 and LC4), to which relatively large volumes of water were added early in the study, were the first to be depleted. The columns packed at higher density, LC5 and LC6, which were the last to flow, were the last to be depleted. LC1 and LC2 were intermediate in both flow rate and time to depletion of the highly soluble elements, relative to LC1, LC2, LC5, and LC6. In addition to the ions shown in Figure 4-4, Se and Mo also followed this patfern with maximum Mo values in the 100 ppm range and Se maximizing around 3 ppm. Since with the exception of hydroxyl ions, Na and Cl are by far the most prevalent ions in the leachate waters, conductivity followed trends similar to those shown in Figure 4-4 as well.

The second type of leaching pattern for LC-LC6, illustrated by the plots of Ca, Mg, and B in Figure 4-5, appears to correlate with leachate pH. For all three plots, ion concentrations varied inversely with pH. Even the 'hump' in Ca ion concentration around week 10 in LC1 and LC3 corresponds to a dip in pH that occurred at that time. At high pH, Ca and Mg
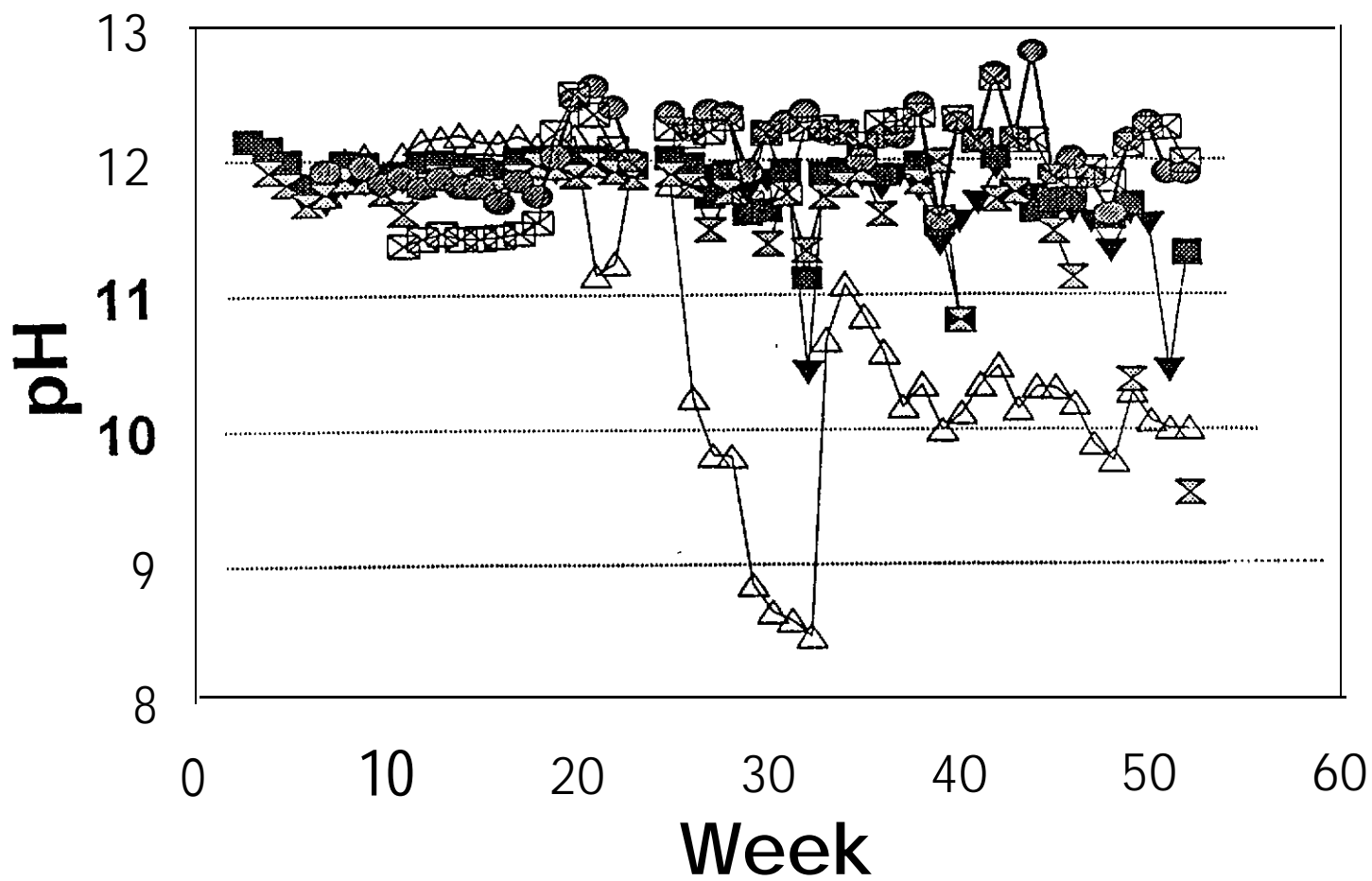
Figure 4-3. pH of the leachate waters collected from LC1 -LC6.
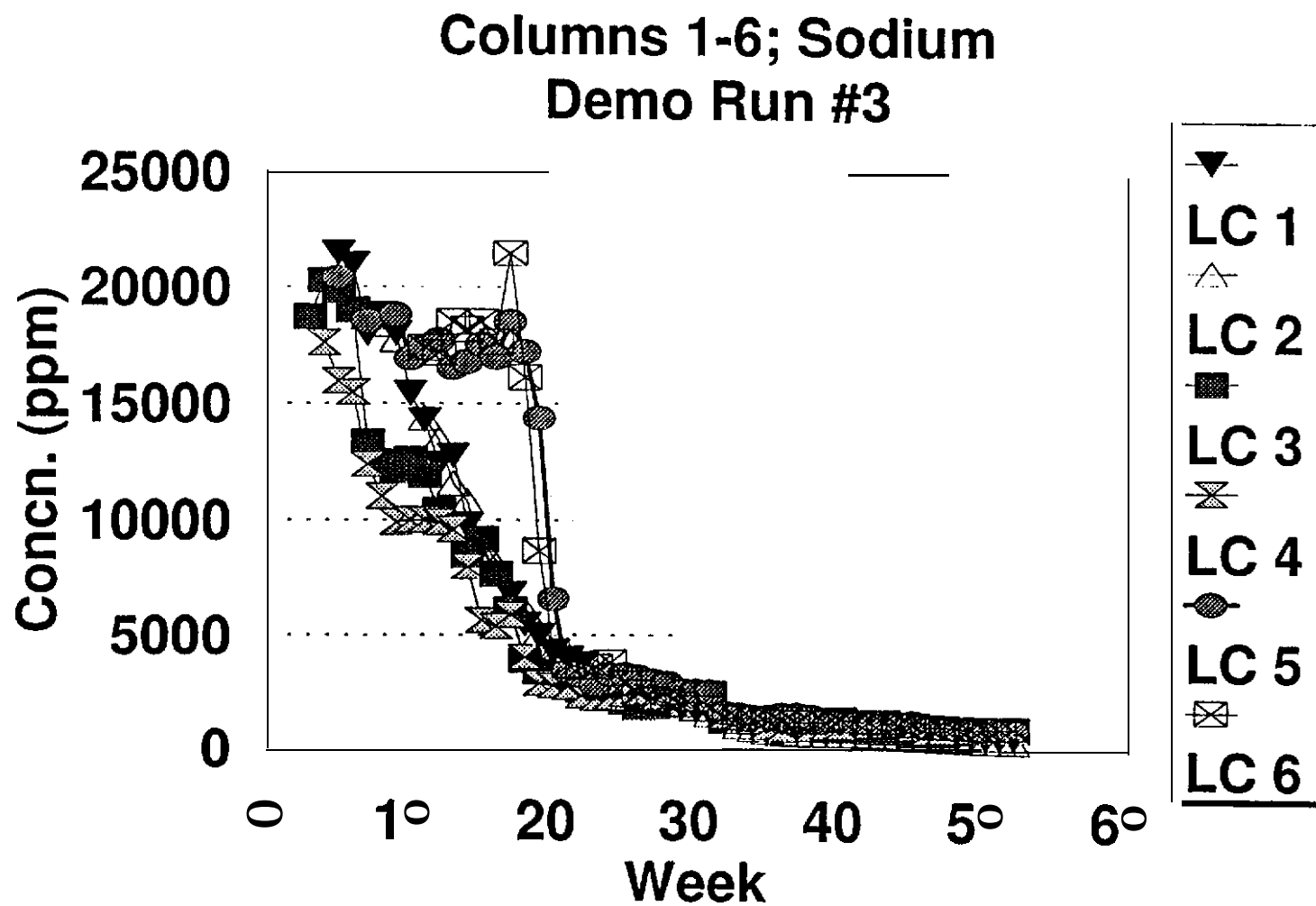
Figure 4-4a. Flow-rate-controlled leaching patterns for LC1-LC6 (Na-t).
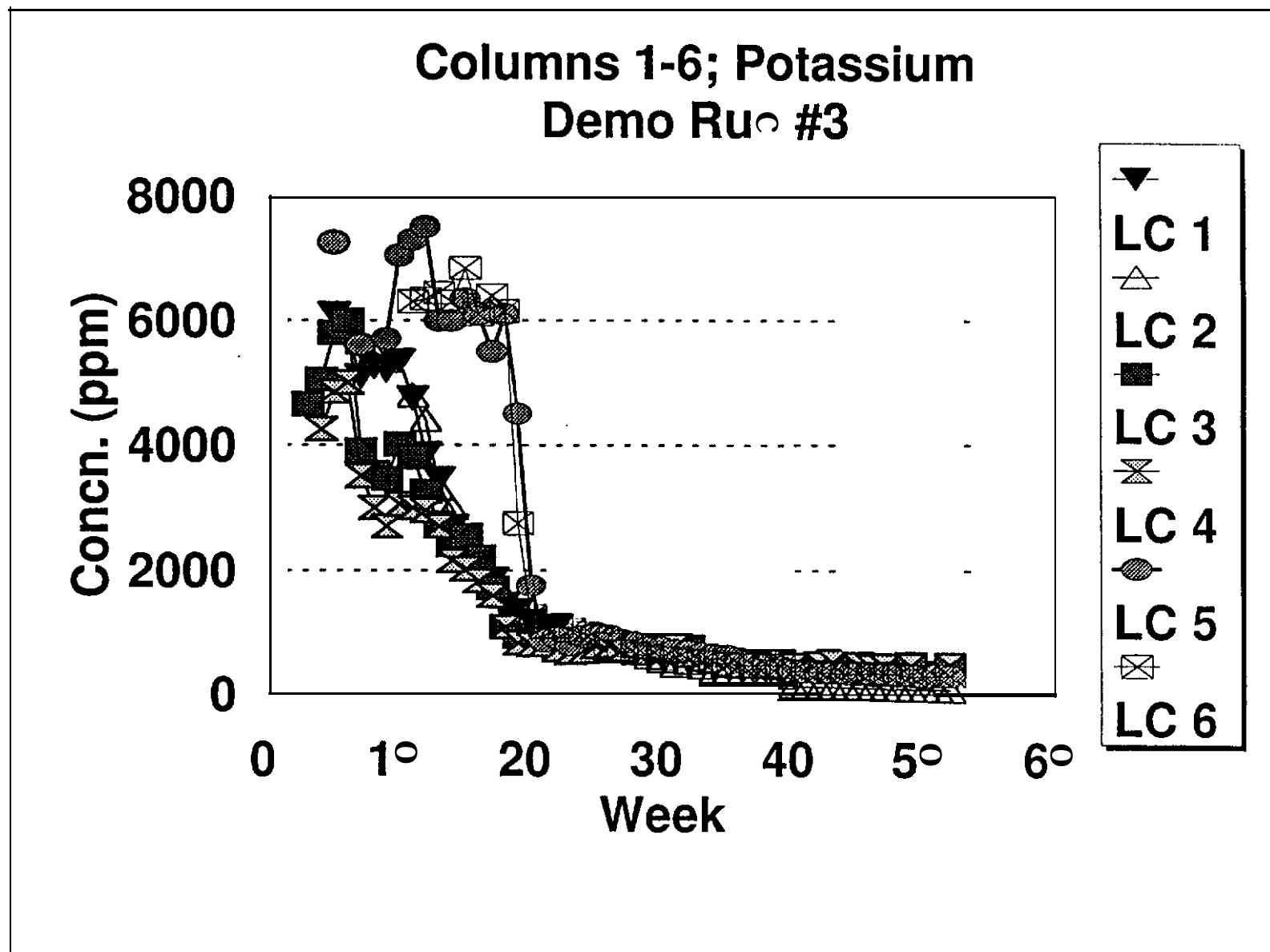
Figure 4-4b. Flow-rate-controlled leaching patterns for LC‌-LC6 (K-m).
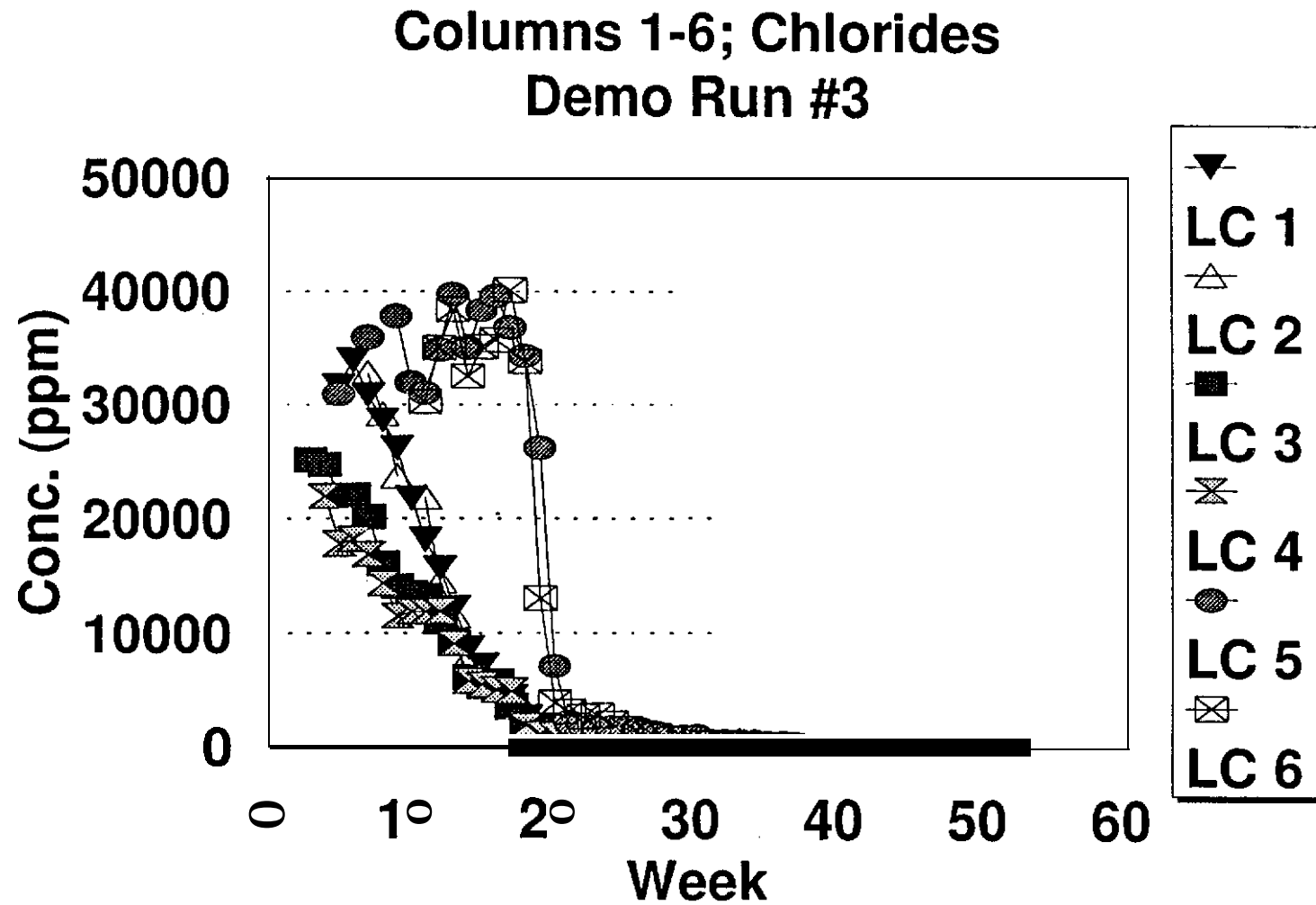
Figure 4-4c. Flow-rate-controlled leaching patterns for LC1-LC6 (Cl-b).
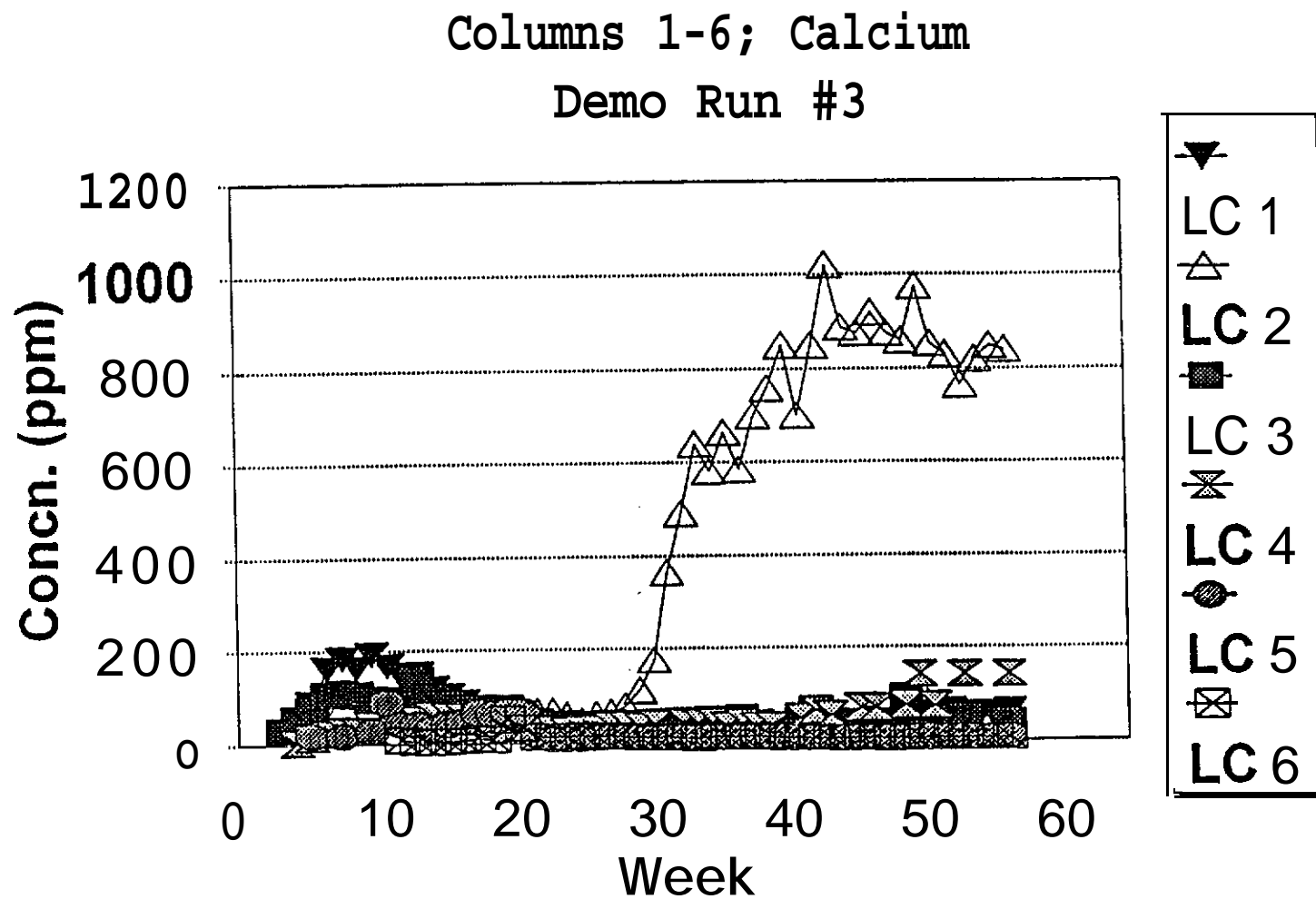
Figure 4-5a. pH-correlated leaching pattern for LC1 -LC6 (calcium).
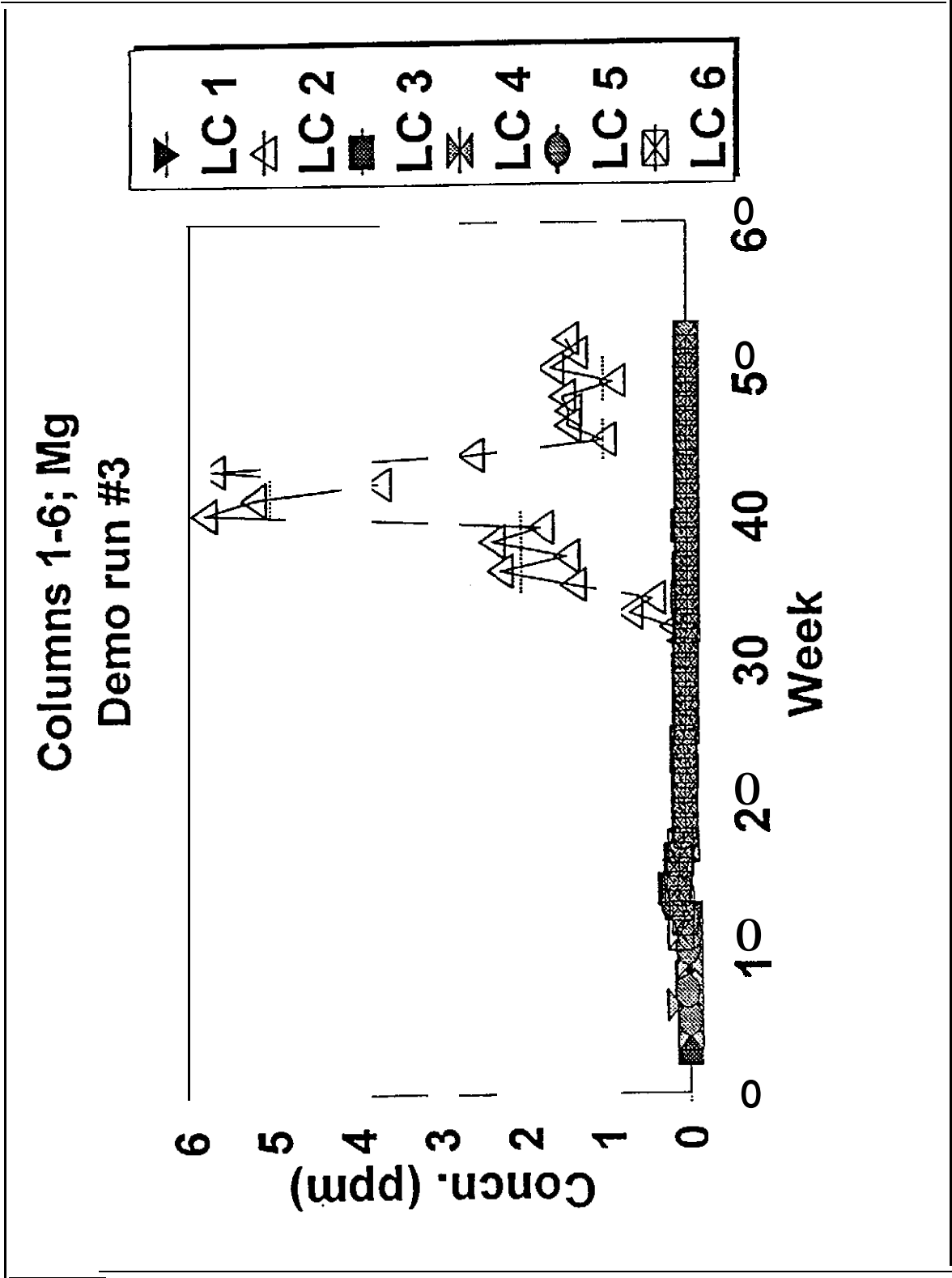
Figure 4-5b. pH-correlated leaching pattern for LC1-LC6 (Mg).

177
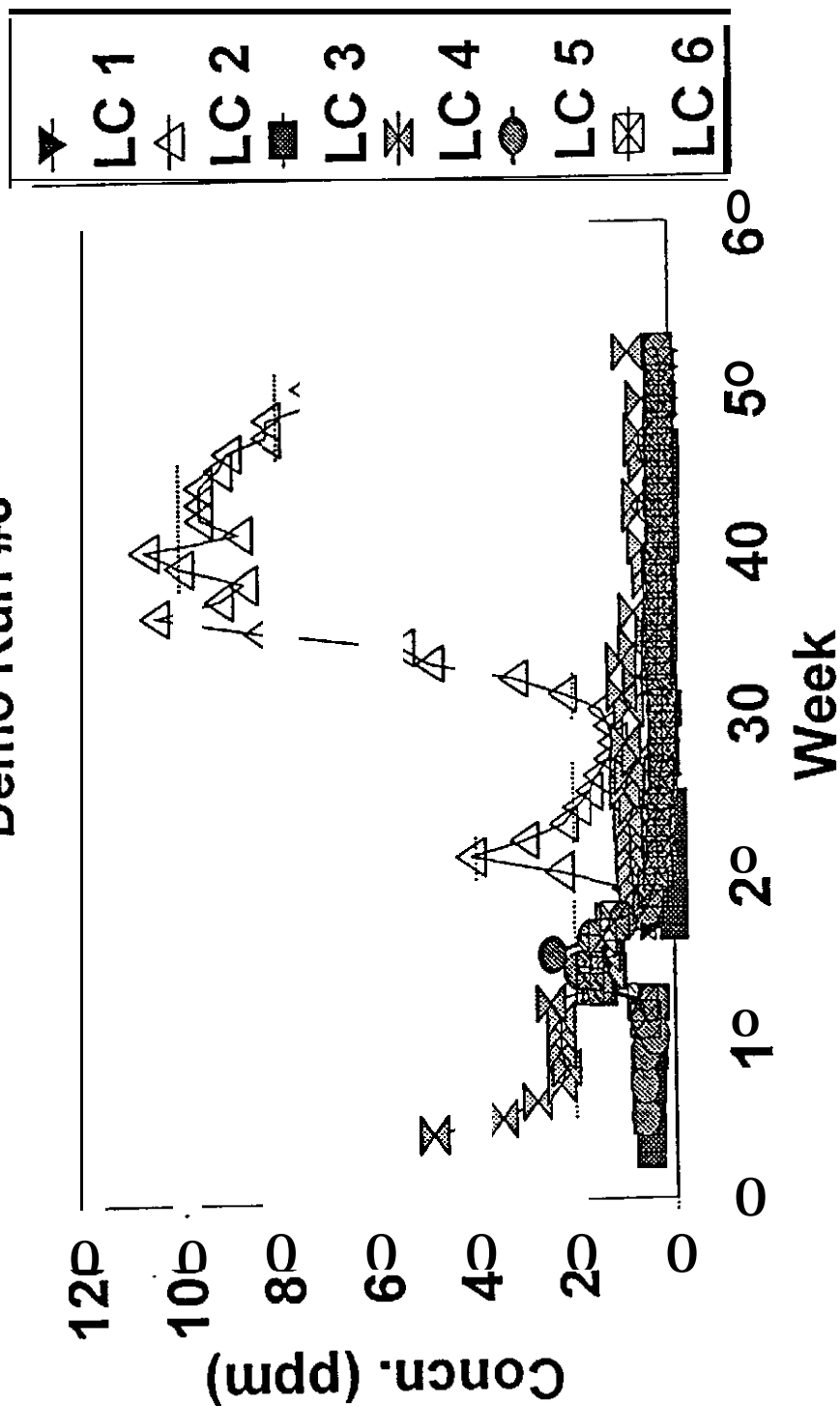
Figure 4-5c. pH-correlated leaching pattern for LC1-LC6 (Boron).

remain in the solid phase largely as portlandite [$Ca(OH)_2$] and brucite [$Mg(OH)_2$]. However, in those leachates in which PH declines following the uptake of CO_2 and subsequent reaction with hydroxyl (OH") to form carbonates (HCO_3^-), the release of Ca and Mg to the leachate increased substantially. This effect is most obvious in the leachate from LC2 (Figure 4-5) which was blanketed with the highest concentration of CO_2 (5%). Unlike Ca which continued to increase in concentration once the pH declined in LC2, Mg concentrations rose sharply before dropping to 1-2 ppm around week 45. This is believed to reflect the depletion of Mg ions from the packed bed. Boron follows a similar pattern with the exception of relatively high levels of B released from LC4 in the initial 3-4 leachate collections. In contrast to its behavior in LC2, boron from LC4 passed through a minimum before increasing inversely with pH. Since pH was initially near 12 in the leachate from LC4, the reason for the early B release from LC4 is not understood. It is notable that the concentrations of Ca, Mg, and Bin the leachate from LC6 never exhibited an increase with time as in LC2 and LC4. As previously discussed, LC6 was packed a higher density and the leachate pH did not exhibit a decline wfth time as did LC2 and LC4 which were also blanketed with elevated levels of CO_2.

The third type of leaching pattern is represented by Al, SO_4, and V in Figure 4-6 (As and Br also followed this pattern). This pattern is similar to that exhibited by Cl, Na, and Kin Figure 4-4 (flow controlled) only with a more prolonged rate of release. The primary factor(s) that dictate the slower release is unknown but is believed to be related to either the slow kinetics of dissolution-transformation of the minerals that retain these ions in the solid phase, the formation of oxyanions, or perhaps a combination of the two. For example, in LC2 which was blanketed wfth 5% CO_2, XRD analysis (discussed in a later section) indicated early formation of ettringite in the hydrated starting materials. However, by the end of the study, ettringite was completely depleted from the upper and middle cores, apparently having been replaced by calcite in the top and gypsum in the middle. Ettringite had also disappeared from the top of both LC2 and LC4 (blanketed with enhanced levels of
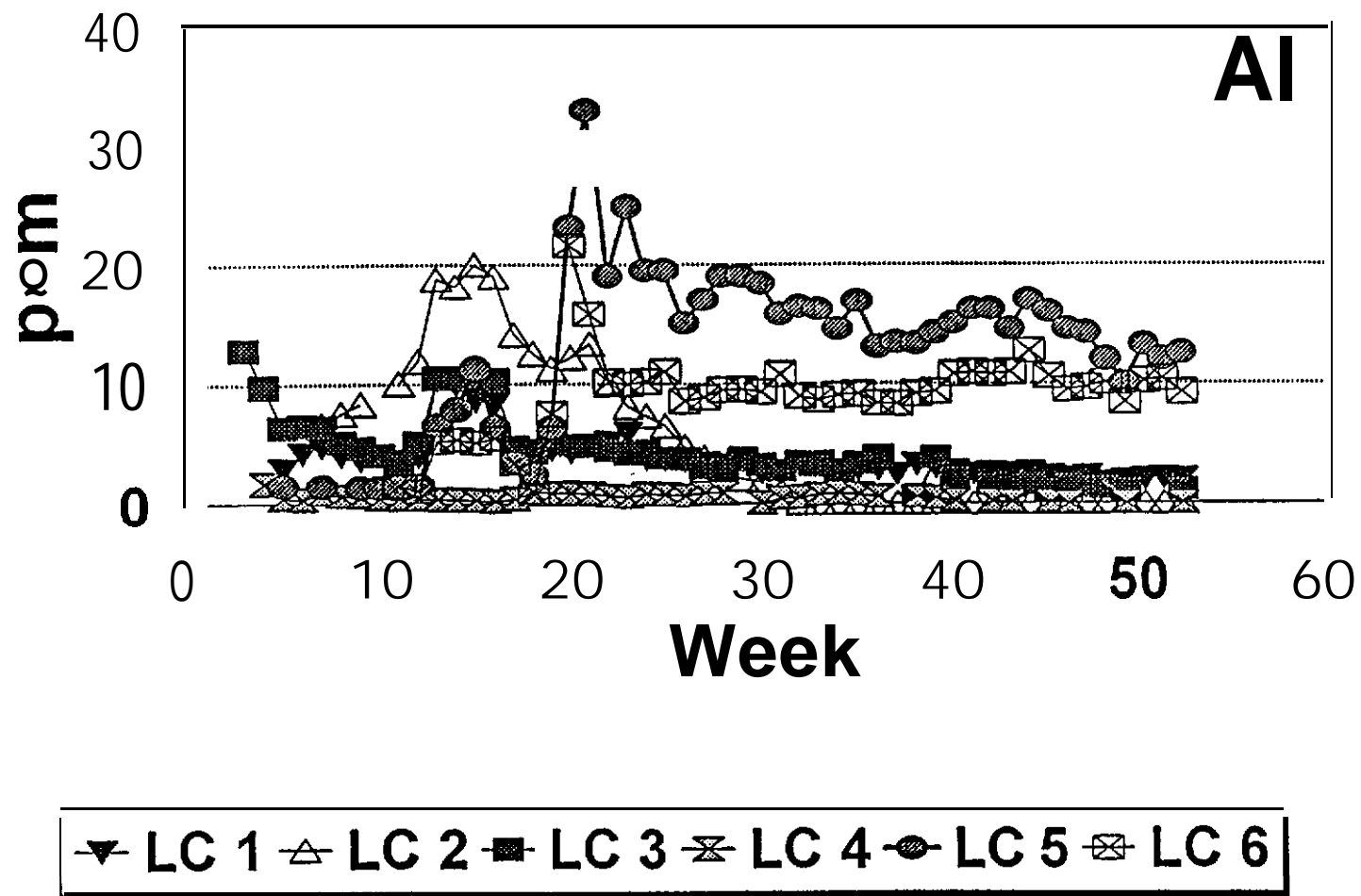
Figure 4-6a. Examples of ions exhibiting more prolonged release patterns from LC1 -
LC6 (Al-t).
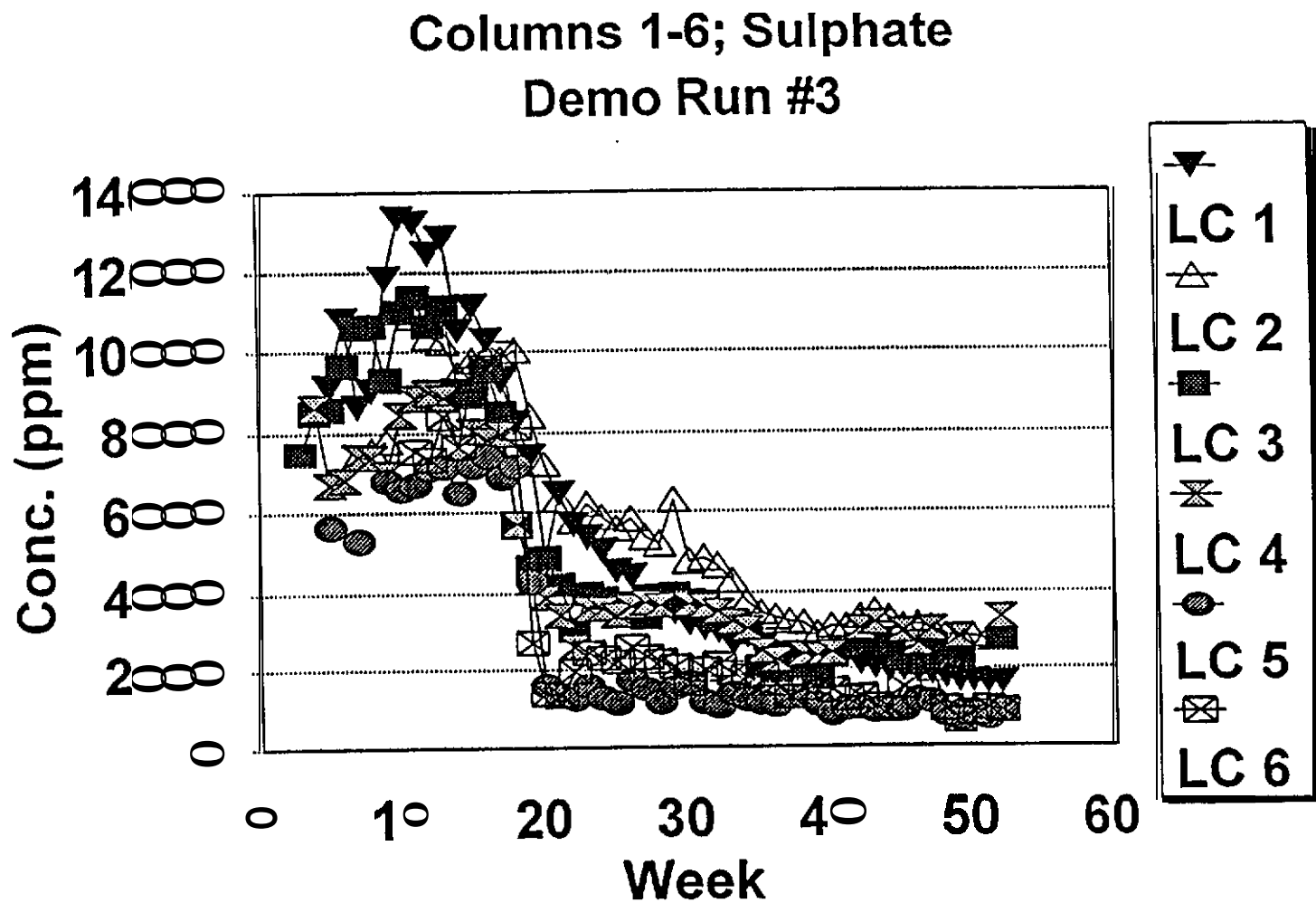
Figure 4-6b. Examples of ions exhibiting more prolonged release patterns from LC1-
LC6 (SO$_4$-m).

Columns 1-6; Vanad um Demo Run #3.

Legend: LC 1, LC 2, LC 3, LC 4, LC 5, LC 6

Y-axis: Concn. (ppm) — 0, 0.5, 1, 1.5, 2, 2.5, 3

X-axis: Week — 0, 1, 2, 3, 40, 50, 60
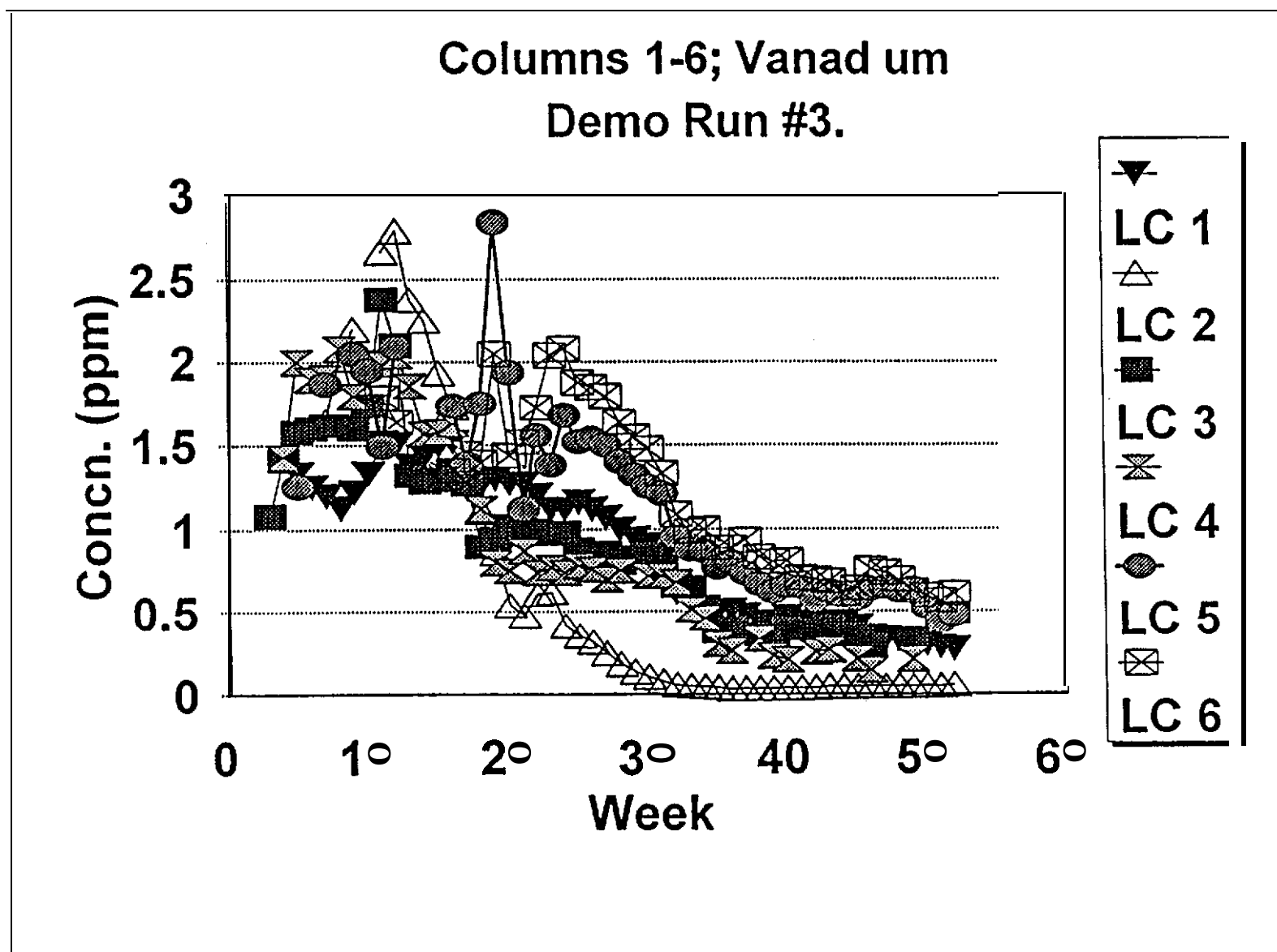
Figure 4-6c. Examples of ions exhibiting more prolonged release patterns from LC1-LC6 (V-b).

CO_2) but remained throughout the three columns blanketed with room air and LC6 (dense packing/2.5% CO_2).

Formation of calcite was observed in the upper portions of LC2 and 4 but not in LC6. Thus, the early formation of ettringite would tend to initially retain Al. This ion maybe released at a later time as the ettringite is depleted whereas the Ca initially present in ettringite is incorporated into calcite or gypsum. The net effect would be prolonged release of Al. Similar arguments can be made for SO_4 which is also present in ettringite. Though a portion of the SO_4 would be incorporated to gypsum, SO_4 release would be greater in those portions of the column where CO_2 is available and calcite formation is favored. It is speculated that the delayed release of V may be due to slow kinetics of formation of oxyanions of vanadium.

CO_2 Effects. All three columns exhibited essentially free flow from about week 5 onward with the exception of LC1 O. This latter lysimeter flowed erratically until about week 18a which time a large slug of water passed through the column followed by free flow for the remainder of the study (Figure 4-7). Essentially the same cumulative volumes of water passed through each of these columns during the study.

In the initial leachate collections, pH levels were in the 12.5-12.6 range for all three lysimeters (Figure 4-8), indicative of pH control by portlandite. However, with time, pH values exhibited clear declines that varied inversely with the concentration of CO_2 in the lysimeter headspace. By the end of the study, pH levels for LC1 O (0% CO_2) were approximately 12.0, approximately 11.4 for LC11 (2.5% CO_2), and in the 9.5-10.0 range for LC12 (5.0% CO_2). As discussed previously, such behavior is consistent with carbonate buffering following absorption of CO_2 (CO_2 + OH --> HCO_3^-).
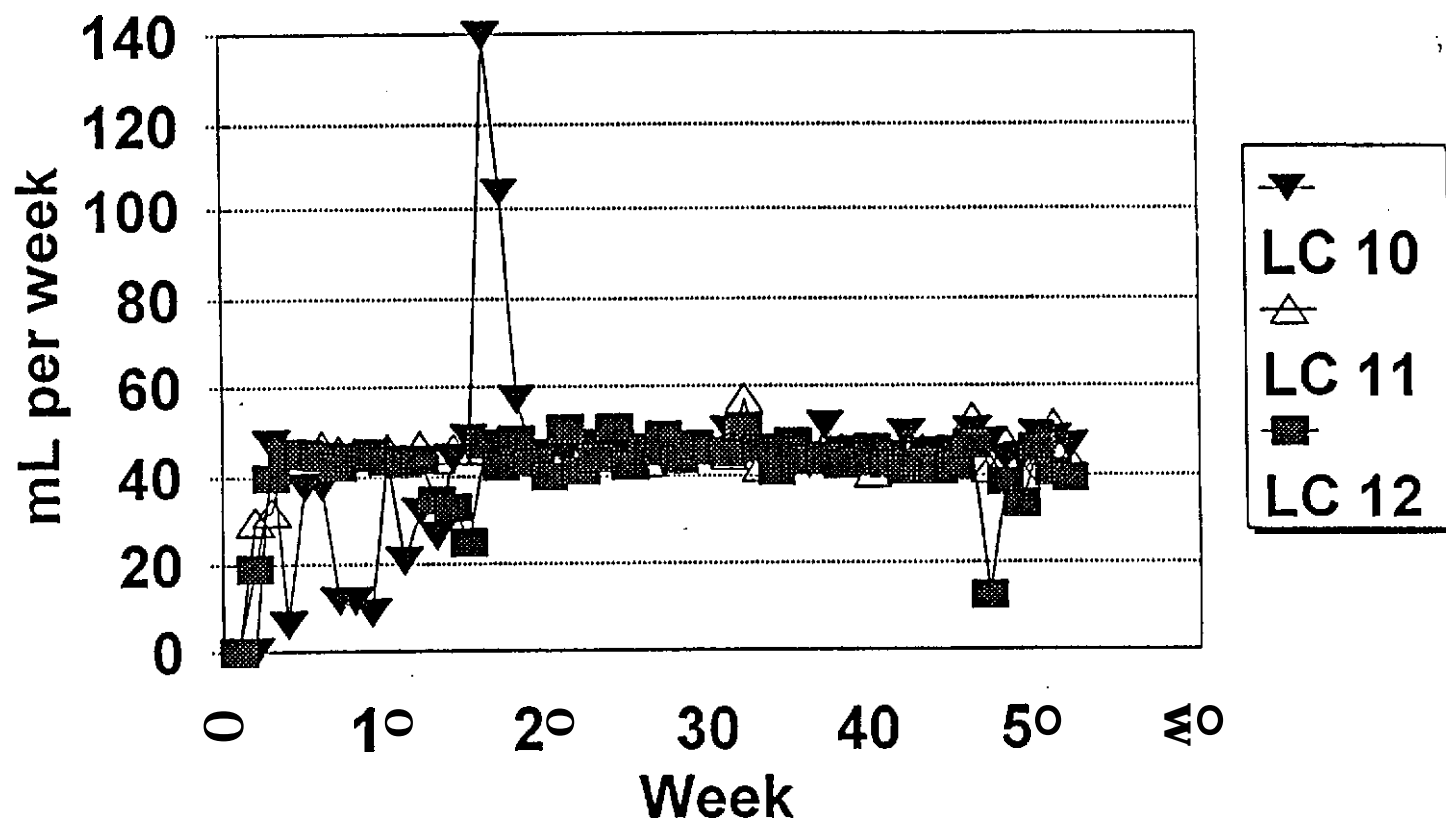
Figure 4-7. Water flow through LC10-LC12.
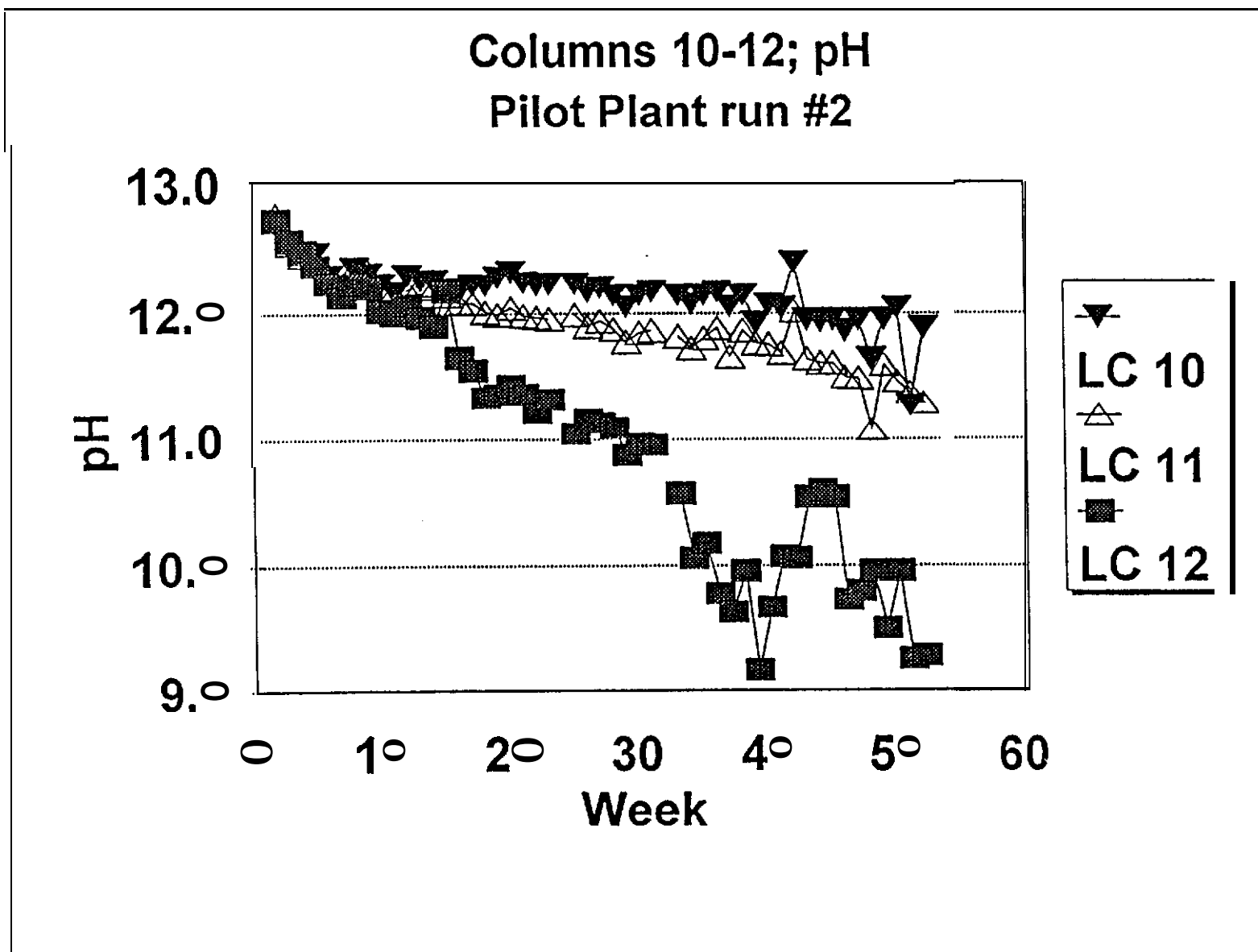
Figure 4-8. pH values of the leachates from LC10-LC12.

Many of the ions measured in the leachate waters from LC1 0-LC1 2 either eluted too early in the study or their concentrations were too low to demonstrate clear trends as a function of CO_2 concentration (As, Zn, Ba, Mn, Se, Cl, Me). The release rate for several other ions, such as K and Na, appear to have been unaffected by the uptake of CO_2 and exhibited release patterns similar to those of the highly soluble ions shown in Figure 4-4. These ions rapidly eluted from the columns until depleted. However, the leachate concentrations for Ca, Mg, B, Al, V, and SO_4 did exhibit variations which appear to correlate with the concentration of CO_2 in the lysimeter headspace.

The relative concentrations of Ca, Mg, and B in the leachate waters increased with decreasing pH as illustrated in Figure 4-9. This trend is particularly apparent for the leachates from LCI 2 which was blanketed with a higher concentration (5%) of CO_2. This inverse relation between pH and ion concentration is similar to that previously discussed in the CO_2-enriched columns in the LC1 -LC6 series with the same arguments being applicable to the behavior of this set of lysimeters.

In contrast to the inversely related plots of Figure 4-9, Al and V concentrations in the leachate waters directly correlated with higher pH (lower CO_2 headspace concentrations) as illustrated by the plots in Figure 4-10. The behavior exhibited by Al in this plot is consistent with release from $Al(OH)_3$ (gibbsite) as a function of pH.[3] The more prolonged release of V from LC1 O is again believed to be related to the slow formation of soluble oxyanions.[4] On a relative basis, SO_4 concentrations increased fromLC1OtoLC12 (Figure 4-1 1). As will be discussed in more detail in a later section, XRD of cores taken from these columns showed ettringite from top to bottom of LCI O, some formation of gypsum and calcite in the top and middle cores of LCI 1, and complete destruction of ettringite and formation of gypsum and calcite in all three mres from LC12. The release of SO_4 is believed to be retarded by incorporation of SO_4 into ettringite in LCI O and the partial

Columns 10-12; Calcium
Pilot Plant run #2.
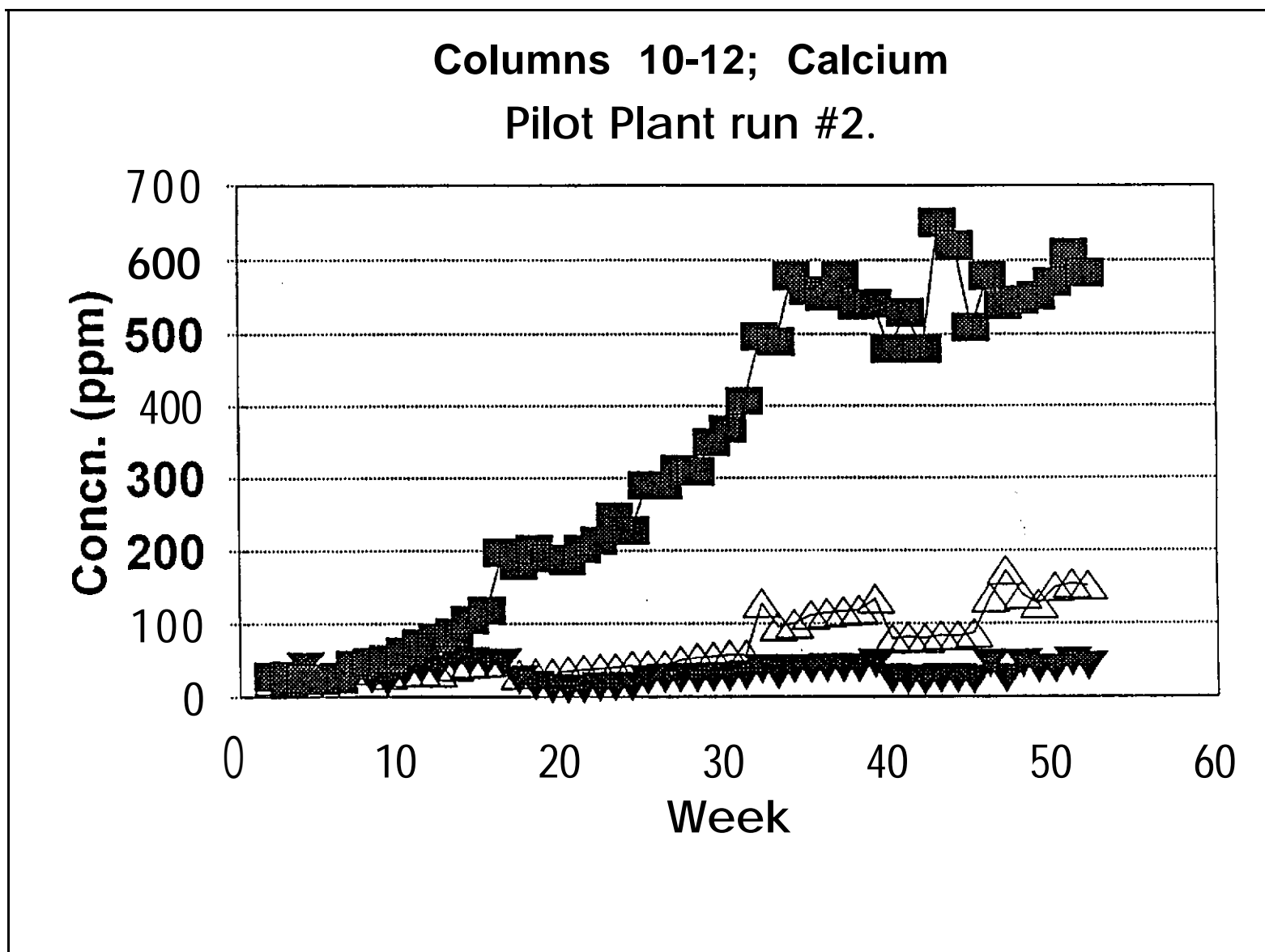
Figure 4-9a. The impact of an enriched CO_2 atmosphere on the release of Ca (t) from LC1O-LCl2.
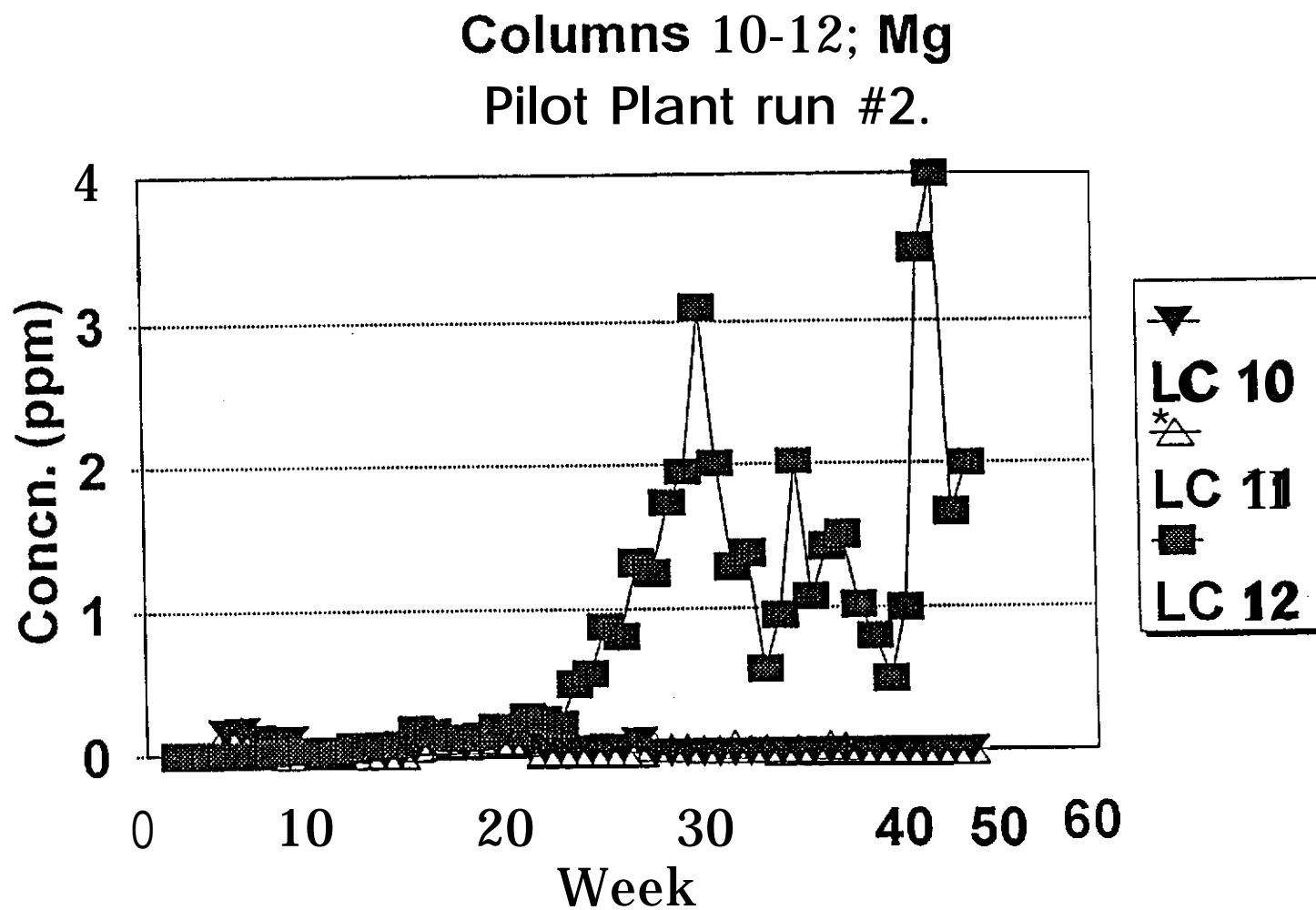
Figure 4-9b. The impact of an enriched CO_2 atmosphere on the release of Mg (m) from LC1 0-LC1 2.

Columns 10-12; Boron
Pilot Plant run #2.
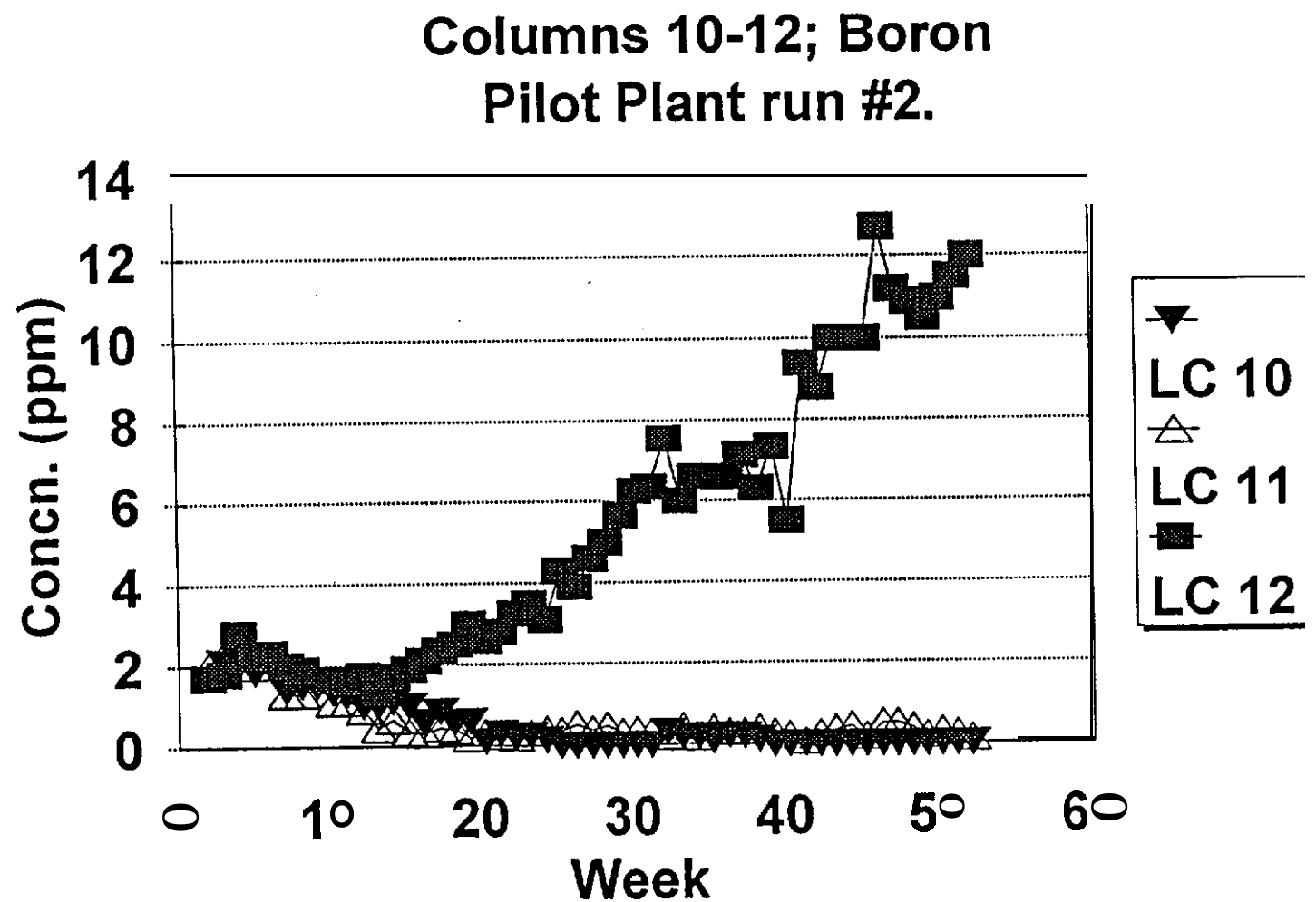
Figure 4-9c. The impact of an enriched CO_2 atmosphere on the release of B (b) from LC10-LC12.
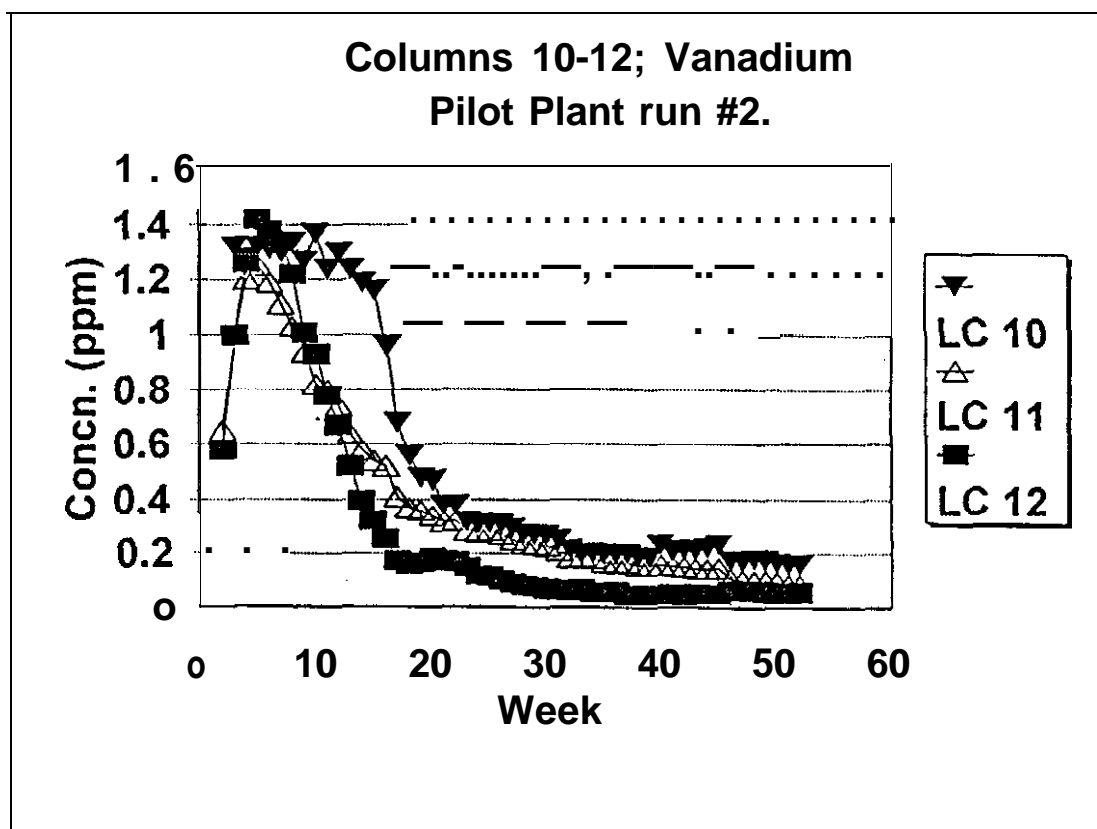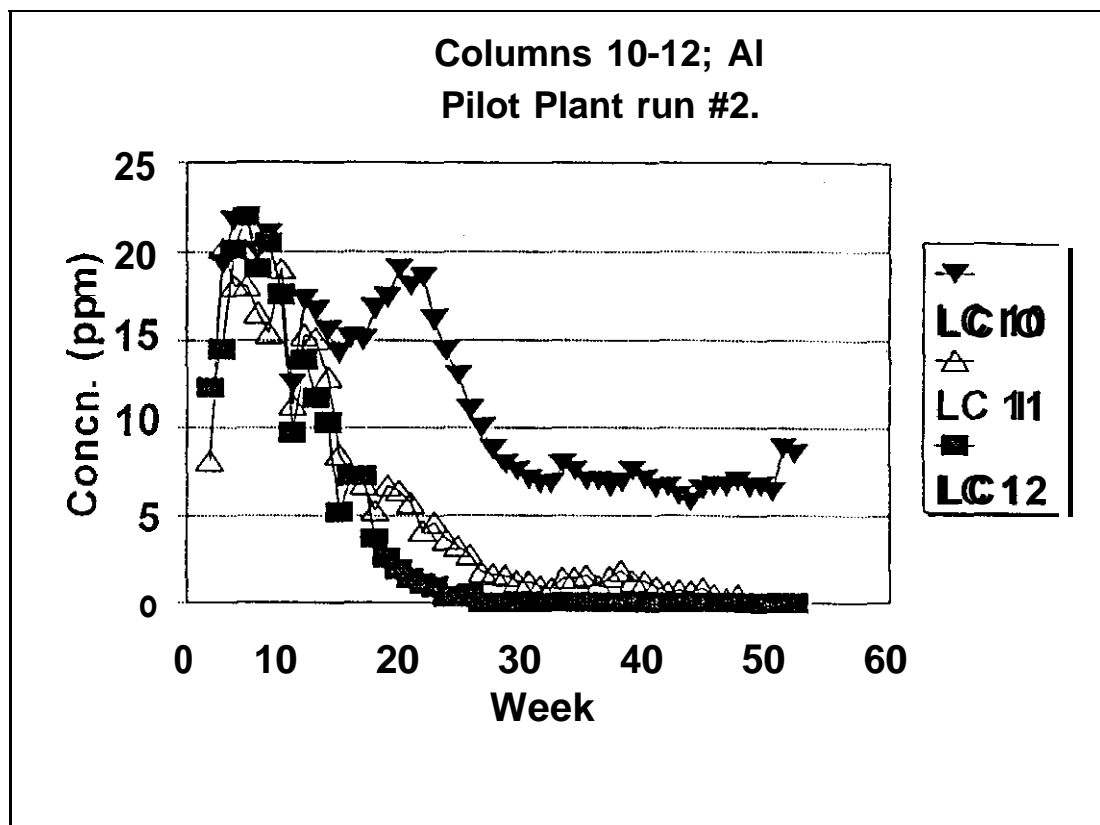
Figure 4-10. The impact of enriched CO_2 atmosphere on the release of Al (l) and V (r) in LC10-12.

Columns 10-12; Sulphate Pilot Plant run #2.
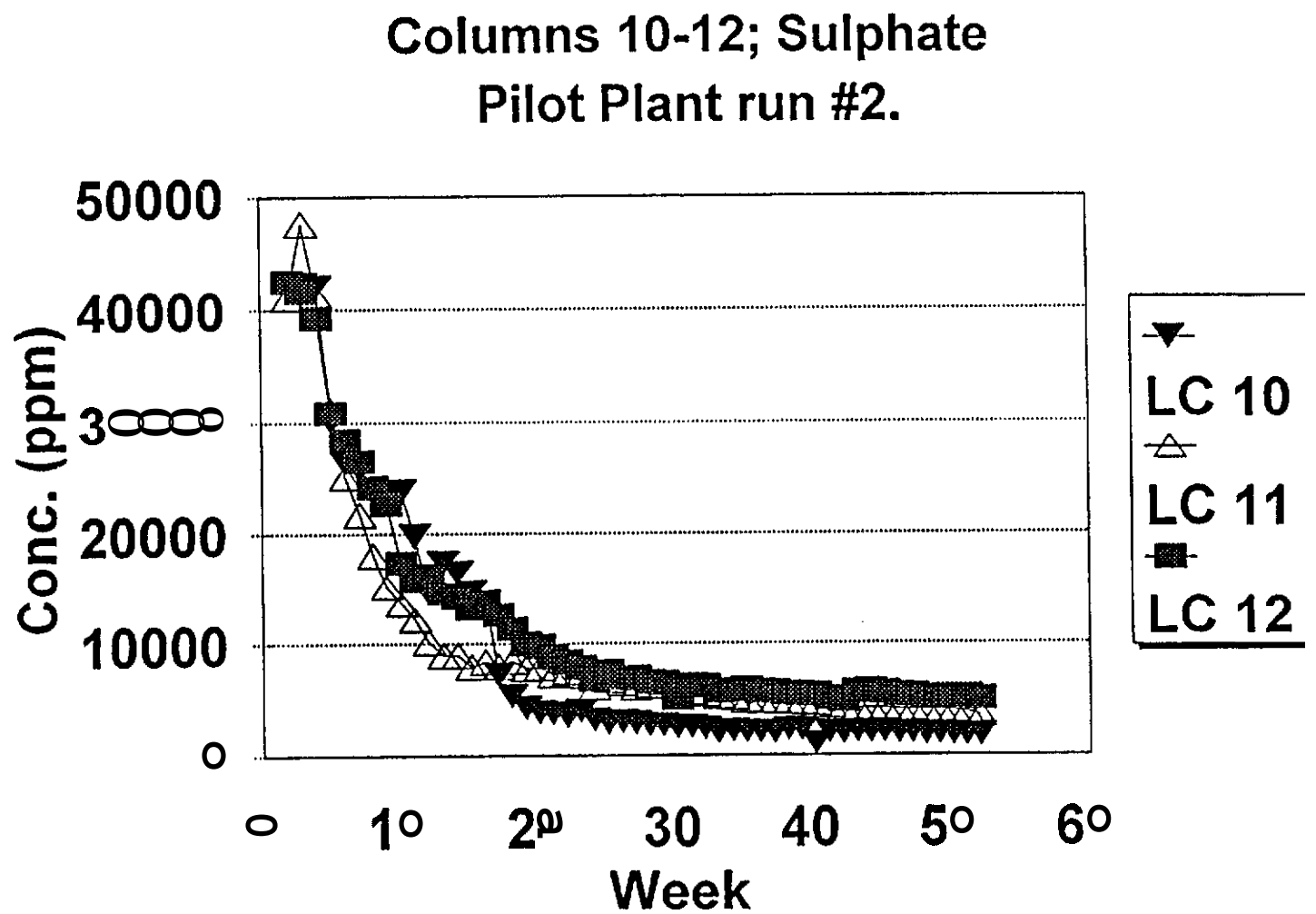
Figure 4- 1. The impact of enriched CO_2 atmosphere on the release of SO_4 in LC10-12.

destruction of the same with concurrent sulfate release and gypsum formation in Cl 1 and LC12.

Prehydration Effects. LC33-LC36 were devised to examine the effect of sample prehydration on leaching behavior. The most notable effect was reflected in differences in the rate of water flow through these columns (Figure 4-12). None of the columns flowed until about week 12 to 14 at which time LC34 and LC35 (15 and 30% prehydration, respectively) exhibited breakthrough followed by free flow around week 15. LC33 (O% prehydration water) began to flow slowly at week 15 then slowly increased to -20% of the feed rate around week 30. LC36 (45% prehydration) never flowed. LC25 and LC26 which were included in the original set of columns and were prehydrated at O% and 40%, respectively, showed similar trends, i.e., LC25 flowed slowly while LC26 did not flow. Thus, the level of prehydration water added to the FGD materials prior to packing appears to have significantly affected the bed permeability. This has implications with respect to disposal in that excess hydration of FGD wastes prior to disposal may produce a material that is effectively impermeable to or at least substantially reduces the percolation of groundwater through the bed.

The leachate chemistry was very similar for LC34 and LC35, the two columns that exhibited similar flow rates during the study. pH values for the leachates from these columns was initially around 12.5 before declining to 11.5-12.0 near the end of the study (Figure 4-13). LC33 which began to flow later and continued to flow more slowly exhibited a relatively low pH of 9.5-11.5 in the initial collections before increasing to the 12.0 range.

Elemental release from LC34 and LC35 was also similar with the exception of Cl⁻ which was more concentrated and shifted about plus 10 weeks for LC35 relative to LC34. Leachate concentrations for LC33, which exhibited slower flow rates, were substantially delayed relative to both LC34 and LC35. Examples of these patterns are shown in the plots of
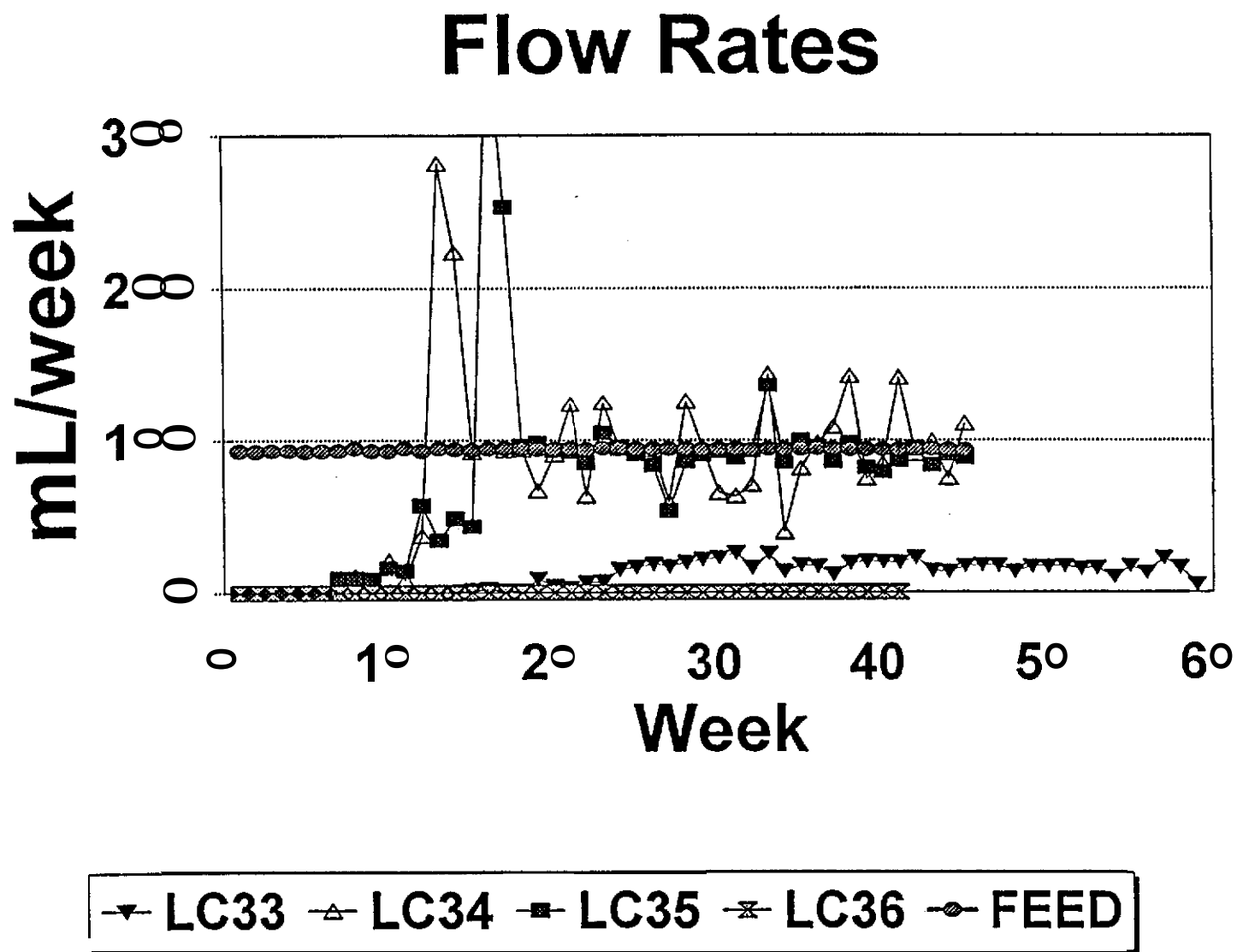
Figure 4-12. Flow rates through LC33-LC36.
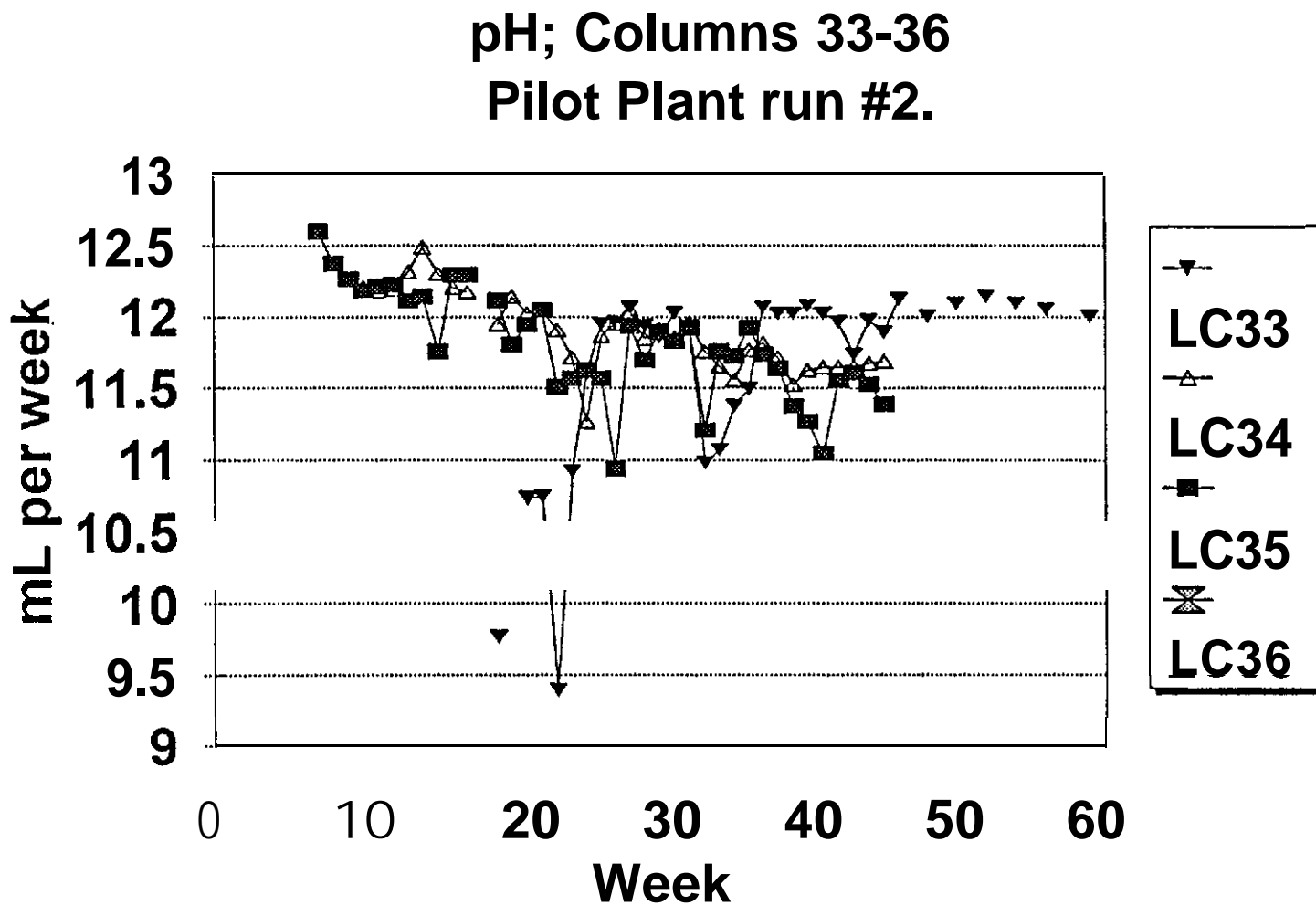
Figure 4-13. pH of leachates from LC33-LC35.
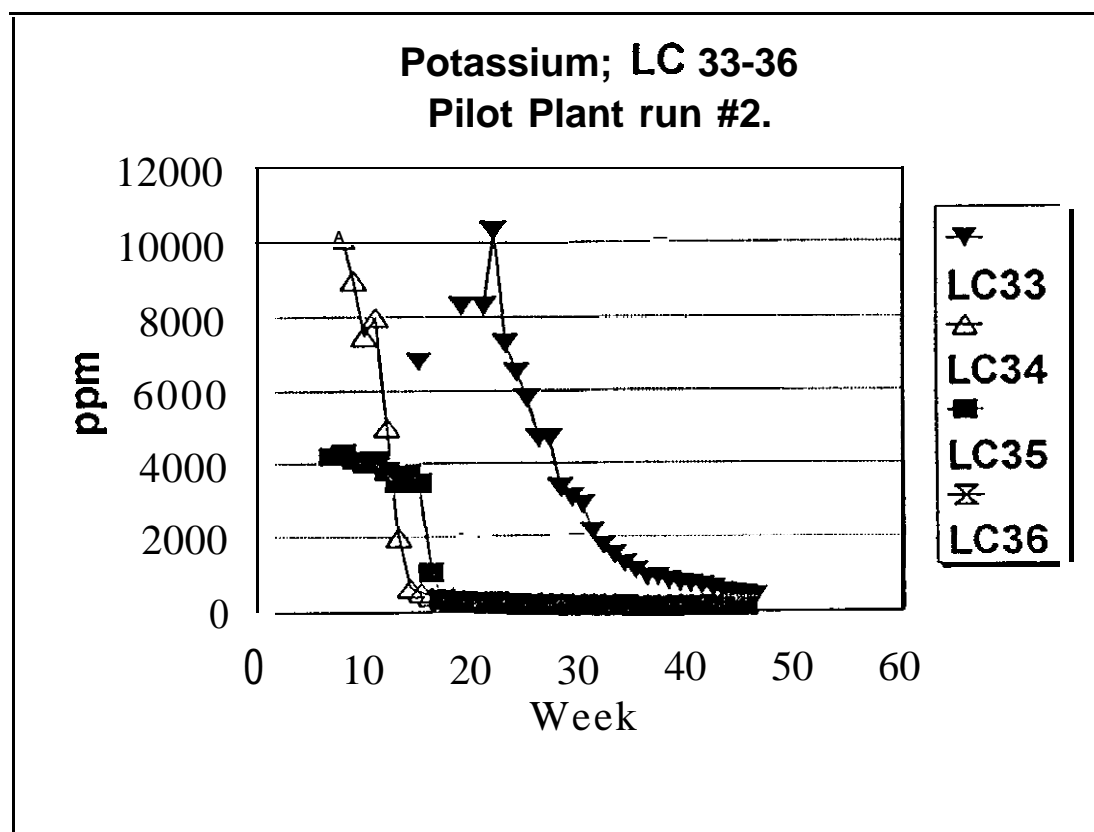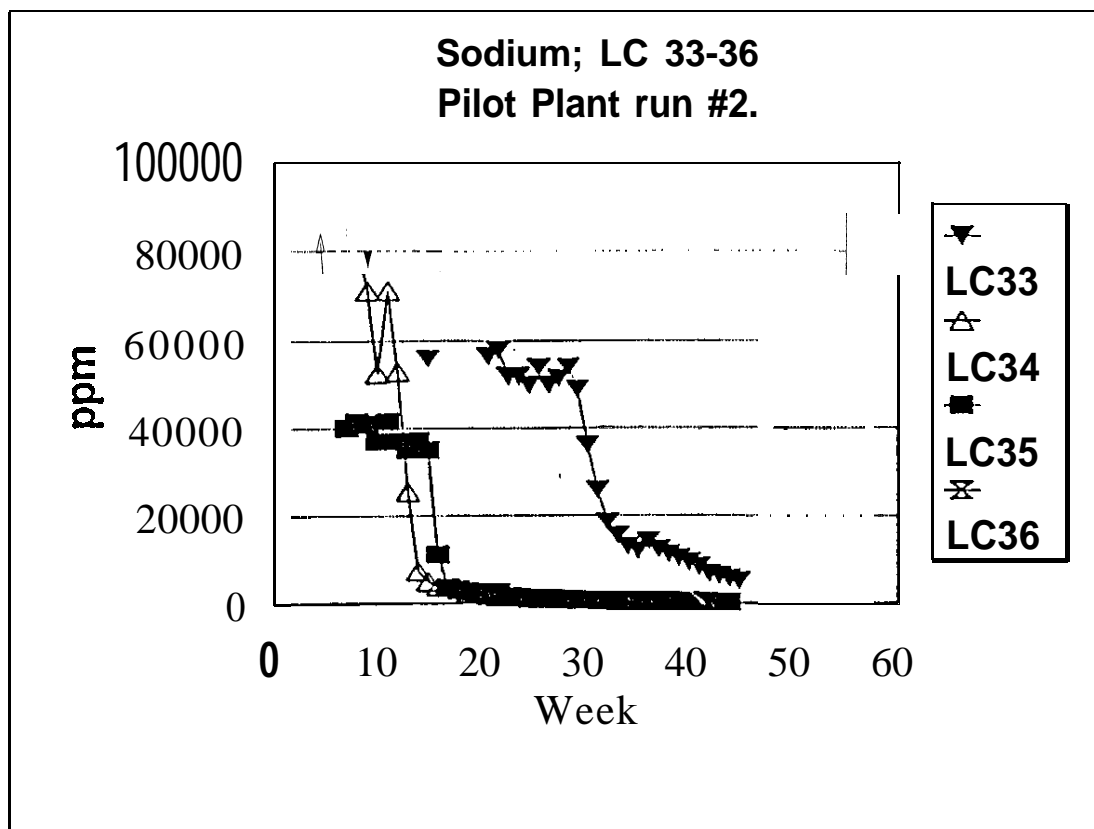
Figure 4-1 4a, b. Leaching behavior for selected ions collected from LC33-LC35 (sodium, potassium).
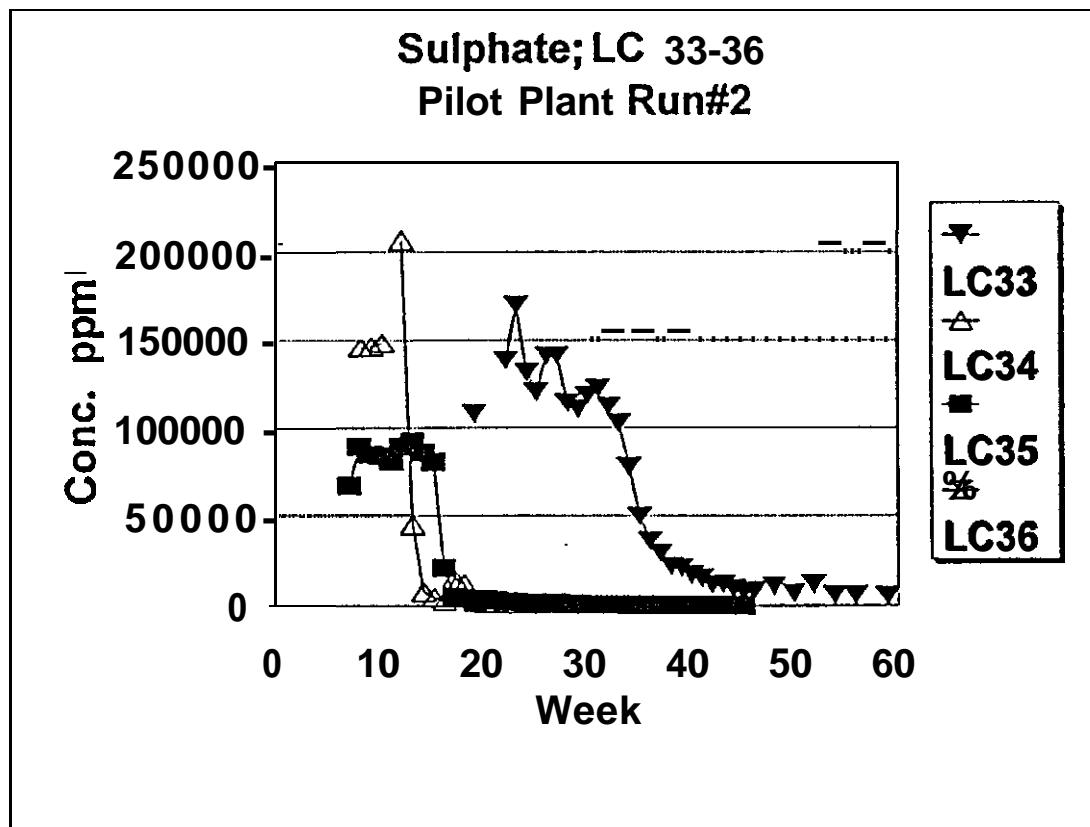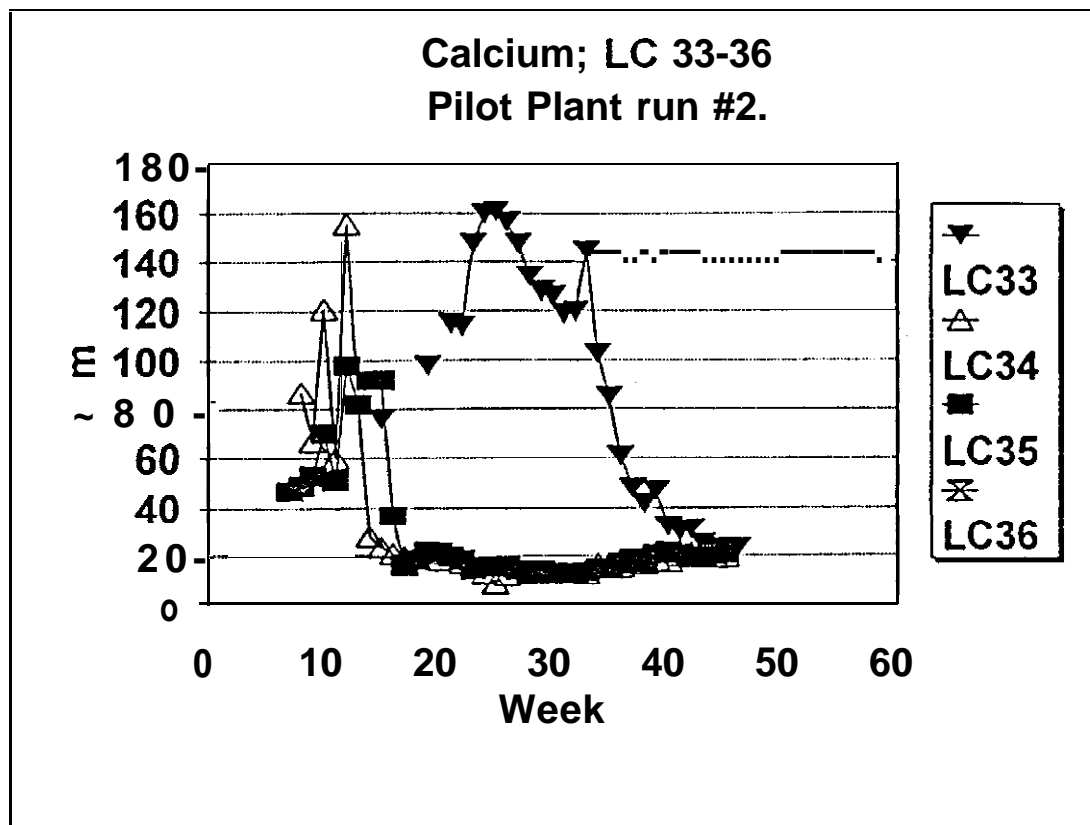
Figure 4-1 4c, d. Leaching behavior for selected ions collected from LC33-LC35 (calcium, sulphate).

Figure 4-14. When ion concentrations were examined as a function of total flow, release patterns for all three lysimeters were similar. That is, release appeared to be governed by the volume of water passing through the columns and not by differences in mineralogy. Thus, although the rate of release is affected by the level of prehydration, release as a function of the volume of water flow through the columns does not appear to be affected. The XRD spectra for post-leaching samples from these columns are presented in a later section.

Summary

The results indicate that packing density, the presence of a CO_2 atmosphere, and extent of prehydration all measurably impact leaching behavior. Packing density and particularly the level of prehydration significantly impacted flow rates which in turn affected leaching kinetics. Packing density also appeared to have some influence on leachate chemistry and CO_2 uptake. Provision of an enriched CO_2 atmosphere in the column headspace was found to lower leachate pH which in turn affects both mineralogy and release patterns for several of the monitored ions including Al, B, Ca, Mg, SO., V, and possibly As and Br. With the exception of Se from the demonstration run #1, none of the ions being monitored were released at concentrations that would be of concern environmentally. Even this material met RCRA standards for non-hazardous waste.

1.   Coolside Waste Management Research *Annual Techn. Progress Report for Period October 1991 through September 1992.* Prepared for the USDoE under Contract No. DE-AC21-91 MC28162 by tbe University of Kentucky-Center for Applied Energy Research and Kentucky Transportation Center; October, 1992; 61 p.

2.   Coolside Waste Management Research *Annual Techn. Progress Report for Period October 1992 through September 1993. Prepared* for the USDoE under Contract No. DE-AC21-91 MC28 162 by the University of Kentucky-Center for Applied Energy Research and Kentucky Transportation Center; October, 1993.

3. R. Garavaglia and P. Caramuscio, Coal Fly-Ash Leaching Behavior and Solubility Controlling Solids, in J.J.J.M. Goumans, H.A. van del Sloot, Th. G. Aalbers (eds.), Proc. Intnl. Corn! on Env. Implications of Construction materials and Techn. Developments, Maastricht, the Netherlands, June 1-31994, Elsevier, Amsterdam, 1994, pp.87-102.

4. Lafferty, C. J,; Robl, T. L.; Schram, W. H.; Yewell, ME.; "Elemental Release Characteristics of Dry Flue Gas Desulfurization By-Products" *10th Annual Intnl. Pittsburgh Coal Conf.* S.-H. Chiaog, Ed.; Univ. of Pittsburgh School of Engineering.-Center for Energy Res.; 1993; 858-863.

CHAPTER 5. CHEMISTRY OF THE FIELD LEACHATES

Sample Collection and Analytical Methodology

Analytical Protocol

Protocols for analysis were established in the project's infancy. Analytical method 1620 was the protocol followed by the CAER analytical staff in the determination of metals concentration. Method 1620 was developed by the Industrial Technology Division (ITD) within the United States Environmental Protection Agency (USEPA) Office of Water Regulations and Standards (WORS) to provide improved precision and accuracy of analysis of pollutants in aqueous and solid matrices. Below is the routine method of analysis for metals concentration:

a) Calibration of Instrument
b) Initial Calibration Verification (ICV)
c) Continuing Calibration Verification (CCV)
d) Interference Check Sample A (ICS A)(interference- Ca, Al, Mg 500 ppm- Fe 200 ppm)
e) Interference Check Sample AB (ICS AB)(analytes mixed with the interference) control limit $\pm$ 20%
f) Reagent Blank (RB) (must follow steps as samples)
g) Quality Control (QC) (Spex QC-19, QC-7 Quality Control Standards)

Prior to analysis of the leachate samples, the initial calibration, check samples, and quality control samples were analyzed and accepted. After every ten samples, a quality control standard was analyzed to secure accuracy of the instrument.

Following the collection of leachate samples from the field lysimeters the following EPA methods of analysis were implemented by the CAER staff on a routine basis. Method 310.1 (Titrimetric, pH 4.5) was the EPA method of analysis for the determination of alkalinity. Method 300.0 was the EPA test method used for the determination of inorganic anions in water by Ion Chromatography. SW-846 Method 9050A was used for the determination of specific conductance. SW-846 Method 9040A was used for the determination of pH. EPA Method 160.2 was used for total residual

non-filterable solids (TDS).

Sample Collection Methodology

The precise chain of events of field and laboratory analytical methods and procedures were as follows. Collection occurred every Monday and Thursday in the beginning of the project (on rare occasions, circumstances dictated alternate days). The early samples were known to have high concentrations of metals, and it was determined that at the onset of leaching samples were to be collected twice a week until the metals trends showed an equilibrium or depletion in concentration.

Upon arrival at the field site the scientific field crew would interpret and record the rainfall data of the preceding week. Moisture readings (counts) were taken with a Troxler Neutron Probe Model 4300 Depth Moisture Gauge within the four lysimeters. The Neutron Probe, containing both a neutron source and a neutron detector encased within a probe, was placed into a 2" OD stainless steel tube positioned in the center of the lysimeter in a vertical position. These tubes were sealed at the bottom and fitted with a cap at the top to prevent moisture from entering the tube. Measurements were taken at.5 feet, at the sand layer, at 2.5,4.5, and 6.5 feet within the Coolside material, and at 8.5 feet, a measurement at the soil layer.

Multiple K-type stainless steel sheathed 1/8 OD thermocouples were placed in specified areas within the lysimeters positioned near the collection tubes. Temperatures were recorded at the soil, Coolside material and sand in the bottom of the lysimeters using an Omega HH11 Portable Digital Thermometer.

It has been proven in previous column leachate studies that CO_2 concentrations can affect the chemistry and mineralogy of the material and leachate, resulting in the decision to measure the CO_2 in the soil and Coolside layers. Four borosilicate glass tubes (suction lysimeters) were placed in each of the four lysimeters in April, 19"94 at

depths of 8, 18, and 30 inches. A 42 inch suction lysimeter was added in April of 1995. The tubes were filled with glass beads, and a rubber septum was placed on the top of the tubes. Measurements occurred by placing a Kitagawa CO_2 Precision Gas Detector Tube through the septum and into the tube. A Kitagawa model 8014-400A hand operated pump was used to pull a vacuum. With the vacuum established, the gas would flow through the Kitagawa detection tube resulting in the recorded measurement of CO_2 concentration.

After an event (precipitation), the volume (L) was determined from each collection port from each lysimeter. The volume (L) in the center collection cell was measured to establish a complete percolation profile. The samples were collected in 25 liter carboys and transported to the laboratory. 500 mls of sample were collected from each carboy for analysis (if more than one carboy was collected from a single port, the sample was mixed homogeneously). The unused portion of the samples was then treated with nitric acid to neutralize the pH, and it was then diluted with tap water and discarded. The 500 ml homogeneous sample was analyzed for pH using the Orion Research Microprocessor Ionalyzer 1901 following SW-846 Method 9040A. A small portion of the sample was then decanted to measure conductivity using the YSI Model 32 Conductance Meter following SW-846 Method 9050A.

200 mls of the sample were then filtered through a .45pm membrane filter, acidified with nitric acid, and analyzed for metals following Method 1620. The aqueous sample was analyzed by a Plasma-Therm ICP 2500 for the determination of trace metals. It was introduced to the ICP via the CETAC U-5000 Ultrasonic Nebulizer. The ultrasonic nebulization system contains a sample inlet, a piezoelectric transducer, an aerosol chamber, a gas inlet, a heating chamber, a condenser, and an interface to the plasma torch. Detection limits obtained with an ultrasonic nebulizer are generally 5 to 25 times better than those achieved with a pneumatic nebulizer. Major elements were obtained by utilizing a Spectrometric DCP Optical Emission Spectrometer.

The determination of mercury was accomplished by using a Perkin Elmer3100 Atomic Absorption Spectrometer along with the Perkin Elmer FIAS 200 following the SW-846 Method 7470 cold vapor generation of Hg.

The unacidfied portion of the sample was used for the determination of alkalinity, anions, and total dissolved solids. 50 mls of the unacidified sample was analyzed by the Fisher Computer Aided Titrimeter to generate alkalinity results following EPA Method 310.1. Another portion of the unacidified sample was used in the determination of anions using a Dionex 2120i Ion Chromatography following EPA Method 300.0. The last portion of unacidified sample was used to determine the Total Dissolved Solids following EPA Method 160.2.

Collection of field samples twice a week continued from approximately March, 1993 at the beginning of the first collected leachate sample to approximately December, 1994 when it was decided to collect once a week because the data had shown a decline in concentration nearing equilibrium of most elements. March 29,1996 was the last visit to the field site by the field operators, ending the 3 ½ year field study. All samples have been analyzed and data recorded.

Chemistry of the Leachates Collected from the Field Lysimeters

Leachate Composition

The samples were analyzed for Ag (0.01), Al (0.05), As (0.05), B, Ba, Be, Ca, Cd, Co, Cr (0.005), Cu (0.01), Fe (0.005), Hg, K, Mg (0.02), Mn (0.005), Mo, Na, Ni (0.01), P (0.05), Pb (0.02), Se (0.03), Si, Ti, V (0.005) and Zn (0.002). Alkalinity was determined and was titrated to both pH 8,3 and pH 4.5 for the samples which were highly alkaline. Cl, sulfate, pH, conductivity, volume, total dissolved solids, total suspended solids and temperature were also determined for all samples. Bromine (Br) was not in the original

protocol, but was added later in the study and was determined for the leachates from the L3 lysimeter.

The chemistry for the leachates is summarized in Tables 5-1 to 5-3. In these tables, leachate data is presented for the lysimeter transport tubes which had the longest continuous collection record. The data are presented by year, starting on March 1.

The data for the soil CO_2 is summarized in Table 5-4. The data was collected from soil gas wells as placed at 8, 18, 30 and 42 inches of depth (20, 46, 76 and 107 cm). The wells were emplaced in April of 1994. The 42-inch deep tube was added in April of 1995.

Of the elements determined, Ag, Be, Cd, Co, Cu, Hg, Ni, P, Pb and Zn were either never detected, or were found only rarely in extremely low concentrations. Similarly, while data is presented in the tables for Cr, Fe, Mn and Ti, they were not found in high enough concentrations to compile meaningful averages and trends. Although one of the primary mineral forms bearing calcium is hannebachite ($CaSO_3.1/2H_2O$), the primary anion from its solution is sulfate SO_4^{-2}, as SO_3^{-2} is quickly oxidized in the weathering environment.

Major *Ions*. The state of compaction of the materials was found to have a strong impact on the chemistry of the leachates with two distinct patterns emerging over the study interval. The lysimeters which were uncompacted or compacted with minimal effort (L1 and L2) initially had much higher elemental concentrations compared to L3 which was compacted to optimum density. Sodium, Cl, K and sulfate were all higher in concentration by factors of 3 to 4 and Ca by a factor of more than 10 in L1 and 2 compared to L3 (Figures 5-1 to 5-4). The elemental release pattern overtime also showed marked contrast, with the less compacted lysimeters showing a rapid decline in leachate elemental concentrations. For example, Na in L1 dropped from a high of 30,000 ppm--which is approaching the concentration of a brine--the first year, to a

Table 5-1 Summary of Chemis... from Feild Leachates for Firs... Project Year (March 1, 1993-February 28, 1994)

	L1-3 N=44			L2-3 N=38			L3-4 N=52			L4-3 N=50		
	Year 1 Mean	Year 1 Min	Year 1 Max	Year 1 Mean	Year 1 Min	Year 1 Max	Year 1 Mean	Year 1 Min	Year 1 Max	Year 1 Mean	Year 1 Min	Year 1 Max
Na	15767	5000	3000C	15863	5300	33000	5480	3200	9100	465	11	830
Ca	800	335	135C	640	220	1340	45	18	90	522	240	730
K	5378	1640	81 0C	4764	1610	8000	1856	1000	3300	1031	56	1690
Al	ns	dl	dl	ns	dl	0,93	14.26	6.00	29.00	0.56	0.05	1.70
As	0.70	0.30	1.50	1.17	0,40	2.30	4.88	0.80	11.20	0.57	0.30	1.00
B	1.79	0.70	3.70	1.37	0.50	2.60	0.96	0.20	2.80	87.16	37.00	115,00
Ba	0.06	0.02	0,08	0.05	0.01	0.10	ns	dl	0.03	0.03	0.02	0.14
Cr	ns	dl	0.04	ns	dl	0,05	ns	dl	0.18	0.52	0.23	0.76
Fe	ns	dl	0.49	ns	dl	1.29	ns	dl	0.62	0.02	dl	0,32
Mg	1.34	0.09	4.94	1.16	0.02	4.00	ns	dl	0.15	7.51	2.59	35.00
Mn	0.01	dl	0.04	ns	dl	0.05	0.03	dl	0.62	ns	dl	0,02
Mo	56.21	6.00	110.00	50.69	6.10	138.00	20.31	5.50	41.00	41.97	2.35	85.00
Se	2.44	0,30	3.70	1.85	0.25	3.55	1.09	0.24	2.00	0.12	0.03	0.33
Si	11.89	4.10	19.70	14.02	4.20	32.00	44.39	23.00	58.00	0.83	0.51	1.95
Ti	0.08	0.03	0.12	0.07	0,02	0.13	0.01	dl	0,02	0.03	0.01	0.53
V	0.54	0,28	0.98	0.85	0.07	1.80	1.56	0.92	3.47	0.41	0.13	0.64
lk-8.3	72	0	128	125	9	315	1905	275	4710			
lk-4.5	186	139	314	249	143	550	3366	1573	7735	540	150	1006
cl	23908	1 M5	37590	23940	2380	46230	6897	2446	13200	153	18	570
Sulphate	17304	9000	20560	14311	2450	21410	2202	1214	3460	3187	1506	4238
Br	nd	nd	nd	nd	nd	nd	1018	506	1960	nd	nd	nd
pH	9.77	8.64	11.10	10.37	8.38	12,24	12.26	12.06	12.48	9.54	8.93	9.78
Cond.	70.18	19.40	102.00	66.21	19.80	108.30	28.56	14.90	48.50	6.50	2.31	9.02
Dis. Solic	65677	16452	112500	59165	15772	107678	18462	8472	31122	6123	921	8504
us. Soli	43	5	136	35	5	84	27	5	427	8	5	48

nd=not determined, ns=not signi;ant, dl= below limits of detec 1

able 5-2 Summary of Chemistry from Feild Leachates for Second Project Year (March 1, 1994-February 28, 1995)

	1-3 N=55			L2-3 N=42			L3-4 N=56			L4-3 N=38		
	Year 2 Mean	Year 2 Min	Year 2 Max	Year 2 Mean	Year 2 Min	Year 2 Max	Year 2 Mean	Year 2 Min	Year 2 Max	Year 2 Mean	Year 2 Min	Year 2 Max
Na	1637	800	4600	2960	1425	6650	2302	1500	3500	12	4	79
Ca	214	129	356	141	78	224	33	24	46	594	525	680
K	687	325	1600	1019	625	2120	660	550	1155	46	25	96
Al	0.43	dl	0.74	1.23	0.41	1.96	11.57	6.70	19.00	ns	dl	dl
As	0.36	0.07	0.63	1.44	0,28	2.08	1.95	1.10	2.90	0.38	0.30	0.47
B	0.66	0.05	1.35	0.91	0.13	1.40	0.48	0.23	0.80	19.65	10.00	36.00
Ba	0.02	0.01	0.04	0.01	0,01	0.04	0.01	0,01	0.02	0.07	0.03	0.22
Cr	0.02	dl	0.15	0.03	dl	0.62	ns	dl	dl	0.08	0.04	0.22
Fe	ns	dl	0.50	0.23	dl	3.00	ns	dl	0.12	ns	dl	0.11
Mg	0.05	dl	0.16	0.03	0.02	0.13	ns	dl	0.12	21.00	13.00	30.00
Mn	0.01	dl	0.02	0.04	dl	0,52	ns	dl	0.02	ns	dl	0.02
Mo	2.10	1.04	5.50	2.37	1.00	7.75	4.65	3,15	6.00	0.75	0.30	2.16
Se	0.14	0.00	0.35	0.16	dl	0.29	0.35	0,18	0.55	0.03	0.02	0.10
Si	20.15	16.50	24.30	29.75	16.00	39.00	41.96	24.30	451.00	1.16	0.58	2.85
Ti	0.03	0.02	0.05	0.03	0.02	0,06	0.01	0.01	0.01	0.01	0.01	0.02
v	0.57	0.11	0.90	1.14	0.23	1.45	0.86	0.65	1.20	0.25	0.22	0.28
-8.3	125	91	158	269	178	348	712	540	890			
-4.5	165	125	186	420	283	541	1301	1100	1528	88	60	150
cl	432	164	1660	740	62	2960	2323	1250	3170	21	0	66
lphate	3987	1964	9455	5761	3890	8550	1140	692	2124	1667	1500	1939
Br	nd	nd	nd	nd	nd	nd	463	228	746	nd	nd	nd
PH	11.14	10.95	11.31	11.54	11.39	11.66	12.08	11.90	12.31	9.20	6.88	9.51
nducti	8.21	4.47	16.90	11.86	7.23	19.70	12.77	8.74	16,40	2.27	1.97	3,00
Solic	7036	3512	17528	9760	4962	17544	7854	5534	9430	2706	1368	3030
sp sol	9	5	32	12	5	33	10	5	21	6	5	17

Table 5-3 Summary of Chemistry from Feild Leachatea for Third Project Year (March 1, 1995-March 29, 1996)

	L1-3 N=39			L2-3 n=26			L3-4 n=35			L4-3 N=23		
	Year 3 Mean	Year 3 Min	Year3 Max	Year 3 Mean	Year 3 Min	Year3 Max	Year 3 Mean	Year 3 Min	Year3 Max	Year 3 Mean	Year 3 Min	Year3 Max
Na	804	495	774	676	352	1635	1436	1035	2180	9	7	17
Ca	109	46	167	83	40	122	33	23	47	473	375	640
K	241	180	330	530	368	715	594	410	780	26	21	32
Al	0.47	0.20	0.92	1.11	0.45	1.74	12. 69	10.50	16.20	ns	dl	0.22
As	0.30	0.21	0,44	0.47	0.15	0.77	1. 16	0.65	1.60	0.43	0.40	0.47
B	0.57	0.30	0,85	0.66	0.30	0.95	0. 21	0.05	0.48	8.76	7.25	9.70
Ba	0.01	0.01	0,02	0.02	0.01	0.03	0. 01	0.01	0.02	0.03	0,03	0.05
Cr	0.01	0.01	0.03	ns	dl	dl	ns	dl	dl	0.05	0.03	0.06
Fe	ns	dl	0.28	na	dl	0.20	ns	dl	0.12	ne	dl	0.08
Mg	ns	dl	0.10	0.06	dl	1.01	ns	dl	0.05	16.40	I 3,00	20,50
Mn	0.01	0.01	0.10	ns	dl	0.01	ns	dl	dl	ns	dl	0.01
Mo	0.93	0.52	2.00	1.36	0,61	2.90	3.40	1.75	5.00	0.45	0.38	0.69
Se	0.06	dl	0.11	0.09	dl	0.18	0. 16	dl	0.45	0.03	dl	0.08
Si	25.10	18.70	34.00	22.03	13.50	28.00	28. 45	23.00	34.00	1.23	0.97	1.84
Ti	0.01	0.01	0.02	0.01	0.01	0.02	0. 01	0.01	0.01	0.01	0.01	0.03
V	0.84	0.68	0.96	0.44	0.19	0.65	0. 58	0.40	0.70	0.25	0.23	0.28
lk-8.3	129	0	262	144	66	256	563	288	920			
lk-4.5	175	121	318	215	104	336	1033	799	1500	53	36	76
c1	109	75	219	46	21	75	1408	838	2213	24	3	40
;ulphate	1506	1031	2052	2652	1671	5680	886	562	1510	1335	907	1591
Br	nd	nd	nd	nd	nd	nd	319	0	523	nd	nd	nd
pH	11.15	10.95	11.34	11.32	10. 91	11.54	12. 00	11.84	12.19	8.97	8.64	9.17
onductiv	3.64	2.77	4.97	5.64	3. 47	8.08	238. 38	6.48	8032.00	1.97	1,60	2.36
ia. Solid	2654	1850	3584	4276	2576	6870	5404	3872	7294	2272	1804	2700
usp Soli	5	5	10	5	5	5	6	5	25	5	5	10

Table 5-4. Carbon dioxide data for lysimeter soil gases. Detection limit =0.01% (-100 ppm). Data in percent atmosphere.

1994 N=25	Depth	MEAN	MAX	MIN	1995 N=24	MEAN	MAX	MIN
L1	8	0.49	1.90	0.05	L1	0.40	1.20	0.05
	18	0.12	0.40	dl		0.13	0.35	dl
	30	ns	0.20	dl		ns	0,05	dl
	42	nd	nd	nd		ns	0.05	dl
L2	8	0.48	1.40	0.10	L2	0.34	1.20	0.05
	18	0.07	0.18	dl		0.16	0.63	dl
	30	ns	0.15	dl		ns	0.05	dl
	42	nd	nd	nd		ns	0.02	dl
L3	6	0.61	1.80	0.05	L3	0.42	0.01	dl
	18	0.78	2.30	dl		0.43	3.20	dl
	30	ns	0.20	dl		ns	2.00	dl
	42	nd	nd	nd		sn	0,02	dl
L4	8	0.15	0.75	dl	L4	0.24	0.80	0.03
	18	0.06	0.30	dl		0.11	0.30	0.03
	30	0.16	0.80	dl		0.25	0.84	0.05
	42	nd	nd	nd		0.25	1.00	0.02

dl=detection limit, ns=not significant
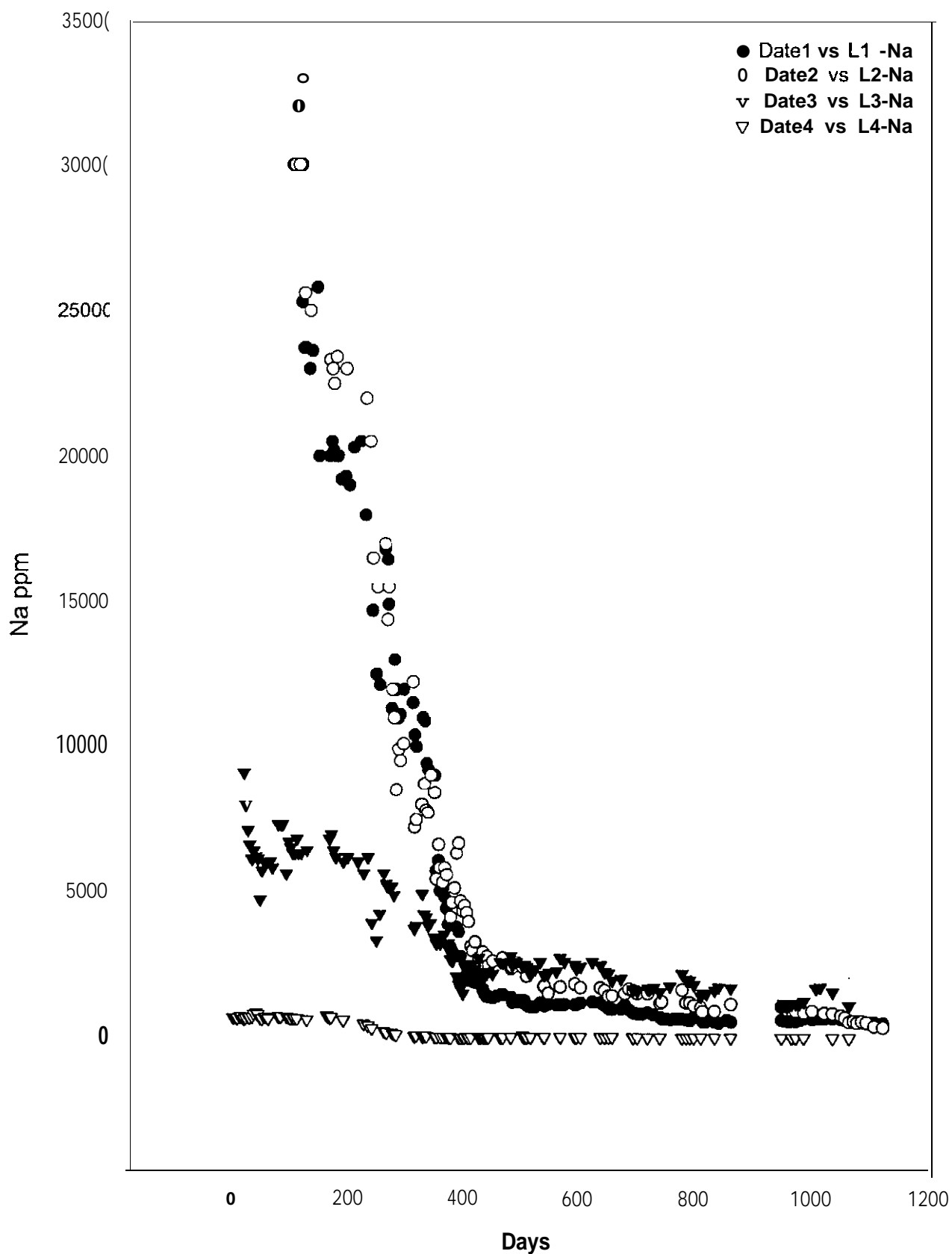
Figure 5-1. Na concentration as ppm in the leachates from the field lysimeters. Data for Ll is from transport tube L1-3, L2 from L2-3, L3 from L3-4 and L4 from L4-3. Day 1 = March 1, 1993.
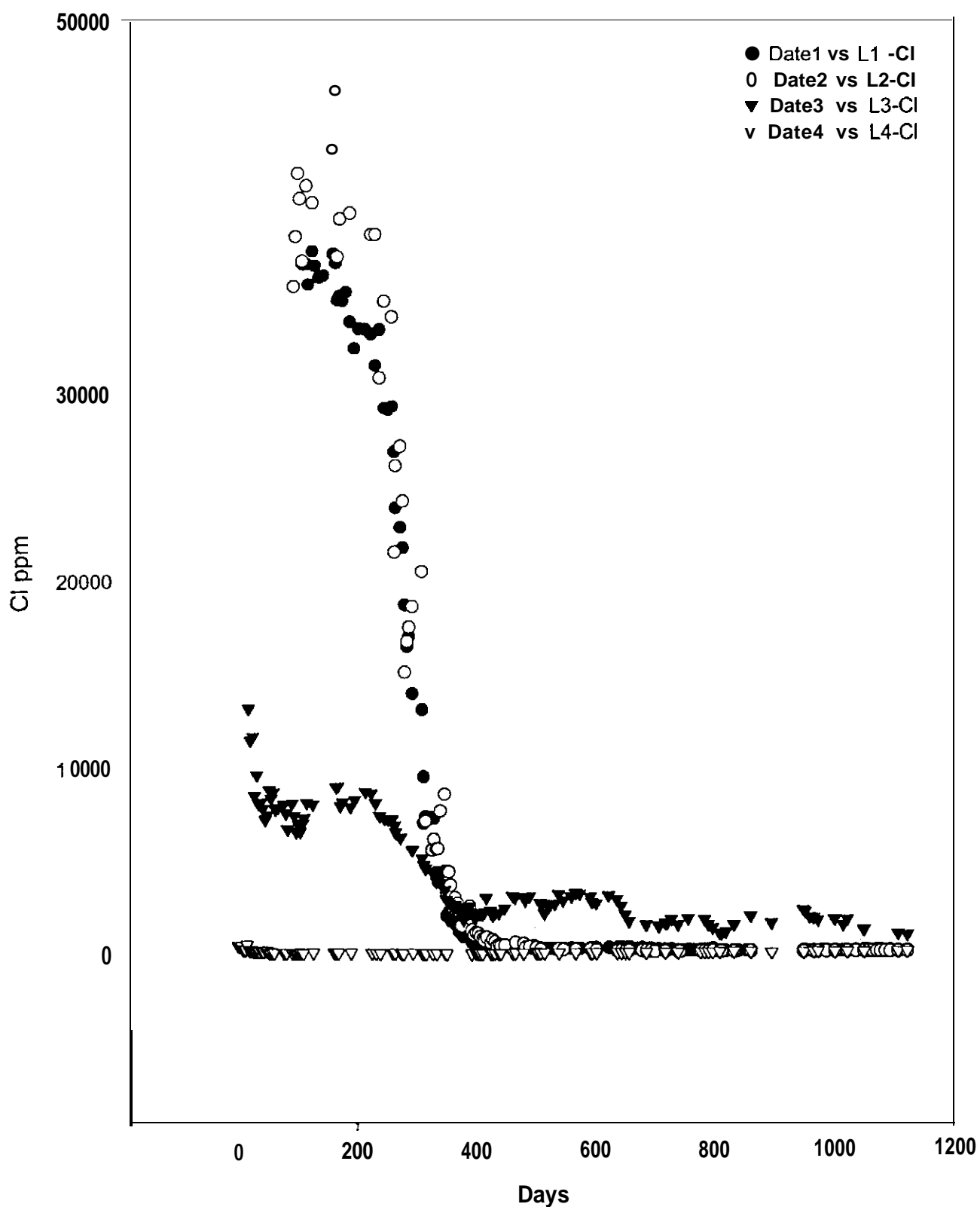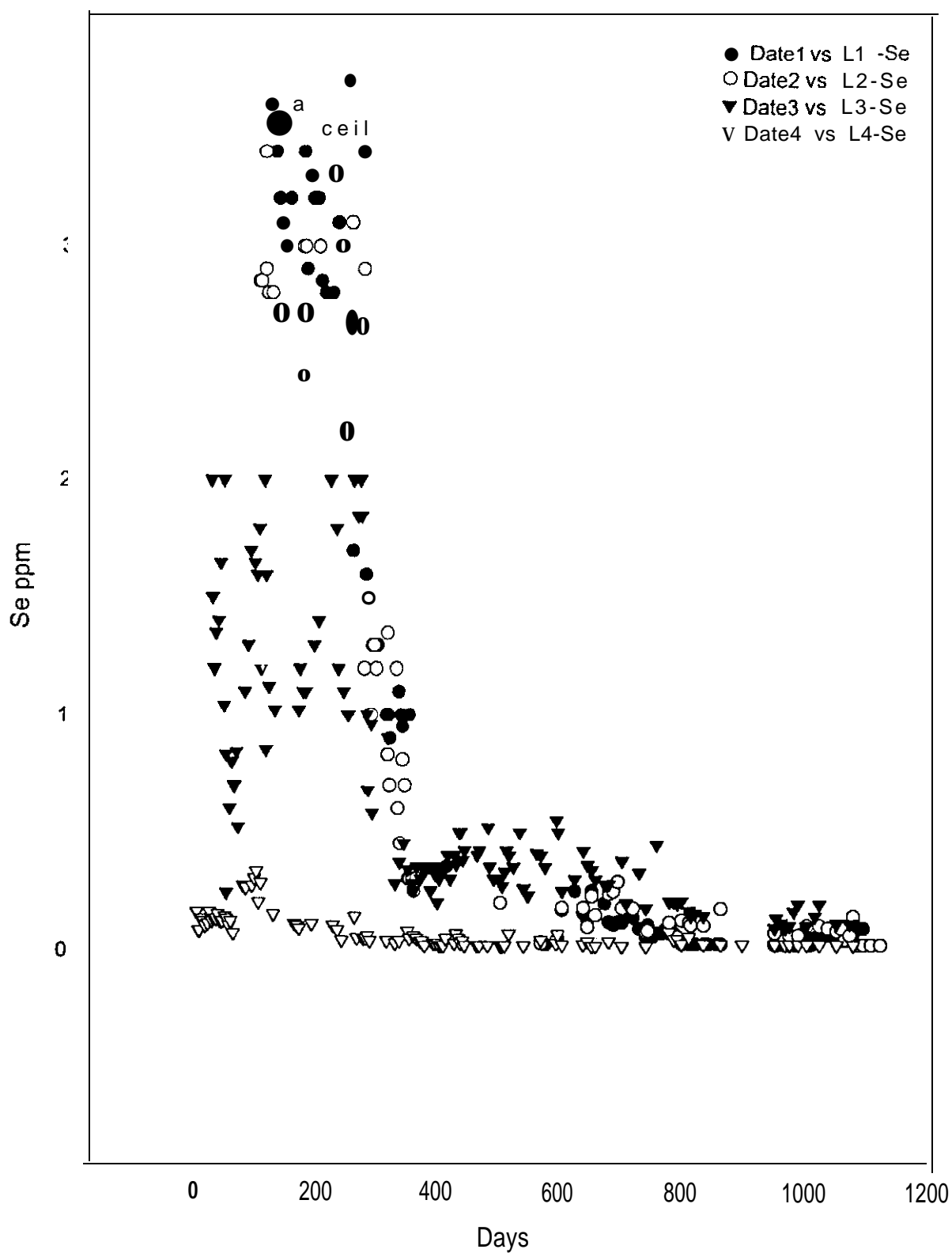
Figure 5-2. Cl concentration as ppm in the leachates **from the field** lysimeters. **Data as Figure 5-1.**
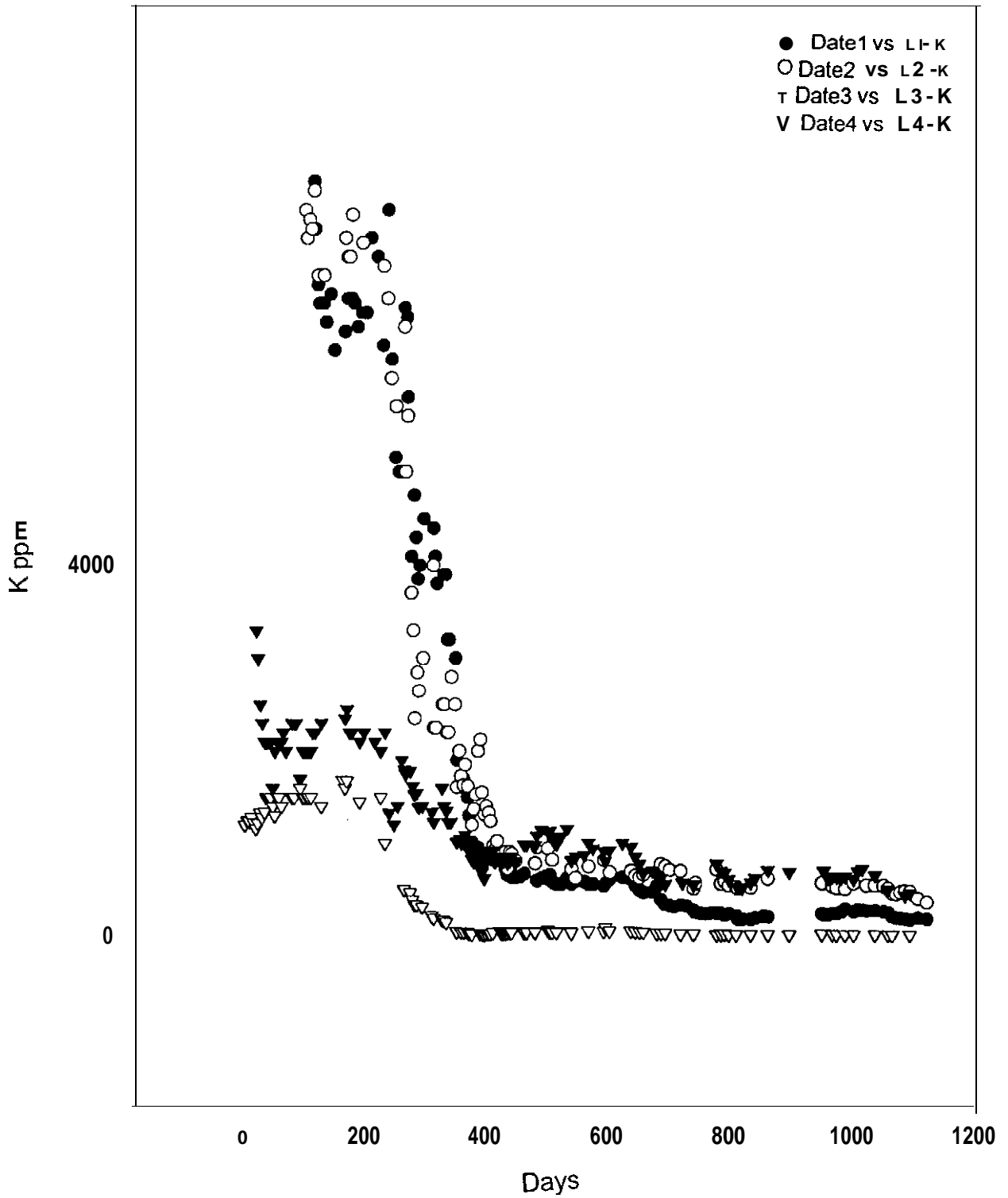
Figure 5-3. K concentration as ppm in the leachates from the field lysimeters.
Data as in Figure 5-I.

maximum of 4,800 ppm the second year, and 774 ppm the third. Thus, the year three maximum was less than 3% of the first years. The decline in L3 was much less, with a maximum of 9,100 ppm the first year, followed by maximums of 3,500 ppm and 2,180 ppm the second and third year (Figure 5-4).

The control lysimeter, L4, filled with Class F fly ash, also showed these patterns, although the maximum concentrations were much less. For example, Na dropped from a maximum of 830 ppm the first year to 79 ppm the second and 17 ppm the third in the L4 leachates.

Minor and Trace *Iens.* The leaching patterns for the other elements do not necessarily show a similar pattern to that of the major elements. For example, Al and Si increased in concentration during the second year of the study in the L1 and L2 leachates (Figure 5-5, 5-6). These trends can be related to increases in the pH of the leachates over time (Figure 5-7). The average pH of the L1, L2 and L3 leachates was 9.7, 10.4, and 12.3 during the first year of collection. pH increased as a function of material density. Most transition elements such as Fe, Co, etc. are essentially insoluble under these conditions. However, the higher pH resulted in the mobilization of elements which can form oxyanionic complexes such as Mo (MoO_4^{-2}), Se (SeO_4^{-2}), As (AsO_4^{-3}) and V (VO_4^{-3}) (e. g., Figures 5-8, 5-9). Additional equilibria with hydroxide, for example, is also expected.

In comparison to the Class F fly ash used for control, the concentrations of Al, As, Mo, Se, Si, Ti and V were higher in the Coolside leachates. On the other hand the concentrations of B and Mg were significantly higher in the Class F leachates (Figure 5-10, 5-1 1).

Leachate elements of environmental concern include As and Se, which have an RCRA limit of 5 Pam and 1 ppm respectively. Many of the samples from the L3 (Figure 5-12) lysimeter exceeded the 5 ppm limit during the first year of the study with a maximum
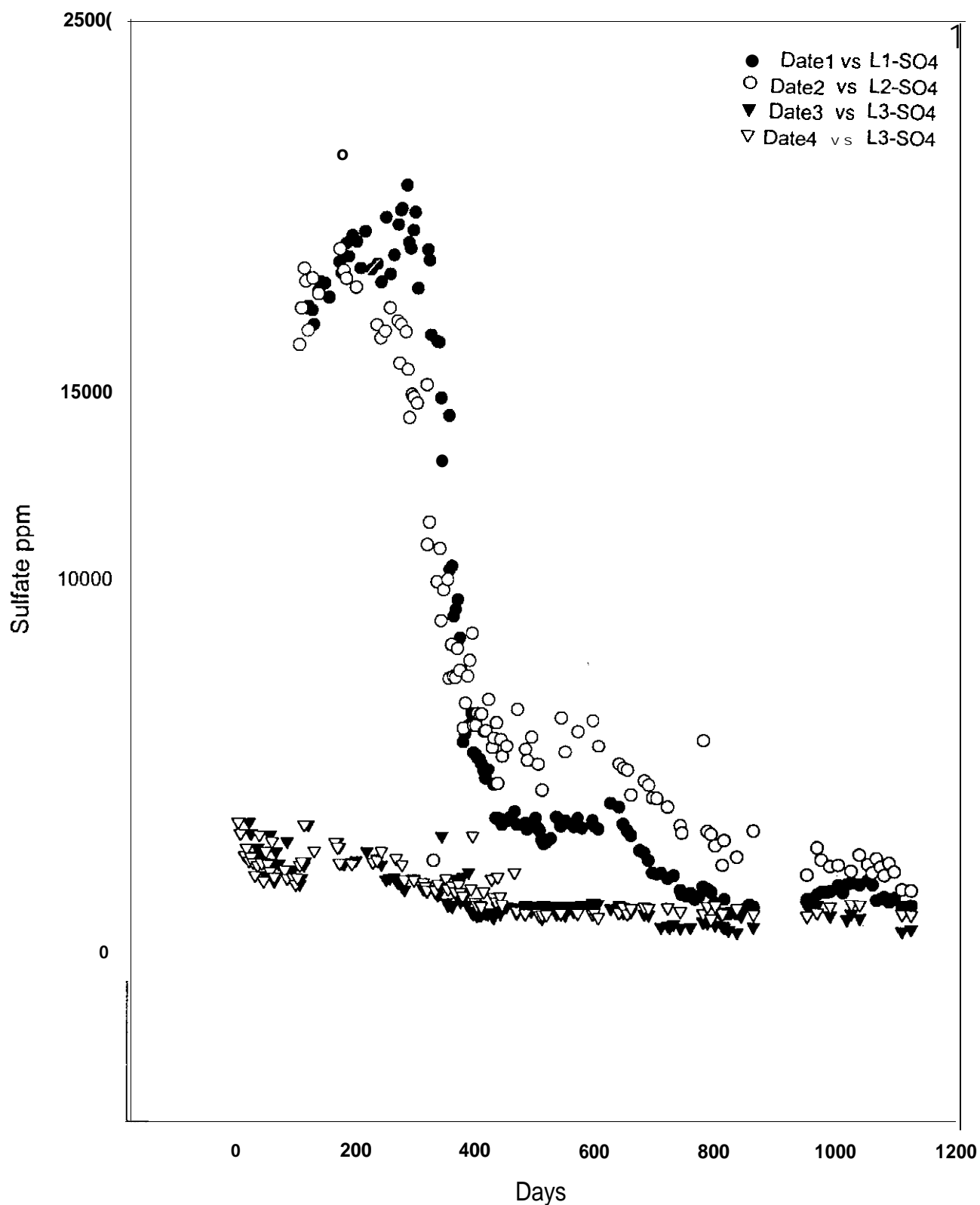
Figure 5-4. Sulfate concentration as ppm in the leachates from the field
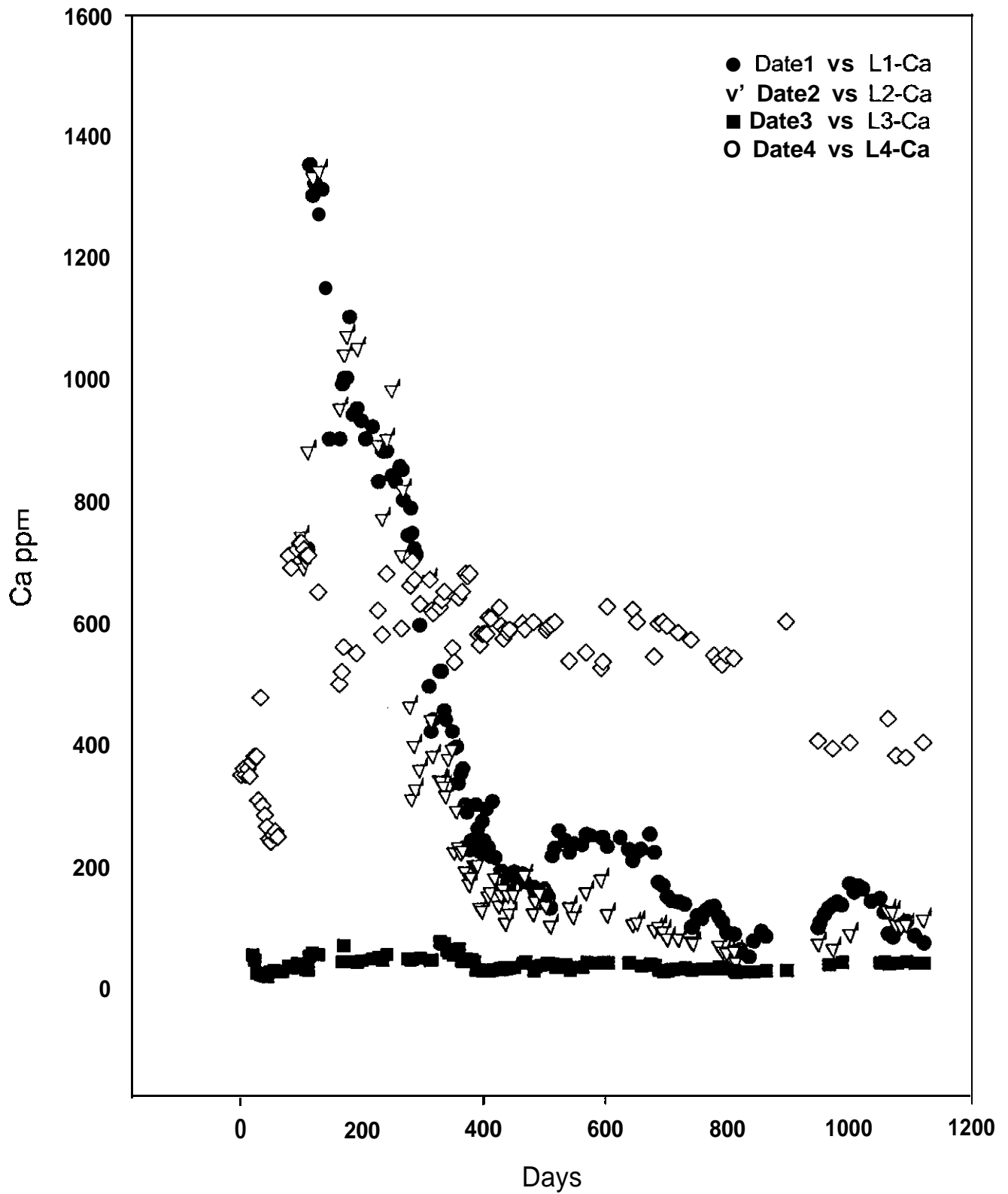lysimeters. Data as in Figure 5-1.

Al in Leachates
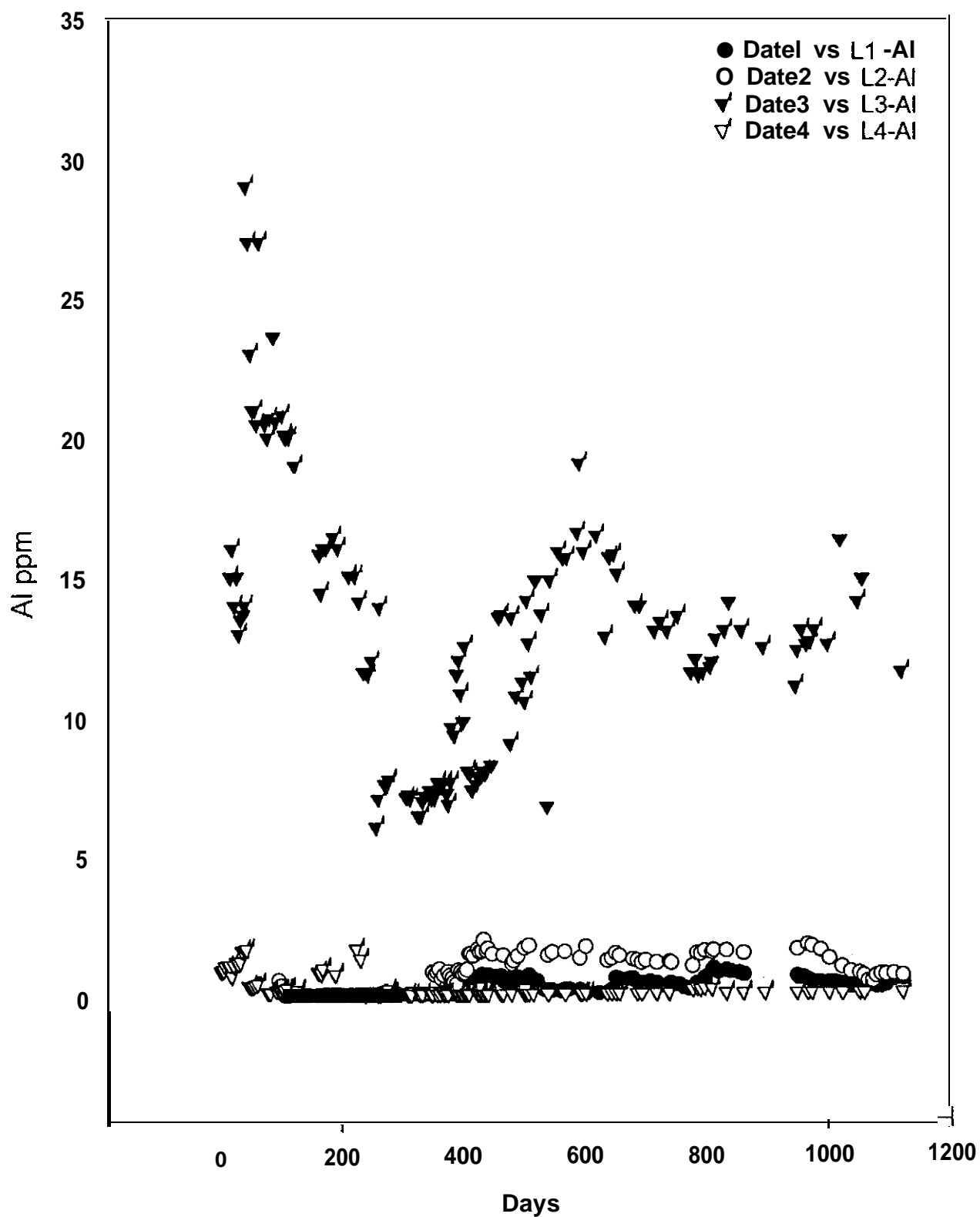
Figure 5-5. Al concentration as ppm in the leachates from the field lysimeters. Data as in Figure 5-1.
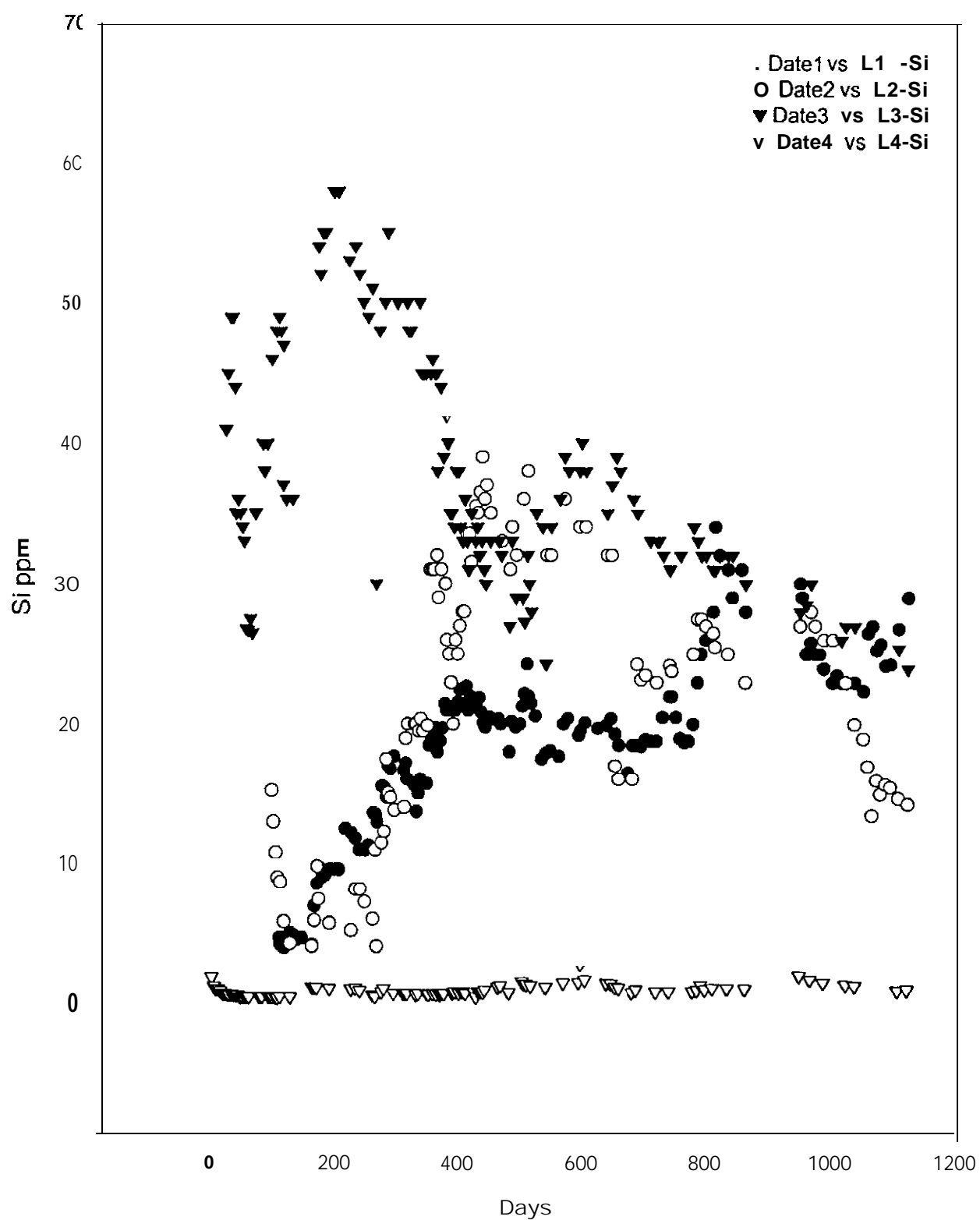
Figure 5-6. Si concentration as ppm in the leachates from the field lysimeters.
Data as in Figure 5-I.
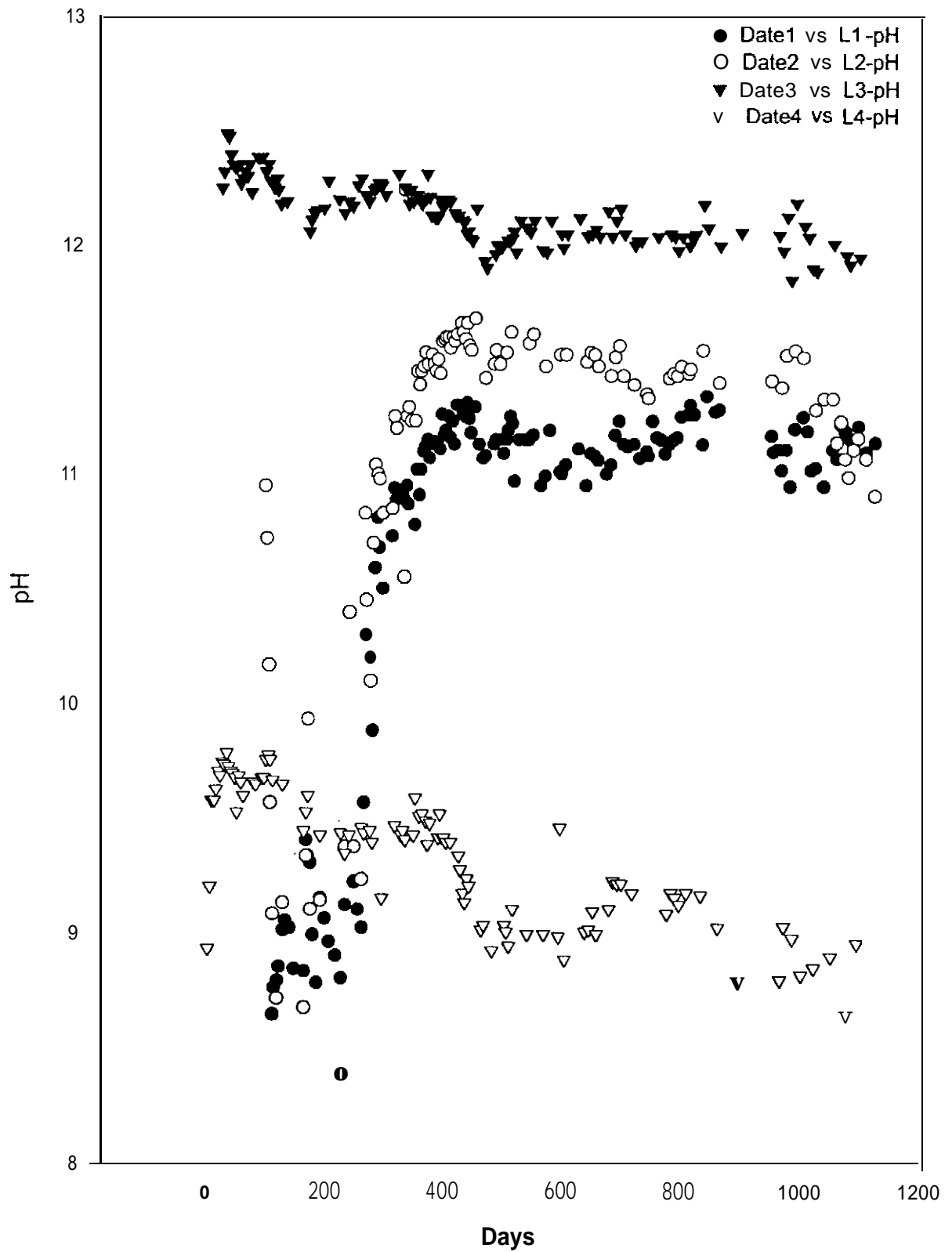
Figure 5-7. pH of the leachates from the field lysimeters. Data as in Figure 5-1.
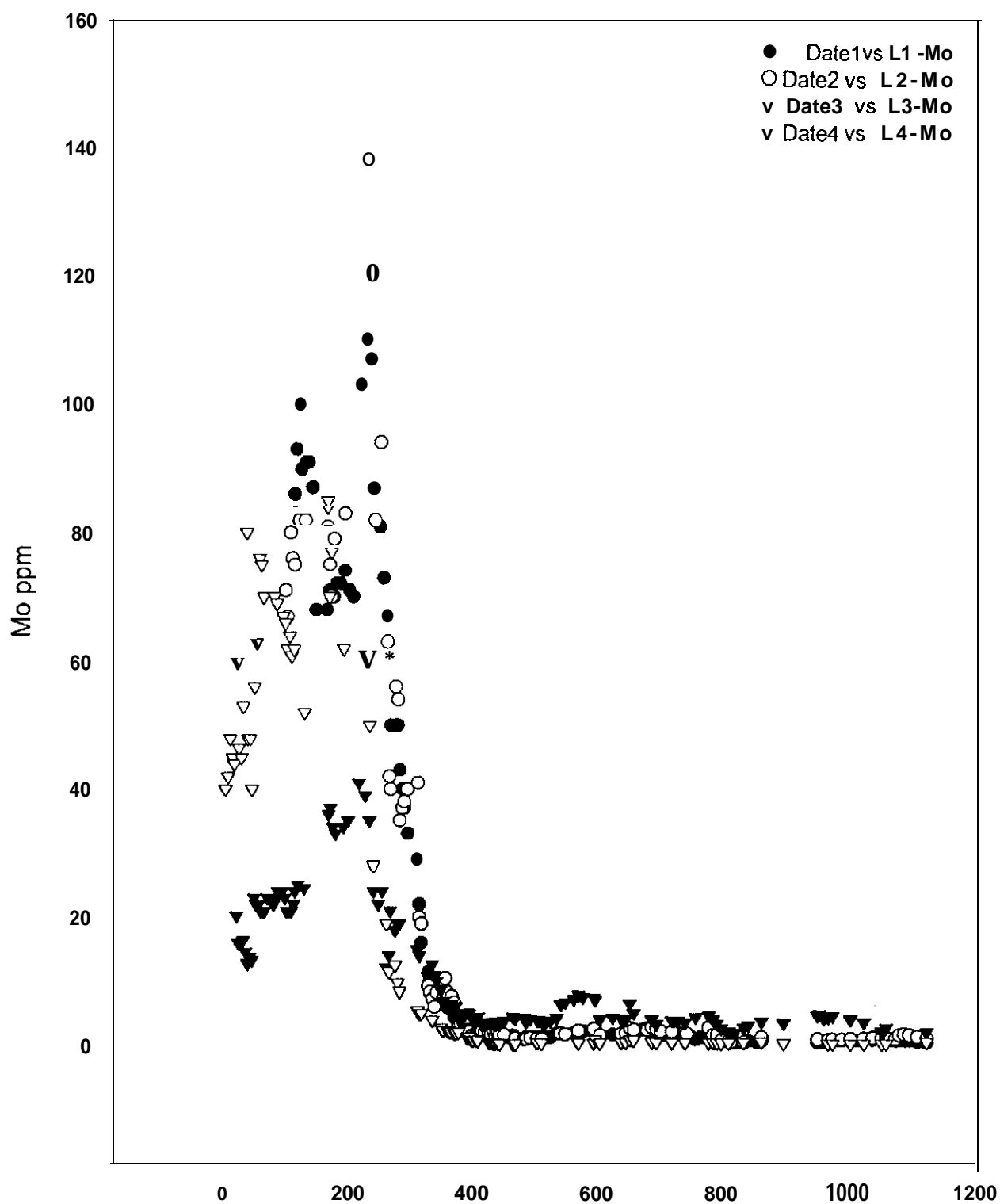
Figure 5-8. Mo concentration as ppm in the leachates from the field lysimeters.
Data as in Figure 5-1.

V in Leachates
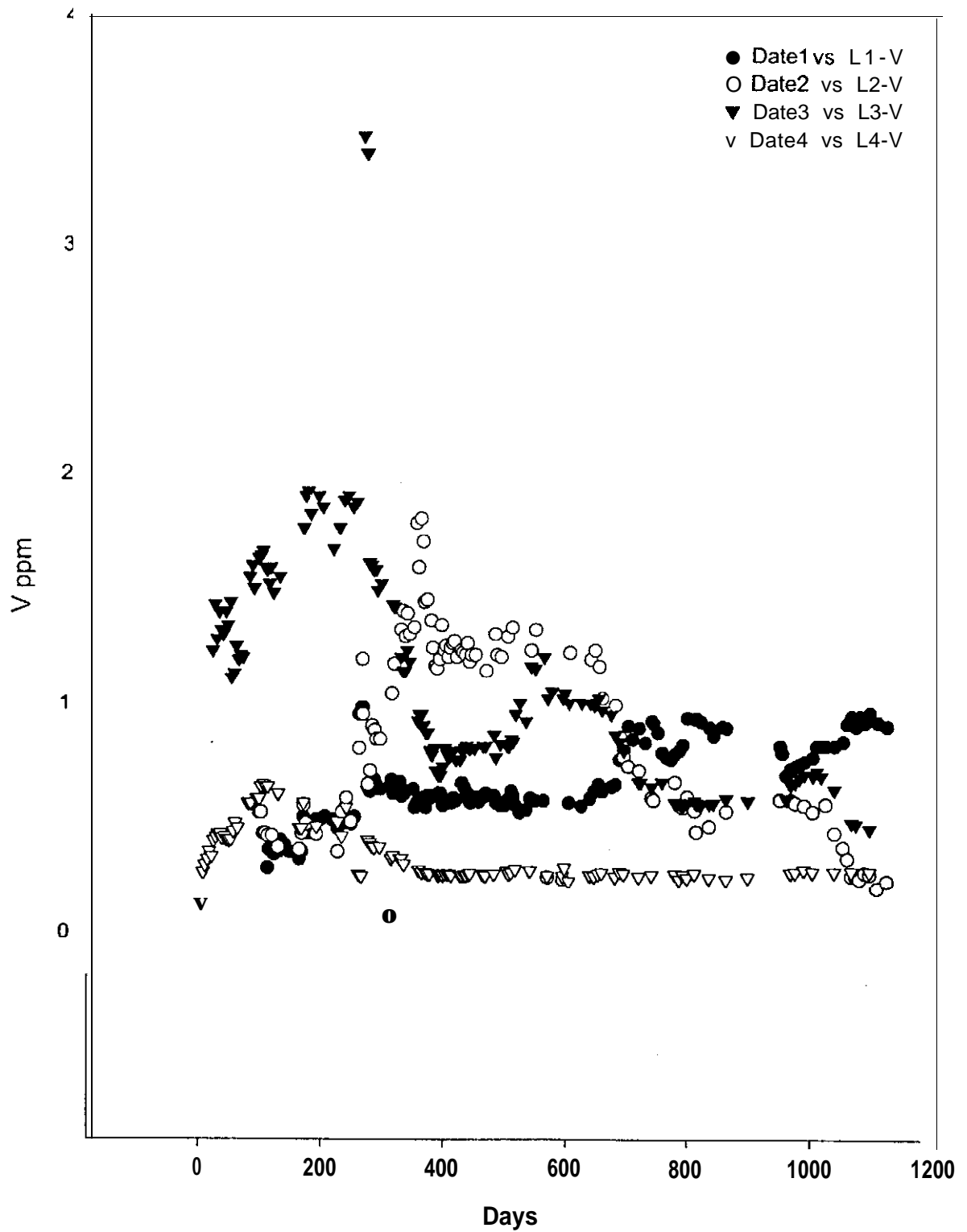
Figure 5-9. V concentration as ppm in the leachates from the **field** lysimeters.
Data as in Figure 5-1.

217
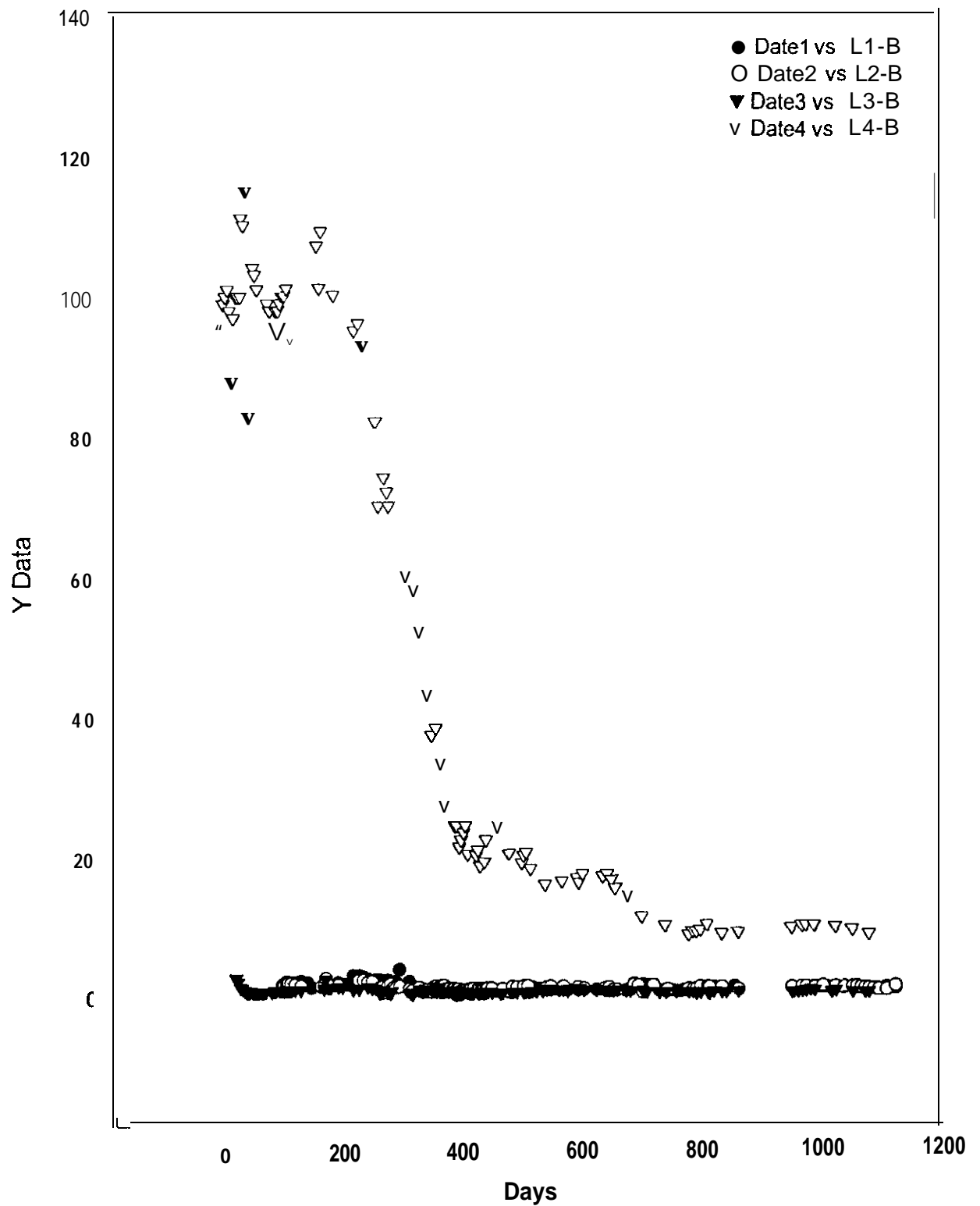
Bin Leachates

Figure 5-10. B concentration as ppm in the leachates from the field lysimeters. Data as in Figure 5-1.
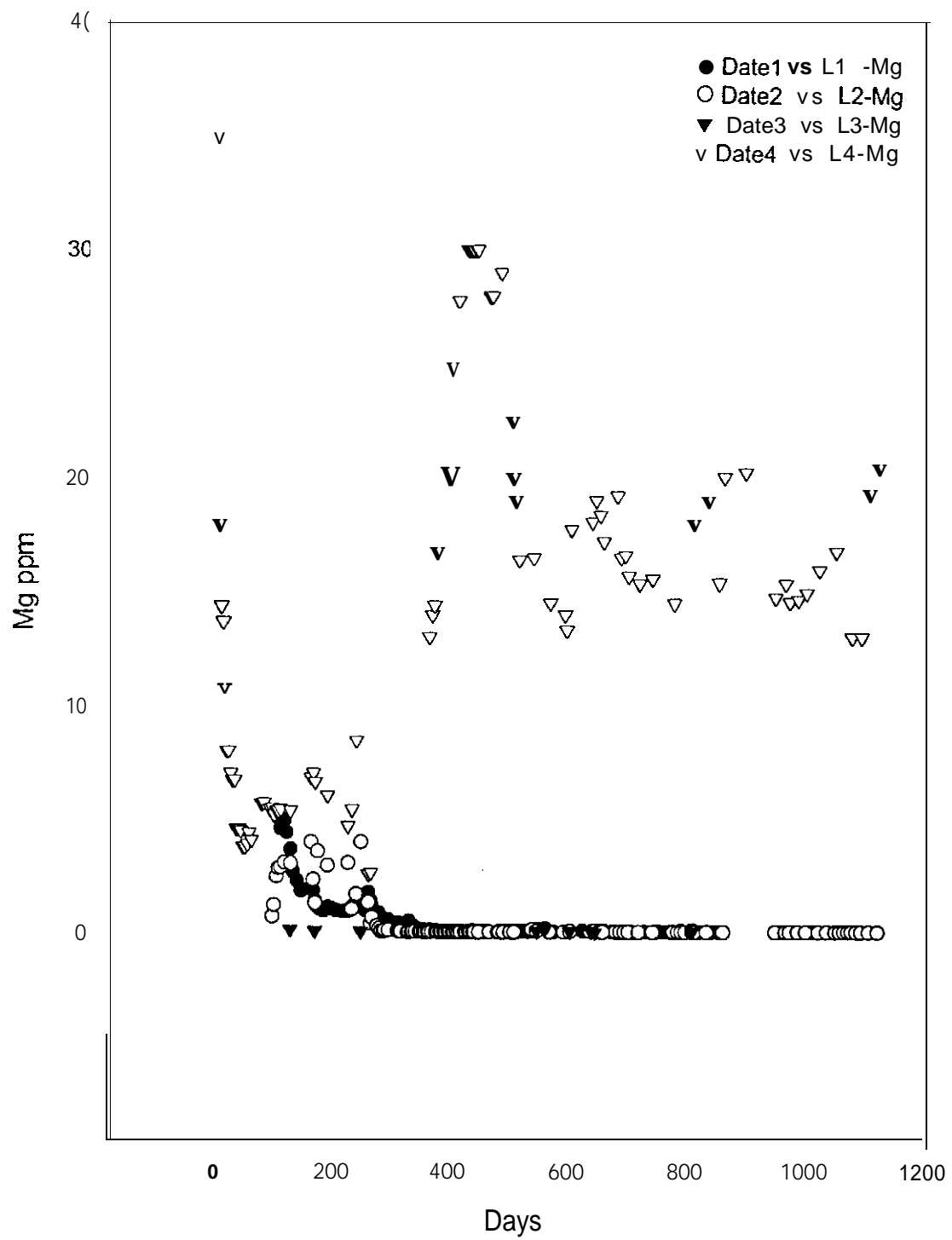
Figure 5-11. Mg concentration as ppm in the leachates from the field lysimeters. Data as in Figure 5-1.
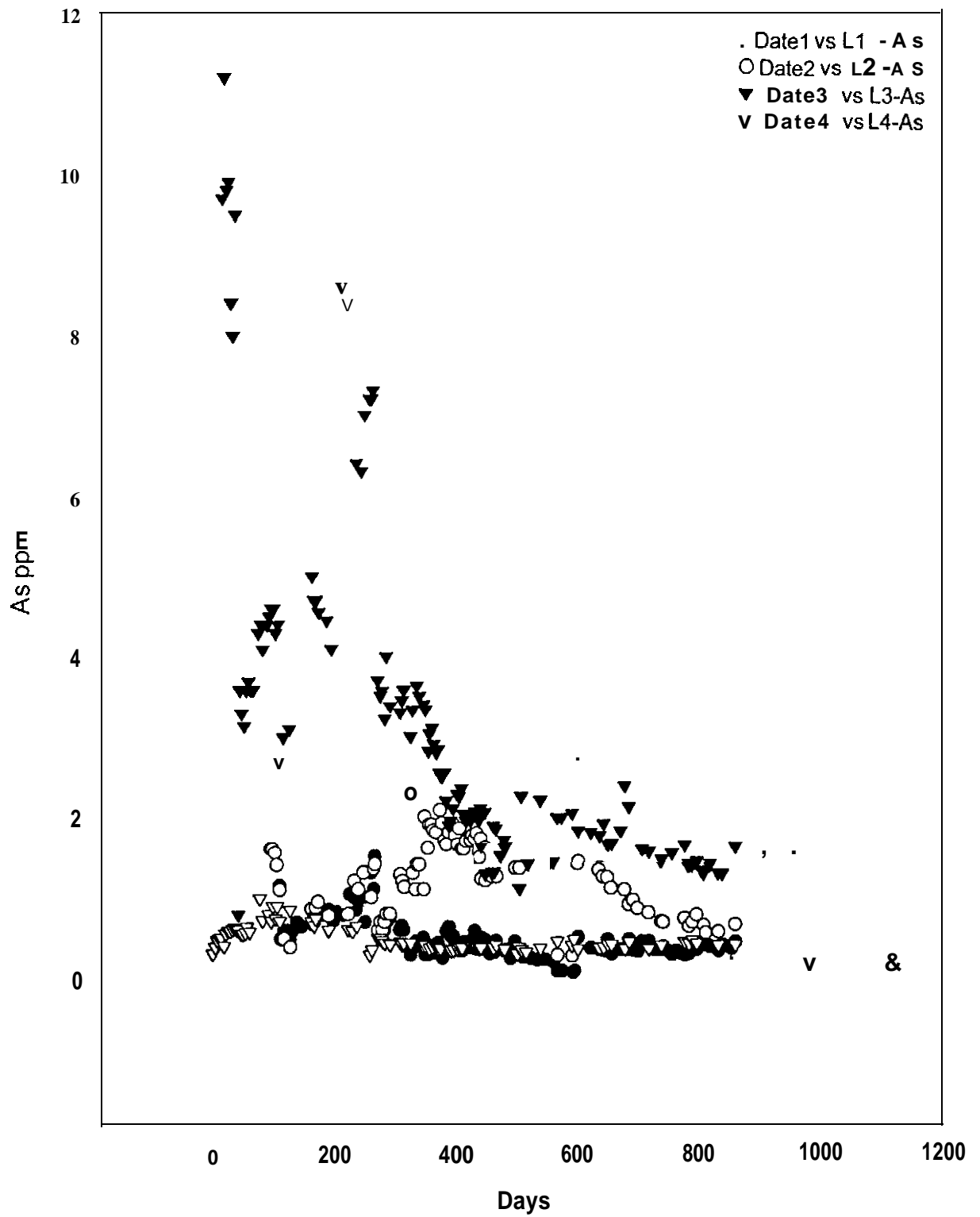
Figure 5-12. **As concentration as ppm** in the leachates from the field lysimeters. **Data as in Figure** 5-1.

concentration of 11.2 ppm in L3-3 and 19 ppm in L3-5. The Se concentration for the L1-3, L2-3 and L3-4 leachates during the first year of the study (Figure 5-13) averaged 2.44 ppm, 1.85 ppm and 1.09 ppm, respectively, well above the RCRA limit. These elements did not exceed the RCRA limits in the TCLP extractions (see Chapter 4).

Carbon Dioxide. After the first few months of the study, grasses and other plants established themselves on the top of the lysimeters. The plants were entirely volunteers, no attempt was made to either seed or fertilize the soil capping the lysimeters. There was considerable variation in plant density and, therefore, rate of respiration, as the best growth was found on the lysimeters with the Coolside material, most notable L1 and L2. Lysimeter L4 had the sparsest growth. Soil gas monitoring began in April 1994 and lasted to the end of the project.

Carbon dioxide concentrations varied throughout the year as a function of time and depth of collection. In general, the highest concentrations were reached during the summer and the lowest during mid-winter (e.g. Figure 5-14). This is a function of respiration. Plants generally conduct photosynthesis in their leaves and respire in their roots, e.g.:

1) $CH_2O + O_2 = CO_2 + H_2O.$

Also contributing to CO_2 in the soil zone is bacterial respiration.

The concentration of CO_2 in the soil zone typically greatly exceeds that of the atmosphere. For example, the highest reading recorded in the study, from the 18 level of L2, was 3.2% (32,000 ppm). Typical atmospheric concentration in the study area is -350 ppm (0.035%), thus soil activity increased the level of CO_2 by two orders of magnitude. The amount of CO_2 in the soil is also a function of its defusivity which is related to permeability. In general, CO_2 concentrations increase with soil depth. The profiles are typified by that of L4. The profiles for L1 through L3 are not typical. In fact,

221

Figure 5-13. Se concentration as ppm in the leachates from the field lysimeters.
Data as in Figure 5-1.
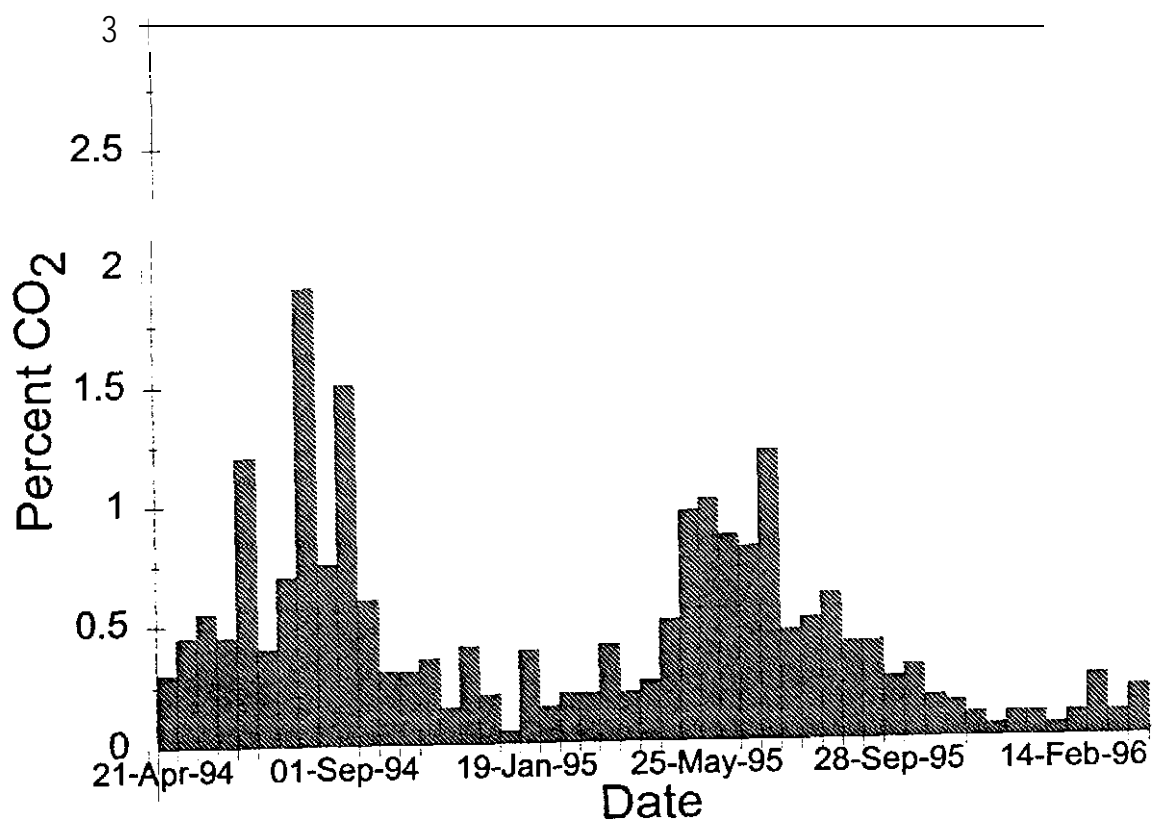
Figure 5-14. CO_2 concentration as measured in the gases of the soils overlaying the L1 Lysimeter. Data is from the 8-inch soil gas well.

the gases within the Coolside material typically were below the detection limit of the equipment employed (-100 ppm), well below atmospheric CO_2. This is clear and conclusive evidence of how reactive the Coolside materials are with respect to CO_2.

Factors Affecting Leachate Chemistry

<u>*Early*</u> **Reactions.** As discussed in other chapters of this report, the Coolside materials are highly reactive and undergo extensive physical and chemical changes during and after emplacement. The principal early changes include completion of hydration reactions, the partial solution of portlandite,

2) $Ca(HO)_2 = Ca^{+2} + 2 0 H$
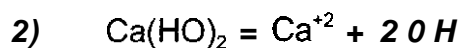
the partial solution and oxidation of hannebachite

3) $2CaSO_3.1/2H_2O +02= 2Ca^{+2} + 2SO_4^{-2} + H_2O$

and the formation of ettringite:

4) $6Ca^{+2} + 2Al^{+3} + 3SO_4^{-2} + 120 H- + 26H_2O = Ca_6Al_2(SO_4)_3OH_{12} 26H_2O$
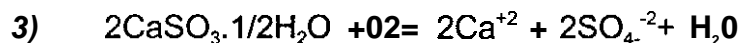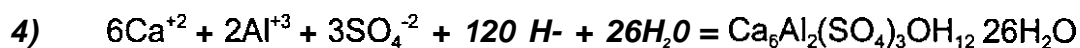
Ettringite is the principal cementitious mineral formed and is responsible for the high strength of the materials, particularly that of the L3 lysimeter. Ettringite is found in all of the lysimeters as well as all of the lab test columns.

<u>*Longer Term Weathering Reactions.*</u> Weathering begins upon the first infiltration of meteoric water. The most important factor in the early weather is the rapid solution of the most readily soluble components, particularly Na and Cl, resulting in brine-like solutions which are very high in ionic strength. High ionic strengths enhance the solution's ability to dissolve additional ionic species. For example, an equilibrium

224

Ca in Leachates

Figure 5-15. Calcium concentration as ppm in the leachates from the field lysimeter. **Data as in Figure 1.**
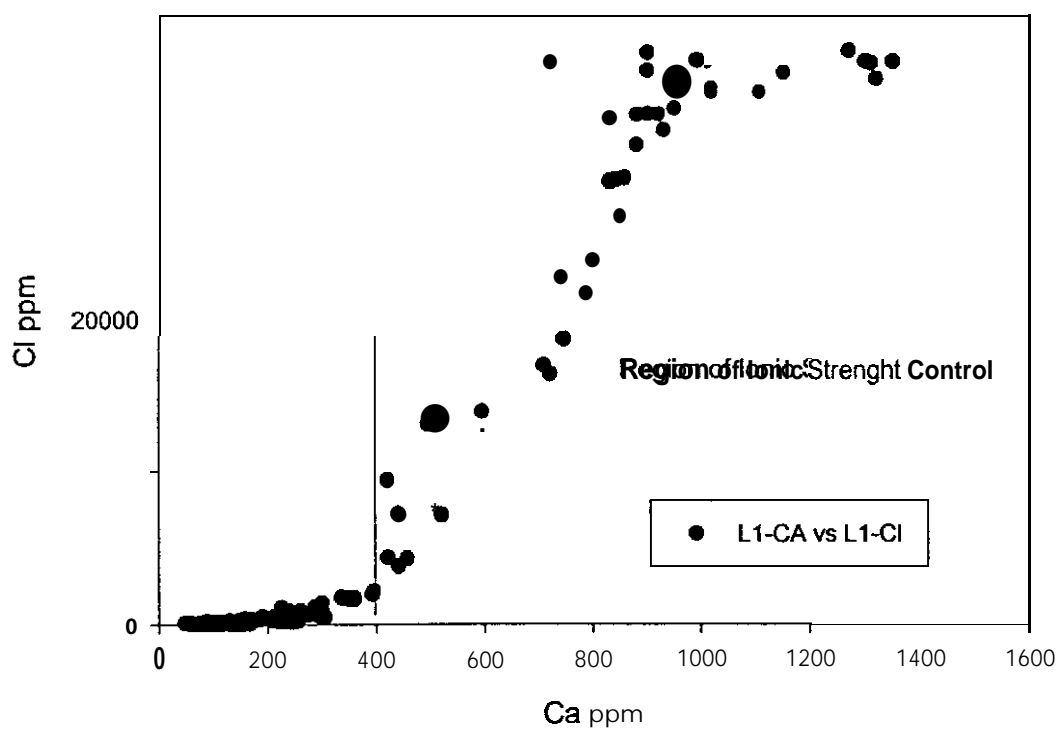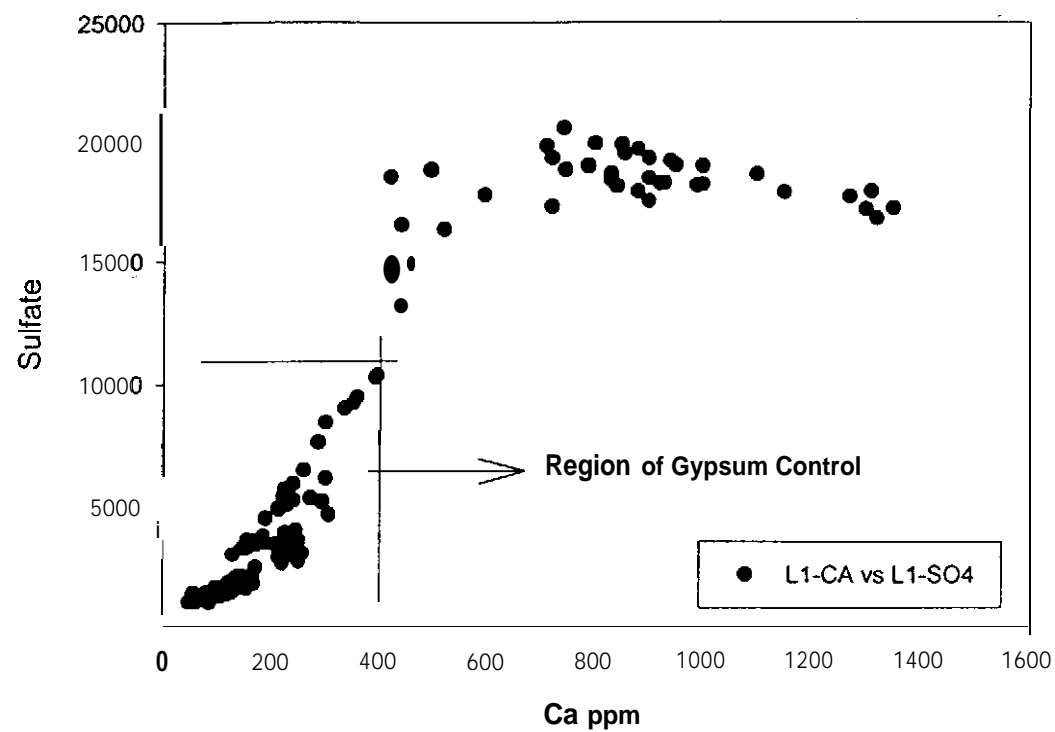
Figure 5-16. Plot of Ca versus Sulfate and Cl for L1-3. The plots illustrate the influence of gypsum dissolution and ionic strength on Ca in solution.

solution of gypsum contains 1,480 ppm of SO_4^{-2}. One with 2,500 ppm of dissolved NaCl will contain 1,800 ppm SO_4^{-2}. This is illustrated in Figures 5-15 and 5-16 which suggests a strong influence on Ca concentration in the high ionic strength region. This correlation changes as ionic strength decreases to one of Ca and sulfate, as would be expected from the thermodynamic data.

As noted above, the absorption of CO_2 is important. At pH's above -10, CO_2 reacts directly with hydroxide and forms a carbonate ion,

5) $\quad CO_2 + 2OH^- = HCO_3^- = H^+CO_3^{-2}$
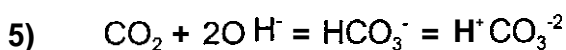
We know from the thermodynamic analysis as presented in Chapter 6 of this report that the leachates are all supersaturated with respect to calcite and undersaturated with respect to gypsum and hannebachite. Thus the materials are both dissolving and precipitating minerals simultaneously. The carbonation of the hannebachite to calcite may be summarized as follows:

6) $\quad CaSO_3 \cdot 1/2\ H_2O + 1/2O_2 + CO_3^{-2} = CaCO_3 + SO;'+ 1/2H_2O$
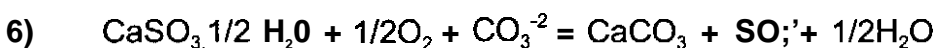
The mineralogical and thermodynamic data all indicate that in the longer term, the most stable set of minerals in the longer term are calcite quartz and ettringite. Both the mineralogical and thermodynamic data indicate that ettringite will also break down over time. However this does not appear to proceed until the sulfate is largely exhausted. Thus, in effect, the sulfate acts as a buffer to extend the stability of the ettringite.

Material Compaction and Leachate Chemistry. One of the more interesting findings of the study is the strong effect of compaction on the chemistry of the leachates. The L1 and L2 leachates have considerably higher elemental concentrations, higher sulfate and lower alkalinity than the L3 leachates.

We believe that this is largely a function of ettrfngite formation. The higher compaction allowed the more extensive formation of ettringite, which tied up the available sulfate in unreactive mineral form. Thus, instead of sulfate carbonation, the reaction with portlandite is more significant, or

7) $Ca(OH_2) + CO_3^{-2} = CaCO_3 + 20H$

This contributes to the significantly higher alkalinity from L3 and also the higher pH. The leachates from LI and L2 eventually increase in both pH and alkalinity as the amount of readily available sulfate (or sulfite) declines. The greater amount of ettringite also decreases pore volume, reduces percolation, and increases strength. This reduces the rate of weathering, resulting in the slower release of soluble salts.

Summary

The leachates from the Coolside material were found to be initially highly alkaline and contained high concentrations of dissolved ions. During the three years of the study the elemental concentration in leachates declined by factors of three to more than an order of magnitude. Initially, the overall leachate chemistry was controlled by the rapid dissolution of highly soluble salts and the formation ettringite. Later, the carbonation of calcium sulfite and calcium hydroxide played important roles.

Overall the Coolside material had significantly higher concentrations of Na, Cl, sulfate, Ca, K, alkalinity, Al, As, Se, Mo, Si, Ti and V in its leachates compared to PCC Class F fly ash used as a control. The Coolside material also had lower B, Ba, Cr and Mg concentrations compared to the fly ash.

Compacting the material resulted in higher alkalinity and pH and a significantly lower rate of release for highly soluble salts. It also appeared to greatly enhance material's strength and improve its resistance to weathering.

Elements of environmental concern which were found in concentration which exceeded RCRA limits included Se and As. Some of the leachates from the L3 lysimeter exceeded 5 ppm As during the first year of the study. The average concentration of Se from all of the leachates from the Coolside material exceeded the limit for Se (1 ppm).

CHAPTER 6. THERMODYNAMIC DATA BASE

Introduction

The data obtained from the lysimeters include pH, conductivity and ionic concentrations. This solute data must be manipulated to infer chemical species concentrations and the mineral phases present in the leaching environment. For this a public domain program WATEQ4F[1] was selected. This program, written in Fortran, expects a single input file and produces a single output file.

Given the large amount of data collected in lysimeter experiments and the difficulty of extracting relevant data from the volumnious output provided by this program, the original program was converted from Fortran to C and tested in DOS using WATEQ4F test case one, modified to run under Windows 3.0/3.1 with menu items and input screens, using Borland C++ v3.l and debugged with all four test cases. Batch data input via Windows clipboard, and output of user-selected data to either comma-delimited files or Windows clipboard was implemented. Options were added to allow saving, reloading or editing input preferences (input species, redox options, input units, and alkalinity options), output preferences (convergence criteria, triggers for species percentage and mineral equilibrium departure for inclusion in output, whether or not to include a thermodynamics table and/or weight/molar concentration ratios in the output), and paste preferences (selection of input and individual output items for inclusion in a "cut/paste" process). The resulting program is referred to as WATEQ, to differentiate it from the 4F (Fortran) version.

---

[1] **WATEQ4F with Revised Thermodynamic Data Base and Test Cases for Calculating Speciation of Major, Trace, and Redox Elements in Natural Waters.** USGS Open File Report 91-183. James W. Ball and D. Kirk Nordstrom

The WATEQ program attempts to infer theoretically, given PH and ionic concentrations of water-borne ions, the active chemical species and approach to saturation of multiple mineral entities of the water. It measures mineral approach to equilibrium by comparing the products of the activities of the constituent ions (Ion Activity Product or IAP) with the equilibrium volubility product (K_{sp}): specifically $\log(IAP/K_i)$, where K is corrected for temperature. A value greater than zero indicates supersaturation. Individual ion activities are the product of the ion concentration and an activity coefficient which attempts to correct for the ionic strength of the solute. The concentrations are determined by an iterative mass and charge balance over the possible species present given the analytical input data of concentrations and pH.

Caveats to Computation

There are enough sources of error inherent in these calculations that measures of approach to equilibrium must not be viewed as absolute indicators of the presence or absence of a particular mineral, or that any equilibrium has been reached. One source of error is the equilibrium volubility product, K, for each mineral. The range of solubilities depend on the degree of crystallinity, particle size effects, order-disorder phenonema, defect structures, range of solid solutions, interlayering and meta-stability. For instance, the Calcite ($CaCO_3$) group consists of Calcite plus the substitution in varying amounts of Mg, Mn, Zn, Fe, and Cd in the matrix for Ca, depending on availability. Thus, formation of Calcite may also include Magnesite ($MgCO_3$), Rhodocrosite ($MnCO_3$), Smithsonite ($ZnCO_3$), Siderite ($FeCO_3$) and Otavite ($CdCO_3$) as part of the solid solution. These individually do not have equal solubilities. At primary saturation, or thermodynamic equilibrium, the aqueous phase will be undersaturated with respect to the solid components. Conversely, a high degree of supersaturation of the most soluble components will exist at stoichiometric saturation. Other examples exhibiting this behavior include Quartz, Gibbsite, Kaolinite, Sepiolite, Oxides and

Hydroxides, Feldspars and Micas. Additionally, the solid phase initially formed may be meta-stable with respect to the thermodynamically preferred state. For example, Calcite is thermodynamically preferred over Aragonite, but Aragonite may form initially as a very fine solid phase with a disordered lattice and slowly convert to the more stable, relatively inactive, less soluble Calcite form. Silica (SiO_2) forms, Anhydrite/Gypsum and Hydroxides also exhibit this behavior.

Another source of error is the determination of the ion activity coefficient over large ranges of ionic strength. In very dilute solutions, the activity coefficient is 1, so that the ion activity is equal to the molar concentration. As ionic strength increases, the coefficient first increases. This increase in ion activity drives the equilibrium toward formation of the neutral species, resulting in a "salting out" of the solid phase. As the ionic strength increases toward and past one, the activity coefficient may drop below one due to greater ionic association in the solute. The solid phase "sees" less ionic activity and the equilibrium is driven towards dissolution of the solid phase. For ionic strengths above about 0.5, the activity coefficients become increasingly uncertain. The ionic strengths encountered in the Coolside leachate range from --0.01 to 3.5. For comparison, the effective ionic strength of a free flowing stream is --0.01, groundwater -0.1, seawater -1. Ionic strength also affects alkalinity. WATEQ estimates available carbonate by correcting measured alkalinity for non-carbonate alkalinity, primarily OH". It is also known that other species, notably silicate forms, introduce errors in measured alkalinity. Despite these uncertainties in volubility constants and ion activity products, the equilibrium calculations performed are useful as an aid in interpreting observed fact.

Many mineral forms addressed by WATEQ show regions of supersaturation but do not control leachate chemistry and are unlikely to be formed in any but the most minor amounts. Albite is a Sodium feldspar. Its saturation index generally has an inverse

232

relation with pH (Figures 6-13 through 6-15). Diopside is a Ca-Mg pyroxene which follows pH (Figures 6-16 through 6-18). These are the most common behaviors seen. The mineral forms which must be suspected of having control of the leachate chemistry are those whose saturation indices remain not far from zero and do not show wild variability, such as Calcite, Diaspore, Gypsum and Silica (Figures 6-22 and 6-23).

Preliminary Investigations

As an initial premise, it was assumed that, regardless of lysimeter contents and degree of compaction, pH will be the controlling parameter affecting leachate species and lysimeter mineralization, Ifso, then theapproach tosaturation ofvarious minerals should vary smoothly with pH, except for errors derived from inherent inaccuracies in test results; any departure from this assumption indicates that there are, indeed, differences in the lysimeters and their leachates. Totestthis, WATEQruns were made on a composite of individual collections of various initial column and field results which gave a total pH range of 13.13 to 8.00. While pH trends were evident, the result indicated there are lysimeter differences.

A second preliminary investigation involved selecting mineral phases approaching saturation within five orders of magnitude ($\log[\text{IAP/kT}] > -5$). 108 of the 322 mineral forms treated by WATEQ met this criteria. Plots of saturation behavior over time were produced. Based upon these plots, the minerals were partitioned into groups exhibiting like behavior for both initial laboratory column 25 (Coolside compressed pellets, wet/dry with average pH about 11.5, rising slightly) and field lysimeter 3, level 3 (Edgewater Coolside, 66#/ft^3@37% H$_2$O with average pH about 12.25, falling slightly) in order to compare saturation behavior. While the partitioning remains valid, saturation behavior is different, again indicating differences in the lysimeters and their resulting leachate.

The third preliminary investigation compared the behavior of selected species with concentrations greater than one ppm in the same two lysimeters. The results also show differences in the lysimeters.

The results of the preliminary investigation, therefore, indicated that lysimeter contents, compaction and CO_2 loading may all affect leachate chemistry.

Selection of Primary Mineral Forms and Ionic Species and Results

Note: Due to the volume of data, graphical illustrations will be restricted to the field lysimeter results in most instances. As the different sample levels of the field lysimeters generally do not show major differences, only one representative level will normally be shown. In addition, as field lysimeters 1 and 2 (the least compacted) are very similar thermodynamically, only one will usually be illustrated.

The initial group of mineral forms and ionic species were further investigated to select those which may drive leachate chemistry, are driven by the chemistry and may be present in significant amounts, or are the predominant carriers of minor ions of interest. Thirty-three aqueous species and seventy-one mineral species were selected for final analysis of the lysimeters based on the following reasoning.

Ionic Species

The major components of coal combustion waste are normally oxides of Mg, Na, Fe, Ti, Si, Ca, K, P, and Al. In addition there are significant amounts of Cl and SO_3. There are trace amounts of other metals such as Zn, Cu, Ni, Co, Cr, Ba, V, As, B, V, Mn, Sr, Zr and Cd. The Coolside sulfur control regime results in the addition of Anhydrite ($CaSO_4$) / Gypsum ($CaSO_4{*}2H_2O$), Portlandite ($Ca(OH)_2$), Dolomite ($CaMg(CO_3)_2$) and, in some cases, Na. Co, Cr, Mo, Ti, Zr, V, B and Se are given little or no treatment in WATEQ,

so will not be considered further. Upon leaching, it would be expected that hydrolysis would result in the release of the metal ion and OH" into solution, resulting in a highly alkaline solute. Free trivalent ions, such as those of Al, Fe and Mn, are not expected to be seen in large amounts, as they tend to form under conditions of low ionic strengths and high acidity. With the exception of $Al^{"3}$, they tend to form insoluble hydroxides. Therefore, $Al(OH)_3^0$ and $Al(OH)$; are expected, as are divalent Ca, Mg, Zn, Cu and Ba, monovalent Na and K ions, and OH". The leaching water is generally in equilibrium with a CO_2 source. This source may be the atmosphere or soil. The partial pressure of CO_2 (pCO_2) in water in equilibrium with the atmosphere is approximately $10^{"3'5}$. The pCO_2 in soil maybe much higher due to organic respiration. It is expected that leaching will introduce significant amounts of CO_2 into the solute. The steps in CO_2 hydration are

$$1: CO_2 + H_2O = H_2CO_3^0$$
$$2: H_2CO_3^0 + H_2O = HCO_3^- + H_3O^+$$
$$3: CO_2 + OH^- = HCO_3$$
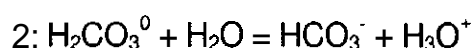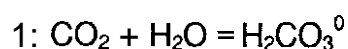
Step 2 is rapid at room temperature while steps 1 and 3 are slow. At higher pH, however, excess hydroxide increases the relative importance of step 3. Therefore, $H_2CO_3^0$, HCO_3^- and CO_3^{2-} are expected. Quartz (SiO_2) is slowly acted upon by alkali at room temperature, with long equilibrium time. This reaction rate increases rapidly above pH 9 due to ionization of silicic acid (H_4SiO_4 or $Si(OH)_4$) and formation of monomeric or multimeric domains, so that $Si(OH)_4^0$ and $SiO(OH)_3^-$ are expected. SO_4^{2-} and HSO_4^- are expected to be available from the dissolution of Anhydrite/Gypsum.

Based on these arguments, the following solute species were initially selected for analysis:
CO_2 total, $Al(OH)_4^-$, Ca, Cl, CO_3^{2-}, HCO_3^-, Na, OH, PO_4^{2-}, SiO_2^0, SO_4^{2-}, Zn, Al, H, K, Mn,

$Al(OH)_3^0$, $CaCO_3^0$, $CaHCO_3^+$, $CaOH^+$, $CaSO_4^0$, $CaHSO_4^-$, HCO_3^-, $MgCO_3^0$, $MgHCO_3^+$, $MgOH^+$, $MgSO_4^0$, $NaCO_3^-$, $NaHCO_3^0$, $NaHPO_4^0$, $NaSO_4^-$, $PbCl^+$, $PbCO_3^0$, $PbHCO_3^+$, $Pb(OH)_4^{2-}$, HPO_4^-, SiO_2^0, $Si(OH)_4^0$, $SiO_2(OH)_2^{2-}$, SO_4^{2-}, $ZnCl^+$, $ZnCO_3^0$, $ZnHCO_3^+$, $ZnOH^+$, $Zn(OH)_4^{2-}$, $ZnOHCl^0$, $ZnSO_4^0$ and $MnCO_3^0$.

After further investigation, all Pb, Zn and PO_4 forms were dropped due to very low concentrations and lack of effect on leachate chemistry. In addition, the following items were also selected:

pH, $-\log(pCO_2)$, Effective Ionic Strength, aH_2O (activity of water), $-\log(Ca$ activity) and $-\log(Mg$ activity).

Mineral Forms

Given the nature of Coolside waste, the characteristics of the oxides are of immediate importance. Of greatest interest are those present in large amounts: those of Ca, Al, Fe, K, and Na. It is expected that hydrolysis of these oxides will result in free aqueous hydroxides and metal ions, with a resulting high PH. On introduction of atmospheric CO_2, metal carbonate precipitation will act to lower pH to some equilibrium value over some unknown period. The pH range seen in Coolside leaching roughly corresponds to that of Portlandite $(Ca(OH)_2)$ in equilibrium with pure water (about 12.45) down to Calcite $(CaCO_3)$ in equilibrium with water that is in equilibrium with atmospheric CO_2 (pH about 8.4 at $\log(pCO_2)=-3.5$). The dissolution of silica and Gypsum/Anhydrite add the possibility of silicate and sulfate mineral formation.

<u>*Silica*</u>. The forms of SiO_2 possible are Quartz, Cristabolite, Chalcedony and Silica Gel. The higher forms, such as Tridymite would naturally convert to the lower forms over time. XRD data show the presence of Quartz. Cristabolite is formed under high temperature up to melting and persists in metastable form on cooling, with eventual conversion to Quartz. Its highly symmetric, open structure is thermodynamically slightly

favored over Tridymite and Quartz. Chalcedony is a fibrous silica, often occurring in small residues as crusts or cavity filling. It is readily soluble in alkaline solutions. Silica Gel is a form favored on formation at STP, most soluble, and ages into poorly crystallized Cristabolite. Quartz is most easily recognized by XRD, and is the expected initial form, least soluble. Earlier inspection of initial leachate column indicated that, of the Silica members, Quartz most nearly approaches equilibrium, but usually remains below. If any other form predominated, then Quartz would be supersaturated, as discussed earlier. Its dissolution is expected to supply SiO_2 to the solute. Silica formation, if any, would be expected to be of the Silica Gel dimorph. Quartz was chosen as the Silica member of interest. The field lysimeter results indicate that Quartz remains in dissolution under higher pH conditions, under low pH conditions in the fly ash lysimeter, and may initially approach equilibrium durng the low pH excursion for those lysimeters which exhibit an initial pH drop. (Figures 6-1 through 6-3)

Na. The initial Sodium mineral forms selected based on approach to equilibrium were Halite (NaCl), Nahcolite ($NaHCO_3$), Trona ($Na_3H(CO_3)_2{}^*2H_2O$), Thermonatrite ($Na_2CO_3{}^*H_2O$), Natron ($Na_2CO_3{}^*10H_2O$), Mirabilite ($Na_2SO_4{}^*10H_2O$) and Thenardite (Na_2SO_4). All of these are extremely water soluble, however, and are not expected to be formed. Na may be involved in minor silicate mineral formation mentioned later. It is expected that Na from oxide dissolution and Na addition due to Sulfur control regimes will be found as a free ion in the solute and will be involved in a very minor way in mineral formation. Its major effect on leachate chemistry is in contributing to the ionic strength of the leachate. Inspection of results for a representative group of these minerals (Figures 6-4 through 6-6) reveals uniform dissolution, except initially in the fly ash lysimeter, where Mirabilite and Analcime (a Sodium Alumino-Silicate) are indicated to possibly form, then go into dissolution.

Cl. No major cation interacts significantly with the Chloride ion. Minor cations Pb, Zn,
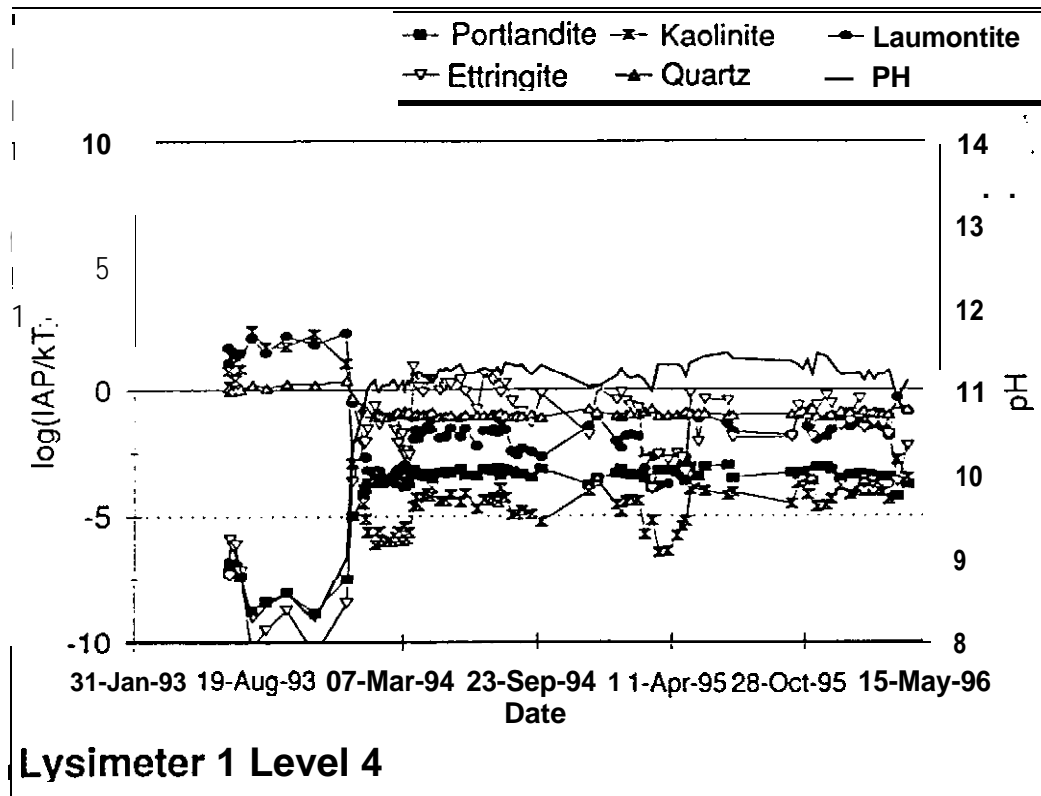
Figure 6-1. Portlandite, Kaolinite, **Laumontite, Ettringite, and Quartz variations by date and** pH **in** Lysimeter **1, Level 4**
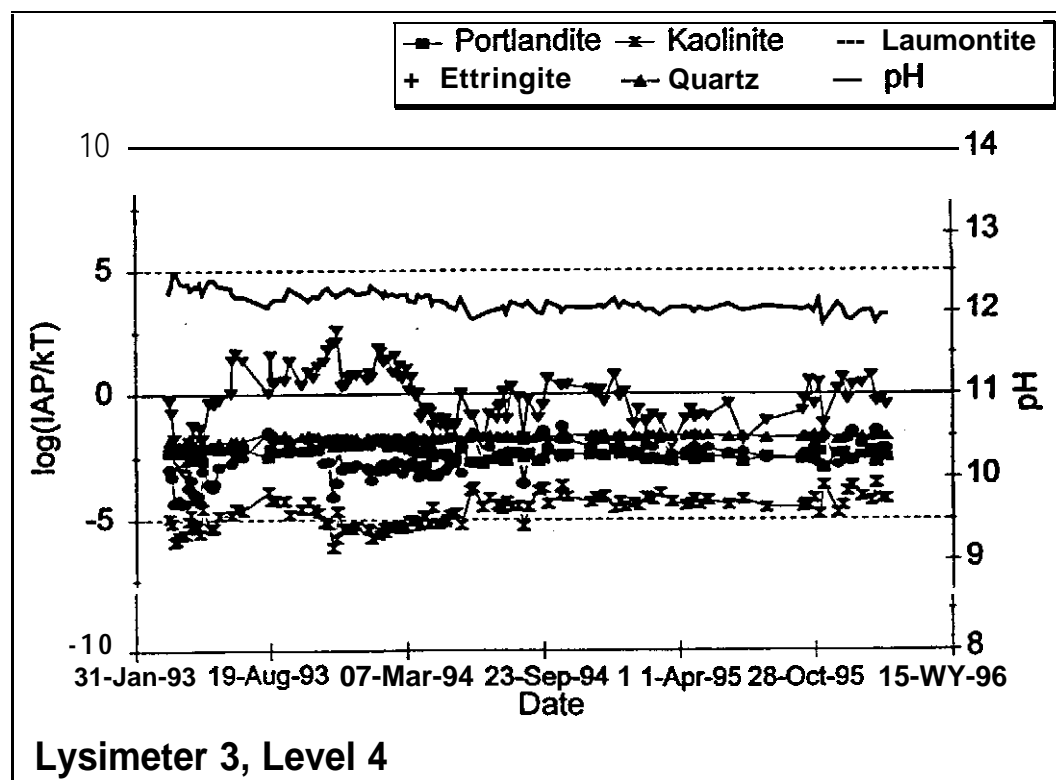
Figure 6-2. Portlandite, Kaolinite, **Laumontite, Ettringite, and Quartz variations by date and** pH **in** Lysimeter 3, **Level 4**
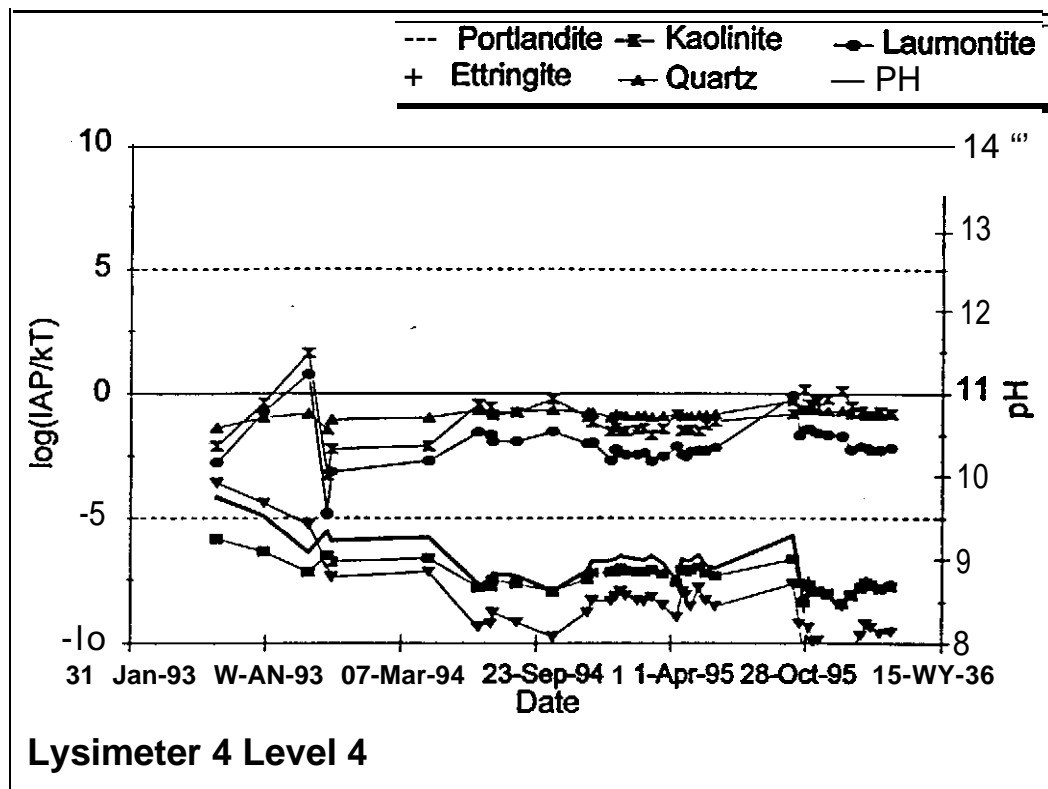
Lysimeter 4 Level 4

Figure 6-3. Portlandite, Kaolinite, Laumontite, Ettringite, and Quartz variations by date and pH in Lysimeter 4, Level 4
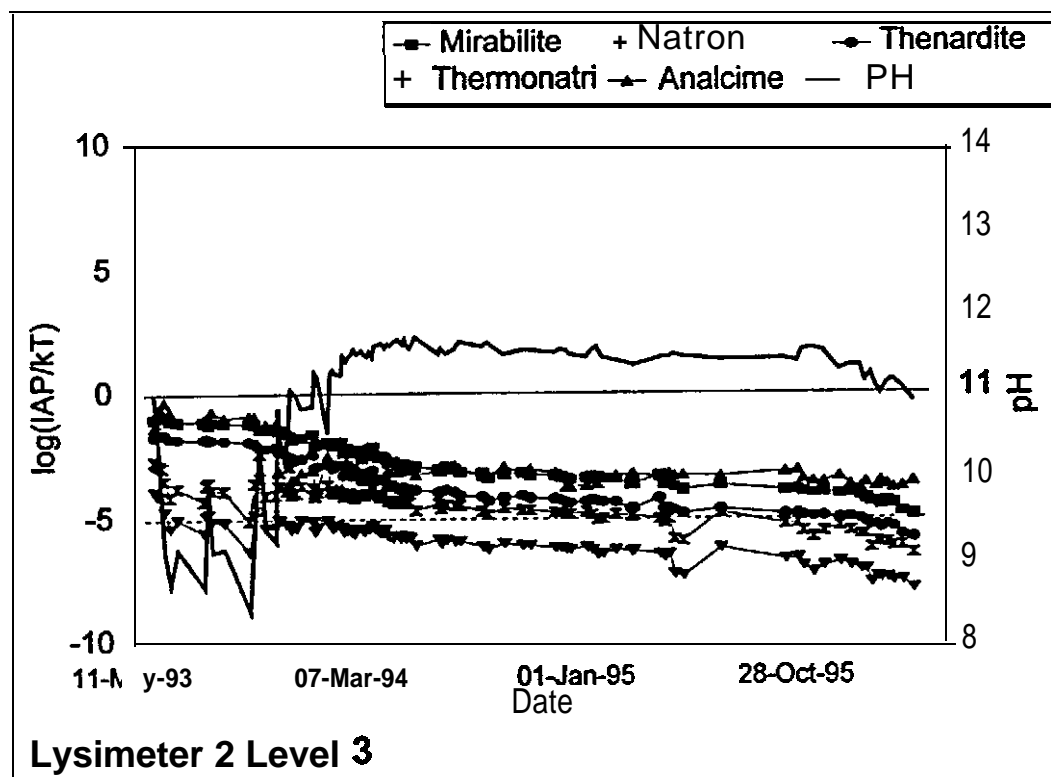
Lysimeter 2 Level 3

Figure 6-4. Mirabilite, Natron, Thenardite, Thermonatrite, and Analcime variations by date and pH in Lysimeter 2, Level 3
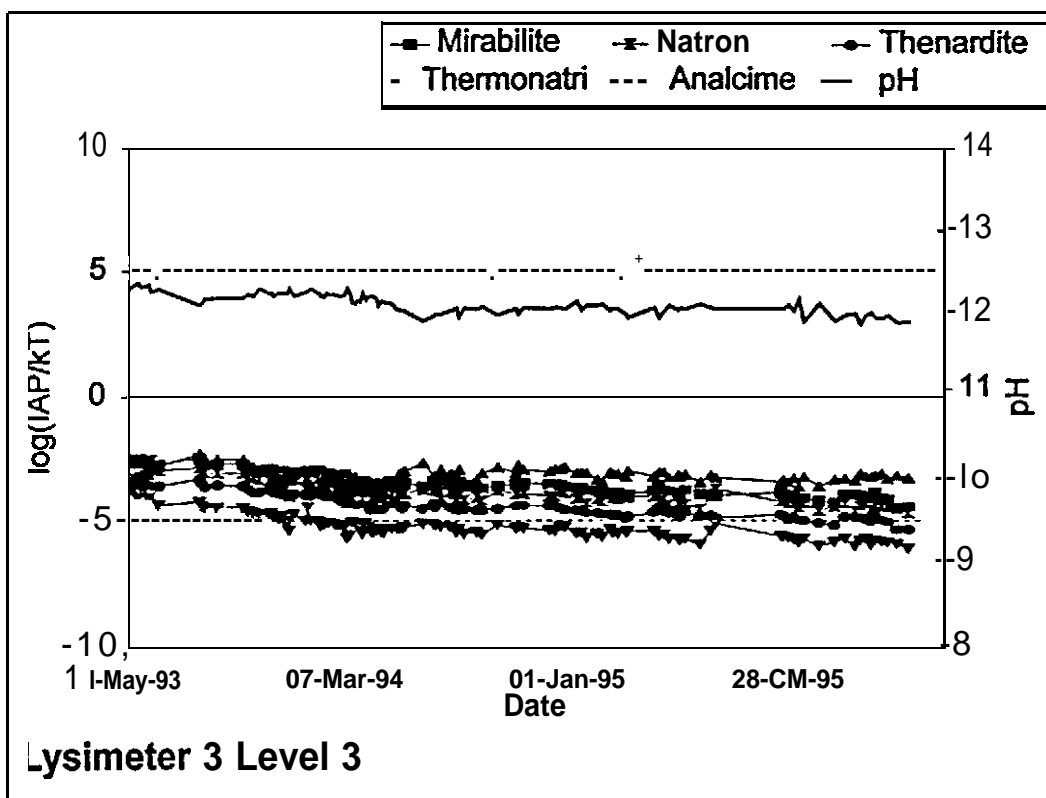
Figure 6-5. Mirabilite, Natron, Thenardite, Thermonatrite, and Analcime variations by date and pH in Lysimeter 3, Level 3
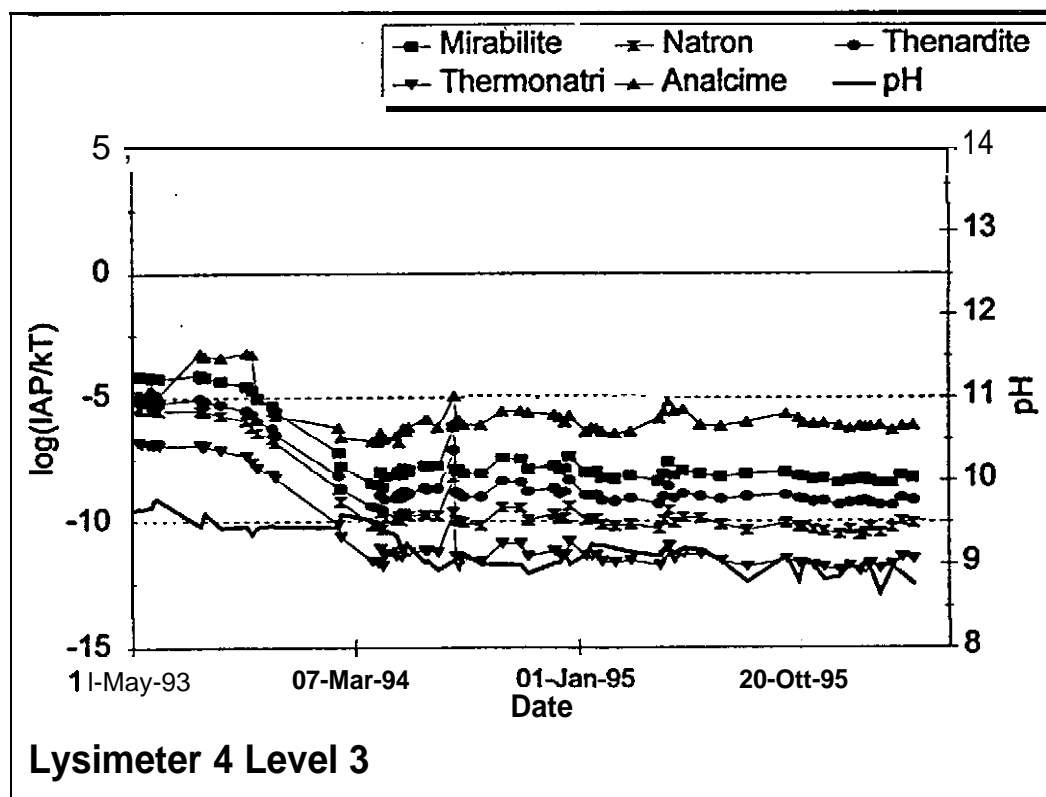
Figure 6-6. Mirabilite, Natron, Thenardite, Thermonatrite, and Analcime variat ᵒns by date and pH in Lysimeter 4, Level 3

240

Fe and Mn may form minor amounts of hydroxy-chloride minerals. Its major effect is also in contributing to the ionic strength of the leachate. Representative samples, $Pb_5(PO_4)_3Cl$ and $Pb_2(OH)_3Cl$ (Figures 6-7 through 6-9), show occasional indications of supersaturation of the phosphate containing member during the low pH transients of the Coolside lysimeters and small supersaturation at the end of the fly ash lysimeter sampling period. Only extremely minor amounts of any Cl containing minerals may be formed.

_Al._ Free Al will be available from the dissolution of glassy alumino-silicates. It is the only trivalent ion which forms a soluble hydroxide. Initially formed is dimorphous Boehmite/Diaspore (AlOOH or Al_2O_3*H_2O), the basic oxide of Alumina. Diaspore is favored over Boehmite by -0.1 kcal/mole. Further hydration in high pH solutions yields $Al(OH)_4^-$, the major ionic carrier of available Aluminum. Diaspore/Boehmite hydrates slowly to Gibbsite ($Al(OH)_3$ or Al_2O_3*$3H_2O$) at room temperature. Gibbsite is also artificially formed by passing CO_2 into alkali aluminate solution, which describes Coolside leachate conditions. Kaolinite ($Al_2Si_2O_5(OH)_4$), which WATEQ indicates approaches or passes saturation at lower pH levels, also dissolves to or forms from Gibbsite and Silicic acid. Diaspore, Gibbsite and Kaolinite were chosen as minerals of interest. For further discussion of Gibbsite and Diaspore, see the discussion of Ettringite below. Various other Aluminosilicates are discussed in the sections on micas, feldspars, pyroxenes and Ca/Mg mineral forms.

A clay-like deposit was reported during sample augering in the field lysimeters. Inspection of Kaolinite saturation indices indicate that clay mineral formation is possible very early in the low pH portions of the lysimeter sample periods (Figures 6-10 through 6-12) and is not indicated at high PH. As XRD data do not generally support the existence of detectable amounts of kaolinite, it is probable that the clay-like deposit is a diffuse alumino-silicate gel consisting of poorly consolidated mixtures of, for example,

Chlorides Lysimeter 2 level 3
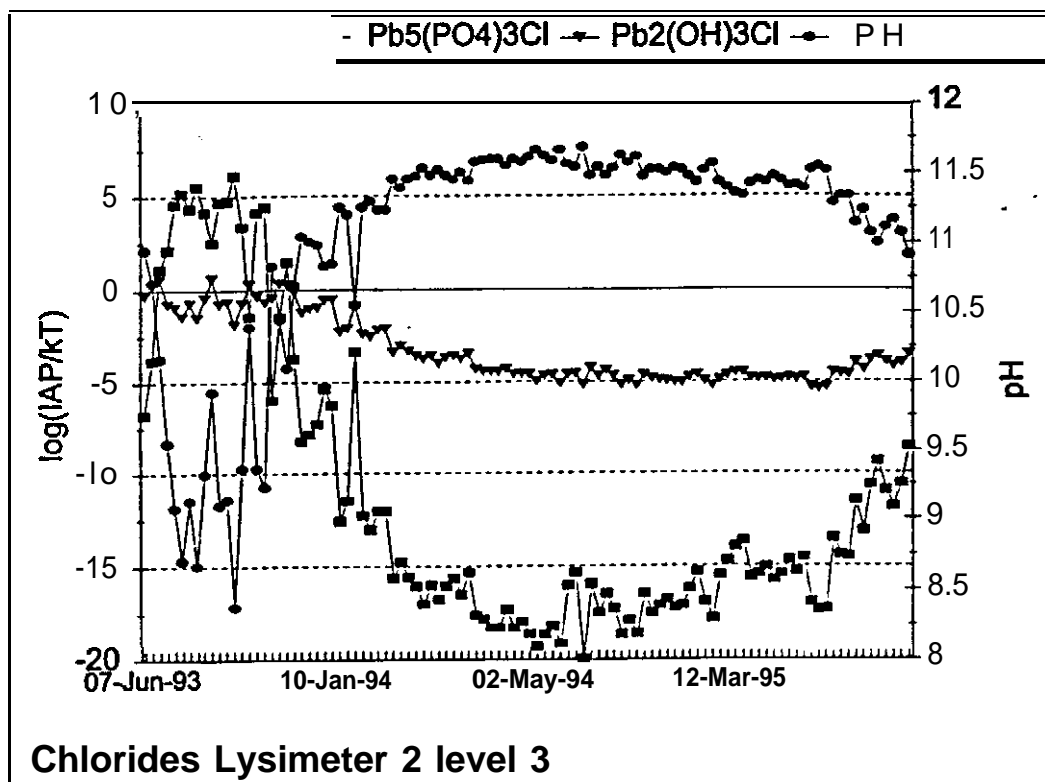
Figure 6-7. $Pb_5(PO_4)_3Cl$ and $Pb_2(OH)_3Cl$ variations by date and pH in Lysimeter 2, Level 3

Chlorides Lysimeter 3 level 3
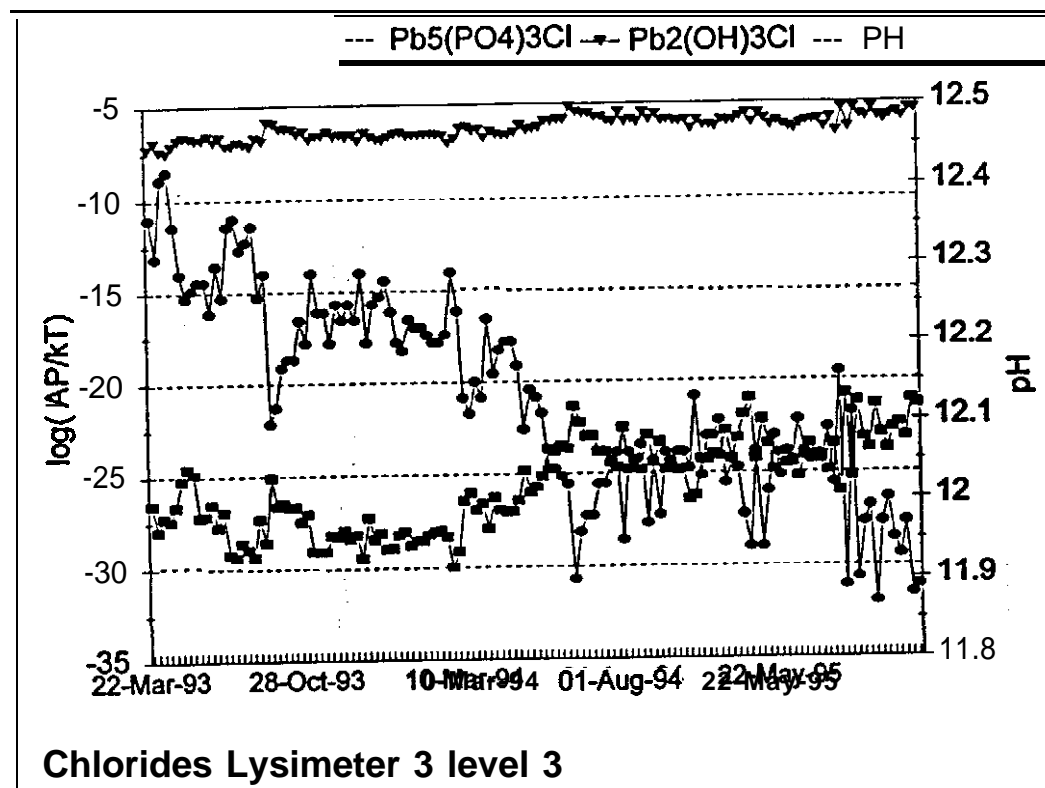
Figure 6-8. $Pb_5(PO_4)_3Cl$ and $Pb_2(OH)_3Cl$ variations by date and pH in Lysimeter 3, Level 3

Chlorides Lysimeter 4 level 3
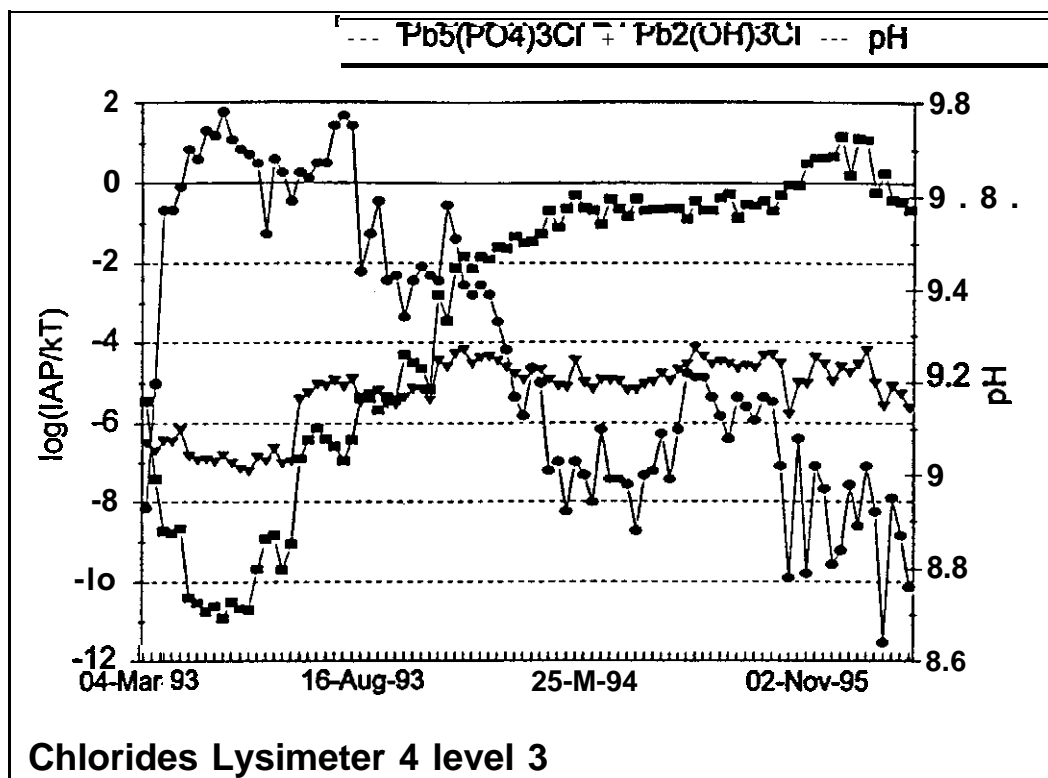
Figure 6-9. Pb$_5$(PO$_4$)$_3$Cl and Pb$_2$(OH)$_3$Cl variations by date and pH in Lysimeter 4, Level 3
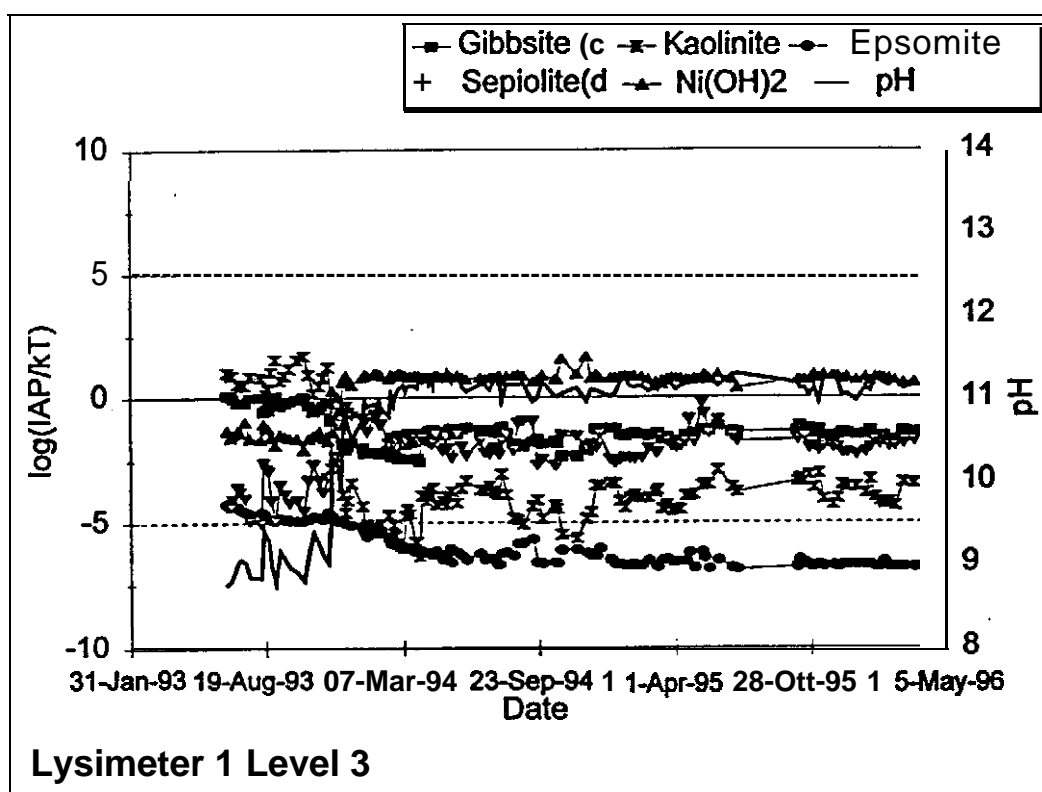
Lysimeter 1 Level 3

Figure 6-10. Gibbsite, Kaolinite, Epsomite, Sepiolite, and Ni(OH)$_2$ variations by date and pH in Lysimeter 1, Level 3
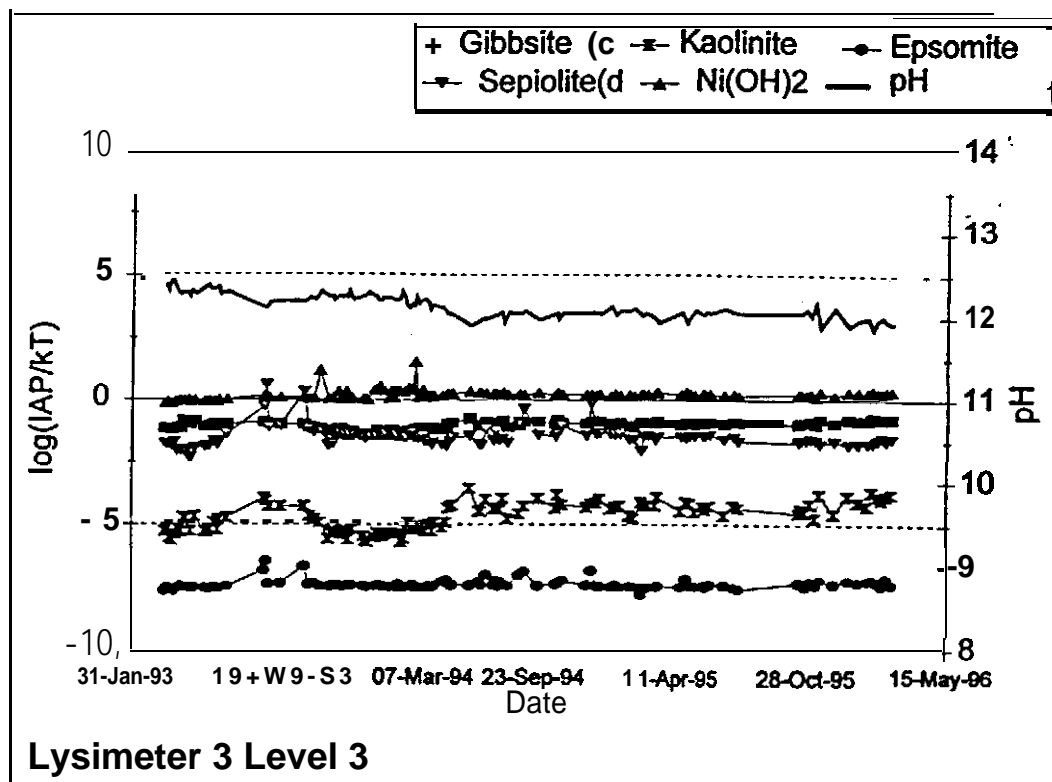
Figure 6-11. Gibbsite, Kaolinite, Epsomite, Sepiolite, and Ni(OH)$_2$ variations by date and pH in Lysimeter 3, Level 3
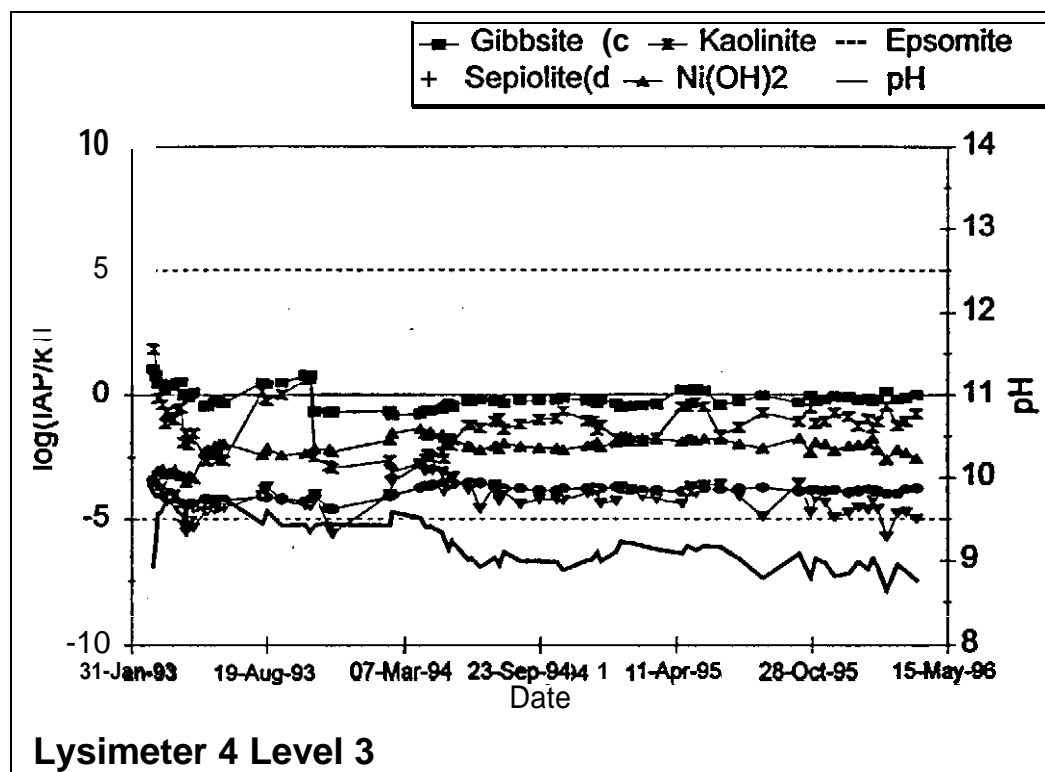
Figure 6-12. Gibbsite, Kaolinite, Epsomite, Sepiolite, and Ni(OH)$_2$ variations by date and pH in Lysimeter 4, Level 3

Adularia, Albite, Anorthite, Pyrophillite, Kaolnite, Wairakite and Halloysite. XRD results generally support this.

Micas. K-mica ($KAl_2(Si_3Al)O_{10}(OH)_2$) remains supersaturated under nearly all lysimeter conditions and shows a sometimes extreme supersaturation at lower leachate pH (Figures 6-13 through 6-15). Micas have never been shown to control water chemistry. Reversibility has not been shown, so there is no reason to believe that they attain equilibrium solubilities or will form. The supersaturation merely reflects the solute availability of the component ions.

Feldspars. The Feldspars Anorthite ($CaAl_2Si_2O_8$), Al bite ($NaAlSiSi_2O_8$) and Adularia ($KAlSiSi_2O_8$) were invesitgated. These minerals forma substitutional solid solution with degree of saturation generally Adularia > Albite > Anorthite. They appear to be driven by leachate chemistry. The dominant members, Adularia and Al bite (Figures 6-13 through 6-15), show supersaturation at low pH and dissolution at high pH in the Coolside lysimeters, and general undersaturation in the fly ash lysimeters. Formation of these minerals is expected to be slight and contributes only to the broad aluminosilicate peak detected by XRD.

Pyroxenes. Clinoenstatite ($Mg_2Si_2O_6$ or $MgSiO_3$), Analcime ($NaAlSi_2O_6 \cdot H_2O$) (hydrated Jadeite) and Diopside ($CaMgSi_2O_6$) at times exhibit supersaturation. Diopside generally appears to be driven by pH mediated silica availability (Figures 6-16 through 6-1 8). Its often very high degree of supersaturation argues against its importance in leachate chemistry. Clinoenstatite, the major Magnesium Silicate, only approaches saturation at high pH in the most compacted lysimeter, and not at all in the others (Figures 6-13 through 6-1 5). This also reflects Silica availability at high pH and low Silica availability even in the presence of elevated Mg in the fly ash lysimeters. Analcime (Figures 6-4 through 6-6) approaches or exceeds saturation only in the early
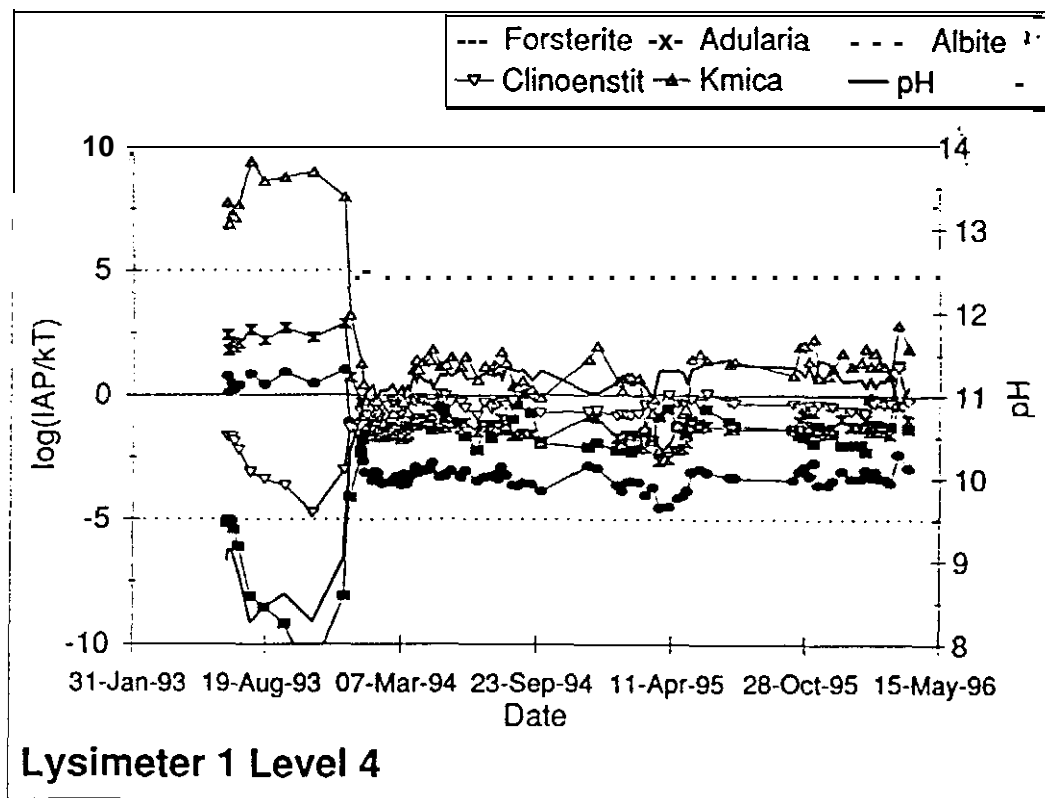
Figure 6-13. Forsterite, Adularia, Albite, Clinoenstatite, and Kmica variations by date and pH in Lysimeter 1, Level 4
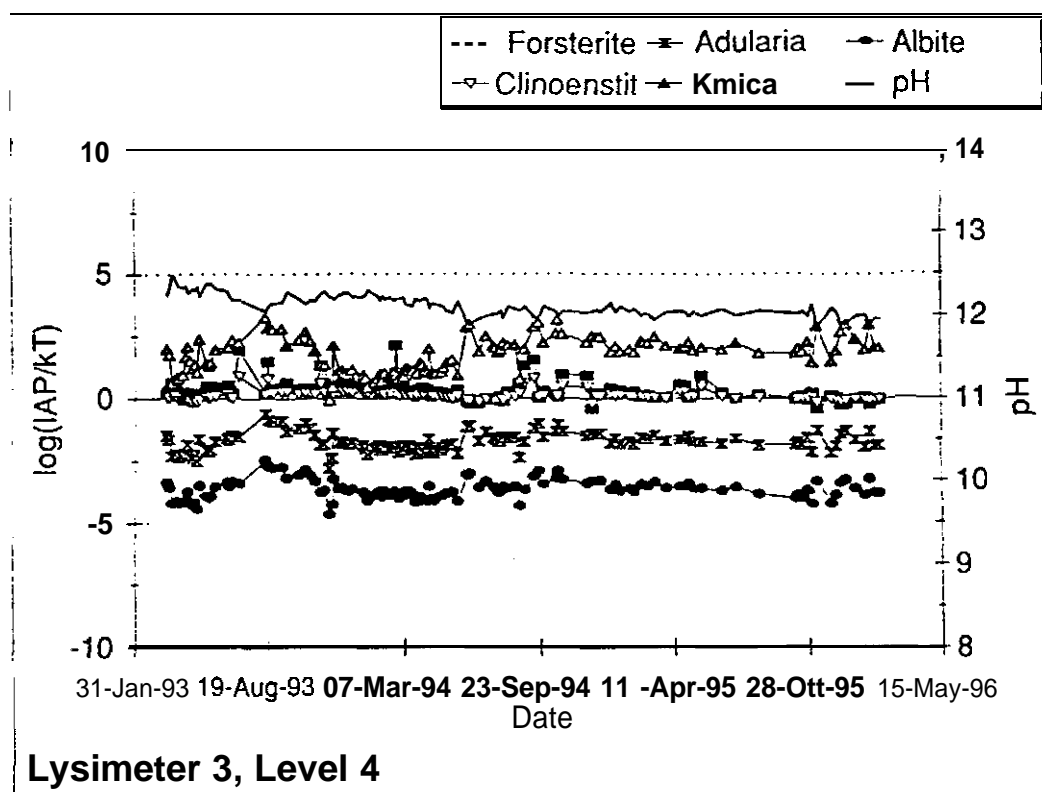
Figure 6-14. Forsterite, Adularia, Albite, Clinoenstatite, and Kmica variations by date and pH in Lysimeter 3, Level 4
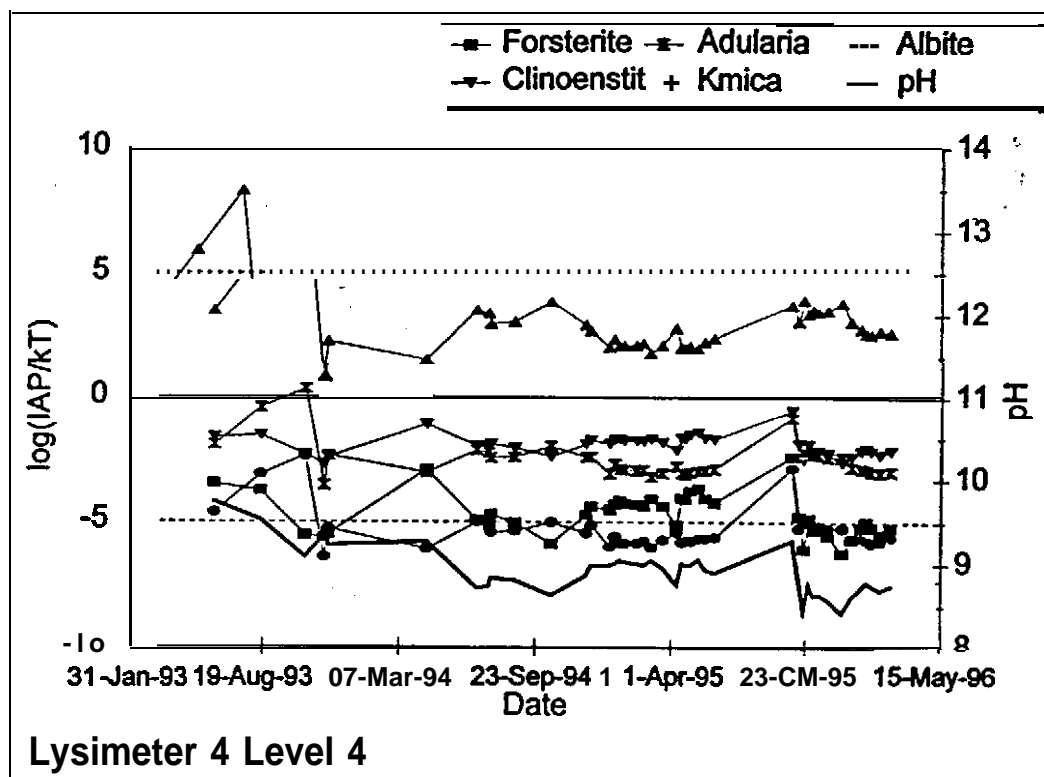
Lysimeter 4 Level 4

Figure 6-15. Forsterite, Adularia, Albite, Clinoenstatite, and Kmica variations by date and pH in Lysimeter 4, Level 4
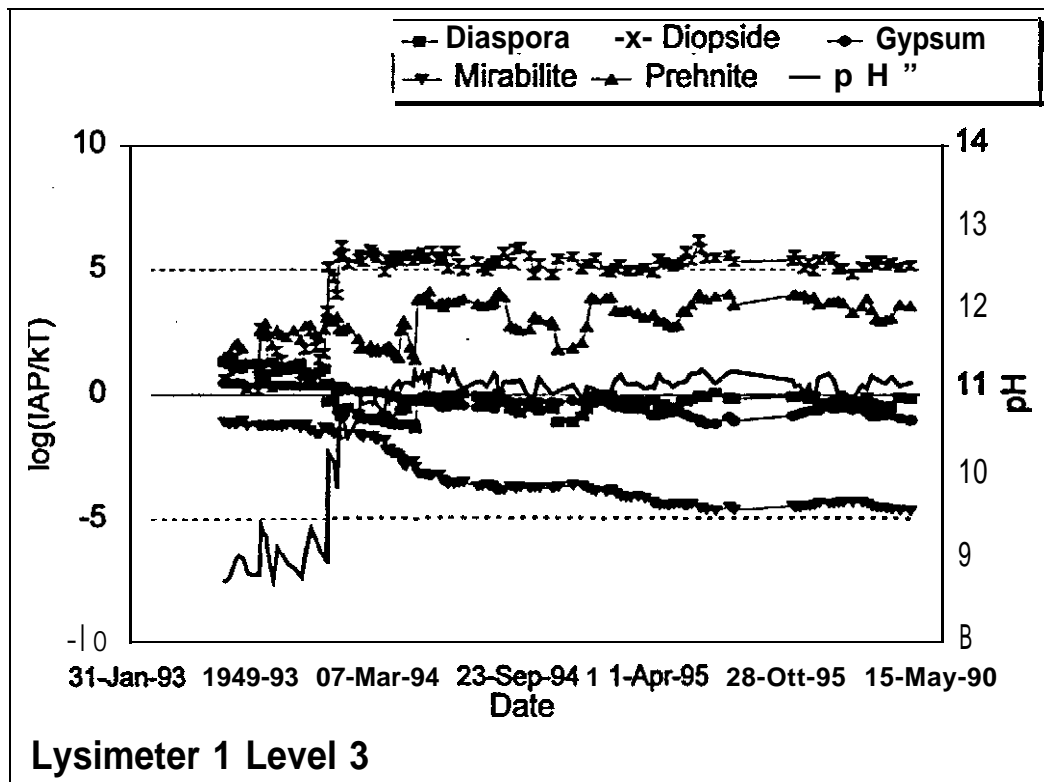
Lysimeter 1 Level 3

Figure 6-16. Diaspore, Diopside, Gypsum, Mirabilite, and Prehnite variations by date and pH in Lysimeter 1, Level 3

247
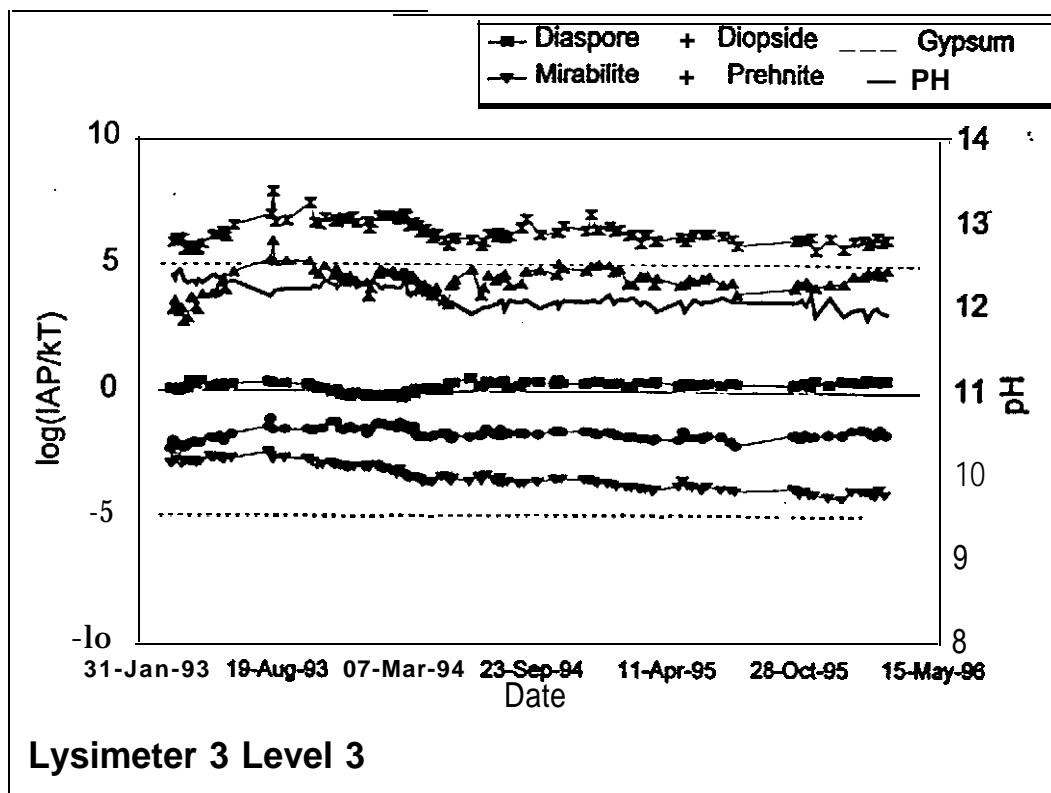
Lysimeter 3 Level 3

Figure 6-17. Diaspore, Diopside, Gypsum, Mirabilite, and Prehnite variations by date and pH in Lysimeter 3, Level 3
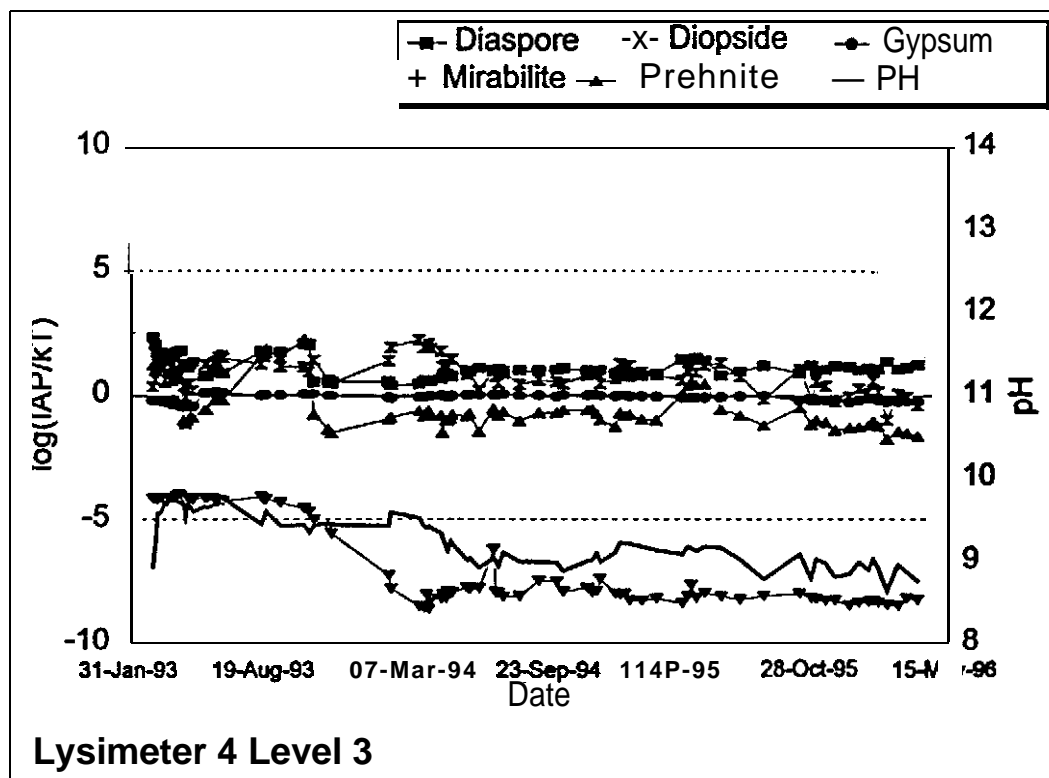
Lysimeter 4 Level 3

Figure 6-18. Diaspore, Diopside, Gypsum, Mirabilite, and Prehnite variations by date and pH in Lysimeter 4, Level 3

stages of fly ash leaching and also appears to be driven by leachate chemistry. Pyroxenes are not expected to form in any measurable amount nor exert any control on lysimeter conditions.

SO_4. Sulfate availability is controlled by the equilibrium dissolution of Anhydrite ($CaSO_4$) and Gypsum ($CaSO_4*2H_2O$). Anhydrite crystals are not common. Anhydrite converts slowly to Gypsum with a corresponding increase in volume giving long-term swell. It is also slightly more soluble than Gypsum. WATEQ indicates that both are uniformly at or slightly under saturation, with Anhydrite slightly less saturated, as expected. There are ranges of local environmental conditions which lead to more efficient congruent dissolution of the least favored form and simultaneous precipitation of the most favored. The primary SO_4 mineral in arid Coolside waste is Anhydrite. This will spontaneously hydrate to Gypsum with concomitant swell due to differing densities. Comparison of saturation indices of Gypsum and Anhydrite illustrate this. Note that the pH range maybe fairly narrow for the most efficient conversion, with Anhydrite in dissolution and Gypsum in formation in the case of the least compacted lysimeters (Figure 6-19). Excess or insufficient hydration and the resulting pH (as exhibited by the pH differences in the least (Figure 6-19) and most compacted lysimeters (Figure 6-20)) may control the pace of this congruent dissolution/precipitation phenomena. When both are thermodynamically likely to precipitate (log(IAP/kT) above O) or dissolve (log(IAP/kT) less than O) (Figure 6-20), equilibrium formation/dissolution will still result in conversion, but at a lower rate. The fly ash lysimeter (Figure 6-21), interestingly, indicates efficient conversion during the entire sampling period. In addition, as Gypsum remains at or near saturation independently of pH swings, it is probable that it will exert a significant control over the fly ash lysimeter chemistry. For comparison, the saturation indices of two corresponding Calcium Carbonate forms, Calcite and Aragonite, were included in Figures 6-19 through 6-21.
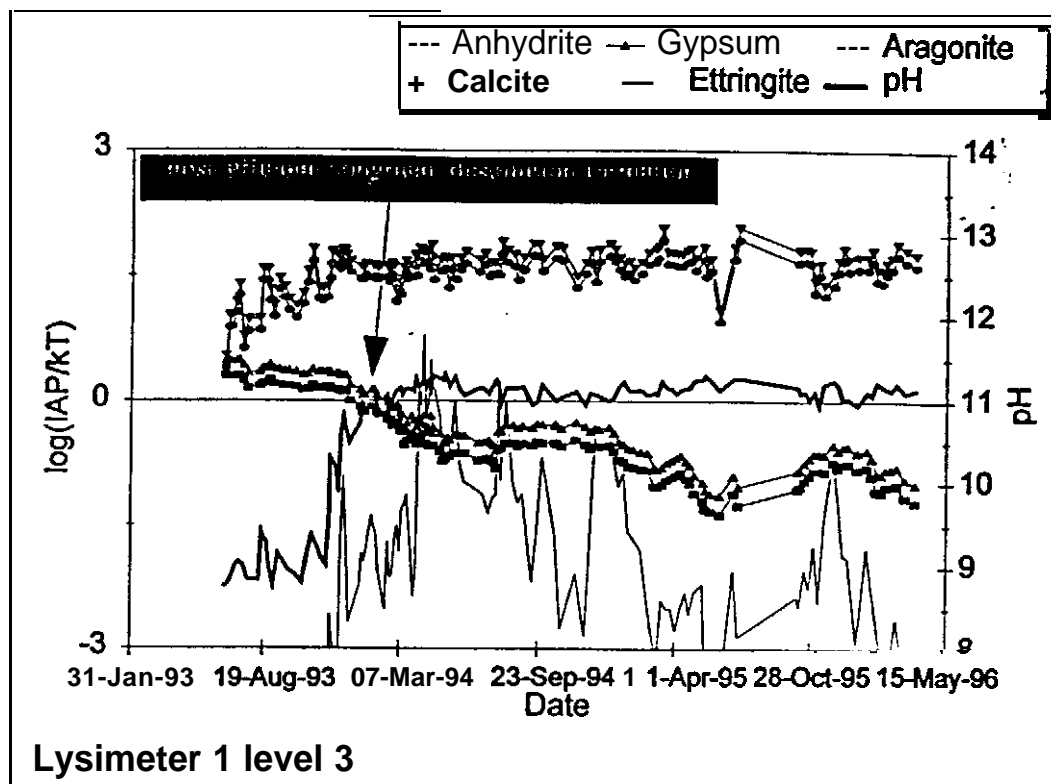
Lysimeter 1 level 3

Figure 6-19. Anhydrite, Gypsum, Aragonite, Calcite, and Ettringite variations by date and pH in Lysimeter 1, Level 3
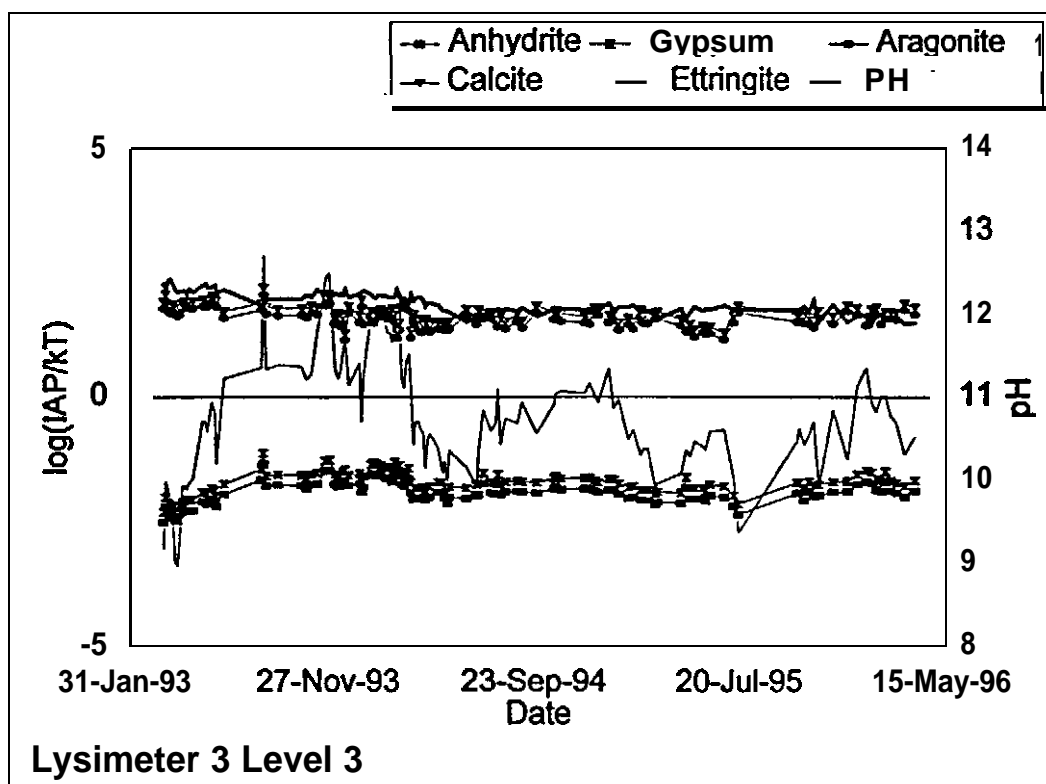
Lysimeter 3 Level 3

Figure 6-20. Anhydrite, Gypsum, Aragonite, Calcite, and Ettringite variations by date and pH in Lysimeter 3, Level 3
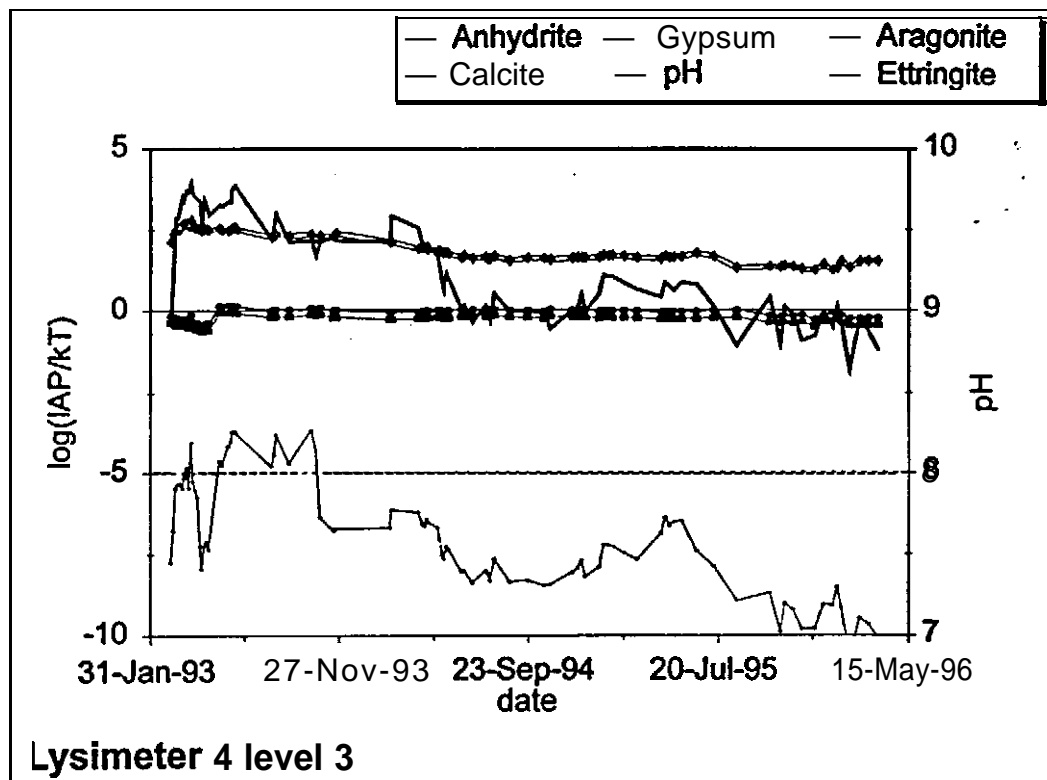
Figure 6-21. Anhydrite, Gypsum, Aragonite, Calcite, and Ettringite variations by date and pH in Lysimeter 4, Level 3
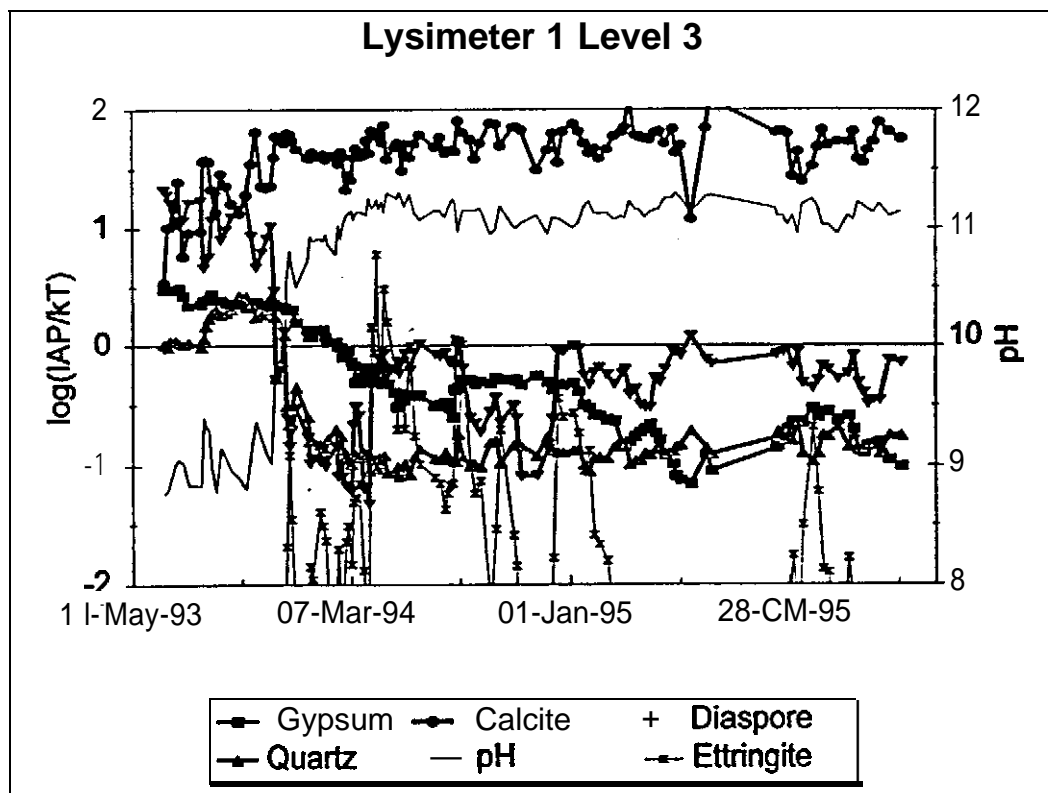
Figure 6-22. Gypsum, Calcite, Diaspore, Quartz, and Ettringite variations by date and pH in Lysimeter 1, Level 3

251

Another source of Sulfate is the dissolution of Epsomite ($MgSO_4*7H_2O$) (Figures 6-10 through 6-1 2). It is extremely soluble and is expected to contribute to the very high initial Sulfate concentration in the leachate but is not expected to be present or control chemistry except initially.

Ettringite. ($Ca_6Al_2(SO_4)_3(OH)_{12}*26H_2O$) is commonly found in $CaO-Al_2O_3-CaSO_4-H_2O$ systems on mineral surfaces and in pore spaces. It is partly decomposed by water to an alkali. Because of its implications in swell and indications of presence in XRD results, it was added to the program calculations. While in the proper pH range, Ettringite formation will be controlled by the availability of Calcium, Sulfate and Aluminum and by competition with other minerals for these ions. Comparison of volubility indices of Calcite and Gypsum show no obvious correlation (Figures 6-22 and 6-23). This is expected, as the solute contains an abundance of free Sulfate and Calcium, as well as OH". It was considered probable, therefore, that Ettringite formation is controlled by the availability of soluble Aluminum. Diaspore ($AlOOH$) is the basic oxide of Al_2O_3 formed by hydration. Further hydration in a high pH solution yields $Al(OH)_4^-$, the major ionic carrier of available Aluminum. However, comparison of Ettringite saturation and Diaspore (Figures 6-22 and 6-23) and $Al(OH)_4^-$ (Figure 6-24) also reveals no obvious correlation. Also, comparison of Ettringite (Figure 6-25) and Diaspore (Figure 6-26) for second laboratory column lysimeters 1 through 6, which comprise a wide range of packing density and CO_2 regimes, shows no correlation. It is concluded that the precipitation of Ettringite is a locally controlled phenomenon rather than a function of the bulk lysimeter/solute thermodynamics.

Other Sulfate minerals will be mentioned below.

Ca and Ma, Carbonates and Hydroxides. The interactions between these drive much
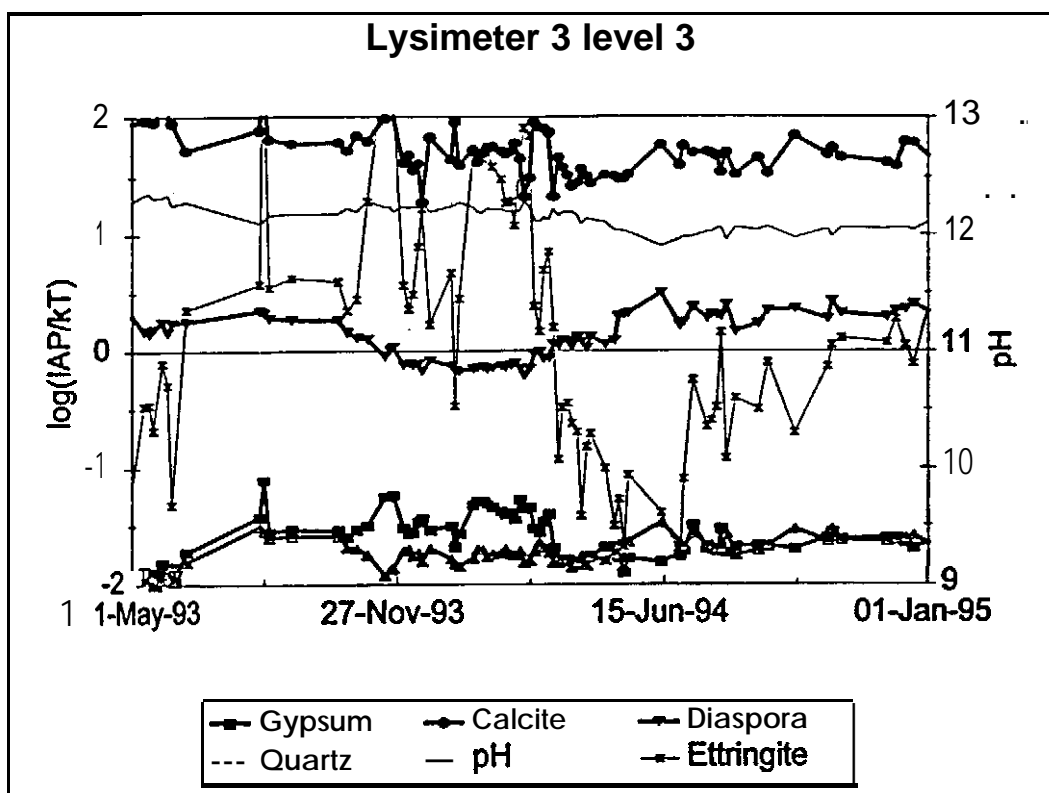
Figure 6-23. Gypsum, Calcite, Diaspore, Quartz, and Ettringite variations by date and pH in Lysimeter 3, Level 3
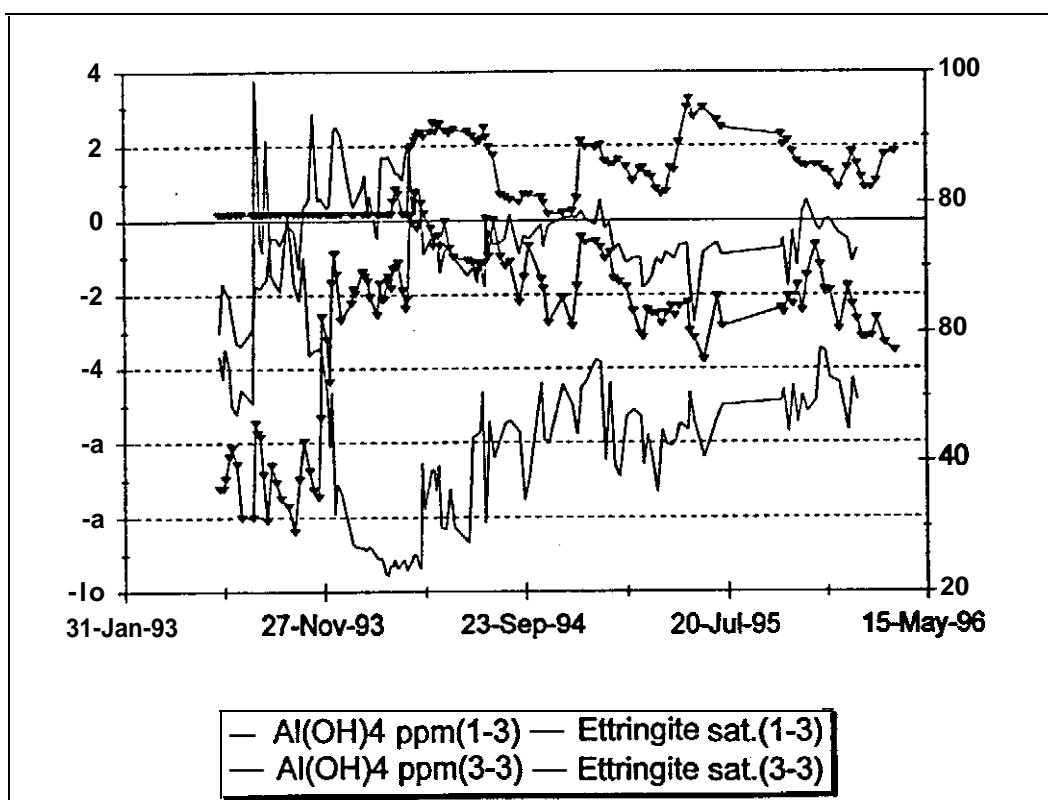
Figure 6-24. Comparison of Ettringite saturation and Al(OH)₄ variations over time

253
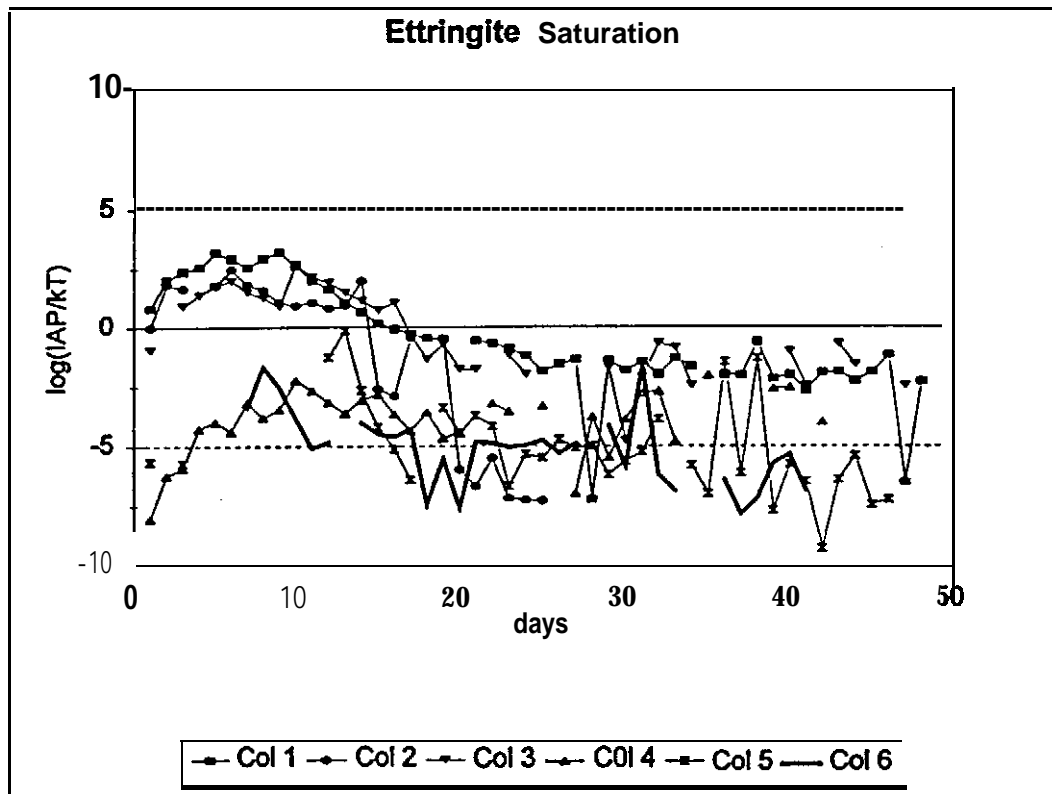
Figure 6-25. Ettringite saturation variations for second laboratory column lysimeters 1 through 6 over 50 days
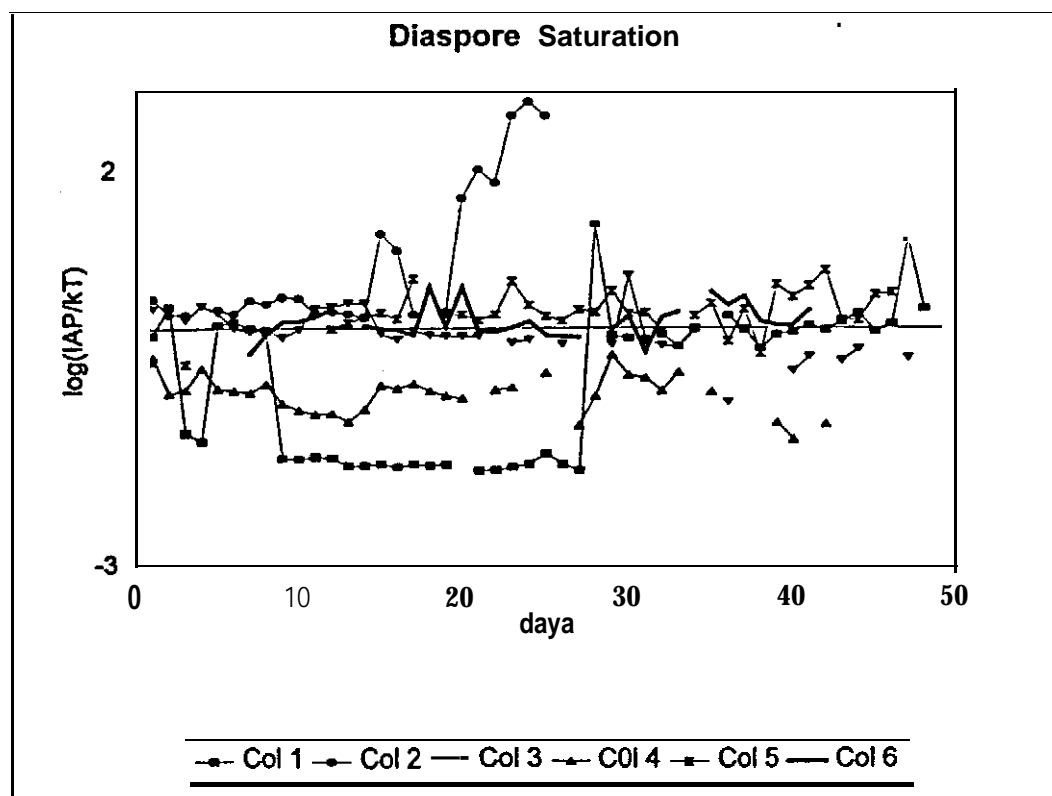
Figure 6-26. Diaspore saturation variations for second laboratory column lysimeters 1 through 6 over 50 days

254

of the leachate chemistry: Ca because of its abundance, Mg because of its interchangeability with Ca, when available, and Carbonates and Hydroxides because of their implication in pH. Possible major mineral forms which WATEQ indicates are often or always supersaturated are Calcite ($CaCO_3$), Aragonite ($CaCO_3$), Dolomite ($CaMg(CO_3)_2$), Brucite ($Mg(OH)_2$), Hydromagnesite ($Mg_5(CO_3)_4(OH)_2*4H_2O$), Magnesite ($MgCO_3$), dimorphic $MgCO_3$, and Huntite ($Mg_3Ca(CO_3)_4$). Periclase (MgO) hydrates to Brucite, which may further alter to Magnesite and Hydromagnesite. A precipitate of the hydrate Nesquehonite($MgCO_3*3H_2O$), whose slight volubility is enhanced by the presence of CO_2, NaCl, and Na_2SO_4, may also be formed at STP. To determine which forms are likely at leachate conditions, an equilibrium diagram which uses log[(activity Ca)/(activity Mg)] vs log(pCO_2) to predict equilibrium conditions was plotted over the leachate collection periods (Figures 6-27 and 6-28). It was found that the Calcitic domain is favored for Coolside lysimeters, with brief movements into Brucite, Aragonite or Dolomitic regimes. For fly ashes, with a lower Ca/Mg ratio, most of the collection period remains in the Dolomitic regime.

The conditions under which Dolomite ($CaMg(CO_3)_2$) is precipitated in nature are not well understood. Attempts to precipitate a Dolomite phase from an oversaturated solution have not been successful. It is possible, however, that Dolomite might be formed under conditions of oversaturation and high ionic strength found in Coolside leachate but this is not confirmed. It is more likely that Dolomite is present originally due to the Coolside Sulfur control regime. Artinite ($Mg_2CO_3(OH)_2*3H_2O$) is significantly favored at pH above about 9.5 in the Coolside lysimeters (Figures 6-29 and 6-30) and briefly favored at the beginning of fly ash lysimeter sampling (Figure 6-31). It is one of the few mineral forms which may be detectable by XRD in the Coolside samples. Forsterite (Mg_2SiO_4) formation is indicated in minor amounts only in the most packed lysimeter (Figures 6-13 through 6-15). Sepiolite ($Mg_4Si_6O_{15}(OH)_2*6H_2O$) only rarely becomes supersaturated and should rarely form (Figures 6-10 through 6-12). The
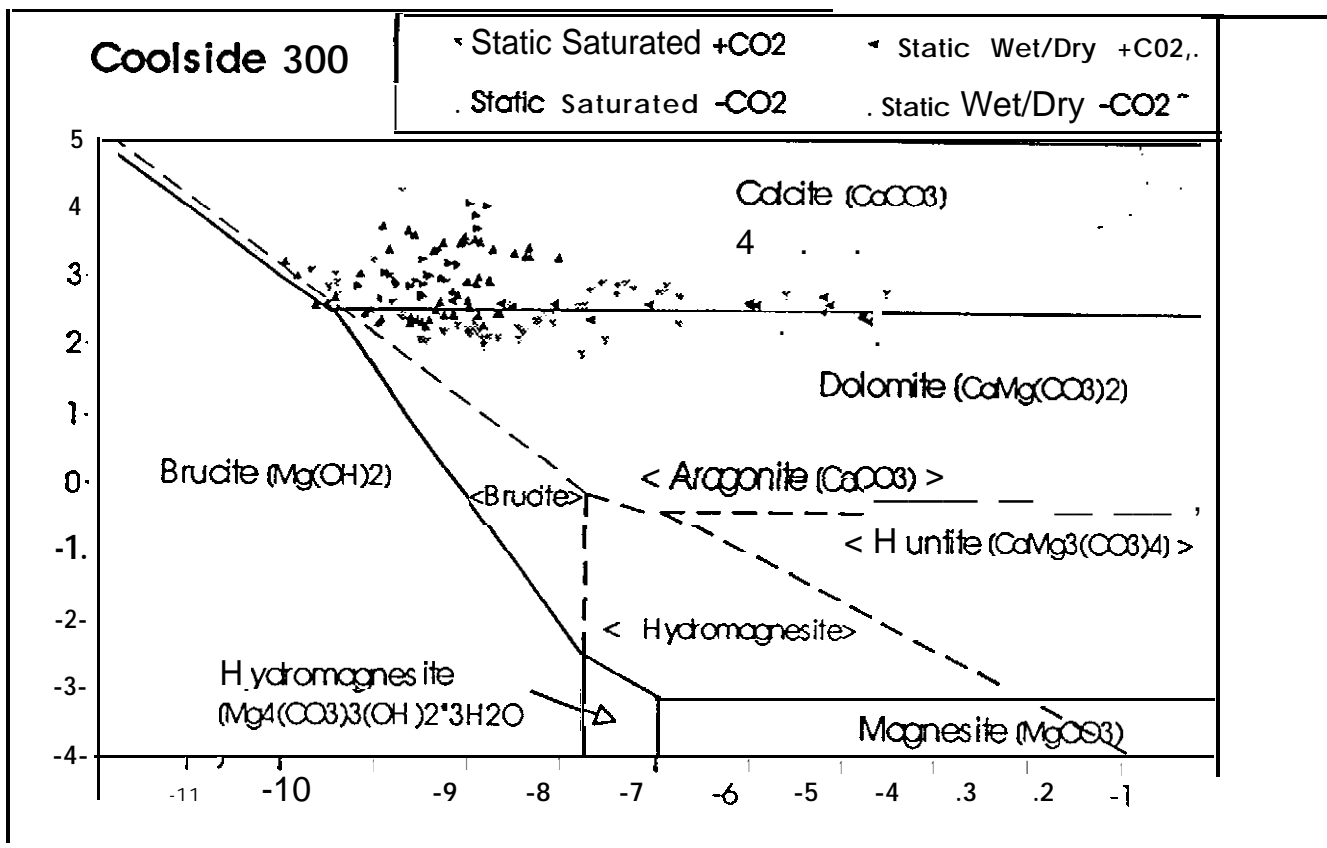
Figure 6-27. Representative Coolside equilibrium - log[(Ca activity)/(Mg activity)] vs log(pCO₂)
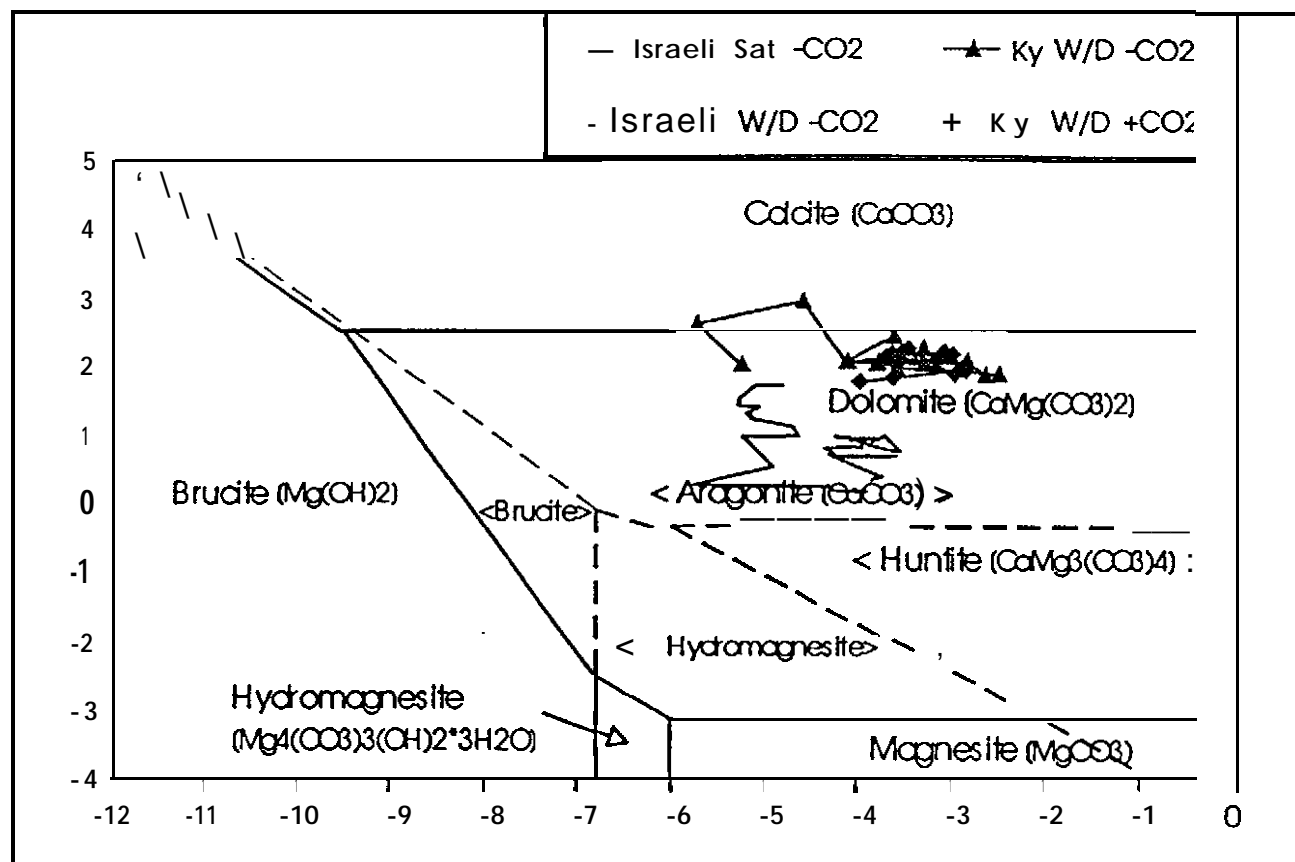
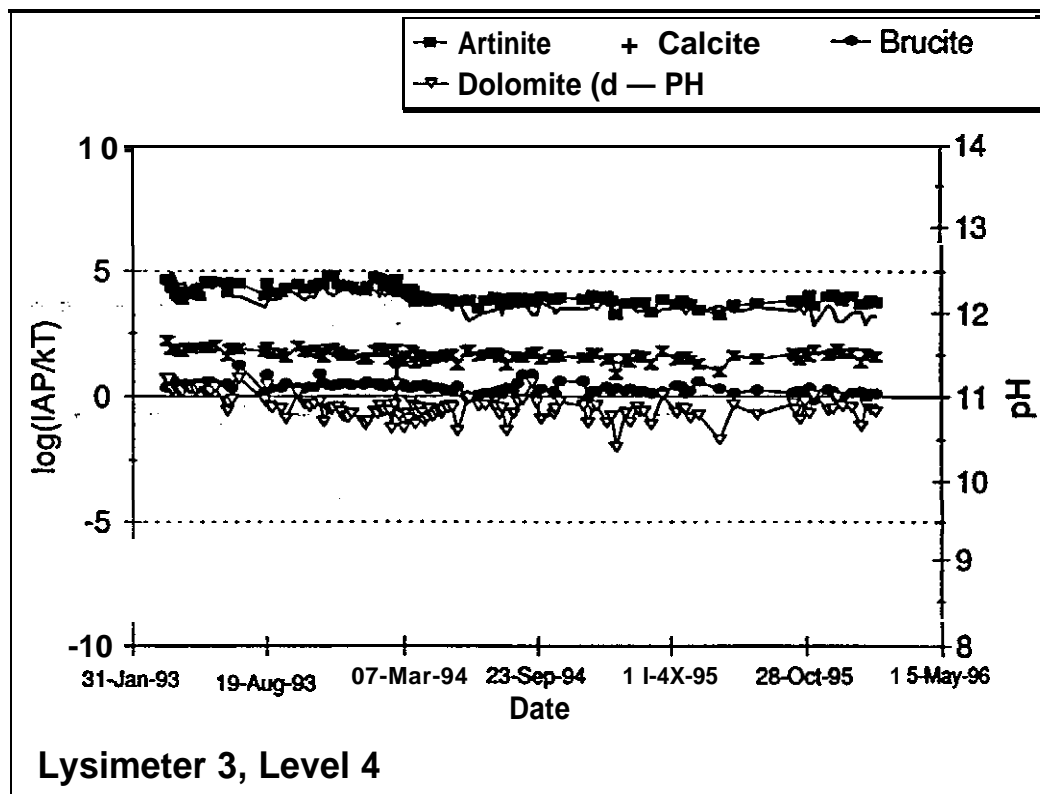Figure 6-28. Fly ash equilibrium diagram - log[(Ca activity)/(Mg activity)] vs pCO₂
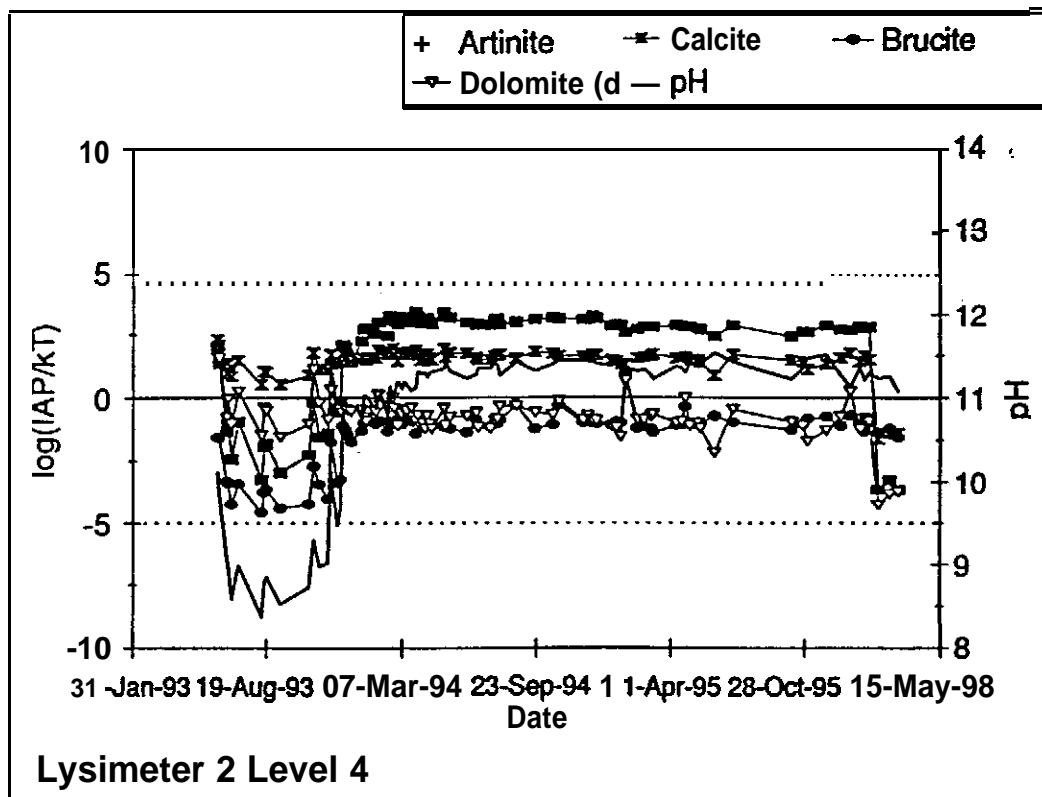
Figure **6-29.** Artinite, Calcite, Brucite, and Dolomite variations by date and pH in Lysimeter 2, Level 4

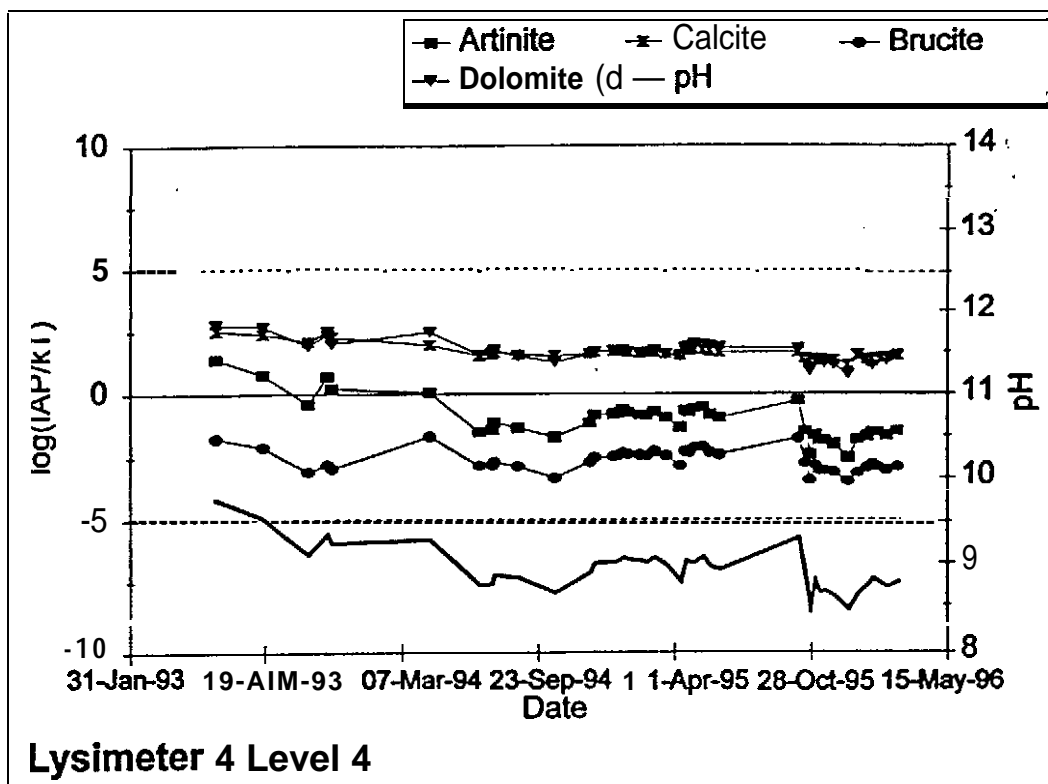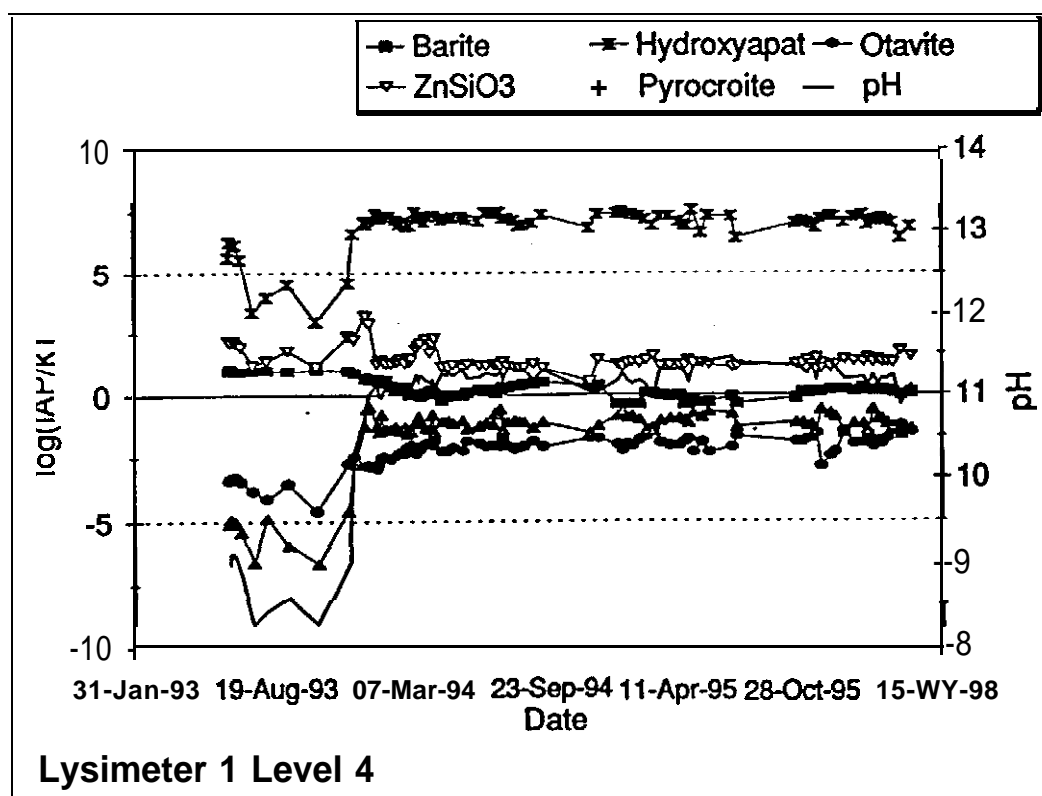Figure **6-30.** Artinite, Calcite, Brucite, and Dolomite variations by date and pH in Lysimeter 3, Level 4

257

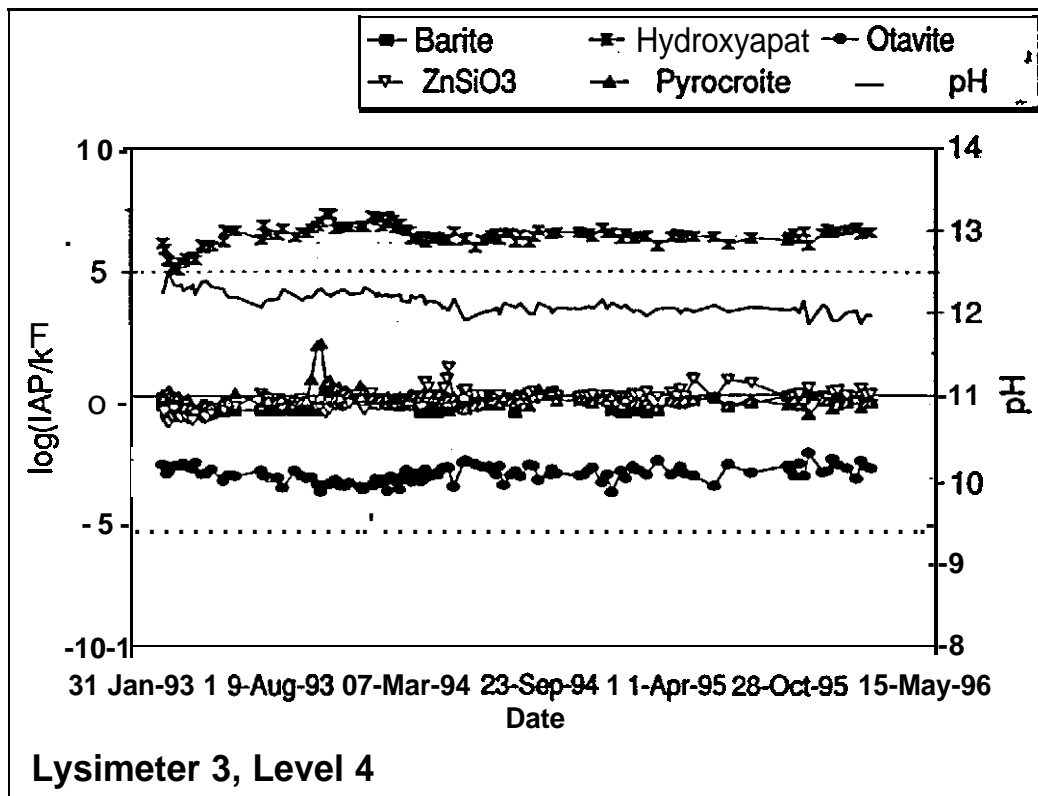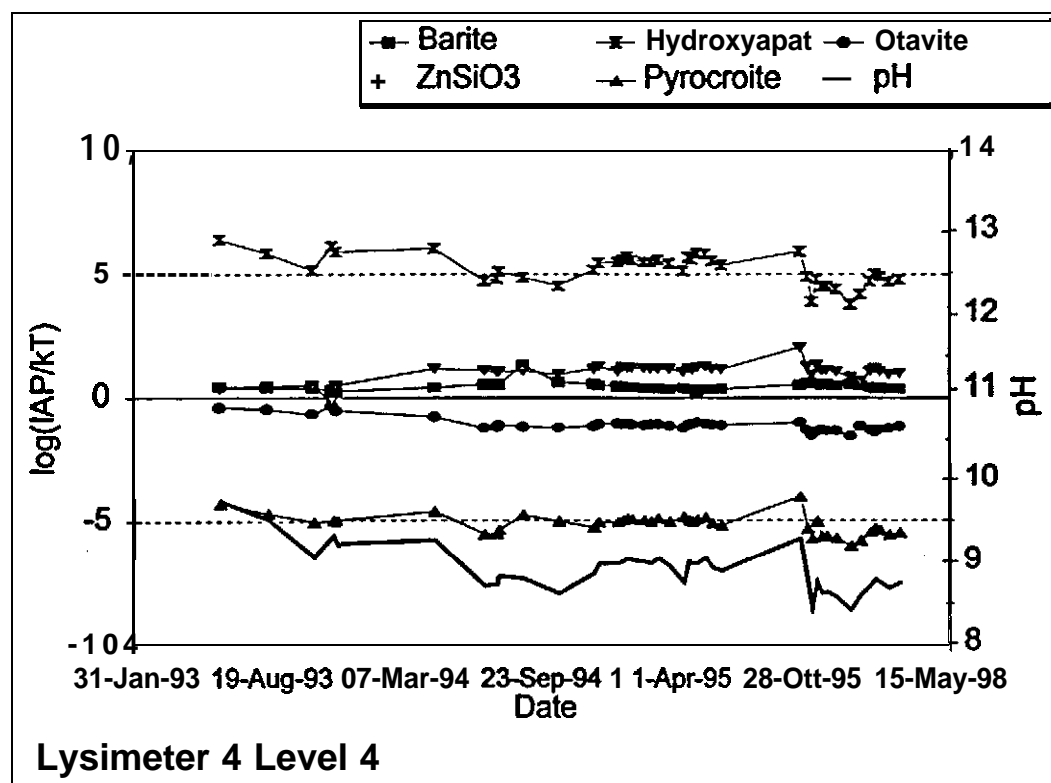Figure 6-31. Artinite, Calcite, Brucite, and Dolomite variations by date and pH in Lysimeter 4, Level 4

Figure 6-32. Barite, Hydroxylapatite, Otavite, $ZnSiO_3$, and Pyrocroite variations by date and pH in Lysimeter 1, Level 4

formation of Sepiolite would have been significant as its precipitation lowers pH. Talc $(Mg_3Si_4O_{10}(OH)_2)$, formed in high ionic strength brines at low temperature, is indicated to be supersaturated, but should not be formed, as Sepiolite tends to precipitate preferentially and is not found to form significantly. Brucite $(Mg(OH)_2)$ shows a slight tendency to form only in the most packed lysimeter (Figures 6-29 through 6-31). Two other Calcium-Aluminum silicates, Prehnite $(Ca_2Al_2Si_3O_{10}(OH)_2)$ (Figures 6-16 through 6-1 8) and Laumontite $(CaAl_2Si_4O_{12}{}^*4H_2O)$ (Figures 6-1 through 6-3), show occasional supersaturation but neither their formation nor affect on leachate chemistry should be significant.

Minor Species Carriers

Mineral carriers of minor ions have little effect on leachate chemistry but are followed to predict which might be dominant at points in the leachate cycle because the ions are of general interest. It is doubtful that any of these could be confirmed by XRD as the amounts would be very small. In general, the oxide, hydroxide, carbonate and silicate forms are indicated at appropriate times in the collection cycle.

Ba. Barite $(BaSO_4)$ is relatively insoluble, but becomes more so in a salt solution. WATEQ indicates that it is sometimes slightly supersaturated at lower pH (Figures *6-32* through 6-34). Witherite $(BaCO_3)$ is indicated to be supersaturated, but less often.

PO_4. Ca-Hydroxylapatite $(Ca_5(PO_4)_3OH)$ is the major phosphate carrier. WATEQ indicates a fairly significant degree of supersaturation (Figures *6-32* through 6-34). If Fluorine were present, the Fluor-apatite would be thermodynamically preferred. It forms a solid solution with Ca>Pb>Na>K.

Pb. Litharge/Massicot (PbO dimorphs) may hydrate and form minor amounts of $Pb(OH)_2$ under high pH conditions (Figures 6-35 through 6-38). Other Pb minerals

Figure 6-33. Barite, Hydroxylapatite, Otavite, $ZnSiO_3$, and Pyrocroite variations by date and pH in Lysimeter 3, Level 4

Figure 6-34. Barite, Hydroxylapatite, Otavite, $ZnSiO_3$, and Pyrocroite variations by date and pH in Lysimeter 4, Level 4
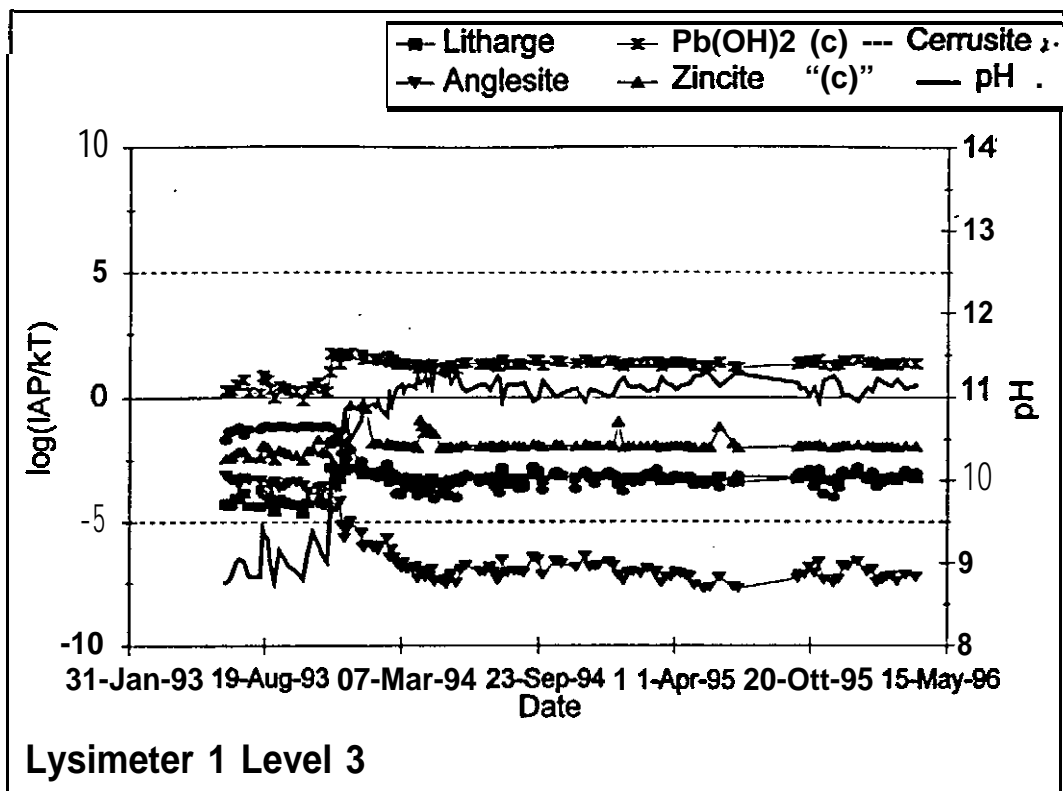
260

Figure 6-35. Litharge, $Pb(OH)_2$, Cerrusite, Anglesite, and Zincite variations by date and pH in Lysimeter 1, Level 3
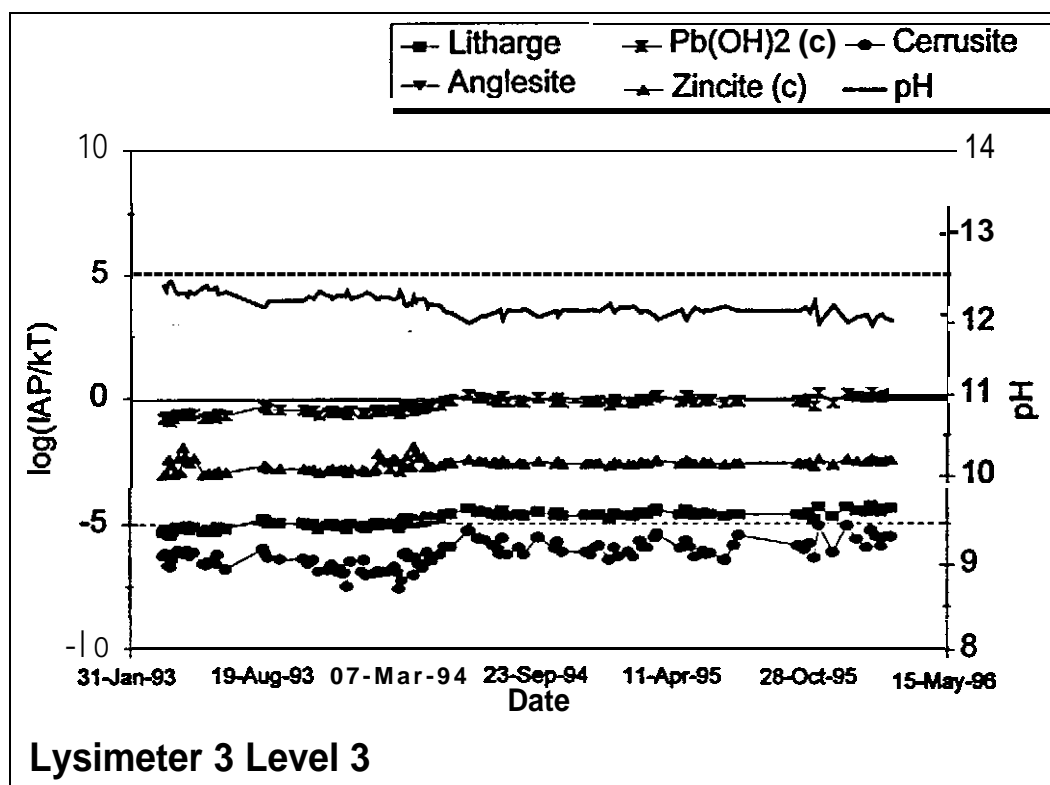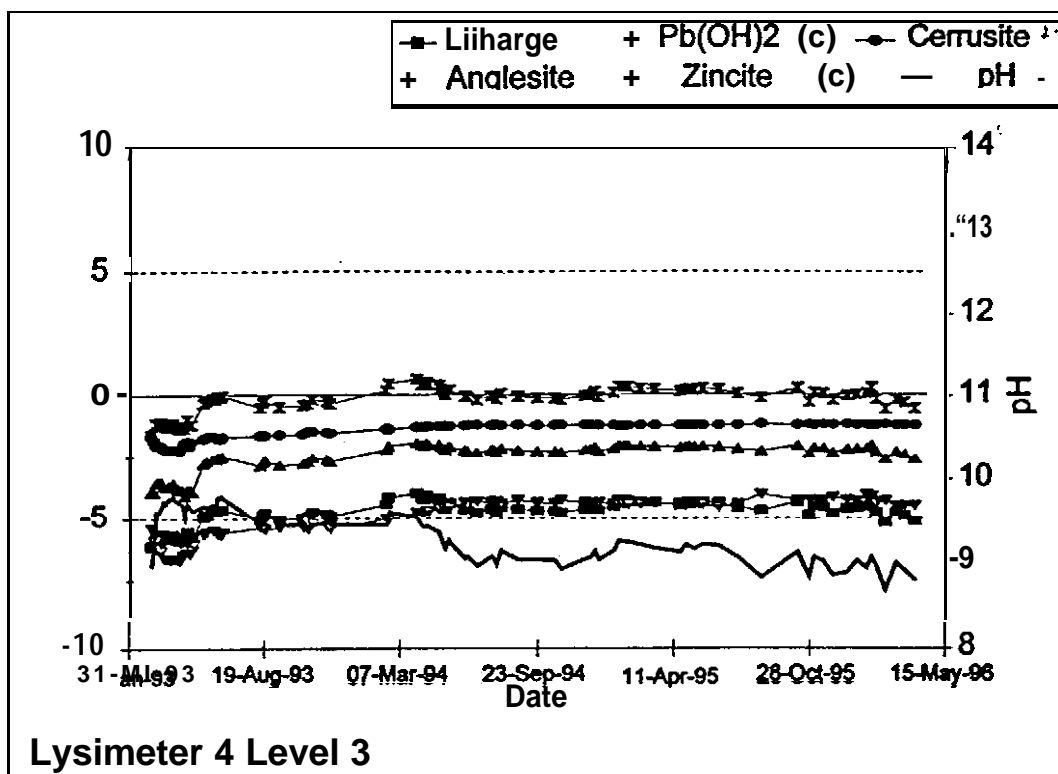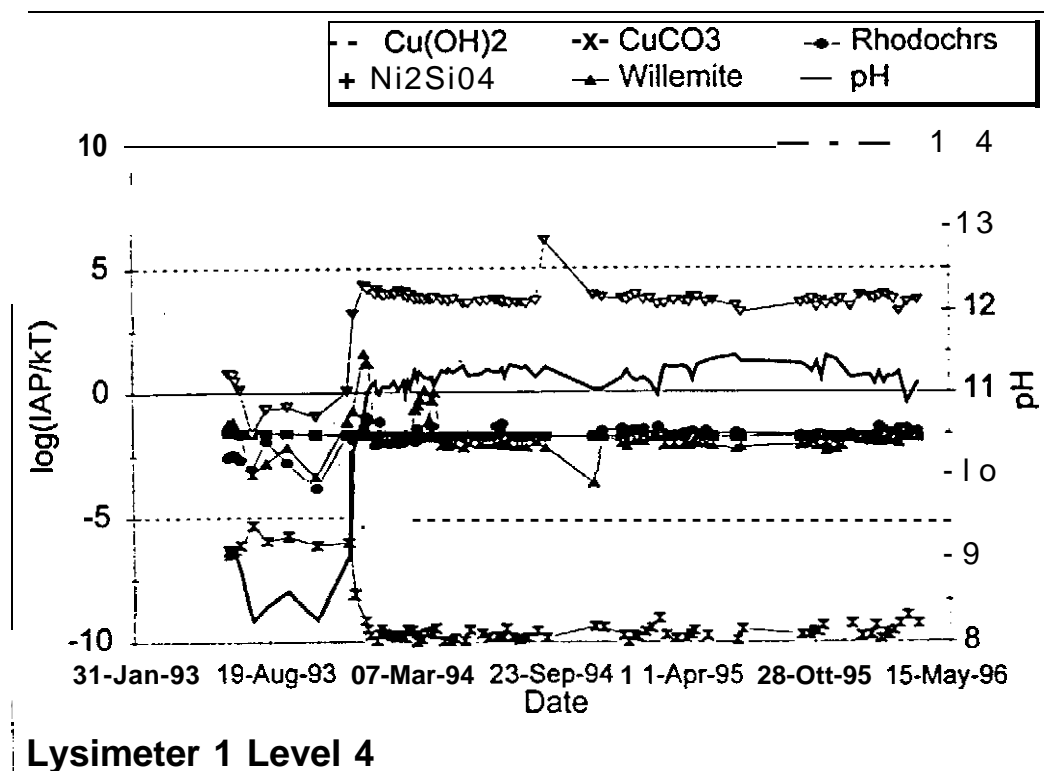

Figure 6-36. Litharge, $Pb(OH)_2$, Cerrusite, Anglesite, and Zincite variations by date and pH in Lysimeter 3, Level 3

Figure 6-37. Litharge, Pb(OH)$_2$, Cerrusite, Anglesite, and Zincite variations by date **and** pH in Lysimeter 4, Level 3

Figure 6-38. Cu(OH)$_2$, CuCO$_3$, Rhodocrosite, Ni$_2$SiO$_4$, and Willemite variations by date and pH in Lysimeter 1, Level 4

possibly formed include Cerrusite ($PbCO_3$), Anglesite ($PbSO_4$) (Figures 6-35 through 6-38). Larnakite ($Pb_2(SO_4)O$), and Laurionite ($Pb(OH)Cl$) are indicated as unlikely to form. Pb compounds, however, are not known for volubility.

_Cu_. Copper is probably initially available as Tenorite (CuO) and slowly hydrated to free copper and hydroxide, as $Cu(OH)_2$ remains undersaturated (Figures 6-38 through 6-40). Malachite ($Cu_2(CO_3)(OH)_2$)(crystals rare, but slightly water-CO_2 soluble), $CuCO_3$ (Figures 6-38 through 6-41) and Atacamite ($Cu_2(OH)_3Cl$)(another of the few Cl minerals; alters to malachite; formed by oxidation of other Cu minerals, especially in arid saline environments) are indicated as unlikely to form. Tsumebite ($CuPb_2(PO_4)(SO_4)(OH)$) is unlikely to be found even though supersaturation is indicated by WATEQ.

_Cd_. Monteponite (CdO), $Cd(OH)_2$, $Cd(OH)Cl$, $CdSiO_3$ and Otavite ($CdCO_3$) (Figures 6-32 through 6-34) exhibit varying degrees of supersaturation. Otavite is supersaturated only in the fly ash system. In the Coolside leaching, the higher Ca/Mg ratio leads to preferential Calcite formation.

_Zn_. Zincite (ZnO) maybe present initially. It is indicated to remain in dissolution in all lysimeters (Figures 6-35 through 6-37). $Zn(OH)_2$ and $ZnCO_3 \cdot H_2O$ may form under appropriate pH conditions. $Zn_2(OH)_3Cl$ is unlikely. $ZnSiO_3$ formation may take place in the least compacted lysimeters and in fly ash lysimeters (Figures 6-32 through 6-34). Willemite (Zn_2SiO_4) is unlikely to form (Figures 6-38 through 6-40).

_Mn_. Pyrocroite ($Mn(OH)_2$) (Figures 6-32 through 6-34) and Rhodochrisite ($MnCO_3$) (Figures 6-38 through 6-40), as well as the oxide form, Pyrolusite, generally remain undersaturated, indicating that Mn from oxide dissolution should primarily contribute to solute ionic strength.
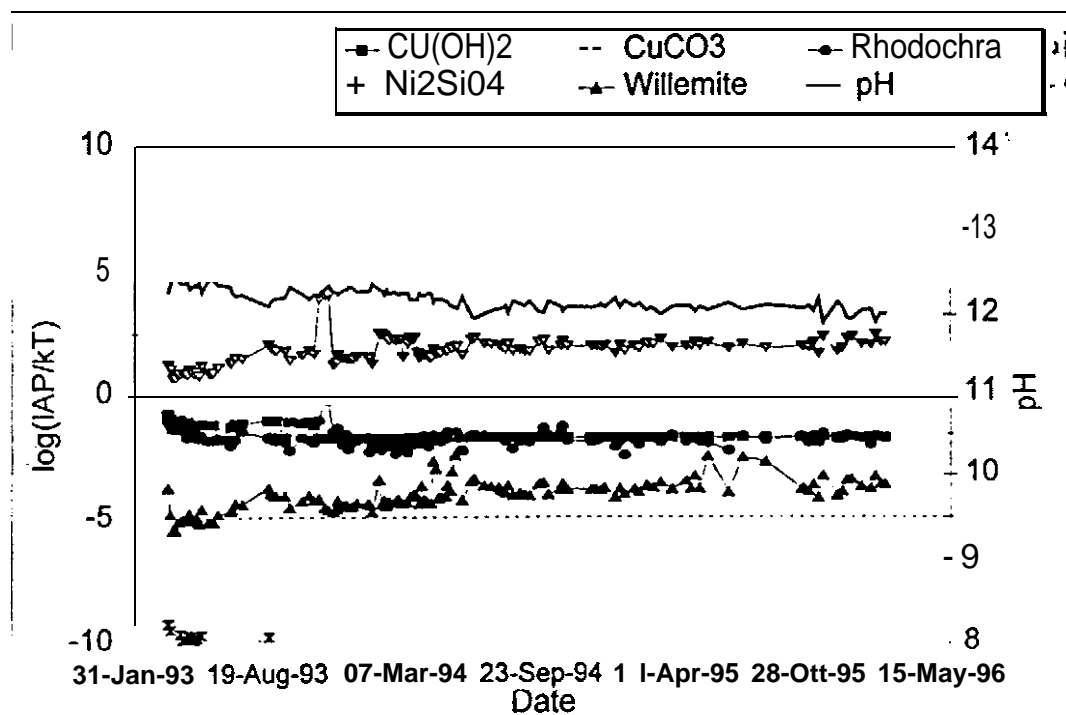
, **Lysimeter** 3, Level 4

Figure 6-39. Cu(OH)$_2$, CuCO$_3$, Rhodocrosite, Ni$_2$SiO$_4$, and Willemite variations by date and pH in Lysimeter 3, Level 4
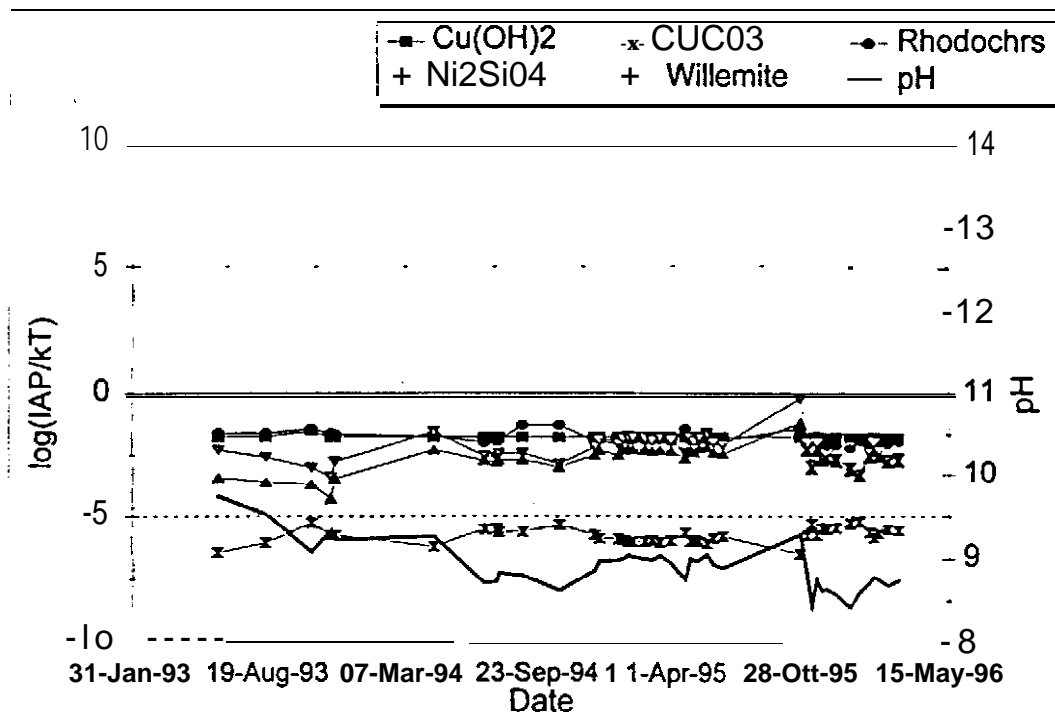
Lysimeter 4 Level 4

Figure 6-40. Cu(OH)$_2$, CuCO$_3$, Rhodocrosite, Ni$_2$SiO$_4$, and Willemite variations by date and pH in Lysimeter 4, Level 4

264

Ni. Nickel is initially present primarily as Bunsenite (NiO). $Ni(OH)_2$ (Figures 6-10 through 6-1 2) and Ni_2SiO_4 (Figures 6-38 through 6-40) may form under higher pH conditions.

Fe. There is no analytical information on relative amounts of divalent and trivalent Fe. Goethite ($FeOOH$), the trivalent analogue to Diaspore ($AlOOH$), does not show saturation. Also, no divalent Fe mineral approaches saturation, so it is probable that Hematite/Maghemite (Fe_2O_3) and Magnetite ($FeFe_2O_4$) are nearly insoluble.

investigation of Initial PH Dip, Field Lysimeters 1 and 2

The ionic strength of the solute appears to have a great deal of influence on the pH behavior. A comparison of ionic strength over time for the field lysimeters shows that the lysimeters with anomolous pH behavior also have the highest initial ionic strength (Figure 6-41). The three Coolside lysimeters approach the same ionic strength and about the same pH overtime but the two least compacted exhibit the pH lowering during the high ionic strength period. Additional graphic illustration of the relationship of pH and ionic strength (Figure 6-42) shows a transition in behavior between ionic strengths of about 0.5 to 1 for the field lysimeters. The three data sets corresponding to the fly ash lysimeter, the most compacted lysimeter, and the group representing the two least compacted lysimeters can easily be seen.

Ionic strength has a direct effect on the volubility of mineral species, as discussed in the section on caveats to calculation. As an example, the volubility of Calcite ($CaCO_3$) increases by a factor of three as ionic strength increases from 0.5 to 2.0. Another effect of high ionic strength is the reduction in activity of H_2O because of polar bonding with species in solution. That portion of the water is no longer available as a solvent.
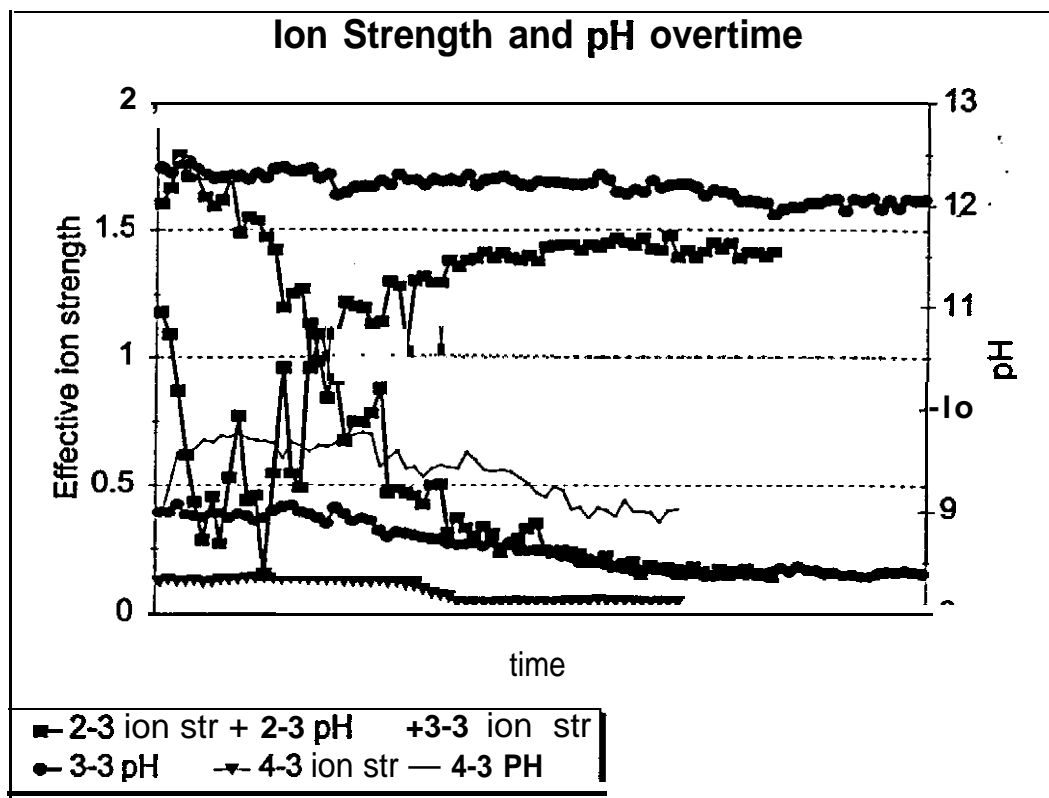
265

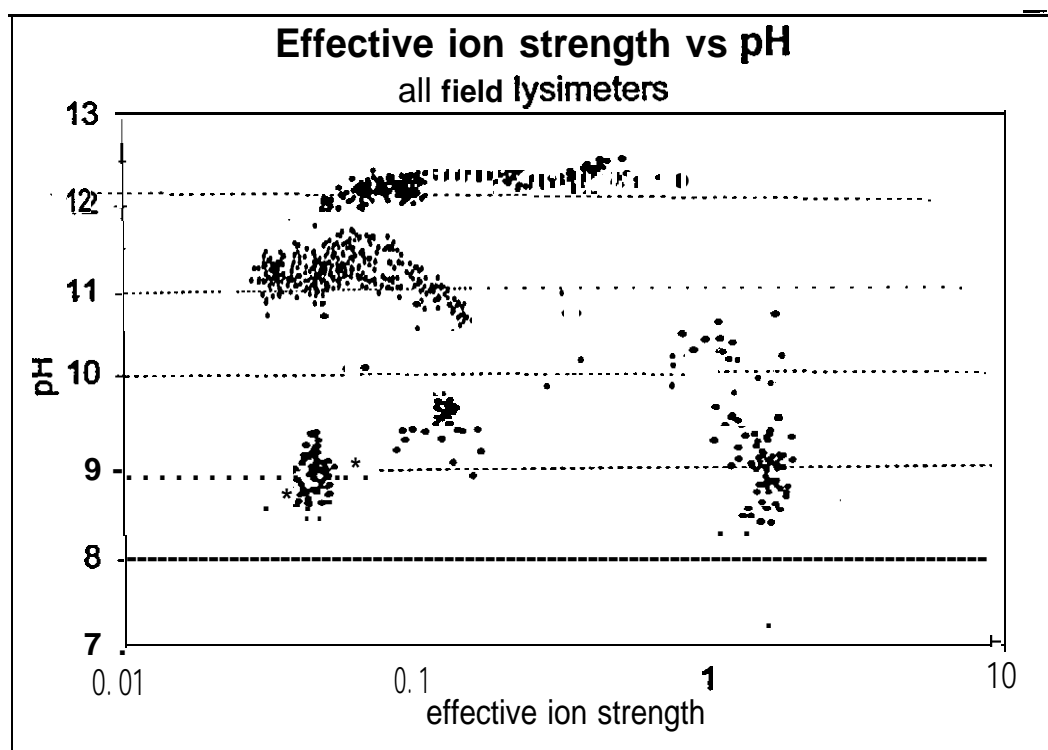Figure **6-41.** Ion strength variations and pH variations over time

Figure 6-42. Effective ion strength vs pH in all field lysimeters

266

The effect is evident when comparing the computed activity of H_2O with observed pH (Figure 6-43). The initial lowering of pH does not appear to be related to leachate water carbonate loading (Figure 6-44, no loading for column 10 through high loading for column 12). The effect is content related. Pilot plant run 2 material (Figure 6-44) shows no dip. Coolside 3 laboratory column (Figure 6-45) shows a slight, but measurable dip. The field lysimeters (Figure 6-41) show a significant dip. The lack of observed dip in the column lysimeters could also be related to column size. It is concluded that the initial high ionic strength plays a major role in the initial lowering of pH, similar to the observed high buffering capacity of sea water, which has an ionic strength of approximately 1.0. This capacity is enhanced by the diversity of ionic constituents available for the formation of neutral aqueous species and polar bonding, as illustrated by plots of major ion elution for the least compacted (Figure 6-46) and most compacted (Figure 6-47) field lysimeters.

It is known that Calcium and Sodium Oxide readily absorb CO_2 from the atmosphere to form Carbonates. WATEQ also predicts a significant carbonate-bicarbonate buffering from both the Ca and Na forms during the low pH transient (Figures 6-48 through 6-49). It is proposed that the pH dip is flow related. In the least compacted lysimeters, higher flow results in increased ionic strength. The higher ionic strength simultaneously increases the solubility of the Calcium and Sodium Carbonates, resulting in significant carbonate-bicarbonate buffering, and reduces the activity of water, thereby lowering the availability for oxide hydration. This results in an initial lower PH. As the major ions are eluted (Figure 6-46), the ionic strength decreases and oxide hydration returns pH to high levels. At lower flows in the most compacted lysimeter, the ionic strength is reduced, favoring oxide hydration over carbonate dissolution.
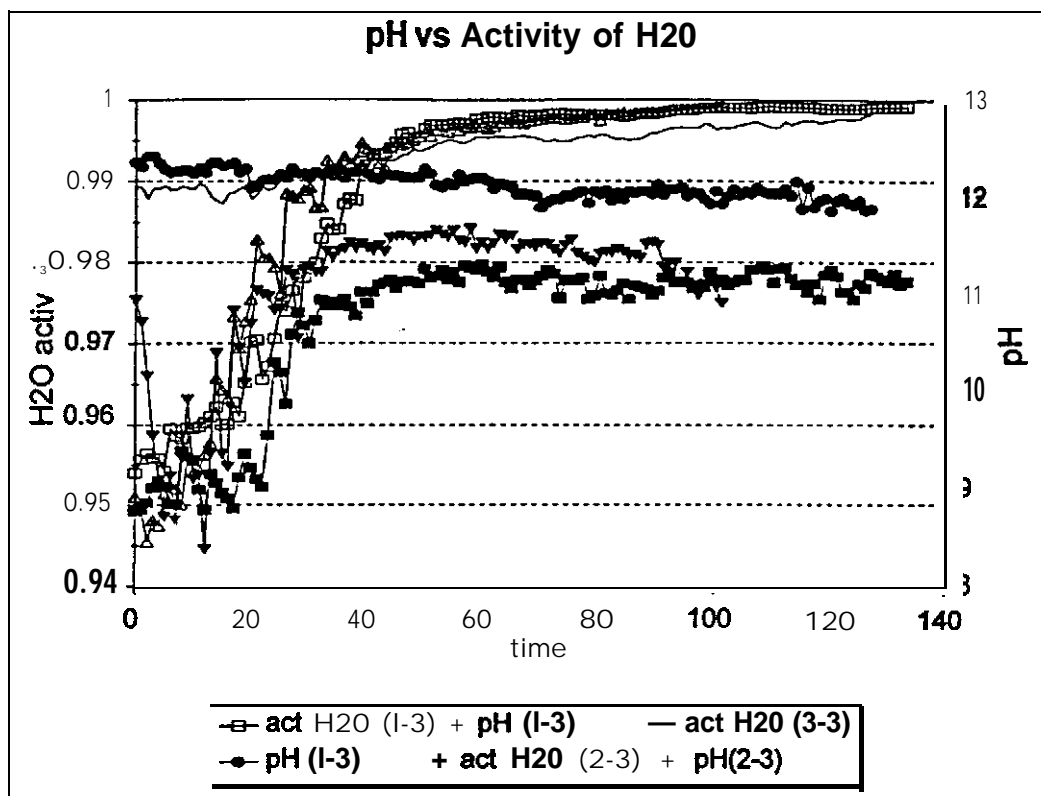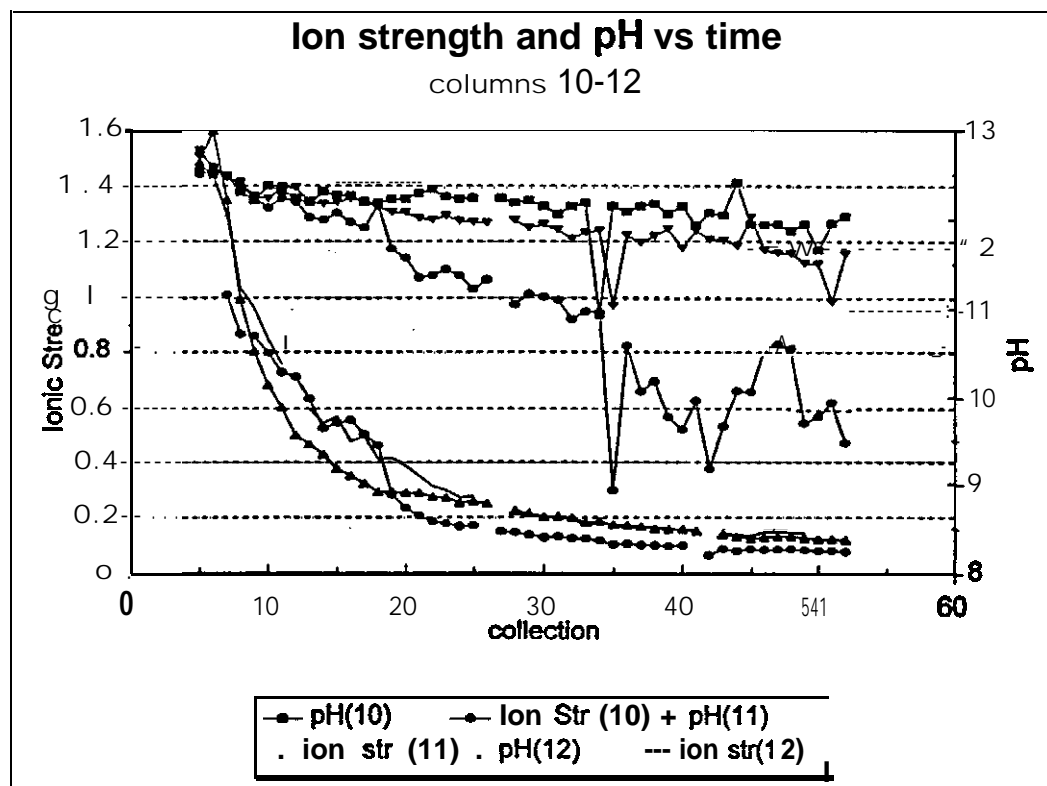
Figure 6-43. pH vs activity of H_2O over time

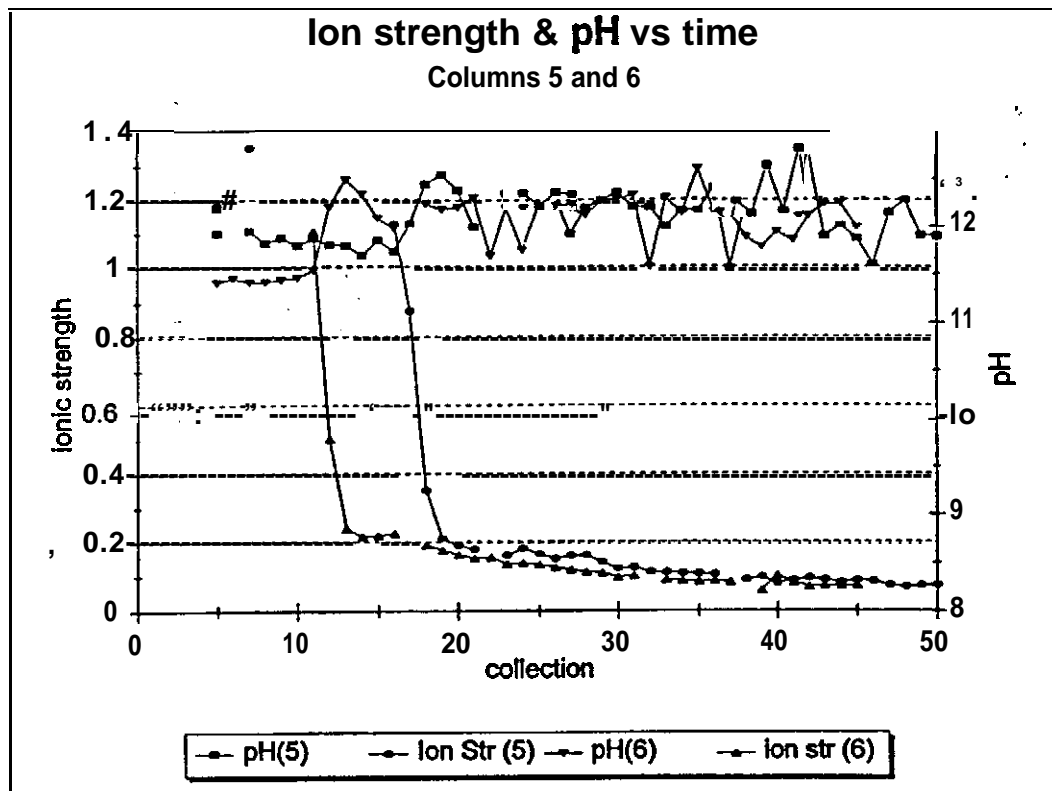**Figure** 6-44. Ion strength and pH vs time in columns 10-12

268

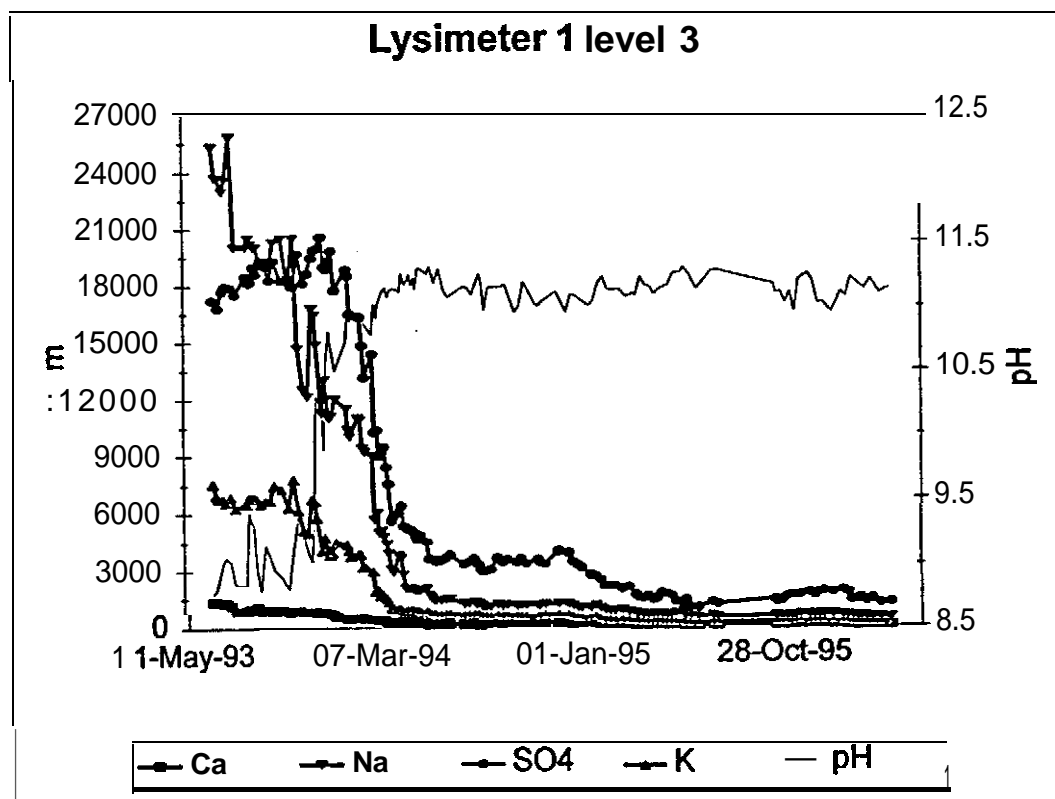**Figure** 6-45. **Ion strength and pH vs time in columns** 5 and 6

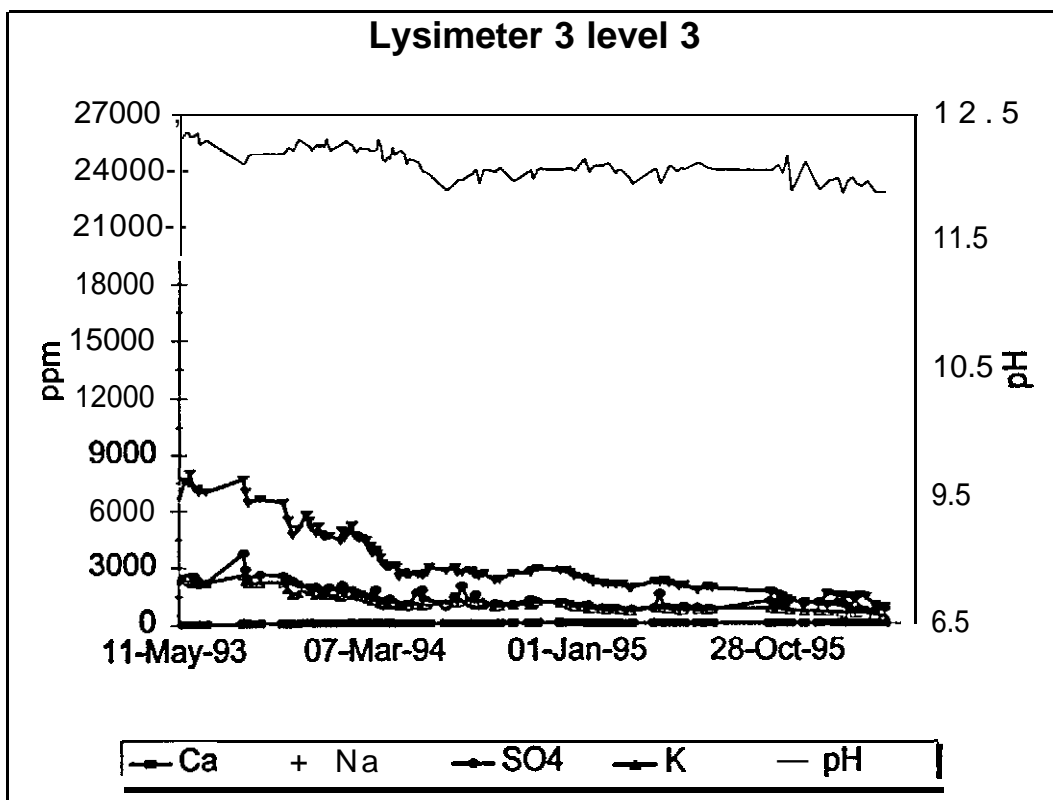**Figure** 6-46. **Ca,** Na, SO₄, and K variations by date and PH in Lysimeter 1, Level 3

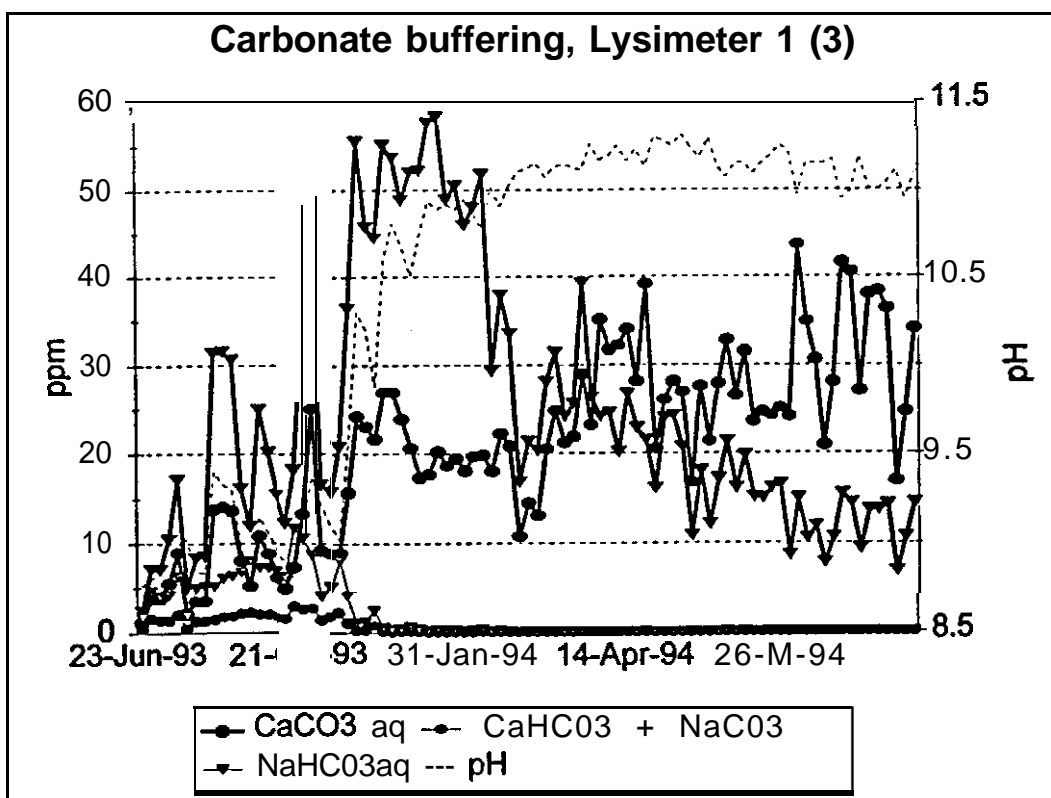Figure 6-47. Ca, Na, SO₄, and K variations by date and PH in Lysimeter 3, Level 3
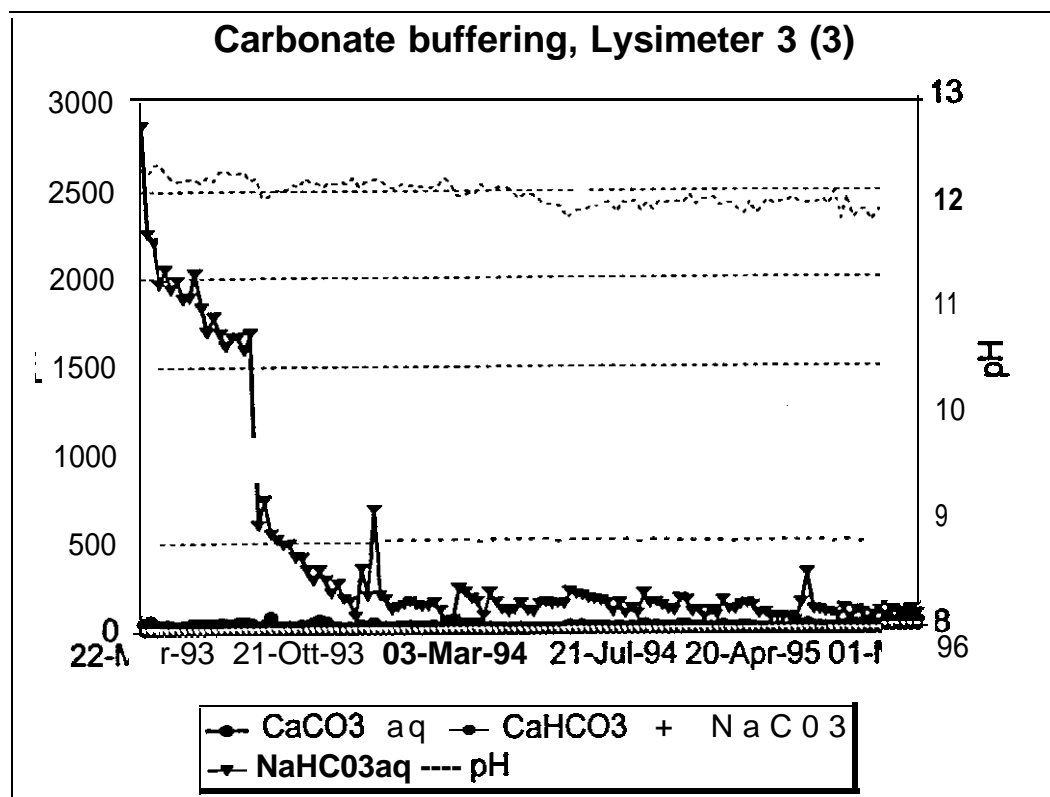

Figure 6-48. Carbonate buffering over time in Lysimeter 1 (3)

Figure 6-49. Carbonate buffering over time in Lysimeter 3 (3)